

bradscholars

Optimal scheduling, design, operation and control of reverse osmosis desalination. Prediction of RO membrane performance under different design and operating conditions, synthesis of RO networks using MINLP optimization framework involving fouling, boron removal, variable seawater temperature and variable fresh water demand.

Item Type	Thesis
Authors	Sassi, Kamal M.
Rights	
The University of Bradford theses are licenced under a Creative Commons Licence.
Download date	2026-05-12 03:17:22
Link to Item	http://hdl.handle.net/10454/5671



University of Bradford eThesis

This thesis is hosted in [Bradford Scholars](#) – The University of Bradford Open Access repository. Visit the repository for full metadata or to contact the repository team



© University of Bradford. This work is licenced for reuse under a [Creative Commons Licence](#).

Optimal Scheduling, Design, Operation and Control of Reverse Osmosis based Desalination

Prediction of RO membrane performance under different design and operating conditions, synthesis of RO networks using MINLP optimization framework involving fouling, boron removal, variable seawater temperature and variable fresh water demand

Kamal M. Sassi

BSc Chem. Eng., MSc Chem. Eng.

Submitted for the Degree of

Doctor of Philosophy

School of Engineering Design and Technology

University of Bradford

United Kingdom

2012

Abstract

Key words: RO desalinations, modelling, simulation, optimization, variable fresh water demand, flexible scheduling, control, MINLP, gPROMS

An accurate model for RO process has significant importance in the simulation and optimization proposes. A steady state model of RO process is developed based on solution diffusion theory to describe the permeation through membrane and thin film approach is used to describe the concentration polarization. The model is validated against the operation data reported in the literature.

For the sake of clear understanding of the interaction of feed temperature and salinity on the design and operation of RO based desalination systems, simultaneous optimization of design and operation of RO network is investigated based on two-stage RO superstructure via MINLP approach. Different cases with several feed concentrations and seasonal variation of seawater temperature are presented. Also, the possibility of flexible scheduling in terms of the number of membrane modules required in operation in high and low temperature seasons is investigated

A simultaneous modelling and optimization method for RO system including boron removal is then presented. A superstructure of the RO network is developed based on double pass RO network (two-stage seawater pass and one-stage brackish water pass). The MINLP problem based on the superstructure is used to find out an optimal RO network which will minimize the total annualized cost while fulfilling a given boron content limit. The effect of pH on boron rejection is investigated at deferent seawater temperatures.

The optimal operation policy of RO system is then studied in this work considering variations in freshwater demand and with changing seawater temperature throughout the day. A storage tank is added to the RO layout to provide additional operational flexibility and to ensure the availability of freshwater at all times. Two optimization problems are solved incorporating two seawater temperature profiles, representing summer and winter seasons. The possibility of flexible scheduling of cleaning and maintenance of membrane modules is investigated.

Then, the optimal design and operation of RO process is studied in the presence of membrane fouling and including several operational variations such as variable seawater temperature. The cleaning schedule of single stage RO process is formulated as MINLP problem using spiral wound modules. NNs based correlation has been developed based on the actual fouling data which can be used for estimating the permeability decline factors. The correlation based on actual data to predict the annual seawater temperature profile is also incorporated in the model. The proposed optimization procedure identified simultaneously the optimal maintenance schedule of RO network including its design parameters and operating policy.

The steady state model of RO process is used to study the sensitivity of different operating and design parameters on the plant performance. A non-linear optimization problem is formulated to minimize specific energy consumption at fixed product flow rate and quality while optimizing the design and operating parameters. Then the MINLP formulation is used to find the optimal designs of RO layout for brackish water desalination. A variable fouling profile along the membrane stages is introduced to see how the network design and operation of the RO system are to be adjusted

Finally, a preliminary control strategy for RO process is developed based on PID control algorithm and a first order transfer function (presented in the Appendix).

Acknowledgment

I would like to express my most sincere gratitude to my supervisor, Professor I.M. Mujtaba for his support, constant guidance and invaluable technical advice during the course of this work.

Special thanks are due to my government for their encouragement and financial support throughout my study.

Thanks also go to Dr Mujahed AlDhaifallah members of staff in King Fahd University of Petroleum and Minerals, Systems Engineering Department, Saudi Arabia, who helped me with my PID control analysis. Also, I would like to thank my colleagues from the School of Engineering, Design and Technology for their moral support and ideas generated during our constant discussions.

My deepest gratitude, as always, to my parents, brothers and sisters for their consistent support and encouragement through this period, although they are far away, they have provided me with encouragement and support. I acknowledge and deeply appreciate the love and support of my wife, whose patience has been endless, and her everlasting support, and my daughter, Sara, for being a source of motivation during this period.

Above all, I express my deepest thanks to almighty Allah for blessing me with the health, wisdom, perseverance, patience, understanding, skills and motivation needed to successfully complete this research.

Table of Contents

Contents	Pages
Abstract	i
Acknowledgment	iii
Table of Contents	iv
List of Figures	xi
List of Tables	xv
Nomenclature	xvii
List of publication	xx
Chapter 1: Introduction	1
1.1 Background	1
1.2 RO Prospective	2
1.3 Membrane Separation Process	3
1.4 Pressure Driven Membrane Processes	3
1.5 Principle of Reverse Osmosis	4
1.6 Membrane Element	5
1.6.1 Spiral Wound	5
1.6.2 Hollow Fibre	6
1.7 Scope of This Research	7
1.8 Aims and Objectives of This Work	10
1.9 Outlines of the Report	11
Chapter 2: Literature Review	15
2.1 Introduction	14
2.2 RO Process Description	14
2.3 RO Membrane Modelling	15

2.3.1 Membrane Transport Theories	16
2.3.1.1 Solution-Diffusion Membrane Models	17
2.3.1.2 Solution-Diffusion Membrane Assessment	17
2.3.2 Concentration Polarization	18
2.3.3 Membrane Fouling	21
2.3.3.1 Understanding Membrane Fouling	21
2.3.3.2 Fouling and RO Staging	23
2.4 Review of Past Work on Simulation and Optimization of RO Process	27
2.4.1 Modelling and Simulation of RO Desalination Process	27
2.4.2 Modelling of RO Process Using Neural Networks (NNs)	30
2.4.3 Optimization of RO Process	31
2.4.3.1 Overview of Operation Optimization of RO Process	32
2.4.3.2 Overview of Control Systems for RO Desalination	35
2.5 Design of Reverse Osmosis Network	36
2.5.1 State Space Approach	36
2.5.2 Review of Previous Work on Design of Reverse Osmosis Network	39
2.6 Literature on Boron Rejection by RO membranes	43
2.7 Methods for Solving Optimization Problems	44
2.7.1 NLP Solution Techniques	44
2.7.1.1 Successive Linear Programming Method	45
2.7.1.2 Successive Quadratic Programming Method.	45
2.7.2 MINLP Solution Techniques	46
2.7.2.1 Branch and Bound Method	46
2.7.2.2 Outer Approximation Method	47
2.8 Conclusion	48

Chapter 3: Modelling and Optimization of Reverse Osmosis Process	51
3.1 Introduction	51
3.2 Modelling of Reverse Osmosis Process	51
3.2.1 Model of RO Module	53
3.2.1.1 Spiral Wound Membrane Element	53
3.2.1.2 Hollow Fibre Membrane Element	56
3.2.1.3 Energy Recovery and Consumption	57
3.2.1.4 Physical Properties	58
3.3 Reverse Osmosis Optimization	59
3.3.1 Superstructure	60
3.3.2 Model Reduction	61
3.3.3 Mathematical Model for the Superstructure	62
3.3.4 Cost Functions	66
3.4 gPROMS simulator	67
3.4.1 Model Development Using gPROMS	68
3.4.2 Solvers in gPROMS	69
3.5 Conclusion	69
Chapter 4: Effective Design of RO Process under Variable Seawater Temperature	71
4.1 Introduction	71
4.2 Modelling of RO Process	72
4.2.1 Membrane Model	72
4.2.2 Network Model	72
4.2.3 Temperature Effect on Membrane Permeability	72
4.3 RO Network Optimization Validation	73
4.3.1 Results	75

4.4 MINLP Formulation	76
4.5 Case Study	78
4.5.1 Specifications	78
4.5.2 Results	79
4.4.3 Maintenance Scheduling	85
4.5 Conclusion	86
Chapter 5: Optimal Design of RO Desalination Process with Boron Removal	88
5.1 Introduction	88
5.2 Discussion on Boron	89
5.2.1 Occurrence and Toxicity	89
5.2.2 Boron Standards in Drinking Water	90
5.2.3 Boron in Seawater Chemistry	91
5.3 Boron Removal by Reverse Osmosis	92
5.4 Mathematical Model for Boron Rejection by RO	95
5.4.1 Effect of pH on Boron Permeability	97
5.5 Synthesis of RO Process Including Boron Removal	98
5.5.1 Network Model	98
5.5.2 MINLP Problem Formulation	100
5.5.3 Cost Function	102
5.6 Case Study	103
5.7 Results	104
5.7.1 Case Study 1: Optimization of RO Design Without pH Adjustment	105
5.7.2 Case Study 2: Optimization of RO Design with pH Adjustment	107
5.8 Conclusion	110
Chapter 6: Optimal operation of RO System with Daily Variation of Fresh Water	111

Demand and Seawater Temperature	
6.1 Introduction	111
6.2 Variable Operation in RO Systems	112
6.3 Estimation of Dynamic Seawater Temperature and Freshwater Demand Profiles	113
6.4 Model Development	114
6.4.1 Storage Tank Dynamic Model	115
6.5 RO process optimization involving storage tank	116
6.5.1 Process constraints	116
6.5.1.1 Tank level	116
6.5.1.2 Tank Salinity	117
6.5.2 Optimization Problem Formulation	119
6.5.3 Optimization Methodology	120
6.6 Presentation of the Illustrative Example	122
6.7 Results and Discussion	123
6.6.1 Case study 1: Optimization of RO Operation in Summer	123
6.6.2 Case study 2: Optimization of RO Operation in Winter	126
6.7.3 Comparison between Case Study One and Two	130
6.8 Conclusion	132
Chapter 7: Optimal Design and Cleaning Scheduling of RO Process	134
7.1 Introduction	134
7.2 Previous Formulations of RO Maintenance Scheduling	134
7.3 Estimation of Dynamic Seawater Temperature Profile	135
7.4 RO Network Model	136
7.5 Maintenance scheduling formulation	138
7.6 Development of Neural Network Model	139

7.6.1 Neural Networks Applications	139
7.6.2 Estimation of Water and Salt Permeability Coefficients Using NNs	142
7.7 Fouling Model Formulation	149
7.8 MINLP optimization formulation	153
7.8.1 The Objective Function	155
7.9 Case Study	156
7.10 Optimal Design and Scheduling Results	156
7.11 Conclusion	163
Chapter 8: Brackish Water RO Process: Simulation and Optimization	165
8.1 Introduction	165
8.2 Fouling Description	166
8.3 Model Validation	167
8.4 Case Study 1: Sensitivity Analysis	171
8.4.1 Sensitivity of Operating Variables	173
8.4.1.1 Pressure	173
8.4.1.2 Number of Element in Pressure Vessel	174
8.4.1.3 Feed Salinity	175
8.4.2 Sensitivity of Design Variables	175
8.4.2.1 Length of Filament Mesh in Feed Spacer	176
8.4.2.2 Filament Diameter to Spacing Ratio	177
8.4.3 Energy Recovery	177
8.5 Optimization Study	178
8.5.1 Case study 2: Optimization of Operating and Design Parameters (OP1)	180
8.5.2 Case study 3: RO Network Optimization	180
8.5.2.1 Effect of Membrane Fouling on RO Performance	182

8.5.2.2 RO Network Optimization Result	184
8.6 Conclusion	187
Chapter 9: Conclusions and Future Work	190
9.1 Conclusions	190
9.2 Future Work	195
References	197
APPENDIX A: PID Control of RO Process	214
A.1 Introduction	214
A.2 Process control variables	215
A.3 Modeling of RO Process	215
A.3.1 Estimation of Water and Salt Permeability Coefficients	216
A.4 Case Study	218
A.5 System Identification	218
A.6 Controller Design and Response	220
A.7 Conclusion	221

List of Figures

Figure 1.1	Global desalination capacity increase by technology, 1980-2016	3
Figure 1.2	Pressure driven membrane processes	4
Figure 1.3	Representation of the Theory of Osmosis	5
Figure 1.4	Schematic view of a spiral wound membrane element	6
Figure 1.5	General view of hollow fibre element	6
Figure 2.1	RO process system	15
Figure 2.2	Transport through membranes	16
Figure 2.3	Schematic diagram of concentration polarization	19
Figure 2.4	Dependence of permeate flow on transmembrane pressure	20
Figure 2.5	Schematic fouling layers	22
Figure 2.6	Reverse Osmosis configuration	24
Figure 2.7	Occurrence of fouling in RO desalination plants	25
Figure 2.8	Pressure drop profile in Zarzis desalination plant	26
Figure 2.9	Pressure drop profile for two stages nanofiltration installation	27
Figure 2.10	Superstructure of reverse osmosis configuration	38
Figure 3.1	Reverse osmosis membrane element	52
Figure 3.2	Pressure Vessel Construction	56
Figure 3.3	RO superstructure	61
Figure 3.4	Superstructure of two stages RO network	63
Figure 4.1	Optimal design and operating conditions for the RO network (this work)	76
Figure 4.2	Tapered design with brine bypass (El-Halwagi, 1992)	76
Figure 4.3	Optimum RO networks	83
Figure 4.2	Unit cost for the optimal RO networks as a function of temperature at different feed salinity	85

Figure 5.1	Distribution of boric acid and borate in seawater at different pH	92
Figure 5.2	Schematic drawings of (a) one pass design (b) the two pass design (c) hybrid design and (d) Cascade design2	94
Figure 5.3	Boron permeability factor predicted vs Chillon Arias et al. (2011b)	98
Figure 5.4	General superstructure for double-pass RO process	98
Figure 5.5	Optimum configurations for boron removal by RO process	109
Figure 6.1	Daily time schedule for fresh water consumption by the user	114
Figure 6.2	Seawater temperature profiles	114
Figure 6.3	RO system with storage tank	115
Figure 6.4	Schematic diagram of a storage tank	115
Figure 6.5	(a) Typical tank level profile and (b) Tank level violations	117
Figure 6.6	(a) Tank salinity profile and (b) Tank salinity violations	118
Figure 6.7	The RO process flow diagram with storage tank	121
Figure 6.8	Daily RO operation cycle at summer season	124
Figure 6.9	Optimal operating pressure profile using summer temperature profile	124
Figure 6.10	Storage tank level profiles at summer operation	125
Figure 6.11	Fresh water consumption and RO production profiles (Scenario 1)	126
Figure 6.12	Salt concentration of fresh water from RO and tank profiles ((Scenario 1)	126
Figure 6.13	Optimal operation schedule of RO at winter season	127
Figure 6.14	Tank operating levels over a cycle of 24 h at winter season	128
Figure 6.15	Fresh water production and consumption during the day.	129
Figure 6.16	Optimal operating pressure profile at summer season	129
Figure 6.17	RO permeate salinity and tank salinity profiles at winter (scenario 3)	129
Figure 6.18	Comparison of different operation schedules	131
Figure 6.19	Pressure pattern for summer and winter (Scenario 1)	131

Figure 6.20	RO permeate salinity in summer and winter (Scenario 3)	131
Figure 7.1	Evolution of feed temperature in one year	135
Figure 7.2	The RO process flow diagram	137
Figure 7.3	RO process configurations for different maintenance schedules	140
Figure 7.4	Scheduling of cleaning of RO membrane and corresponding flow diagram	141
Figure 7.5	Different Neuron transfer Functions	142
Figure 7.6	Four layer neural network	143
Figure 7.7	Actual water permeability decline factor and the predicted by NNs	151
Figure 7.8	Actual salt permeability decline factor and the predicted by NNs	152
Figure 7.9	Actual and predicted water permeability decay factor	152
Figure 7.10	Actual and predicted salt permeability decay factor	152
Figure 7.11	Total production cost of optimal maintenance schedule	159
Figure 7.12	Optimal feed pressure profile for one maintenance cycle and 2 inter-maintenance cycles	160
Figure 7.13	Optimal trajectory of feed pressure and permeate salinity	163
Figure 8.1	Schematic diagram of RO process	168
Figure 8.2	Water and salt fluxes for different elements	171
Figure 8.3	Average concentration polarization factor and Mass transfer coefficient for the different elements	171
Figure 8.4	Dependence of RO process performance on operating pressure	174
Figure 8.5	Effect of the number of membrane element on the recovery ratio	175
Figure 8.6	Effect of mesh length on water recovery and axial pressure drop	176
Figure 8.7	RO performance for different circular spacer diameters and filament spacing	177
Figure 8.8	RO energy recovery for different recovery devices	178

Figure 8.9	Variation of water permeability with different fouling levels for RO stages	182
Figure 8.10	Water recovery decline for various fouling percentage at different stages	183
Figure 8.11	Water flux profile for different fouling levels	184
Figure 8.12	Second stage feed concentration at two levels of fouling	184
Figure 8.13	The optimum process arrangements	186
Figure 8.14	Predicted feed pressure at various fouling levels	187
Figure 8.15	Annual operating cost profiles at various fouling levels	187
Figure A.1	Identification Input Signal	219
Figure A.2	Identification Output Signal	220
Figure A.3	Closed-Loop Response	221

List of Tables

Table 2.1	Location of fouling in NF/RO plants	25
Table 2.2	Summary of the past work on RO modelling	29
Table 2.3	Summary of the past work on RO operation optimization	33
Table 2.4	A summary on control of membrane processes	37
Table 2.5	Summary of RO process design works	40
Table 2.6	Summary of boron rejection modelling	43
Table 4.1	Hollow fibre RO modules specifications (El-Halwagi, 1992)	74
Table 4.2	Input Data for the hollow fibre optimization case study	75
Table 4.3	DuPont hollow fibre RO modules specifications	79
Table 4.4	Input data for MINLP optimization	80
Table 4.3	MINLP optimization results	82
Table 5.1	Regulations for boron in drinking water	91
Table 5.2	RO seawater desalination process for boron removal	95
Table 5.3	The characteristics of spiral wound membranes (Lu et al., 2007)	104
Table 5.4	Input data for MINLP optimization	104
Table 5.5	MINLP results for seawater desalination considering boron limit in fresh water and without pH adjustment	105
Table 5.6	MINLP results for seawater desalination considering boron limit in fresh water and with pH adjustment	108
Table 6.1	Input data for optimization	123
Table 6.2	Specific power consumption (kwh/m ³ of permeate)	132
Table 7.1	Water and salt permeability coefficients vs. seawater temperature throughout one year	144
Table 7.2	NNs parameters for estimation water permeability factor	150

Table 7.3	NNs parameters for estimation salt permeability factor	151
Table 7.4	Input data for MINLP optimization	157
Table 7.5	Cost breakdown for optimal RO systems at different maintenance schedules in (k\$/year)	158
Table 7.6	MINLP results for spiral wound membrane scheduling problem	161
Table 8.1	Membrane parameters and operating conditions	168
Table 8.2	Comparison operational data with Abbas data and this work results	169
Table 8.3	Comparison of data predicted by Abbas and this work (Feed concentration 2540 ppm, Feed flow 20.4 m ³ /h)	169
Table 8.4	Compression of data predicted by Abbas and this work (Feed concentration 2540 ppm, Feed pressure 12.2 bar)	169
Table 8.5	Predicted profiles by this work for the three stages reverse osmosis	172
Table 8.6	Optimization Results of Problem 1 (OP1) results	180
Table 8.7	Input parameters for optimization calculations	181
Table 8.8	Summary of MINLP optimization results	185
Table A.1	Permeability coefficients and experimental data	217
Table A.2	Comparison of predicted with experimental data	218
Table A.3	B10 hollow fibre module (6440-T) specifications	219

Nomenclature

A	Area (m^2)
A_b^T	Boron permeability as a function in temperature (m/s)
$A_b^{T_o}$	Boron permeability at reference temperature (m/s)
A_s^f	Salt permeability decay factor
A_s^T	Salt permeability as a function in temperature (m/s)
$A_s^{T_o}$	Salt permeability at reference temperature (m/s)
A_w^f	Water permeability decay factor
A_w^{fo}	Water permeability with fouling (m/ bar.s)
A_w^T	Water permeability as a function in temperature (m/ bar.s)
$A_w^{T_o}$	Water permeability at reference temperature (m/ bar.s)
B	Binary variable
BW	Brackish water pass
BY	Bypass fraction
BY^{BW}	Brackish water pass bypass fraction
c	Salt concentration (kg/m^3)
C_{BW}	Concentration associated with BW pass (kg/m^3)
C_{ERD}	Turbine capital cost (\$)
C_f	Feed salt concentration (kg/m^3)
$C_{f,t}$	Salt concentration in the total feed (kg/m^3)
CH_{cost}	Caustic and acid costs per cubic meter (euro cent/ m^3)
C_{me}	Membrane module cost (\$)
C_p	Permeate salt concentration (kg/m^3)
CP	Concentration polarization factor
$C_{p,avg}$	Average salt concentration in total permeate (kg/m^3)
C_{pu}	Pump capital cost (\$)
C_{PV}	Pressure vessel cost (\$)
C_r	Brine salt concentration (kg/m^3)
$C_{r,t}$	Outlet brine concentration (kg/m^3)

C_{SW}	concentration associated with SW pass (kg/m^3)
C_{tu}	Turbine capital cost (\$)
C_{WIP}	Pretreatment cost (\$)
d_h	Hydraulic diameter (m)
D^T	Salt diffusivity at any temperature (m^2/s)
D^{T_0}	Salt diffusivity at reference temperature (m^2/s)
E_c	Electricity price (\$)
E_{pu}	Pump power consumption (kWh)
E_{PX}	Specific energy consumption (PX as ERD) (kWh/m^3)
ERD	Energy recovery device
$E_{t,recv}$	Total energy recovered by turbine (kWh)
E_{tu}	Specific energy consumption (Turbine as ERD) (kWh/m^3)
F	Fouling factor
F^1	Fouling factor of first stage
F^2	Fouling factor of second stage
h_{sp}	Height of spacer channel (m)
j^T	Flux at any temperature ($(\text{m}/\text{s}$ or $\text{kg}/\text{m}^2\text{s}$)
k	Mass transfer coefficient (m/s)
k_{dc}	Constant in equation 3.8
L	Fiber bundle length or membrane leaf length (m)
l_f	Load factor
L_f	Feed spacer filament length (m)
N	Number of membrane modules in j^{th} RO stage
ne	Number of elements in each PV
N_{pu}	Number of pumps
N_{tu}	Number of turbines
OC_{ch}	Chemical cost (\$/y)
OC_{me}	Membrane module capital cost (\$)
OC_{me}	Membrane operating cost (\$/y)
OC_{pu}	Pump energy cost (\$/y)
OC_{reag}	Cost of increasing pH in BW pass (\$/y)
OC_{sc}	Spare cost (\$/y)
P_f	Feed pressure (bar)

pH_f	Boron permeability factor account effect solution pH
PX	Pressure exchanger
Q_{BW}	Flow associated with BW pass (m^3/h)
Q_f	Feed flow (m^3/s)
$Q_{f,in}$	Fresh feed flow(m^3/h)
$Q_{f,t}$	Total feed flow (m^3/h)
Q_{HP}	Total flow entering pump or turbine (m^3/h)
Q_p	Permeate flow (m^3/s)
$Q_{p,t}$	Total permeate flow (m^3/h)
Q_r	Brine flow (m^3/s)
$Q_{r,t}$	Total outlet brine flow (m^3/h)
Q_{SW}	Flow rate associated with SW pass (m^3/h)
R	2 nd stage brine recycled fraction
Re	Reynolds number
r_i	Inner fiber radius (m)
R_i	Fiber bundle inner radius (m)
r_{ot}	Outer fiber radius (m)
R_{ot}	Fiber bundle outer radius (m)
S	Number of RO stages
Sc	Schmidt number
sh	Sherwood number-
SR	Salt rejection
SR_b	Boron rejection
SW	Seawater pass
t	Time
T	Temperature ($^{\circ}C$)
TAC	Total annualized cost ($\$/y$)
T_o	Reference temperature ($^{\circ}C$)
t_p	Time in the period p (h)
u	Axial velocity (m/s)
U	Superficial velocity (m/s)
U_i	Inner superficial velocity (m/s)
U_{ot}	Outer superficial velocity (m/s)

w	Width of the membrane (m)
WR	Water recovery (%)
X	Total number of streams leaving splitter
X_{f1}	Fouling fraction in first stage
Y	Total number of streams leaving mixer
ΔP	Pressure drop across the membrane element (bar)
ΔP_{HP}	Pressure difference across the pump or turbine (bar)

Creek letters

η	Efficiency
ε	Feed spacer void fraction
μ^{T_0}	Dynamic viscosity at reference temperature (Pa s)
μ^T	Dynamic viscosity at any temperature (Pa s)
φ	Osmotic pressure (bar)
ρ	Bulk density (kg/m^3)

Subscript

B	Bulk
b	boron
f	Feed
fo	Fouling
j	The j^{th} RO stage
m	Membrane surface
mx	Total streams from mixer
p	Permeate
pu	Pump
r	Brine
s	Salt
sp	Total streams from splitter
tu	Turbine
w	Water
x	The x^{th} mixer
y	The y^{th} mixer

List of publication

Journal papers

- 1) Sassi, K.M. and I.M. Mujtaba (2011), Optimal design and operation of reverse osmosis desalination process with membrane fouling, *Chemical Engineering Journal*, 171, 582–593.
- 2) Sassi, K.M. and I.M. Mujtaba (2011), Optimal Design of Reverse Osmosis Based Desalination Process with Seasonal Variation of Feed Temperature, *Chemical Engineering Transactions*, 25, 1055-1060.
- 3) Sassi, K.M. and I.M. Mujtaba (2012); Effective design of reverse osmosis based desalination process considering wide range of salinity and seawater temperature, *Desalination*, 306, 8-16.
- 4) Sassi, K.M. and I.M. Mujtaba (2012) Coping with variable demand by flexible design and operation of reverse osmosis process, to submit to *chemical engineering Journal*.
- 5) Sassi, K.M. and I.M. Mujtaba (2012) General superstructure and MINLP optimization for boron removal by reverse osmosis membranes, submitted to *Journal of membrane science*.

Conference papers

- 1) Sassi, K. M., and Mujtaba, I. M. (2010) Simulation and Optimization of Full Scale Reverse Osmosis Desalination Plant, *20th European Symposium on Computer Aided Process Engineering*, 28, 895-900.
- 2) Sassi, K.M. and I.M. Mujtaba (2011), Optimization of Design and Operation of Reverse Osmosis Based Desalination Process Using MINLP Approach Incorporating Fouling Effect, *21st European Symposium on Computer Aided Process Engineering*, 29, 206–210.

- 3) Sassi, K.M. and I.M. Mujtaba (2012), Optimal operation of RO system with daily variation of freshwater demand and seawater temperature, *22nd European Symposium on Computer Aided Process Engineering*, 30, 817-821.
- 4) AlDhaifallaha, M.M., Sassi, K.M. and Mujtaba, I.M. (2012) PID control of RO desalination process, *22nd European Symposium on Computer Aided Process Engineering*, 30, 812-816.

Chapter 1

Introduction

1.1 Background

Water is the most abundant compound on earth's surface but in fact a very small portion of it is accessible or suitable for human consumption. About 97% of the global water resource is salt water and only 3% of total water capacity is represented by freshwater including water frozen in glaciers and polar ice caps (Bielik et al., 2010).

Freshwater is a renewable resource, but the globe's resources are steadily depleted. The current demand for freshwater already exceeds the supply in many parts of the world. Water shortages problems are expected to grow worse in the near future for many regions in the world. Recently, some industrial nations such as Australia and Spain have experienced severe water shortages (Martin-Rosales et al., 2007).

The scarcity of fresh water resources and the growth of population, industry and agriculture have increased the reliance on water production using desalination technology. Some countries such as gulf areas rely completely on desalinated water (Abuzinada et al., 2008). Therefore, much attention is being paid to seawater and brackish water desalination technologies including Reverse Osmosis (RO) in attempts to improve the reliability and the performance of freshwater production processes.

Thermal and RO processes are, by far, the major desalination systems used now-a-days. RO process is less energy intensive which makes it most cost efficient (Fritzmann et al., 2007). For instance, energy consumption for seawater RO desalination is about one-half of that of multiple effect evaporator process (Singh, 2008).

Recently, seawater desalination by RO has been the main source of drinking water supply in many regions that have freshwater lake (Geraldés et al., 2005). RO membranes used in sea water desalination are capable of producing good water quality by removing most of the salts and some other contaminants from water sources. During

the last decade, tremendous advances were made in the research related to development of RO membranes, which has resulted in the production of new membranes able to work within wide pH ranges, higher temperatures and pressures, increased productivity, reduced salt concentration in the product, and low capital and operating costs (Grote et al., 2012).

1.3 RO Prospective

The RO process seems to be the most promising technology for water desalination. Recently, the RO market share is significantly increased compared with thermal desalination technologies with the highest number of new desalination plants around the world. The RO desalination capacity reached 53% of worldwide desalination capacity in 2008 (IDA, 2008-2009), and in 2010, RO desalination accounted for 60 % of desalination plants capacity while MSF represents only about 26 % (IDA, 2010-2011). Significant advances have been made in the research related to water desalination using RO membranes in the last decades. The application of RO process in the water desalination has grown rapidly and has become the leading technology in desalination market. Figure 1.1 shows a dramatic increase in the new RO worldwide desalination capacity in the period 1980 to 2016 compared to thermal desalination. The RO desalination capacity is increased about 20 times in this period, while thermal processes capacity remained in their initial level.

The cost of fresh water produced by membrane treatment has shown dramatic reduction trend. This remarkable progress has been made mainly through two aspects, huge improvements in membrane material and incorporation of the energy recovery devices in RO systems (Greenlee et al., 2009) which significantly reduce the energy requirements. Khawaji et al. (2008) reported that the unit energy consumption for seawater desalination have been reduced to as low as 2 kWh/m³ significantly lower than thermal process such as Multi-stage flash distillation (MSF) which typical 4 kWh/m³.

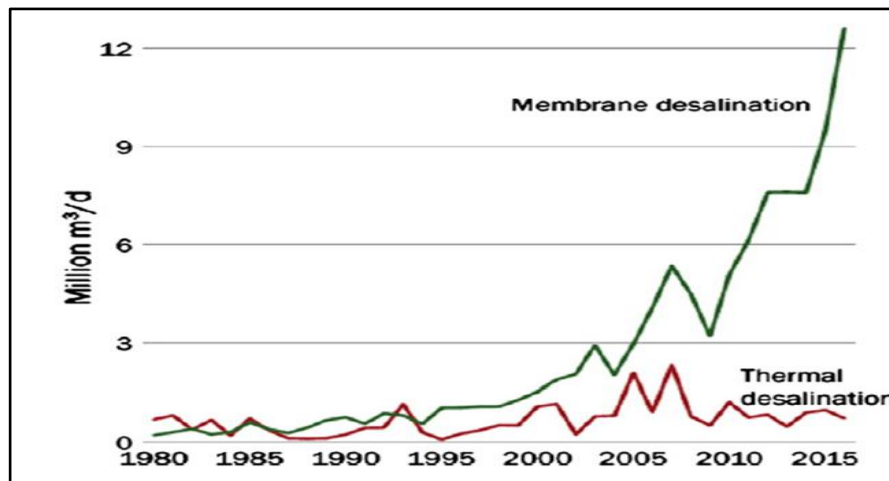


Figure 1.1 Global desalination capacity increase by technology, 1980-2016
(Desalination Market, 2010)

Another potential growth of RO process is that by utilizing the renewable energy resources. Ghobeity and Mitsos (2010) suggested that RO plants can operate at variable load without any technical problems. Therefore, RO plants can cope even with instantaneous energy fluctuations as in the case of RO installations powered by renewable energy. Nowadays, 51 % of the total renewable energy sources powered desalination systems were used to operate the RO processes (Eltawil et al., 2009).

1.3 Membrane Separation Processes

Membrane filtration is a process in which a membrane is used to separate compounds or concentrate a solution by applying a certain driving force across the membrane, which may be a pressure gradient, concentration gradient, electrical potential gradient or temperature gradient. Membrane processes are designed to carry out physical or physicochemical separations. These are more recent developments and have not yet achieved widespread implementation. The development of membrane-based bulk water and wastewater treatment processes is significant and offer many advantages over conventional techniques in terms of complexity and cost.

1.4 Pressure Driven Membrane Processes

In the pressure driven membrane processes, the driving force is a pressure difference across the membrane. It differs mainly in the pore size of their membranes, which

makes a particular membrane effective for the removal of a specific range of impurities. Four pressure driven membrane filtration processes can be distinguished based on differences in feed pressures and membrane rejection capacities: Reverse Osmosis (RO), Nanofiltration (NF), Ultrafiltration (UF), Microfiltration ranked by increasing pressure as shown in Figure 1.2 (Cheryan, 1998). Microfiltration and ultrafiltration processes need low pressure membranes to accomplish the filtration process while high pressure is required for nanofiltration and reverse osmosis processes.

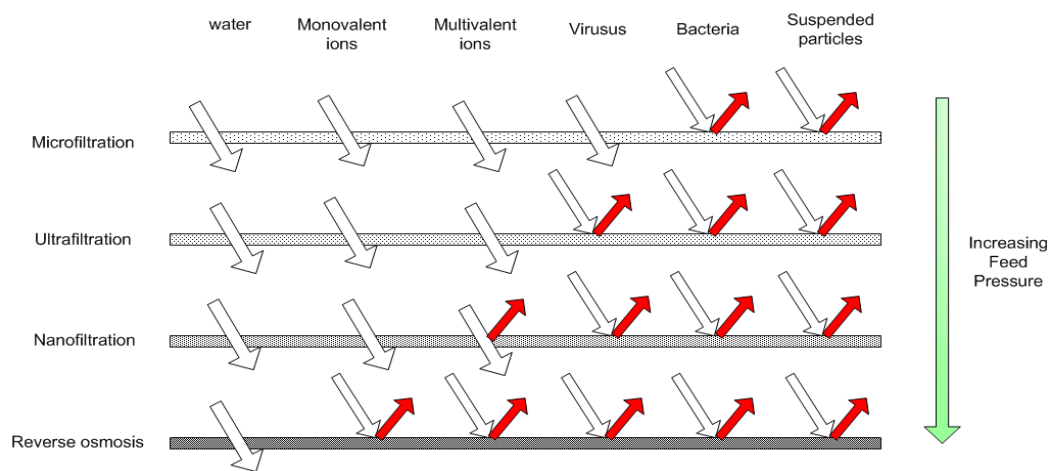


Figure 1.2 Pressure driven membrane processes

1.5 Principle of Reverse Osmosis

Osmosis is a natural flow of water through a semipermeable membrane from a solution with low salt into a more concentrated solution (Figure 1.3) until osmotic equilibrium between the two solutions is reached (Ian et al., 2003). The driving force for this passage of water is known as the osmotic pressure and depends on the difference in solutes concentrations of the two solutions.

RO is pressure driven membrane separation process in which a dense membrane allows diffusion of the solvent and solutes. Diffusion of solutes, like salts, is low compared to water results in a rejection for those substances. When pressure is applied to the concentrated solution, larger than the osmotic pressure, the flow of diffused solvent through the membrane is reversed as shown in (Figure 1.3) and solvent flows from the

concentrated solution side through the membrane to the diluted solution while dissolved ions and small molecules that contaminate aqueous solutions and impurities are rejected by the membrane. This process is called reverse osmosis (Sourirajan and Agrawal, 1969).

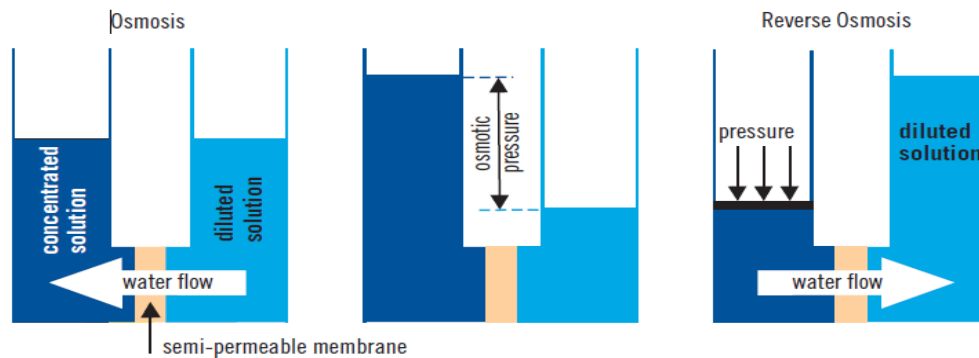


Figure 1.3 Representation of osmosis theory (Sourirajan and Agrawal, 1969)

The commercial RO membranes are made up of mainly from cellulose acetate in the past. Recently, aromatic polyamide membranes were largely accepted in the real applications (Mallevalle et al., 1996). The polyamide membranes have several advantages over the cellulose acetate membranes such as high solute rejection, high resistivity to fouling and more stability.

1.6 Membrane Element

The large membrane area required for commercial separations is tightly packaged into membrane modules. Different membrane geometries have been developed for this purpose including spiral wound, hollow fibre tubular and plate and frame, which are offering high separation efficiency and are economically feasible (Baker et al., 2004). This thesis focuses on spiral-wound and hollow-fibre modules because of their greater commercial and technical importance.

1.6.1 Spiral Wound

Spiral wound membrane elements are produced from flat membrane sheets which are rolled into along a central perforated permeate collection tube (Figure 1.4) and

separated by highly porous spacer material facilitating the transport of product water to the central product collection tube. The spacer keeps the membrane layers apart and also promotes turbulence and mixing, which improve mass transport near the membrane surface and reduce concentration polarization. Spiral wound module is designed to offer as much surface area as possible into a given volume (Senthilmurugan et al., 2005).

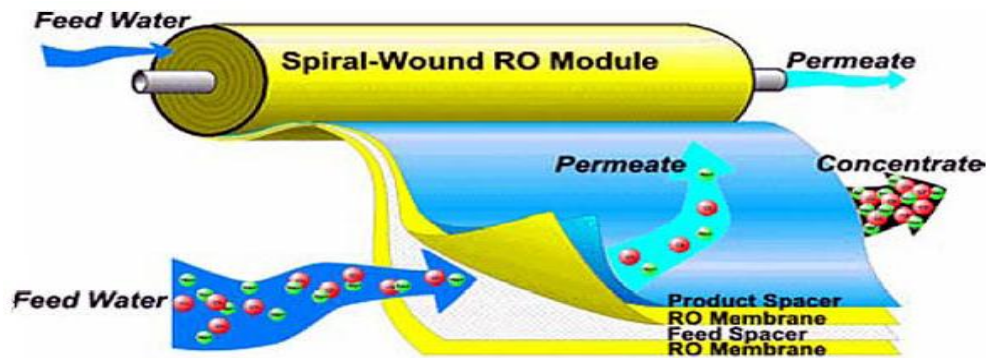


Figure 1.4 Schematic view of a spiral wound membrane element (Mareth, 2006)

1.6.2 Hollow Fibre

Hollow-fibre modules contain a large number of membranes tubes which are housed in a U tube bundle of several thousand fibres as illustrated in Figure 1.5. Feed is usually introduced outside the hollow fibre, distributed from a tube in the centre of the bundle and may flow through the fibre bundle radially or parallel to the hollow fibres. The permeate is collected at the tube sheet end of the vessel (Khan, 1986). Hollow fibre elements have very high packing density and require minimal space. The product recovery is high, typically 50– 60% of the feed flow.

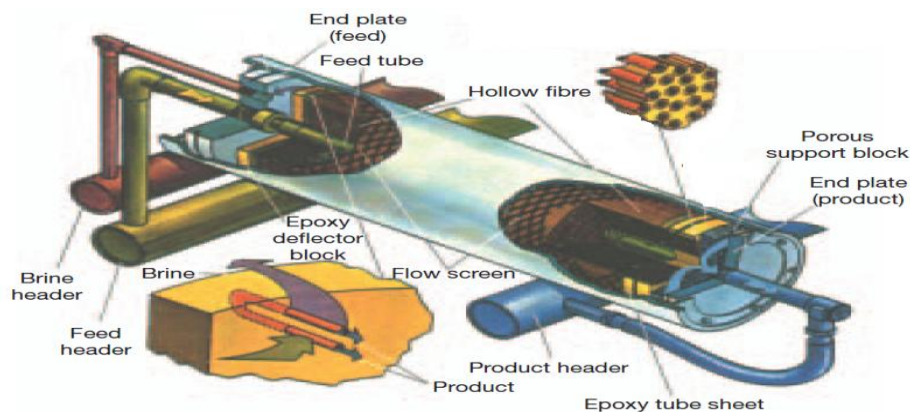


Figure 1.5 General view of hollow fibre element (Khan, 1986).

1.7 Scope of This Research

This research is focused on simulation and optimization of RO based desalination process. The optimal design of RO system for seawater and brackish water are investigated in order to achieve the goal of reducing the production cost while at the same time increasing the freshwater productivity and quality incorporating the influence of the several operation and design parameters such as fouling, variable fresh water demand, variation in seawater temperature, salinity and pH value.

Researchers have often looked into minimizing the energy consumption of RO, neglecting the variability in seawater temperature and fresh water demand during a day and year and assumed constant operation (Starov et al., 1995; Wilf et al., 2001; Guria et al., 2005; Geraldles et al. 2005; Abbas 2007; Gilau and Small 2008; Zhu et al. 2009. Hyun et al., 2009; Lee et al., 2009; Bartman et al., 2010; Peñat et al., 2011). In reality the fresh water demand and seawater temperature vary significantly throughout the year and even during a day. To the author's best knowledge, no studies have been reported on the optimization of RO desalination process including variable seawater temperature and variable demand throughout the day or year.

In order to design and optimize RO processes that are capable of removing boron from permeate, detail understanding of the boron chemistry and its permeation properties in RO membrane is crucial to balance the trade-off between boron concentration reduction and energy consumption. The flow and permeation properties should be modelled with the consideration of the effects of several operation and design parameters of RO process on boron rejection. Although there exist an abundant literature on optimal design and operation of RO systems, most studies carried out so far on the boron removal by RO membranes have been focused on experimental or lab scale analysis. In fact only few publications were found in the literature which studied this issue theoretically (Taniguchi et al. 2001; Sagiv and Semiat, 2004; Hyung and Kim, 2006;

Hung et al. 2009; Manea et al., 2009). Flexible network superstructure approach has not been studied extensively until to date.

One of the more serious problems encountered in a RO process is the occurrence of membrane fouling, which limits both operation efficiency and membrane lifetime. Most of previous studies for RO process have not considered RO membrane fouling. Few of them considered fouling rate in all membrane stages equally distributed; in modelling and simulation (Boudinar et al., 1992; Van der Meer et al., 1998; Abbas, 2005; Zhu et al., 2009; Li, 2010); RO network layout optimization (Evangalista, 1985; El-Halwagi, 1992; Voros et al., 1996; Zhu et al., 1997; Villafafila and Mujtaba, 2003; Lu et al., 2007; Saif et al., 2008; Sarkar et al., 2008).

The optimization of design and operation of RO network to include scheduling for membrane cleaning is an important issue that has received relatively little attention. Only limited studies on maintenance and cleaning scheduling of RO membranes are found in the literature (Zhu et al., 1997; See et al., 1999 and Lu et al., 2006). Although, spiral-wound module occupies the largest market share (Kaghazchi et al., 2010), all the RO scheduling optimization problems were investigated using hollow fibre modules. In addition, all of these studies (RO maintenance scheduling) did not include the effect of seasonal changes such as seawater temperature and seawater salinity variations on the optimal maintenance scheduling of RO process.

The accuracy of optimal cleaning schedule of a membrane desalination plant depends largely on the accurate estimation of fouling model (See et al., 1999). However, most of the fouling models used were simple exponential function and implemented simple model to represent the system performance decay which might not be adequate to represent the real application.

As seen from the literature, simulation and optimization of RO separation systems incorporating different fouling extents in membrane stages are not often found in the

literature. Therefore, this work is focused on investigating the role of varying fouling rate into membrane stages and its effect on the operation and design of RO process.

Proportional–integral (PI) or proportional–integral–derivative (PID) control algorithms have been used to regulate process variables such as water flux and adjust the system control variables such as feed flow rate and pressure in order to achieve a fresh water production target (Alatiqi et al., 1989; Singh, 1999; Martins, 2005; Kim et al., 2008).

Furthermore, there have been substantial efforts that were made to reduce energy consumption by RO desalination process including controlling the operating variables subject to process fluctuations (Perrot, 1996; Abbas, 2006; Greenlee et al., 2009; Ali, 2010). However, little of these studies take into account the membrane fouling effects on RO performance (Van Boxtel and Otten, 1993; Lee et al., 2009).

With this background, the general focus of this research is developing the following:

- Several steady state RO process models.
- Accurate fouling model based on actual plant data which are used in the formulation of RO maintenance scheduling optimization problem.
- A control strategy that takes into account desired system operating conditions, feed water quality, membrane fouling and different operational limitations.
- Numerous steady state and dynamic optimization frameworks considering different RO operation variations and subject to process constraints including boron concentration, fixed/variable seawater temperature and fresh water demand.

Modelling and optimization frameworks are then used for better understanding, operation, control and design of RO process. The detailed aims and objectives of the thesis are outlined below.

1.8 Aim and Objectives of This Work

The main goal of this thesis is to achieve a stable and reliable operation for the RO process with minimum production cost by optimizing operation and design parameters via mathematical modelling and optimization.

The main objectives of the thesis can be highlighted as follows:

- To develop the general superstructure for two-stage RO process layout and formulate RO network design problem as MINLP problem.
- To investigate the effect of seawater temperature and salinity on the synthesis of RO networks via the application of MINLP approach.
- To develop a novel superstructure of the RO network based on double pass RO network. The RO design problem will be formulated as an MINLP problem constrained with maximum salt and boron concentration in the fresh water.
- To combine a steady state model for RO process with dynamic model of a storage tank in the optimization formulation considering variable seawater temperature and water demand for a 24 h time horizon.
- To formulate the design and cleaning scheduling of RO network as MINLP problem to find the optimal RO network design corresponding to each membrane cleaning schedule.
- To use the MINLP optimization approach to solve the optimal design problem of RO desalination process incorporating different fouling percentages in membrane stages.
- To investigate on how the operation of RO process is to be adjusted to maintain a fixed water flux by developing an optimization-based PID controller.

1.9 Outlines of the Thesis

The layout of this thesis is presented below.

Chapter 1: Introduction

General background of desalination, brief literature review on desalination market, classification of membrane process, background about RO process, also comparison between commercial membrane elements are presented. Finally the scope, the aim and the objectives of the research are highlighted.

Chapter 2: Literature Review

The general description of RO process is presented. A brief description of membrane transport theory, the effect of concentration polarization and membrane fouling on RO performance are highlighted. Past work relating RO process simulation, control and optimization are addressed. Finally, the methods of solving different types of optimization problems are also presented in this chapter.

Chapter 3: Modelling and optimization of reverse osmosis process

This chapter presents mathematical RO process model which is used in this study for spiral wound and hollow fibre modules. Also it introduces the RO network superstructure and the procedure to obtain optimal solutions for the RO network. Application and the advantages of the gPROMS software are also included.

Chapter 4: Effective design of RO process under variable seawater temperature

An MINLP optimization framework is developed here. For fixed water demand, optimization of RO design and operation is conducted for several seawater temperatures and salinity which provides further insight on the RO performance. The possibility of flexible scheduling of cleaning and maintenance of RO membrane modules is also investigated.

Chapter 5: Optimal design of RO desalination process with boron removal

This chapter gives an overview on boron in general and discusses issues related to boron toxicity and current regulations and guidelines governing boron. The focus is placed on boron removal by RO process and the effect of the RO configuration. Then, a mathematical model for boron rejection in RO desalination plants is presented. An MINLP optimization formulation is developed using a superstructure based on double pass RO desalination process. Finally the optimal design of RO network which sustain boron concentration below the maximum limit is determined for two operational cases.

Chapter 6: Optimal operation of RO system with daily variation of fresh water demand and seawater temperature

This chapter considers the dynamic optimization of RO process on the daily basis. Initially, empirical correlations are developed for estimating daily seawater temperature profiles (winter and summer) and fresh water consumption profile. A steady state RO model incorporating the correlations for predicting temperature and fresh water consumption coupled with dynamic model describes storage tank operation is presented. The optimal operation policy is generated using the optimization model for two sea water temperature profiles.

Chapter 7: Optimal design and cleaning schedule of RO process

This chapter presents a systematic technique for the optimal design and scheduling of RO networks. Neural network based correlations for predicting water and salt permeability decline factors have been developed. Also this chapter deals with the formulation of the maintenance and scheduling problem of the RO network as MINLP problem for predicting the optimal RO schedules.

Chapter 8: Brackish water RO process: Simulation and Optimization

Steady state simulation of RO process results are presented here with validation of results from the literature. The effect of changing process and design parameters on the RO process performance are presented and analysed in this chapter. Two types of

optimization problem are carried out here: (i) operation optimisation (NLP problem) and (ii) optimum design of RO network problem (MINLP). Fouling effect on membrane permeability is incorporated in the MINLP optimization problem.

Chapter 9: Conclusions and future work

This chapter presents the conclusions obtained from this study and the suggestions for future work recommendations.

Appendix A: PID control of RO process

The parameter estimation was carried out to predict the values of steady state RO model parameters. Then the RO model used to develop an optimization-based PID controller for hollow fiber RO process.

Chapter 2

Literature Review

2.1 Introduction

This chapter presents a critical review of the past work on the modeling and optimization of RO based desalination process. Overview of basic concepts of the transport phenomena in RO membranes are presented briefly. Concentration polarization and fouling problem coupled with their effects on RO performance are discussed in this chapter.

Then, this chapter will present some literature relevant to RO process modeling, control, and optimization. Two optimization types are reviewed: first, optimization of RO operation and second is optimization of RO network design with and without membrane fouling. The removal of boron by RO membranes, in addition to, mathematical representation of this issue is also briefly addressed. Finally, a brief overview on the methods used for solving both NLP and MINLP optimization problems are presented.

2.2 RO Process Description

RO is a type of membrane process commonly used for seawater and brackish water desalination. In industrial applications, a typical RO water desalination system consists of four main sub-systems: intake, pretreatment, RO membrane units and post-treatment as shown in Figure 2.1 (Fritzmman et al., 2007).

Pretreatment system is the key to successful operation of a RO plant. The type and complexity of the feed pretreatment system mainly depends on the feed water quality. The suspended solids and organic colloids are separated by coagulation process. Filtration is followed which can remove sand and other particles from the feed solution. The common way to minimize scale on the membrane surface is to lower the pH by adding acid, thus increasing the solubility of the precipitated substances or to maintain salts in their soluble pH range.

The pre-treated feed is pressurized with a pump to exceed the osmotic pressure. The quality of the permeate leaving the plant depends on the quality of plant source water and configuration. The produced water from a desalting process requires post-treatment to prepare it for potable use and some industrial uses such as chlorine injection to prevent bacterial growth.

The energy lost in depressurizing the concentrate can be returned efficiently to the feed water by using mechanical turbine or employing efficient pressure exchanger devices. Nowadays energy recovery systems working on the pressure exchange principle are available, the devices can recover up to 50% of the pumping energy (Villafafila and Mujtaba, 2003).

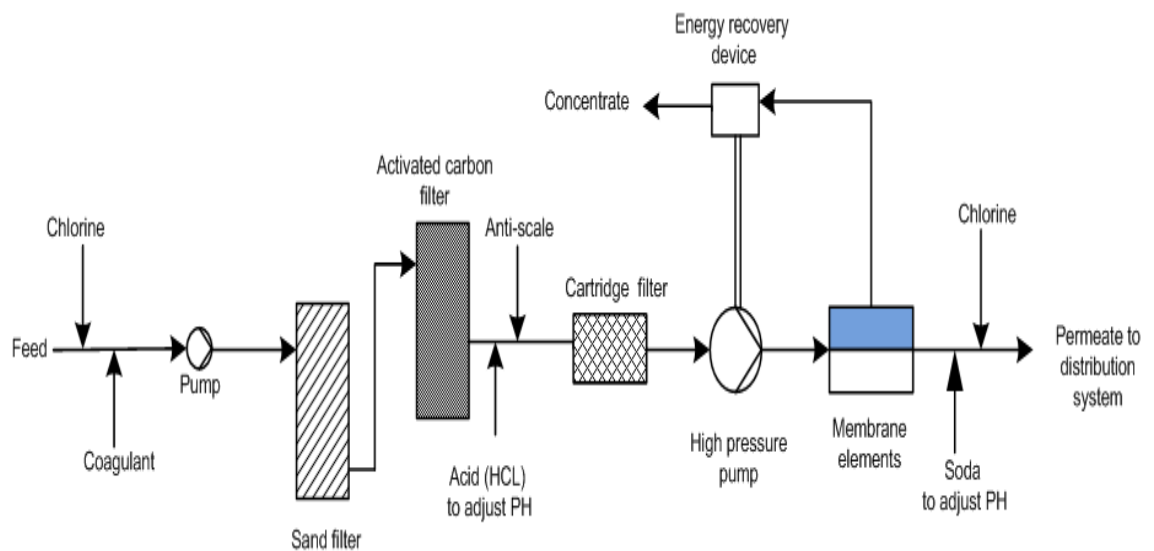


Figure 2.1 RO process system (Kim et al., 2009)

2.3 RO Membrane Modelling

The mathematical modelling of RO systems plays an important role in operation and design the RO process. It can relate the RO performance indicators such as permeate recovery and solute rejection to the operational variables such as feed pressure and design variables such as membrane module dimensions and allow optimizing the process variables without applying these changes on the real plant.

2.3.1 Membrane Transport Theories

Huge efforts have been presented in the literature in an attempt to model the transport mechanisms through membranes (Soltahieh and Gill, 1981). Most models for membrane separation assume diffusion or pore flow mechanism through the membrane as shown in Figure 2.2 (Baker, 2004). In the diffusion model, the permeate dissolves in the membrane material and then diffuses through the membrane down a concentration gradient (Figure 2.2a). The pore-flow model, in which permeates are transported by pressure-driven convective flow through tiny pores where some of permeates are excluded from some of the pores in the membrane through which other permeates pass (Figure 2.2b). Solution-diffusion model was used to explain the transport phenomena through membrane films in reverse osmosis and nanofiltration processes while pore model was more applicable to rationalize ultrafiltration and microfiltration processes (Baker, 2004).

In general, the membrane transport models are derived from three main approaches, homogeneous membrane model, pore-flow model and irreversible thermodynamics theory. Only homogeneous membrane model (Solution –diffusion) will be presented here.

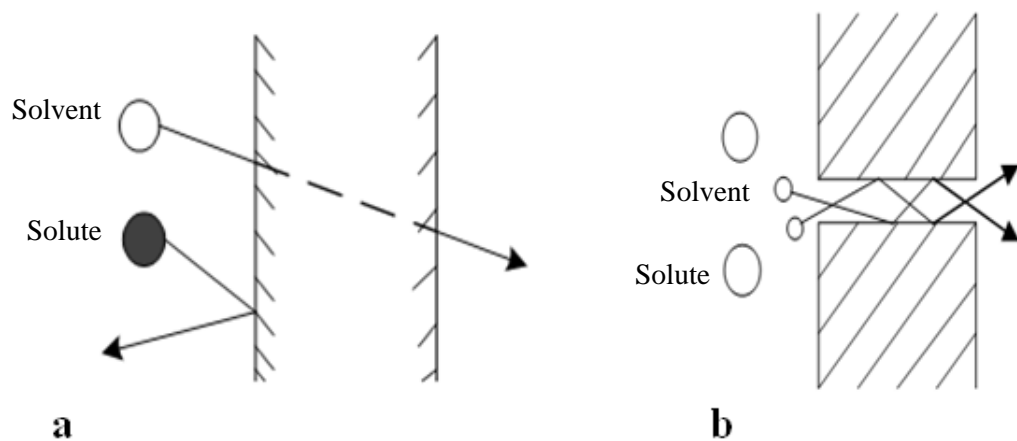


Figure 2.2 Transport through membranes (Baker, 2004)

a) Diffusion mechanism

b) Pores mechanism

2.3.1.1 Solution–Diffusion Membrane Model

This model assumes that the concentration gradient is the major effective factor in the transport from one side to another via the membrane. The model is applicable to a variety of processes as RO, pervaporation and gas permeation (Baker, 2004). The solution-diffusion model is originally developed by Lonsdale et al. (1965). It is based on the assumption that both the solute and permeate are dissolved in the surface layer of the membrane and diffuse through the membrane by the effect of concentration gradient and pressure while the solute and the solvent are diffused, each one separately.

The separation between solute and the solvent occur due to the difference in the solubility of the materials in the membrane and the differences in the rates at which the materials diffuse through the membrane (Paul, 2004). Another assumption in solution-diffusion model is that the pressure throughout the membrane is remained constant at the highest value, which leads to the pressure within a membrane uniform. According to diffusion mechanism, the total solvent and solute fluxes are expressed as:

$$J_w = A_w(\Delta P - \Delta \phi) \quad (2.1)$$

$$J_s = A_s(\Delta C) \quad (2.2)$$

Where ΔP , ΔC and $\Delta \phi$ represent differences of pressure, concentration and osmotic pressure across the membrane, respectively. A_w and A_s are the water and salt permeability coefficients.

2.3.1.2 Solution – Diffusion Model Assessment

Solution-diffusion model was used to predict the experimentally observed performance of the membrane processes of many membrane applications. According to Baker (2004), this model is able to predict the RO performance with good accuracy compared to experimental data. Furthermore, this model has less complexity compared to the other models in terms of number of unknown parameters.

The solution-diffusion model is the most widely used transport model to describe the transport through the membrane layers. The model was applied to gas separation, pervaporation and dialysis as well as to reverse osmosis (Zhao et al., 2005). Marcovecchio et al. (2005) reported that this model is able to provide an accurate prediction of the flow of water and salt through the RO membrane.

Wijmans and Baker (1995) provided more evidences for the validity of the solution-diffusion model such as the good agreement between theory and experiment, and the large number of the permeability coefficient data, obtained for a large number of membrane processes being in good numerical agreement with one another.

2.3.2 Concentration Polarization

During the normal operation of RO, the membrane separates one or more component from binary or multicomponent mixture by allowing some components to pass through a semi permeable membrane and reject the others. This process leads to accumulation of the rejected solutes on the front of the membrane surface and concentration gradient is formed with highest concentrations directly at the membrane surface. This results in equilibrium between the convective transport (permeate flux due to the pressure) and diffusion (from the membrane wall to the bulk feed solution due to the concentration gradient). This phenomenon is called concentration polarization (Fritzmann et al., 2007).

Concentration polarization creates new layer on the membrane surface as shown in Figure 2.3. The concentration profile illustrates that the local surface concentration is greater than the feed concentration. Therefore, it is crucial to determine the concentration of solutes at the surface of membrane and use it in the estimation of the transport parameters for the rigours transport model instead of feed bulk concentration.

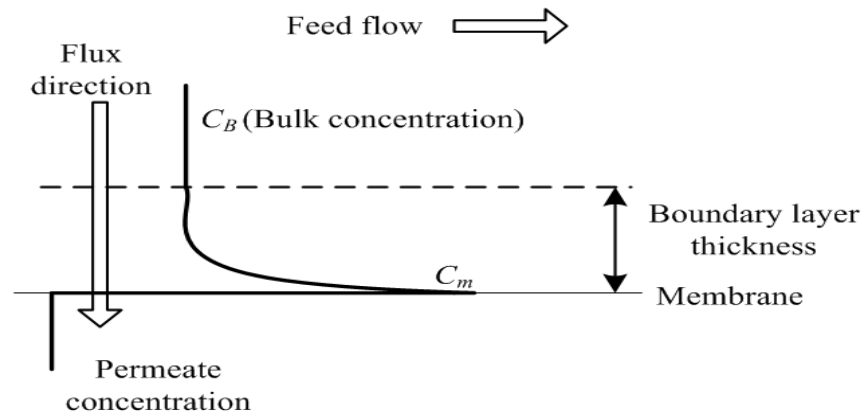


Figure 2.3 Schematic diagram of concentration polarization (Kumar, et al. 2006)

Concentration polarization influences the separation performance in several ways:

- Substantial reduction in the solute rejection due to higher salt flux because of increased salt concentrations at the membrane surface and consequently, high solute concentration in the permeate.
- Saturation solubility limits can exceed especially for concentrated solutions, leading to formation of gel layer on the membrane surface, which enhance the fouling on the membrane surface.
- Solvent flux is reduced due to a reduction in the driving force of the solvent species and higher osmotic pressure associated with higher salt concentration.

The main operational variables that affect the formation of polarized solute layer on the membrane surface are (Kim and Hoek, 2005): a) pressure difference across the membrane, b) solute concentration in the feed, c) hydrodynamics (turbulence).

Increase of feed pressure can enhance the membrane separation performance to a certain limit (Figure 2.4), after that, the permeate flux becomes independent of feed pressure. As feed pressure is increased, there is a corresponding increase in convective transport of solute molecules to the membrane surface and the concentration polarization layer becomes thicker.

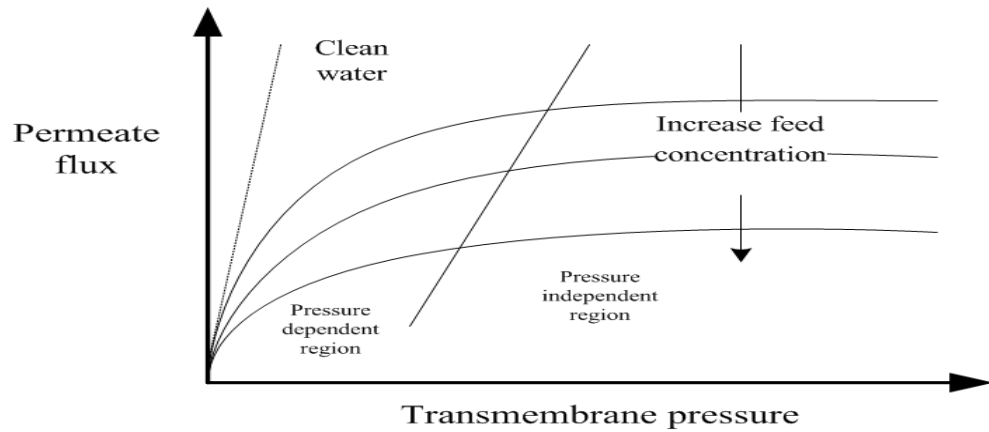


Figure 2.4 Dependence of permeate flow on transmembrane pressure (Cheryan, 1998)

Increase in feed flow can be helpful to reduce the boundary layer because an increase in velocity reduces concentration polarization due to a higher wall shear stress (Schwinge et al., 2002). The thickness of the boundary layer depends on the turbulence of the feed water flow (Kumar et al., 2006). Increase in the turbulence will reduce the thickness of the boundary layer. Membrane spacers are used to promote turbulence in the feed and permeate channels by disrupting fluid flow in the modules channels. Spacers lead to increase in energy consumption by the pump due to increase of the pressure drop across the membrane module. Therefore, optimal spacers were designed based on the optimization of concentration polarization and extra energy consumed by the pumps.

Several models have been used to study concentration polarization and determine the solute concentration at the surface of membrane such as analytical Film Theory (FT) model (Michaels, 1968), Retained Solute (RS) model (Song and Yu, 1999) and Numerical Convection–Diffusion model (Bhattacharyya et al., 1990).

Film theory has been widely used by several researchers to model the concentration polarization phenomena. Many authors reported that film theory can predict concentration polarization accurately at operating conditions of feed flow and flux similar to practical RO applications (Kim and Hoek, 2005; Subramani et al., 2006).

According to the film theory (Micheals, 1968), the transport of the solute in concentration polarization layer can be illustrated as:

$$\frac{C_m - C_p}{C_B - C_p} = \exp\left(\frac{j_w}{k}\right) \quad (2.3)$$

With C_m representing the concentration at the membrane surface, C_p and C_B being the permeate and feed bulk concentrations. k denotes the mass transfer coefficient and j_w is the pure water flux.

2.3.3 Membrane Fouling

2.3.3.1 Understanding Membrane Fouling

The most critical obstacle restricts further growth and wider application of membrane separation processes is fouling. It affects the operational reliability and increase the production cost, therefore many studies are focused on this subject, for example (Karime et al., 2008; Schneider et al., 2005).

Fouling is referred generally as the accumulation of unwanted particles (Chen et al., 2004), colloids and/or salts on the interface. In general, there are four major types of compounds which may led to membrane fouling (Flemming et al., 1997).

- a. **Dissolved solids:** (inorganic scale) such as calcium and barium.
- b. **Suspended solids:** (colloidal) such as metal oxides and silica.
- c. **Biological organisms:** such as bacteria, fungus and algae.
- d. **Non-biological organic:** such as oil.

Scaling by inorganic compounds such as calcium carbonate and sulphates is formed in the feed spacers and on the membrane surface and block the flow. This type of fouling may be controlled by injecting an anti-scalant and/or acid. Fouling can be controlled by pretreatment methods, such as coagulation and flocculation followed by filtration elements. Ultrafiltration may be used to remove colloidal particles and provide a good water quality for the RO process.

Fouling generally results in decreased permeate flux, decreased product quality and increased feed pressure. The fouling phenomena can be described to characterize the reversibility of fouling (Figure 2.5). Reversible fouling refers to the fouling species forming the deposit layer on the outer surface of the membrane which is readily removable from the membrane surface and easy to clean by physical methods such as rinsing or flushing the membrane or applying backwashing (Choi et al., 2005).

Irreversible fouling (as gel layer) on the other hand requires cleaning under severe conditions or with chemical agents. The internal membrane pores are blocked and the foulants could not be removed by simple cleaning method as backwashing.

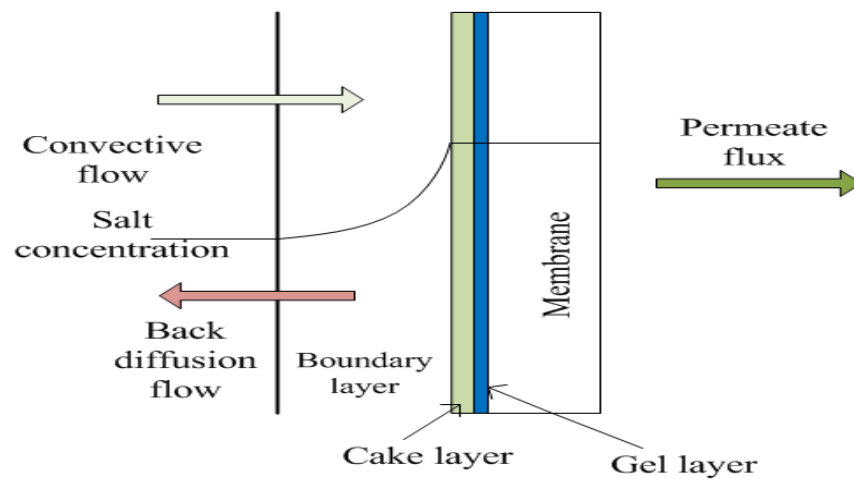


Figure 2.5 Schematic fouling layers (Cheryan 1998).

Normally, in the RO desalination plants, the production capacity is remained relatively constant as well as the solute concentration is kept under certain limit. The permeate flux will vary with filtration time according to the fouling behaviour of the feed solution.

Numerous studies have been carried out to estimate and control of fouling for the RO processes (Chen et al., 2004; Park, et al., 2008; Oh et al., 2009b). Amiri and Samiei (2007) suggested that increasing feed velocity could reduce the fouling area to a thinner layer and consequently less fouling on the membrane layer. Yang et al. (2010)

investigated the use of a pilot plant to explore the seasonal fouling characteristic of RO membrane. The experiments were conducted in summer and winter seasons to emphasize the presence of the inorganic fouling and biofouling on the RO membrane. They found that scaling and biofouling are more serious in summer season.

2.3.3.2 Fouling and RO Staging

A commercial RO unit usually consists of one or multi stage array of membrane modules depending on the product demand and purity. Two kinds of membrane staging are commonly used in RO desalination plants:

- Permeate staging: the permeate from the first stage (pass) becomes the feed to the second stage (pass). The water produced from this type of staging may contain solute concentration less than the required limit.
- Brine staging: the feed of the second stage is the brine from the first stage. Permeate is collected from all modules and sent to the final product stream.

For looser permeate concentration requirement, brine staging configuration is favoured that increase the system recovery ratio while the permeate staging structure is identified for lower permeate quality requirement (Lu et al., 2007).

Generally, the most common arrangements of the membrane modules are: a) Series arrays, b) Parallel arrays and c) Tapered arrays. Figure 2.6a shows a series arrangement of the membrane modules. The entire flow is passed over all the modules. As permeate is recovered, the brine flow is gradually reduced. This can decrease the flow and concentrate the brine at the end of the array and increase scaling especially at the tail elements in the array. In the parallel array (Figure 2.6b), the feed flow is split into large number of parallel streams generating poor cross-flow at the end elements.

To overcome the limitations of the two previous arrangements the tapered array (Figure 2.6c), which is a combination of parallel and series arrangement, is introduced.

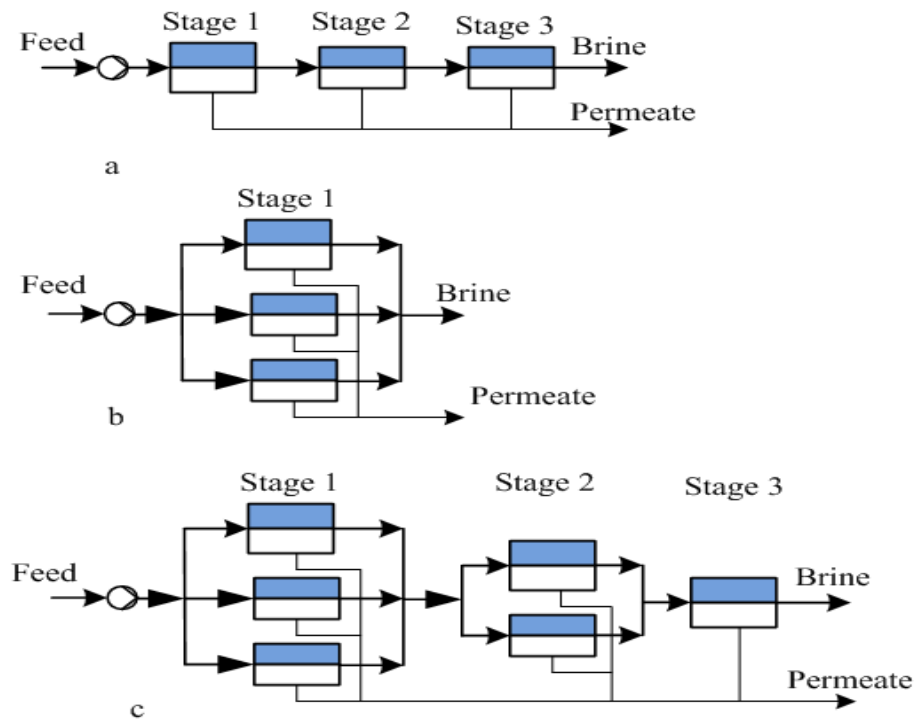


Figure 2.6 Reverse osmosis configurations

a. Series b. Parallel c. Tapered

Although extensive research had been carried out on RO membrane fouling (Zhu et al., 1997; Flemming et al., 1997; Tay and Song, 2005; Hoek et al., 2008; Oh et al., 2009a), the same cannot be said about the local fouling in RO stages. Most of these studies investigate the fouling effect on RO performance by assuming average fouling value for all stages regardless the fouling type and process configuration.

Different fouling types and where they occur in the RO membrane process are shown in Table 2.1 (Huiting et al., 2001). It is clear that the first stage and precisely first element in the first stage (in case of spiral wound element) suffers from high organic fouling and suspended solids. Scaling and silica the only types of fouling deposit in the last stage where the solute concentration becomes high due to permeate recovered along the stages.

The biofouling potential of feed water to RO plants is very high as shown in Figure 2.7 (Khedr, 2000). It reaches up to 50 % of the total fouling occurring in RO plants. Followed by scaling about 20 % of the total fouling which deposited in the last stage.

The remaining fouling will hit the first stage. Biofouling is considered as the major type of fouling in RO processes (Vrouwenvelder et al., 2009a).

Table 2.1 Location of fouling in NF/RO plants (Huiting et al., 2001)

Fouling	Where does it occur first
Scaling/silica	Last membranes in last stage
Metal oxides	First membranes of first stage
Colloids	First membranes of first stage
Organic	First membranes of first stage
Biofouling (rapid)	First membranes of first stage
(slow)	Throughout all the stages

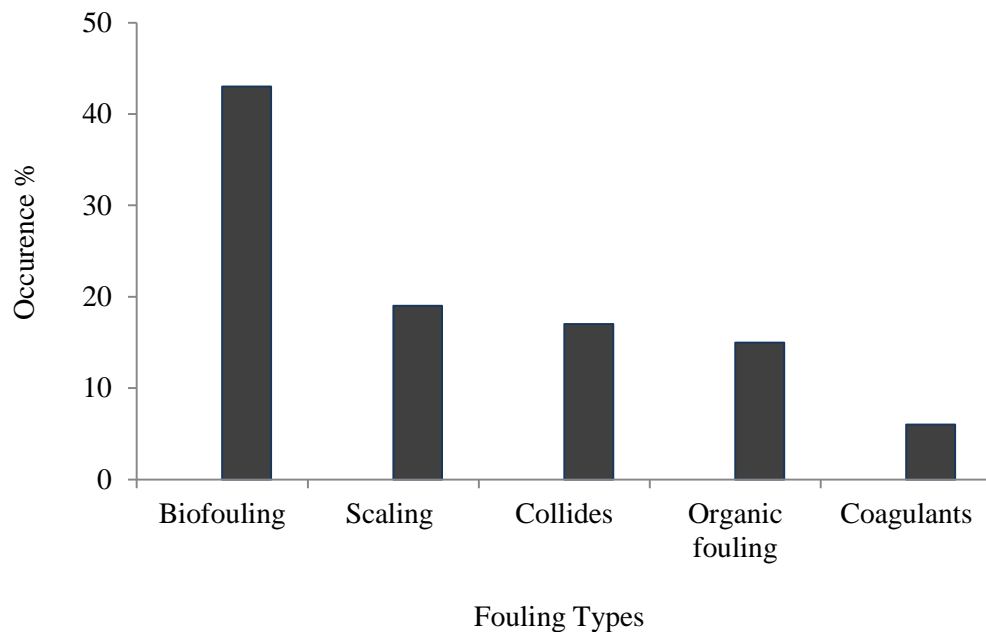


Figure 2.7 Occurrence of fouling in RO desalination plants (Khedr, 2000)

Karime et al. (2008) carried out a study about loss of membrane performances in Zarzis brackish water desalination plant. The pressure drop in first stage caused by fouling is higher than that in second stage as shown in Figure 2.8. The analysed of fouling in membrane element in first stage indicate the presence of biofouling.

A model of RO processes that accounts the effects of fouling on the performance of a RO system was developed by Hoek et al. (2008). Model parameters are determined

based on pilot plant data using brackish water as a feed. The high fouling level in lead elements causing a water flux decline; hence, permeate production compensated by subsequent elements levelling the flux profile from inlet to outlet.

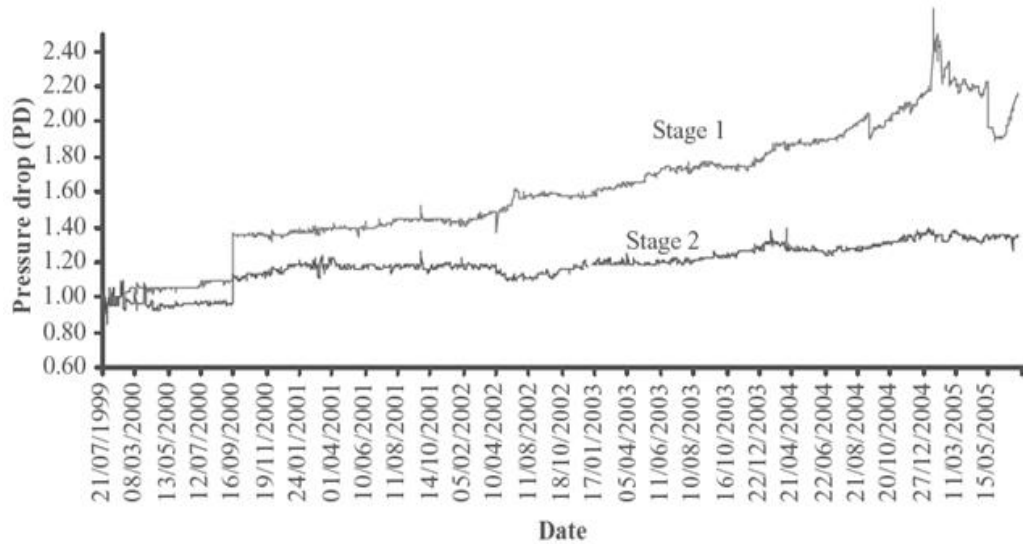


Figure 2.8 Pressure drop profile in Zarzis desalination plant (Karime et al., 2008)

Recently, Vrouwenvelder et al. (2009a) presented a comprehensive study on the detection of biofouling in membrane filtration installations treating low salinity waters. The pressure drop increase in the first stage was higher than the increase in second stage (Figure 2.9). Also most biofouling fouling was present in the lead element in the first stage, consistent with membrane autopsy results obtained in the above studies.

See et al. (1999) mentioned in their work that the fouling factor can be varied between membrane stages in the simulation and optimization purposes. Also, they pointed out those different fouling models could be included for each stage in the mathematical formulation of membrane filtration process.

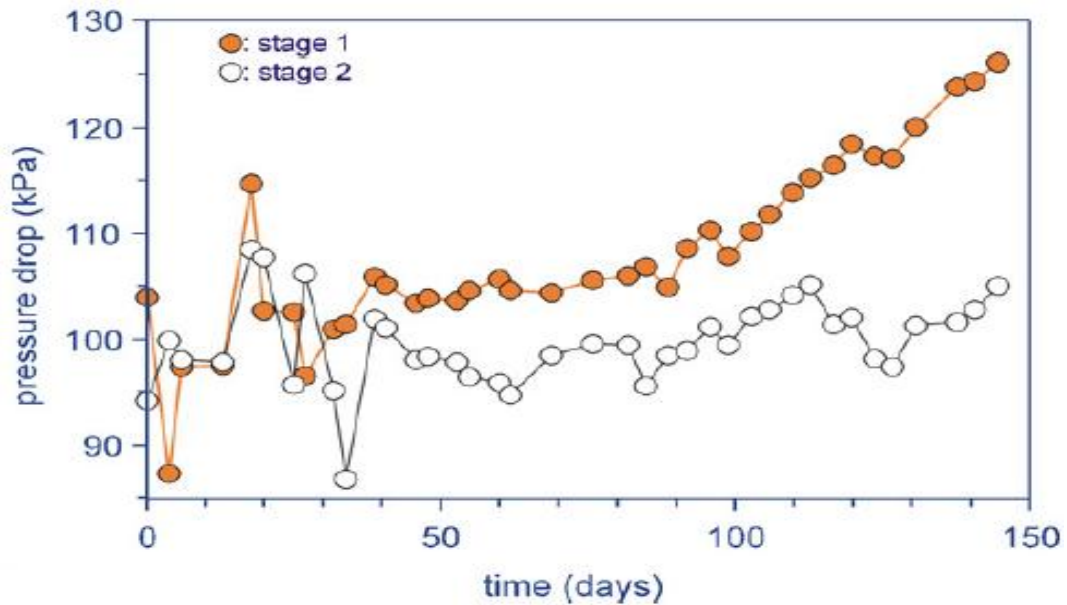


Figure 2.9 Pressure drop profile for two stages (Vrouwenvelder et al., 2009a)

2.4 Review of Past Work on Simulation and Optimization of RO Process

There is an abundant theoretical and experimental literature related the transport theory and practice of RO processes. This section includes studies that are only relevant to the modelling, control and operation optimization of the RO systems.

2.4.1 Modelling and Simulation of RO Desalination Process

The primary objective of this work is to develop a model that can accurately predict the RO process performance under different operating conditions. In order to develop a reliable membrane separation model, it is important to fully understand the operation and all accompanied phenomena related to the interactions between the transport theory through the membrane layer and other operation and design aspects. This section presents some literature for the RO process modeling.

The permeation through membranes was modelled using several approaches include the solution-diffusion model, pore models and irreversible thermodynamic model all these models are special cases of the statistical-mechanical model (Majali et al., 2008) which was originally developed by Lonsdale (1965).

The early works of Kimura–Sourirajan model (Kimura and Sourirajan, 1967) first drew attention to the formulation of the concentration polarization phenomenon in RO modelling. This model combines solution-diffusion equations for the transport across membrane layer with the film theory which describes concentration polarization. Two parameters: water and salt permeability coefficients are involved in the model.

Numerous models describe the performance of RO membranes have been developed over recent years. Simulation models typically fall into two main categories: 1) Analytical Models (e.g Evangelista,1985; Sirkar, 1982; Malek et al., 1994; Marcovecchio et al., 2010); are used for simple design calculations. 2) Numerical Models that incorporate spatial variations in fluid properties throughout the module and are appropriate for accurate simulation studies (ElHalwagi et al., 1996; Ben-Boudinar et al., 1992; Marriot, 2003; Sundaramoorthy et al., 2011). Selected literature describing significant development of RO modeling concept are summarized in Table 2.2.

Concentration polarization and fouling are the major problems challenge the manufactures of RO membrane modules. Both of them can be reduced by varying the hydrodynamics conditions in membrane channel. This can be achieved by the incorporation of the feed spacer in the membrane channel.

Feed spacers improve mass transfer in spiral wound elements but this improvement comes at the cost of increased hydraulic losses. Hence, models for spiral wound modules which include the effect of spacers in the flux comprised a significant share of membrane research (Schock and Miquel, 1987; Geraldés et al., 2002; Dendukuri et al., 2005; Geraldés and Afonso, 2007; Guillen and Hoek, 2009).

Table 2.2 Summary of the past work on RO modelling

Authors	Year	Main Features
Lonsdale	1965	Homogeneous diffusion model for cellulose acetate membrane
Taniguchi	1978	Compared the performance characteristics of two kinds of spiral wound modules based on experimental data
Chiolle	1978	Model investigates fluid dynamics and mass transfer in a channel, made up by two membranes separated by a net spacer for a double-solute system based on two-parameter membrane transport model.
Sirkar	1982	Simple analytical equations to estimate averaged permeate flux and concentration in the case of high rejecting membranes for spiral wound RO module. Pressure drop in feed and permeate channels are neglected, linear approximation for concentration polarization was assumed
Gupta	1985	Analytical design equations by neglecting pressure drops and assuming the mass transfer coefficient to be a constant throughout the channel length.
Evangelista	1985	Explicit analytical equations for water flux for dilute solutions based on assumptions of average and uniform fluid conditions in feed and permeate channels.
Avlonitis	1991	Analytical procedure to determine the brine and permeate friction parameter and membrane water permeability coefficient based on experimental data for spiral wound modules.
Ben Bouldinar	1992	Mathematical model involves differential equations accounts the spatial variations of concentrations, pressures and flow rates in the feed and permeate channels for spiral wound and hollow fibre modules and solved numerically using finite differences method.
Sekino	1993	Formulation for the transport phenomena of salt and water transport through the membrane incorporating Kimura–Sourirajan model and take into account the pressure drop in the fiber bore of a hollow fiber module.
Hawladar	1994	By conducting pure water and salt (NaCl) water experiments, the sensitivity of the product flow rate and concentration as functions of the feed concentration, pressure, temperature and feed flow rate are studied.
Malek	1994	A simple model based on a lumped transport parameter approach for modelling the performance of hollow fiber modules. The model performs a one-dimensional simplification of the permeator hydrodynamics, considering a linear relationship between the shell side concentration and the membrane surface area.
Starov	1995	Analytical model for the performance of hollow fiber membranes according to a balance between fiber productivity and fiber selectivity. Three flow configurations modules for reverse osmosis hollow fiber membranes are considered.
Al-Bastaki and Abbas	1999	Mathematical model based on the solution-diffusion model to predict the performance of hollow fiber membranes. The model considers pressure drop in the fiber bore, pressure drop on the shell side of the fiber bundle. The solution concentration variation on the shell side of the fiber bundle and concentration polarization.
Al-Bastaki and Abbas	2000	The model where the salt and water fluxes are considered as implicit functions of module length and radius was used to investigate the effects of ignoring the concentration polarization and the pressure drop for hollow fiber and spiral wound modules.
Marriot	2003	General approach from rigorous mass, momentum and energy balances for modelling spiral wound and hollow fibre membrane modules.
Jamal	2004	Model combines material balances on the feed tank, membrane module and product tank with membrane mass transfer models incorporating the effect of mass transfer inhibition while concentration polarization was not included. The model considers spatial dependence of solute feed concentration. Differential equations in the model are solved using the fourth order Runge-Kutta method.

cont'd next page

Table 2.2 Summary of the past work on RO modelling (cont'd)

Authors	Year	Main Features
Chatterjee	2004	A mathematical model includes Spiegler–Kedem model for the transport phenomenon and the friction concentration- polarization model for the radial flow in hollow fiber permeators. The model is solved through finite difference method.
Senthilmurugan	2005	Mathematical model for a spiral-wound using Spiegler-Kedem model accounts for pressure drops in feed and permeate channels, and solved using finite differences method.
Kumano	2008	Group Model for hollow fiber to correct an anomaly of the friction concentration polarization model. The boundary layer thickness on the surface of the fiber group obtained by the application of the fiber Group Model.
Marcovecchio,	2010	Model for predicting the permeation performance in RO seawater desalination with hollow fiber module considers, concentration polarization, pressure drop in both fiber and shell side. Finite difference mesh for a hollow fiber module is implemented, dividing the module in its axial and radial directions.
Sundaramoorthy	2011	A mathematical model for spiral wound RO membrane module based on solution–diffusion model and incorporates spatial variations of pressure, flow and solute concentration in the feed channel and uniform conditions of pressure in the permeate channel. Graphical linear fit methods are developed for estimation of model permeability parameters.

Decline in permeate flow rates due to membrane fouling was studied based on the solution-diffusion mass-transfer theory and concentration polarization for spiral wound module by Al-Bastak and Abbas (2004) and Tay and Song (2005), for hollow fibre module by Al-Qahtany and Al-bastaki, (1995). The water and salt permeability coefficients decline over a period of 454 days was predicted for industrial water desalination plant based on solution diffusion model (Pais et al., 2007). Due to the feed temperature effects, it was found that the normalized water permeability coefficient declined only by about 7% and the salt permeability only increased during the summer.

2.4.2 Modelling of RO Process Using Neural Networks (NNs)

Neural networks (NNs) are modelling tools able to solve linear and non-linear multivariate regression problems with some desired accuracy (Lee et al., 2009). Moreover, NNs methodology does not need any governing equations with assumptions to describe the process under study. A number of studies have been reported on the modelling, simulation and optimization of pressure-driven membrane systems using NNs tool (Niemi et al., 1995; Zhao et al., 2005; Lu et al., 2010).

Abbas and Al-Bastaki (2005) developed neural network (NN) model to predict the performance of a RO experimental setup. The model considers ranges of operating conditions as input to the NNs model that include the feed pressure, temperature and salt concentration to predict the water permeate rate. A neural network-based modelling approach with back-propagation was investigated by Libotean et al. (2009). Operation data of normalized permeate flux and salt passage were used as input variables to develop NNs model for estimating RO plant performance.

Predictive models for simulation and optimization of RO desalination pilot plant based on both Response Surface Methodology (RSM) and Artificial Neural Network (ANN) models have been developed by Khayet et al. (2011). They found that RSM was unable to develop a global model to predict the RO performance while ANN approach provides a global model in a wide range of feed salt concentration.

Neural networks (NNs) tool also used in optimization of RO processes. For example, Lee et al. (2009) have developed NNs models using one-year real operational data for the prediction of the performance of a Fujairah RO desalination plant. The input parameters of the NNs model consists of feed temperature, seawater salinity, operating pressure, feed flow rate, and operation time while the output parameters were permeate salinity and production. The NNs model then used to determine the temperature control to optimize the operation of RO plant.

2.4.3 Optimization of RO Process

Nowadays with the recent developments in sophisticated numerical methods, optimization methodologies can handle very large problems in the design and/or operation of various industrial applications (Edgar et al., 2001). Adoption of the operation variables set points at plant start-up time will not guarantee the expected profitability while facing the operational fluctuations. Thus, it is important to determine

the new optimal set points of the individual control variables on a regular basis instead of using the real plant to determine these values (Tanvir and Mujtaba, 2008).

2.4.3.1 Overview of Operation Optimization of RO Process

The general aim of the operation optimization problem is to predict a collection of values of the operation variables of a given process configuration (fixed design) subject to the different constraints expressed in the form of a system of equations or inequalities, which will produce the desired optimum response for the selected objective function. The optimization formulations of RO operation are reviewed and briefly highlighted in this section.

Optimization of the operation of RO process has been studied in the last decades, but with less attention compared to studies on RO process modelling and simulation. The early research such as Hatfield et al. (1970) and Van der Meer et al. (1998) have focused on cost reduction with respect to water recovery, feed flow rate, and the applied pressure. Efforts to reduce the specific energy consumption were considered improving membrane permeability (Wilf, 1997; Zhu et al., 2009b). Recently, few works have focused on the development of RO optimization framework subject to feed conditions fluctuation (Abbas, 2007; Zhu et al., 2009a).

A summary of works carried out in operation optimization of RO process is given in Table 2.3. Optimization of membrane module configuration is also shown in the Table. Geraldés et al. (2005) developed a mathematical model to simulate and optimize the operating conditions and the module configurations for single/two-stage spiral wound module. Different RO fixed configurations and operating variables for several seawater desalination processes are investigated by Wilf and Bartels (2005). They found that efficient energy recovery devices and higher permeability high rejection membranes lead to substantial decrease in the desalted water costs.

Table 2.3 Summary of the past work on RO operation optimization

Author (year)	Variables studied	Objectives	Constrains	Problem type
Hatfield (1970)	<ul style="list-style-type: none"> • Arrangement of modules with respect to fabrication temperature 	Maximizing product flux	Maximum number of modules	Nonlinear programming problem
Van der Meer (1997)	<ul style="list-style-type: none"> • Feed pressure • Feed flow • Module configuration (spiral wound, capillary, feed and permeate channels height) 	Specific Productivity	<ul style="list-style-type: none"> • Permeate productivity per module • Pressure losses in concentrate and permeate channels 	Optimal Operation and PV configurations optimization
Van der Meer (1998)	<ul style="list-style-type: none"> • Hydraulic pressure losses • Osmotic pressure • Number of membrane modules in PV 	Maximize permeate production	<ul style="list-style-type: none"> • Permeate productivity per module • Hydraulic pressure losses in concentrate and permeate channels 	Operation and PV configurations optimization
Wilf (2001)	<ul style="list-style-type: none"> • Recovery ratio • Seawater salinity 	Minimum energy consumption	Permeate salinity	Optimal operation
Geraldes (2005)	<ul style="list-style-type: none"> • Feed velocity • Feed pressure • Number of membrane modules in PV 	Minimize the water production costs	<ul style="list-style-type: none"> • Maximum permeate salt concentration • Maximum concentration polarization 	Economic optimization
Guria (2005)	<ul style="list-style-type: none"> • Operating pressure • Type of module 	<ul style="list-style-type: none"> • Maximize permeate flow • Minimize the cost of desalination • Minimize the permeate concentration 	<ul style="list-style-type: none"> • Maximum throughput • Maximum permissible permeability coefficients 	Optimal operation and membrane module type selection
Djebedjian (2008)	Pressure	Maximization of permeate volumetric flow rate	Permeate concentration	Operation optimization

cont'd next page

Table 2.3 Summary of the past work on RO operation optimization (cont'd)

Author (year)	Variables studied	Objectives	Constrains	Problem type
Zhu (2009)	<ul style="list-style-type: none"> • RO configuration (single-pass, two-pass) • Water recovery • Brine recycle • Existence of energy recovery device 	Minimization of energy consumption	<ul style="list-style-type: none"> • Salt rejection • permeate product • Recovery • Thermodynamic restriction. 	Operation optimization
Oh (2009)a	<ul style="list-style-type: none"> • Feed pressure • Feed flow rate • Feed temperature • Fouling extent 	<ul style="list-style-type: none"> • Minimize energy consumption • Maximize boron rejection 	<ul style="list-style-type: none"> • Recovery ratio • Permeate TDS 	Performance optimization
Li (2010)	<ul style="list-style-type: none"> • Several fixed RO configurations • Driving force • Energy recovery efficiency 	Minimization of specific energy consumption	<ul style="list-style-type: none"> • Thermodynamic limit • Minimum recovery constant 	Non-linear optimization problems (NLP)
Khayet (2010)	<ul style="list-style-type: none"> • Feed temperature • Feed concentration • Feed pressure • Feed flow-rate 	Minimization of specific energy consumption	<ul style="list-style-type: none"> • Salt rejection • Permeate flux • Energy consumption 	Predictive models for simulation and Optimization
This work (2012)	<ul style="list-style-type: none"> • Feed pressure • Feed flow rate • Spacer thickness • Mesh length 	Minimization of specific energy consumption	<ul style="list-style-type: none"> • Fresh water flow • Fresh water salinity • Module design constraints 	Non-linear optimization problems (NLP)

Gilau and Small (2008) studied the performance of a renewable energy powered alternatives for small-scale seawater RO in terms of water productivity and energy cost. The optimum recovery and flux are determined by Hyun et al. (2009) for a given condition of specific energy and boron concentration. The simulated model was also used to optimize the performance of RO process for minimum specific energy consumption and high boron removal.

2.4.3.2 Overview of Control Systems for RO Desalination

Several control strategies may be adopted in the operation of RO systems such as directly increasing or decreasing the feed flow rate and/or pressure to account the fluctuations in water production. In general, dynamic operation policies must be developed by manipulating the operation variables that can provide the best control performance and also, installing new equipment that may improve the system control performance.

Several contributions can be found in the literature on the design and implementation of controllers for RO systems. For instance, in Alatiqi et al. (1999), the authors used open loop step response data from RO plant to construct a Multiple Input Multiple Output (MIMO) model. The RO plant was simulated in closed-loop with BLT (Biggest-log modulus) tuning criteria. Zilouchian and Jafar (2001) have presented the application of fuzzy logic and neural networks based intelligent system in process control of RO desalination plants.

Abbas (2006) used constrained and unconstrained Dynamic Matrix Control (DMC) algorithms to control a simulated RO model developed by Alatiqi et al. (1999). He showed that the DMC algorithms produce faster response than conventional PI control when applied to Alatiqi model. In Kim et al. (2008), the authors demonstrated the use of new genetic algorithm auto-tuned PID controller for the optimal control of simulated RO plant.

McFall et al. (2008) developed model based nonlinear feed-forward/feedback control structures for high recovery which is able to reject disturbances caused by feed water variation.

In Greenlee et al. (2009), a step testing based model was used to design a constrained model predictive control (CMPC) to produce permeate with specific flow rate and salt subject to the constraints that the inlet pH and the trans-membrane pressure are within specified bounds.

Table 2.4 provides a summary of past work in control of RO systems. The existing literature differs from each other in terms of control algorithms, as well as the selection of the variables.

2.5 Design of RO Network

The mathematical modelling of the RO process is used in the design of RO network. RO design problem involves many complicated and interacting choices to meet the technical, environmental and economic requirements. Particular attention was paid to the optimization of RO network design including scheduling for membrane cleaning due to membrane fouling.

Designing a cost effective RO network depends mainly on the determination of optimal operational and structural schemes. Superstructure based on state space approach is the basis of RO design which represents all the possible designs that are to be considered as candidates for the optimal solution is used in design of RO process.

2.5.1 State Space Approach

The state space approach for process synthesis representation was first used in system design to model the mass-heat exchange networks in distillation systems (Bagajewicz and Manousiouthakis, 1992).

Table 2.4 A summary on control of membrane processes

Author (year)	Controlled variables	Manipulated variables	Control procedure
Alatqi (1989)	<ul style="list-style-type: none"> • Permeate flux • Conductivity 	<ul style="list-style-type: none"> • Operating pressure • pH 	PID
Van Boxtel (1993)	Economic return In terms of Permeate flux	<ul style="list-style-type: none"> • Operating pressure • Flow velocity 	Optimal control
Perrot (1996)	Permeate flux	<ul style="list-style-type: none"> • Operating pressure • Cross-flow velocity 	Fuzzy logic
Robertson (1996)	<ul style="list-style-type: none"> • Permeate flux • Permeate conductivity 	<ul style="list-style-type: none"> • Operating pressure • pH 	Model predictive control
Assef (1997)	<ul style="list-style-type: none"> • Operating pressure • Permeate flux • Permeate conductivity • pH 	<ul style="list-style-type: none"> • Pressure control • Acid inlet 	Model predictive control
Singh (1999)	Permeate flux	<ul style="list-style-type: none"> • Pressure • Brine flow 	PID
Zilouchian (2001)	Opening/closing the brine valve	<ul style="list-style-type: none"> • Temperature • Feed TDS • Feed pH • Feed flow rate • Feed pressure • Feed concentrate • Recovery • Scale index 	Neural network and Fuzzy logic control system
Cabassud (2002)	Membrane permeability	<ul style="list-style-type: none"> • Permeate flux • Filtration time 	Model predictive control (NNs)
Abbas (2005)	Permeate flow rate.	<ul style="list-style-type: none"> • Feed pressure • Feed temperature • Feed concentration 	NNs
Abbas (2006)	<ul style="list-style-type: none"> • Permeate flux • Permeate salinity 	<ul style="list-style-type: none"> • Operating pressure • pH 	Model predictive control
Curcio (2006)	Permeate flux	<ul style="list-style-type: none"> • Feed flow rate • Operating and sampling time 	Model predictive control (NNs)
Busch (2007)	Cost function	<ul style="list-style-type: none"> • Operating pressure • pH • Flux 	Optimal control
Lee (2009)	<ul style="list-style-type: none"> • Permeate flow rate • Permeate quality 	<ul style="list-style-type: none"> • Feed temperature • Feed TDS • Operating pressure • Feed flow rate 	NNs
Ali (2010)	<ul style="list-style-type: none"> • Permeate flow • Permeate concentration 	<ul style="list-style-type: none"> • Feed pressure • Feed salinity • Feed flow rate 	Model predictive control
Alahmad (2010)	<ul style="list-style-type: none"> • Recovery ratio, • Permeate TDS • Power consumption 	<ul style="list-style-type: none"> • Feed flow rate • Feed salinity • Feed pressure • pH • Feed temperature. 	Linear Regression and multiple-input single-output
This work (2012)	<ul style="list-style-type: none"> • Permeate flux • Permeate salinity 	<ul style="list-style-type: none"> • Feed pressure 	PID (presence of fouling)
	<ul style="list-style-type: none"> • Fresh water demand • Tank height • Tank salinity • Operation cost 	<ul style="list-style-type: none"> • Feed temperature • Operating pressure • Feed flow rate 	Operation optimization

El-Halwagi (1992) applies this approach to determine the optimal structural of RO networks. This representation provides a large number of alternative process layouts.

To be able to formulate a process synthesis problem as a mathematical optimization problem, a representation that contains all the possible layouts that are to be considered as candidates for the optimal solution has to be developed. The most common way of developing the general representation, called the superstructure, is by using a graphical representation (El-Halwagi, 1992).

The superstructure for RO network represents the arrangement of different types of devices including pumps, turbines and RO stages as shown in Figure 2.10 (El-Halwagi, 1992). The RO networks were described using four boxes: a pressurization/depressurization stream distribution box (PDSDB), a pressurization/depressurization matching box PDMB, a RO stream-distribution box (ROSDB) and a RO matching box (ROMB). The function of the distribution boxes was to represent all possible grouping of stream splitting, mixing, bypass and recycle. The matching boxes determine all possible streams matching to units. With this formulation, all possible structure arrangements could be represented.

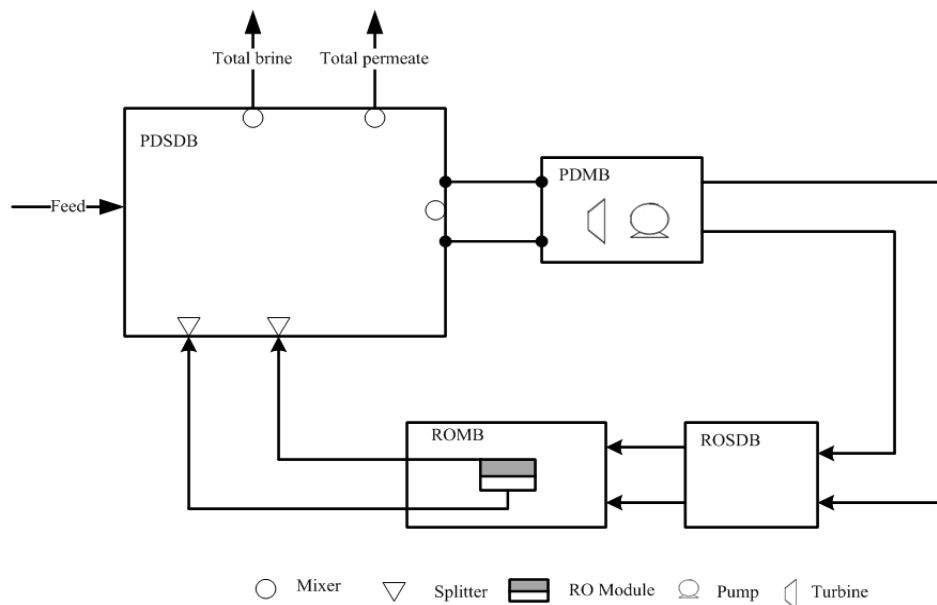


Figure 2.10 Superstructure of reverse osmosis configuration (El-Halwagi, 1992)

2.5.2 Review of Previous Work on RO Network Design

Optimal design and operation of RO process have received significant attention in recent decades since several algorithms have been developed addressing the problem of effectively solving MINLP problems (Goyal and Ierapetritou, 2004). Substantial efforts have been made to optimize the RO systems in search of the optimum system layout and operating conditions.

There are many studies based on a state space approach that are originally developed by El-Halwagi (1992) to optimize the RO networks synthesis under various conditions, for hollow fibre module (Voros et al., 1997; Maskan et al., 2000; Saif et al., 2008) and for spiral wound modules (Lu et al., 2007). Zhu et al. (1997), See et al. (1999) and Lu et al. (2006) considered cleaning schedule as part of the optimization problem using hollow fibre module.

Villafafila and Mujtaba (2003) studied the optimization of both; design (vessel internal diameter and total number of vessels) and operation (feed flow rate and operating pressure) for RO desalination process with tubular module for several objective functions including maximum water recovery, minimum energy consumption and a profit function. An optimization problem was formulated by Marcovecchio et al. (2005) for the design of a two stage RO process using Hollow fiber module. A sophisticated iterative algorithm to solve the optimization problem is developed in this work.

A summary of works carried out in the optimization of RO design is given in Table 2.5. The cleaning scheduling of RO networks issue is also highlighted in the Table.

Table 2.5 Summary of RO process design works

Author	Year	Approach	Objectives	Module type	Constraints	Fouling	Variable salinity	Variable temp.	Water feed type
<i>1-Optimization of RO design</i>									
Evangellsia	1985	Graphical analytical method	Not included	<ul style="list-style-type: none"> • Spiral wound • Hollow fibre 	<ul style="list-style-type: none"> • Maximum water recovery • Module lower and upper bounds of specified flow rates • Concentration factor • Average product concentration 	No	No	No	Brackish and Sea water
El-halwagi	1992	MINLP (superstructure)	Minimize total annualized cost	Hollow fiber	<ul style="list-style-type: none"> • Maximum permeate salinity • Minimum permeate production • Module lower and upper bound flow rates 	No	No	No	Sea water
Voros	1997	NLP (superstructure, variable split ratio)	Minimize the total cost of the RO plant	Hollow fiber	<ul style="list-style-type: none"> • Product flow and salinity • Module lower and upper limit flow rates 	No	No	No	Brackish and Sea water
Maskan	2000	Constrained multivariable nonlinear (RO network)	Maximize annual profit	<ul style="list-style-type: none"> • Tubular • Hollow fiber 	<ul style="list-style-type: none"> • Flow rate of stream range • Concentration of stream range • Minimum and maximum pressure bounds 	No	No	No	Brackish and Sea water
Villafafila and Mujtaba	2003	NLP (successive quadratic programming SQP)	<ul style="list-style-type: none"> • Maximum recovery • Minimum energy consumption • minimum number of tubes 	Tubular	<ul style="list-style-type: none"> • Lower and Upper for feed pressure in terms of (osmotic pressure) • Total number of tubes • Internal diameter • Maximum flux 	No	No	No	Sea water
Marcovecchio	2005	MINLP (simple two stage flow sheet)	Minimize the total annualized	Hollow fiber	<ul style="list-style-type: none"> • Freshwater production • Module maximum feed flow rates 	No	Yes	No	Seawater
Lu	2007	MINLP (superstructure)	Minimize the total annualized cost	Spiral wound	<ul style="list-style-type: none"> • Permeate production • Module Lower and upper bounds of specified flow rates 	No	Yes	No	Brackish and Sea water

cont'd next page

Table 2.5 Summary of RO process design works (cont'd)

Author	Year	Approach	Objectives	Module type	Constraints	Fouling	Variable salinity	Variable temp.	Water feed type
Saif	2008	MINLP, relaxation of non-convex (superstructure)	Minimize the total annualized cost	Hollow fiber	<ul style="list-style-type: none"> Fresh water production and salinity Module lower and upper bounds of specified flow rates 	No	No	No	Seawater
This work	2012	MINLP (two-stage superstructure)	Minimize the total annualized cost	Spiral wound	<ul style="list-style-type: none"> Permeate production and salinity Module lower and upper bounds of flow rates 	Yes	No	No	Brackish water
		MINLP (two-stage superstructure)	Minimize the total annualized cost	Hollow fiber	<ul style="list-style-type: none"> Permeate production and salinity Module lower and upper bounds of specified flow rates 	No	Yes	Yes	Seawater
		MINLP (double pass superstructure)	Minimize the total annualized cost	Spiral wound	<ul style="list-style-type: none"> Boron concentration in final permeate stream Permeate production and salinity Module lower and upper bounds of flow rates 	No	No	Yes	Seawater
<i>2- Optimization of RO design including maintenance scheduling</i>									
Zhu	1997	MINLP (superstructure)	Minimize the total annualized cost	Hollow fiber	<ul style="list-style-type: none"> Freshwater production and salinity Module feed flow rate bound 	Yes (uniform decline model for water permeability)	No	No	Seawater
See	1999	MINLP (fixed configuration and superstructure)	Minimize the total annualized cost	Hollow fiber	<ul style="list-style-type: none"> Freshwater production and salinity Module feed flow rate bound 	Yes (uniform decline model for water permeability)	No	No	Seawater

cont'd next page

Table 2.5 Summary of RO process design works (cont'd)

Author	Year	Approach	Objectives	Module type	Constraints	Fouling	Variable salinity	Variable temp.	Water feed type
Lu	2006	MINLP (single stage RO)	Minimize the total annualized cost	Hollow fiber	<ul style="list-style-type: none"> • Freshwater production and salinity • Module feed flow rate bounds 	Yes (uniform decline model for water and salt permeability)	No	No	Seawater
This work	2012	MINLP (superstructure for one stage)	Minimize the total annualized cost	Spiral wound	<ul style="list-style-type: none"> • Freshwater production and salinity • Module feed flow rate bounds 	Yes (actual decline model based NNs for water and salt permeability)	No	Yes	Seawater

2.6 Literature on Boron Rejection by RO Membranes

Boron is a vital element for growth of creations, but excessive exposure can cause detrimental effects to plants, animals, and possibly humans (Hyung and Kim, 2006). Several studies investigate boron removal by RO membranes. However, the main focus of many of these studies was on experimental analysis and only few published works have investigated boron removal process theoretically. Table 2.6 summarizes the most efforts to illustrate the modelling of boron rejection under different conditions.

Table 2.6 Summary of boron rejection modelling

Author et al. (year)	Model used	Parameters studied	Comments
Taniguchi (2001)	Solution–diffusion	Not included	The permeability factors of salt and boron for UTC-80 membrane are measured experimentally. The relationship linked between the salt and boron permeability is obtained in this study. Another relationship between the salt and boron concentrations enables one to estimate the boron concentration in the permeate if the salt concentration only known.
Sagiv and Semiat, (2004)	Kedem-Katchalsky	<ul style="list-style-type: none"> • pH • Temperature • Pressure • Permeate splitting 	A numerical model was developed in order to identify the parameters that affect boron reduction and analyse each individual effect as well as the combined effects of these parameters to reduce desalination cost and/or permeate boron concentrations
Hyung and Kim (2006)	Spiegler-Kedem	<ul style="list-style-type: none"> • pH • Temperature 	Bench-scale cross-flow filtration experiments were used to estimate the rejection of boron by six commercial RO membranes. A mathematical model which was developed based on the irreversible thermodynamic were used to analysis the experimental results. The model was modified to account for the effect of pH and temperature on the overall boron transport.
Hung et al., (2009)	Solution–diffusion	<ul style="list-style-type: none"> • pH • Temperature • Feed boron conc. • feed salinity 	The permeability of boron through seawater RO membranes was estimated using a lab-scale plate frame RO system. Then , using predicted permeability factors as inputs, computer program was developed to estimate the boron rejection at different operating conditions
Mane et al., (2009)	Spiegler-Kedem	<ul style="list-style-type: none"> • pH • Temperature • Pressure • Overall recovery 	A mechanistic model was developed to simulate boron rejection by pilot- and full-scale RO processes under varying operating. The model was further applied to simulate the performance of a pilot-scale RO process that employed a single spiral wound element, providing suggestions for process design and operation.

Pastor et al. (2001) carried out a study aiming to determine the optimum pH at which a sufficient rejection of boron is obtained to use the water as drinking water. The RO system consists of a third stage in the treatment of the permeate of RO where the pH is increased. This study shows that at around a pH of 9.5 the boron is totally rejected in the membrane.

Redendo et al. (2003) have provided a review on the boron removal techniques using FilmTec seawater RO membranes. A typical examples for boron removal design concepts have been presented in this study including one RO pass with natural seawater feed pH, two passes with increased pH in the second pass, two passes with boron-selective ion exchange resins (IER) and three passes with low and high pH.

The boron removal efficiency in Ashkelon plant which produces 330,000 m³/d of drinking water is investigated for FILMTEC membranes by Gorenflo et al. (2007). They showed that the RO system has a stable performance at pH > 10 with boron concentration less than 0.3 mg/l in final permeate flow.

Tu et al. (2011) have used NF and RO membranes to study the coupling effects of solution pH and ionic strength on boron rejection. They reported that as the salt rejection decreases, the dependency of boron rejection on the feed solution pH becomes more significant.

2.7 Methods for Solving Optimization Problems

The objective of this section is to provide a brief review on the methods that are used to solve different optimization problems. Two techniques, the nonlinear programming (NLP) and mixed integer nonlinear programming (MINLP) will be discussed here.

2.7.1 NLP Solution Techniques

There are a variety of methods for solving NLP problems which can be used to find an optimal solution of the NLP problem such as Generalized Reduced Gradient (GRG) (Onwubiko, 2000), Exterior penalty function methods (Fiacco, and McCormick, 1968)

and Successive Linear and Quadratic Programming methods (Wilson, 1963). The last two methods will be presented in the next few sections:

2.7.1.1 Successive Linear Programming Method

Successive Linear Programming (SLP) Method uses a first-order Taylor's series approximation around an initial point to convert the non-linear functions into approximate linear functions.

The original variables are replaced by the deviations around the initial point (Edgar et al., 2001). The resulting LP problem is solved until there is an improvement in the value of the objective function. The values of the design variables thus obtained now become the initial point for further linearization and resolving of the resulting LP problem. This process is repeated until an optimum is reached. The optimum for the successive LPs will be the optimum of the original NLP if the original NLP is not highly non-linear. If it is highly non-linear, the linear approximations may lead to incorrect search directions.

2.7.1.2 Successive Quadratic Programming Method.

Successive quadratic programming (SQP) method has proved to be highly effective for solving constrained optimization problems (Gill et al., 2005). Quadratic programs have a quadratic objective function and linear constraints. At each iteration of SQP optimisation, a quadratic approximation to the objective function is generated. The SQP approach also linearizes the constraints of the approximate quadratic problem and then can be solved in many ways. The constraints of each QP sub-problem are linearizations of the constraints in the original problem, and the objective function of the sub-problem is a quadratic approximation to the Lagrangian function (Edgar et al., 2001). The inequality constraints may be converted to equality constraints by the use of slack variables (Onwubiko, 2000).

2.7.2 MINLP Solution Techniques

The decision variables in many optimization problems involve discrete and continuous variables (Edgar, 2001). These problems can be modelled as mixed integer nonlinear programming (MINLP) problems. For example, a decision may be whether a unit should exist or not (1 for true and 0 for false) or a decision needed may be integer variables representing the number of workers.

Different methods have been developed to solve MINLP problems. Some of the well-known methods in the literature for solving MINLP problem can be summarized as follows:

- Outer Approximation (OA) methods (Duran and Grossmann, 1986; Fletcher and Leyffer, 1994)
- Branch-and-Bound (B&B) (Quesada and Grossmann, 1992).
- Extended Cutting Plane methods (Westerlund and Petersson, 1995).
- Generalized Bender's Decomposition (GBD) (Geoffrion, 1972).

Branch-and-Bound Outer and Approximation (OA) methods will be discussed in this section.

2.7.2.1 Branch and Bound Method

This approach is developed by many authors (Borchers and Mitchell, 1997).

Mathematically, it can be written as:

$$\begin{aligned} \text{Maximize} \quad & P = f(x) + c^T y \\ \text{s.t} \quad & g(x) = 0 \\ & h(x) + My \leq 0 \\ & x \in X \\ & y \in Y \text{ (Integer or binary)} \end{aligned}$$

Where x is the continuous variables, y is the integer variables; M is the matrix of the binary. Branch and Bound Method can be applied to both linear and nonlinear

problems, therefore for nonlinear problems the integer variables y may be written as y^k (Edgar et al, 2001).

The integer variables are relaxed by allowing them to take continuous values. This is known as LP relaxation (Kallrath, 2000). The initial NLP problem is solved. If a continuous NLP relaxation of MINLP problem does not give a feasible solution, and solution is only found for some of the discrete variables as an integer valued then, two subsequent NLP problems are formulated. One NLP solution is treated as a lower bound, the binary tree search is performed by implicit enumeration, and another solution is considered as the upper bound. This process is repeated until the optimal solution for all discrete variables are obtained (Kallrath, 2000).

2.7.2.2 Outer Approximation Method

The "Outer Approximation" (OA) algorithm was first introduced by Duran and Grossman (1986). Mathematically, it can be written as:

$$\begin{aligned}
 & \text{Maximize} && P = f(x) + c^T y^k \\
 & \text{s.t} && g(x) = 0 \\
 & && h(x) + My^k \leq 0 \\
 & && x \in X
 \end{aligned}$$

It performs iterative calculations; at each iteration two sub-problems are solved. NLP problem is solved in which the discrete variables are held constant; the solution of NLP problem was considered the upper bound. The lower bounds of the original problem are obtained by solving convex problem MILP. At iteration k , it is formed by linearization of all the nonlinear function about the optimal solutions.

MILP sub-problem

$$\begin{aligned}
 & \text{Maximize} && P = f(x) + c^T y \\
 & \text{s.t} && z \geq f(x) + \nabla f^T(x)(x - x_i) && i=1, \dots, k
 \end{aligned}$$

$$h(x^i) + \nabla h^T(x^i)(x - x^i) = 0 \quad i=1, \dots, k$$

$$g(x) + \nabla g^T(x^i)(x - x^i) + My^i \leq 0$$

$$x \in X ; y \in Y$$

The objective and constrains functions are added as constraints. The calculations are stopped when a specified tolerance between the two bounds is obtained.

Outer approximation is significantly studied and improved by many researchers such as Fletcher and Leyffer (1994) and recently, Bergamini et al. (2005) tailoring the outer approximation method. They introduced a new formulation of the piecewise under estimators. The calculation of lower bounds of the global optimum is eliminated. The new version focuses on searching improved feasible solutions that lie below a given upper bound.

2.8 Conclusion

This chapter has reviewed the existing work on modelling, optimization and control of RO desalination process. A brief review of the membrane transport models is presented. Special attention is given to the fouling formation on the membrane surface and the subsequent effects on RO performance.

Superstructure optimization is presented as a tool to generate membrane process networks utilizing state space approach. Previous RO network optimization studies were presented. Also, the roles of the fouling, maintenance scheduling and boron removal in the RO design problem are reviewed. Past works revealing several relevant points, (which have given impetus and direction to this work) are summarized below:

- Most of the recent works relevant to determination of the optimal design and operation of RO process are presented in the literature review. However, their work was limited to determine the optimum RO designs for fixed seawater temperature and fixed fresh water demand. The influences of the seasonal and daily variations in seawater temperature and water demand on the operational

and design parameters and consequently on the production cost are overlooked. In this work, the MINLP optimization framework is linked to water storage tank model to determine the optimal operation policies of RO process throughout the day. The optimal operation strategies are established for different process design in terms of number of membrane modules in operation and including variable seawater temperature and freshwater demand throughout 24h.

- The majority of literature investigates the boron removal by RO membranes in seawater desalination experimentally. In fact only few publications were found in the literature which studied this issue theoretically. This may be illustrated due to the complexation of boron rejection process by RO membranes. A review of boron behaviour and its separation processes is given in Chapter 5. In this work, therefore, MINLP optimization tool is considered to formulate the RO design problem based on double pass RO network and constrained by boron concentration in the final permeate for the first time.
- There are only limited studies on maintenance and cleaning scheduling of RO membranes. In fact, little attention has been paid to the important area of membrane cleaning/regeneration and scheduling (See et al., 1999). In addition, all previous studies used hollow fibre modules in their scheduling problems. They used an exponential function which implements the uniform decline in membrane performance. The effect of seawater temperature variation was not implemented in the optimization model. In this work, an extensive study on RO membranes scheduling optimization was carried out using spiral wound modules. NNs based correlations are developed to estimate the actual RO membrane permeability decline and incorporated in the optimization formulation. Annual seawater temperature variation is considered in the model.

- The optimization design problems of membrane separation systems incorporating fouling effect have rarely been studied. Also, The effect of different fouling extents in membrane stages on the RO network design are not often found in the literature. In this research, these points are addressed. Hence, an optimal design strategy that incorporates local fouling effect is proposed.
- The research work concerning control of RO desalination process was considered by many researchers to achieve reliable and cost effective operation. Very limited work investigates the optimal control of RO process in the presence of membrane fouling.

Chapter 3

Reverse Osmosis Process Model and gPROMS

3.1 Introduction

A simulation model is a mathematical representation of a process by means of a number of variables which are defined to represent the inputs, outputs and a set of equations describing the interaction of these variables. A simulation is the execution of a model, represented by a computer program that gives information about the system being investigated. In the first part, a mathematical model that combines solution diffusion model with the description of concentration polarization is presented for modelling and optimization of RO processes. A simulation approach has been proposed to correlate the permeation phenomena through the membranes for both spiral wound and hollow fibre modules. Next sections describe the synthesis of RO networks for water desalination via a superstructure. The formulation of RO design as MINLP problem is presented. The description of the total production cost function with the main capital and operating cost components are also introduced. This chapter ends with a brief overview on the main features of the gPROMS software.

The ultimate objective is to use these modelling and optimization formulations within a RO process simulation and optimization frameworks in the next chapters.

3.2 Modelling of Reverse Osmosis Process

The RO process relies on the use of a semi-permeable membrane barrier as shown in Figure 3.1. It allows solvent molecules to pass through it, impeding the pass of solutes. The solvent as pure water crosses the membrane with very low salt concentration. The concentrated water or brine is left behind.

The transport through RO membranes is well described by the widely accepted solution diffusion model (Kimura and Sourirajan, 1967). The model is used to illustrate solvent and solute transport through RO membrane and therefore predict the performance of RO

unit. According to Marcovecchio et al. (2005), this model is the most used for this purpose because it is able to provide an accurate prediction of the flow of water and salt through the membrane. A film theory approach which was developed originally by Michaels (1968) is used in this work to describe the concentration polarization. It is simple, analytical, and (reasonably) accurate for most RO separations (Kim and Hoek, 2005).

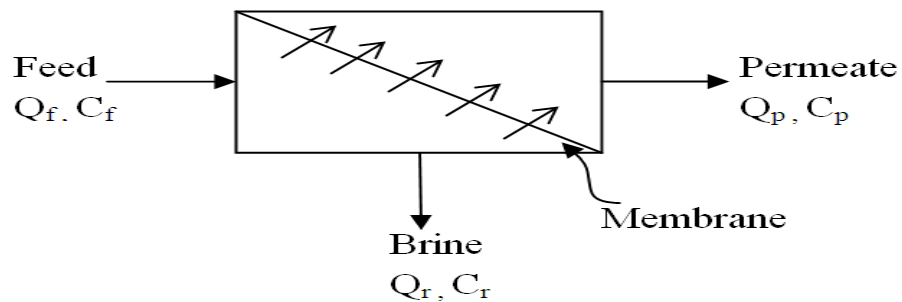


Figure 3.1 Reverse osmosis membrane element

It is important to use models that adequately describe RO process with high accuracy. However, all the models are based on several assumptions and simplifications taking into account the complexity of the problem. RO models are usually difficult to develop because the performance of the membrane units can be influenced by temperature, pressure, feed concentration, and the geometry of the unit, etc. It is difficult to obtain accurate mathematical model accounting all this operation and design aspects of RO process. The following assumptions were used to create the mathematical models for both membrane module configurations (hollow fibre and spiral wound modules) (Murkes and Bohman, (1972); Hameed, (1989); Sekino, (1993); V; Al-Bastaki and Abbas, (1999); Abbas and Al-Bastaki, (2001); Marcovecchio et al., (2005); Abbas (2005); Geraldés et al., 2005; Pais et al., (2007); Lu et al., (2007); Abbas, (2007); Majali et al., (2008); Djebedjian et al., (2008); Oh et al., (2009a); Kaghazchi et al., (2010); Marcovecchio et al., (2010)):

- Membrane structure is uniform throughout the module.

- The feed concentration varies linearly along feed side channel.
- Solution diffusion model is applicable to calculate the transport of water and salt through the membrane.
- Constant membrane permeability coefficients for water and salt.
- Constant temperature; no free convection effects.
- Constant mass transfer coefficient for a given fluid condition.

Most of the models reported in the literature based on the aforementioned assumptions are on validation with salt water desalination data but these models were not tested with wastewater treatment data (Sundaramoorthy et al., 2011).

3.2.1 Model of RO Module

The steady state performance prediction of RO process has been carried out by utilizing a set of implicit mathematical equations which are generated by combining film theory approach with solution diffusion model, mass balance over the membrane element, etc.

3.2.1.1 Spiral Wound Membrane Element

In this section, mathematical modelling of spiral wound module by using Kimura-Sourirajan model and film theory is considered. In addition to the aforesaid assumptions, the pressure drop along permeate channel for 8 inch spiral wound module that has 37 membrane leafs with a length of 1 m is neglected (Gerald et al., 2005). Also, Van der Meer (1997) reported that the curvature of membrane module has insignificant effect on system's performance. Therefore, an unwound flat sheet membrane with same channel height and spacers would adequately represent characteristics of the corresponding spiral-wound RO module.

Referring to Figure 1.4, the following equations can be written for the spiral wound element at steady state conditions. Water and salt fluxes via the membrane can be estimated by Kimura–Sourirajan model (Kimura and Sourirajan, 1967).

$$j_w^T = A_w^T (\Delta P - (\varphi_m - \varphi_p)) \quad (3.1)$$

$$j_s^T = A_s^T (C_m - C_p) \quad (3.2)$$

Where ΔP represent the pressure difference between the high concentration side and low concentration side of the membrane, the subscripts w, m, p, s refer to water, membrane surface, permeate and solute respectively. The subscript T refers to temperature dependence parameters.

The total and salt mass balance equations around the spiral wound element are:

$$Q_f = Q_r + Q_p \quad (3.3)$$

$$Q_f C_f = Q_r C_r + Q_p C_p \quad (3.4)$$

The water permeate concentration and flow can be expressed as:

$$C_p = \frac{j_s^T}{j_w^T} \quad (3.5)$$

$$Q_p = A j_w^T \quad (3.6)$$

The permeate flux cannot be known unless the membrane wall concentration is known. At the same time, this concentration needs the value of water flux to be evaluated. Therefore, an iterative calculation is needed. Concentration polarization on membrane surface phenomenon may be described using the film theory (Michaels, 1968) as:

$$CP = \frac{C_m - C_p}{C_b - C_p} = \exp\left(\frac{j_w^T}{k}\right) \quad (3.7)$$

The mass-transfer coefficient is given by the following correlations developed by (Da Costa et al., 1994) in terms of Sherwood number for spiral wound modules:

$$sh = \frac{k d_h}{D} = 0.664 k_{dc} \text{Re}^{0.5} \text{Sc}^{0.33} \left(\frac{2d_h}{L}\right)^{0.5} \quad (3.8)$$

Reynolds number (Re) and Schmidt number (Sc) are given as:

$$\text{Re} = \frac{\rho d_h u}{\mu^T} \quad (3.9)$$

$$Sc = \frac{\mu^T}{\rho D^T} \quad (3.10)$$

μ^T and D^T are temperature dependence water viscosity and diffusivity coefficients. The average axial velocity in the feed channel is calculated by the following relation:

$$u = \frac{Q_B}{wh_{sp}\varepsilon} \quad (3.11)$$

The pressure drop of the spiral wound element is calculated using the model developed by Da costa et al. (1994). The model takes into account pressure losses due to drag on feed spacer and kinetic losses due to change in direction of flow. The pressure losses due to connections and fitting are not included.

$$\Delta P_f = \frac{\rho u^2 LC_{td}}{2d_h} \quad (3.12)$$

The total water recovery and salt rejection for the RO process, which is the measure of the process performance is defined as:

$$WR = \frac{Q_p}{Q_f} 100 \quad (3.13)$$

$$SR = \frac{C_f - C_p}{C_f} 100 \quad (3.14)$$

Pressure Vessel

In each pressure vessel (PV), normally (2-8) spiral wound elements are connected in series as shown in Figure 3.2. The permeate produced by each PV is the sum of all elements products. The following relations are used to model the whole pressure vessel system:

$$Q_{f,z+1} = Q_{r,z} \quad \text{For } z= 1 \dots ne \quad (3.15)$$

$$C_{f,z+1} = C_{r,z} \quad \text{For } z= 1 \dots ne \quad (3.16)$$

$$P_{f,z+1} = P_{r,z} \quad \text{For } z= 1 \dots ne \quad (3.17)$$

Where ne is the number of membrane elements in PV_i within stage j . Similarly, streams leaving j stage are connected to the inlet of stage $j+1$.

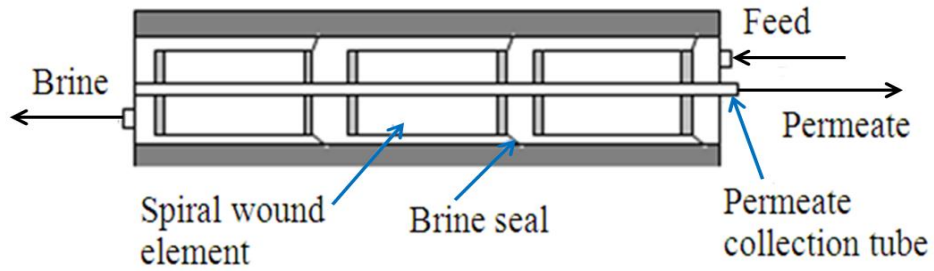


Figure 3.2 Pressure vessel construction

3.2.1.2 Hollow Fibre Membrane Element

A mathematical model of RO membrane based on Kimura-Sourirajan model and film theory has been developed to describe the transport through the membrane and concentration polarization for Hollow Fiber module. The equations from 3.1 to 3.7 are used to describe the permeation properties and mass balance around the hollow fibre module as well as the concentration polarization phenomena.

The mass transfer coefficient on the feed side (k) is related to the Sherwood number through the following equation (Marcovecchio et al., 2005):

$$sh = \frac{k2r_{ot}}{D} = 2.725 Re^{0.33} Sc^{0.33} \quad (3.18)$$

Reynolds number (Re) and Schmidt number (Sc) are given as:

$$Re = \frac{\rho 2r_{ot} U}{\mu^T} \quad (3.19)$$

$$Sc = \frac{\mu^T}{\rho D^T} \quad (3.20)$$

The superficial velocity at the inner radius and outer radius of the fiber bundle are used to calculate the superficial velocity which is used to calculate Reynolds number.

The inner superficial velocity of the fiber bundle:

$$U_i = \frac{Q_f}{2\pi R_i L} \quad (3.21)$$

The outer superficial velocity of the fiber bundle:

$$U_{ot} = \frac{Q_f - Q_p}{2\pi R_{ot} L} \quad (3.22)$$

And the average superficial velocity:

$$U = \frac{U_i - U_{ot}}{\log \frac{U_i}{U_{ot}}} \quad (3.23)$$

The total water recovery (WR) and salt rejection (SR) which are the measure of the process performance is defined as:

$$WR = \frac{Q_p}{Q_f} 100 \quad (3.24)$$

$$SR = \frac{C_f - C_p}{C_f} 100 \quad (3.25)$$

3.2.1.1 Energy Recovery and Consumption

Reverse osmosis system produces concentrate with considerable amount of energy applied through the high-pressure RO pumps. This energy can be recovered and reused to minimize the overall energy cost for seawater desalination. The energy lost in depressurizing the concentrate can be returned efficiently to the feed water by using mechanical turbine or employing efficient pressure exchanger devices. Turbines can be used to recover energy from the concentrate, the pressure of the concentrate turns into water velocity that rotates the blades of the turbines.

The electrical power consumed by the pumps and recovered by the turbine from the brine can be expressed in (kw) as (Oh et al., 2009a):

$$E_{pu} = \sum \frac{\Delta P_{HP,pu} Q_{HP,pu}}{36\eta_{pu}} \quad (3.26)$$

$$E_{t,recv} = \sum \frac{\Delta P_{HP,tu} Q_{HP,tu} \eta_{tu}}{36} \quad (3.27)$$

Where E_{pu} is the total electrical power consumption of all pumps in the candidate process structure and $E_{t,recv}$ is the total energy recovered from the turbines that may exist.

Energy consumption by feed pumps being expressed per cubic meter of permeate which can be calculated as:

$$E_{tu} = \frac{E_{pu} - E_{t,recv}}{Q_{p,t}} \quad (3.28)$$

In case of pressure exchange used as energy recovery device, the specific energy will be expressed as (Villafafila and Mujtaba, 2003):

$$E_{PX} = \frac{\frac{P_f Q_{p,t}}{36\eta_{px}}}{Q_{p,t}} \quad (3.29)$$

3.2.1.4 Physical Properties

For solving the RO model, the following correlations are used to estimate seawater properties:

Water density (kg/m^3) (Pais et al.; 2007):

$$M = 1.0069 - 2.757 \times 10^{-4} T(^{\circ}C) \quad (3.30)$$

$$\rho = 498.4M + \sqrt{248400 M^2 + 752.4cM} \quad (3.31)$$

Brine viscosity (Pa s) (Pais et al.; 2007):

$$\mu = 1.234 \times 10^{-6} \exp\left(0.00212c + \frac{1965}{273.15 + T(^{\circ}C)}\right) \quad (3.32)$$

Diffusivity coefficient (m^2/s) (Pais et al.; 2007):

$$D = 6.725 \times 10^{-6} \exp\left(0.154 \times 10^{-3} c + \frac{2513}{273.15 + T(^{\circ}C)}\right) \quad (3.33)$$

Osmotic pressure φ (bar) (Technical Manual, Dow)

For c (salt concentration) <20

$$\varphi = c10^3 \frac{(T(^{\circ}C) + 320)}{491000} \quad (3.34)$$

For c (kg/m³) >20

$$\varphi = \left(\frac{0.0117 c 10^3 - 34}{14.23}\right) \frac{(T(^{\circ}C) + 320)}{345} \quad (3.35)$$

3.3 Reverse Osmosis Optimization

The main objective of the optimization is concerned with finding the optimum values (solutions) of any variable from among a lot that leads to best value of the process performance. Optimization problems can be classified on the basis of whether or not the objective functions or constraints are linear in the decision variables (Onwubiko, 2000).

In general, optimization problem includes three basic categories:

1. The objective function which is to be optimized (profit function, cost function, etc.).
2. Equality constraints (model equations) as mass and energy balances.
3. Inequality constraints (such as upper and lower bounds of the continuous variables).

Reverse osmosis process performance is affected by several factors. These factors can be classified into two categories:

- *Operation variables*: such as feed flow rate, operating pressures, feed temperature, recovery rate, energy recovered and degree of fouling.
- *Design variables*: membrane element type, size and RO network arrangement such as the existence of booster pumps and energy recovery systems.

Based on the above classification for the variables connected to the RO process performance, the optimization of the RO system is performed in two parts:

1. Optimization of operating variables: specific energy consumption or total operation cost is used as objective function while the operating parameters are optimized. The problem is formulated as non-linear programming (NLP).
2. Optimal Design: optimal synthesis of RO systems using mixed integer non-linear programming approach (MINLP). The total cost is used as objective function.

3.3.1 Superstructure

E1-Halwagi (1992) developed a structural representation based on state space approach which embeds RO systems for a given membrane module type and feed water quality. The superstructure is composed of several unit operations (e.g. Turbines, Pumps, RO membrane stages) which represent the fixed cost of the network. Mixers and splitters nodes provide mixing and splitting for the streams within the network.

Saif et al. (2008) showed a compact representation (Figure 3.3) of the general superstructure (Figure 2.10) which was originally presented by El-Halwagi (1992). This representation contains less mixer nodes and requires fewer binary variables in the optimization formulation and consequently easier optimization procedure.

Figure 3.3 shows RO superstructure representation which has two sets of boxes: a set of distribution boxes (DBs) and a set of matching boxes (MBs). The distribution boxes are responsible for stream mixing, bypass and recycle. On the other hand, the matching boxes are used to determine the optimal assignment of streams to units. Energy recovery devices are used to recover kinetic energy from the effluent high-pressure streams. The feed stream can be mixed with streams from the RO units before pumping stage to allow for possible bypass of some portion of the feed to the final product nodes. Also the outlet streams from the RO membrane units are matched to the inlet feed stream (after passing through turbine) before pumping stage to allow possible full or partial recycle. It can be seen that the unit operations are arranged in series in the

superstructure representation. Each RO stage is assumed to consist of multiple parallel RO membrane modules under the same operational conditions. Each stream in the network is supposed to be connected to all the nodes.

3.3.2 Model Reduction

In the present study, the superstructure in Figure 3.3 represents the most of possible networks design. Several alternatives can be eliminated from the superstructure based on examination the theoretical design of RO network. It is possible to eliminate non-essential streams from the superstructure by screening the options at every mixing point in the DB to locate the possible simplification. The following stream sets can be excluded from the MINLP model:

1. The feed stream should not link to any turbine as it is used to recover energy from the effluent high pressure streams.

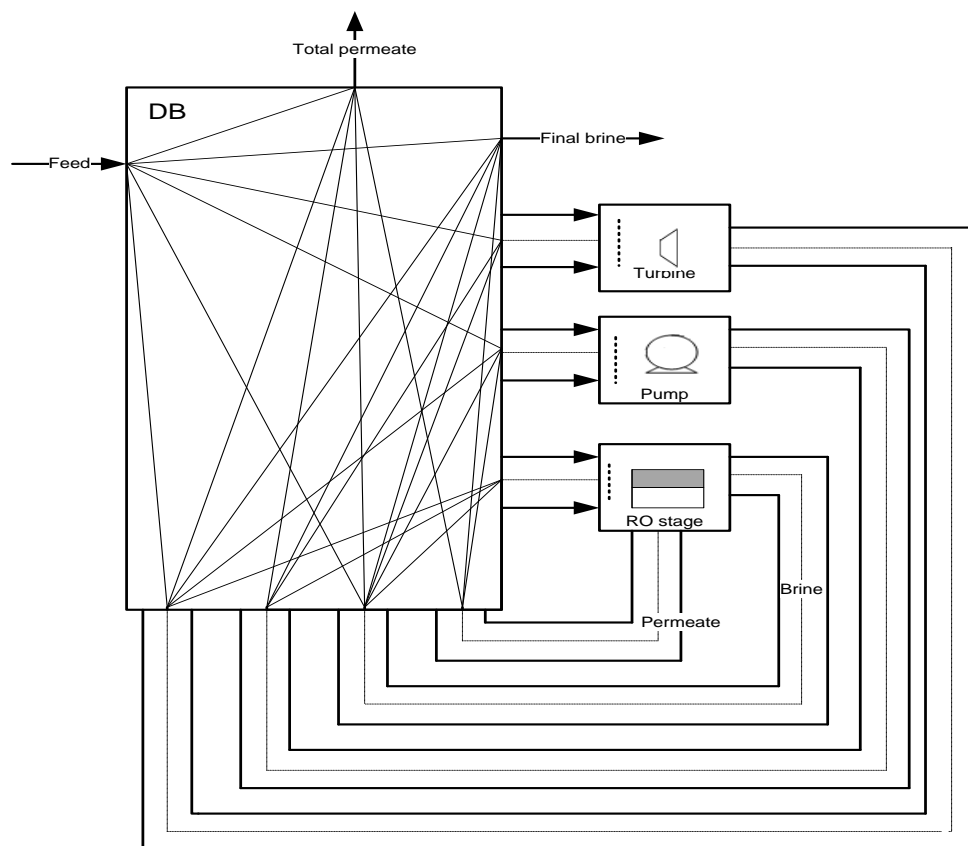


Figure 3.3 RO superstructure (Saif et al., 2008)

2. Any permeate streams should not be connected to other streams or equipment.
3. The only way allowable for the streams to exit from the pumps is the membrane stages.
4. Eliminating the existence of series between turbines and/or pump stages.

Further reductions in the model optimization variables can be achieved by modifying the model to eliminate the binary variables for essential equipment as feed pump, first membrane stage and arrange the streams to the inlet and outlet of mixers and splitters in the way to prevent any flow to the permeate streams and mix streams with different pressure.

3.3.3 Mathematical Model for the Superstructure

The MINLP optimization approach is used to determine the optimal configuration of the process. Continuous variables are defined for the continuous optimization of parameters and discrete variables are used to express discrete decisions as the existence of process units. Both types of variables are handled in the MINLP problem.

The general superstructure in Figure 3.3 could be further improved by considering only the feasible process structures by removing non-essential streams and mixing points from the superstructure (as described above). A reduced superstructure is developed for two-stage RO system (Figure 3.4) by implementing all the proposed reductions such as recycle brine stream to the same stage or mixing permeate stream with the brine. Note that the mixing of streams is only allowable for the streams with equal pressure.

The RO superstructure comprised mainly of two stages. Each RO stage comprised of a number of parallel membrane modules operating under identical conditions. The permeate produced by each stage is the sum of permeates of all parallel membrane elements in the stage. The RO stages are connected in series where the brine output of stage j becomes the input for stage $j+1$. The following relations are used to calculate process variables:

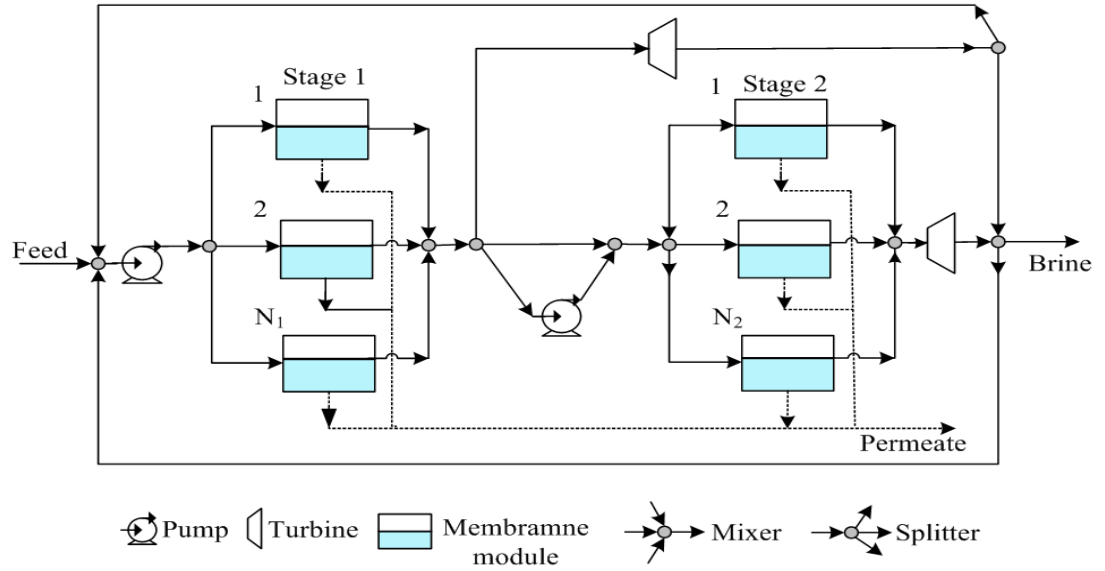


Figure 3.4 Superstructure of two stages RO network

$$Q_{f,j+1} = Q_{r,j} \quad \text{For } j = 1 \dots S \quad (3.36)$$

$$C_{f,j+1} = C_{r,j} \quad \text{For } j = 1 \dots S \quad (3.37)$$

$$P_{f,j+1} = P_{r,j} \quad \text{For } j = 1 \dots S \quad (3.38)$$

S is the number of stages. Similarly, the membrane modules in stage $j+1$ are modelled by the same equations that are used for modules in stage j (Section 3.2.1) but using new input operating conditions.

The inlet feed stream to the first stage consists of fresh feed water and recycle brine streams obtained from all stages. The continuous variable R determines the flow rates of recycled brine mixed with feed stream. For instance, R equals zero means that the brine recycle stream does not exist:

$$Q_{f,t} = Q_{f,in} + \sum_{j=1}^S Q_{r,j} R_j \quad (3.39)$$

The streams leaving the high pressure pump is split into N_1 streams depending on the number of parallel membrane elements exist in the stage:

$$Q_{f,i} = \frac{Q_{f,j}}{N_j} \quad i \in N_j \quad j \in S \quad (3.40)$$

$$Q_{f,i} = \sum_{i=1}^{N_j} Q_{f,j} \quad i \in N_j \quad j \in S \quad (3.41)$$

N_j is an integer variable represents the number of membrane modules exist in the stage j . For $j=1$, $Q_{f,j} = Q_{f,t}$. The optimum number of modules per stage must lead to fulfil the module flow rate constraints.

The total permeate flow and concentration from all membrane modules can be used to determine whether the stage exist or not by introducing a binary variable B_j which has value of 1 when the stage exists and 0 if not. The binary variable for the first stage (B_1) always has a value 1:

$$Q_{p,t} = \sum_{j=1}^S \sum_{i=1}^{N_j} Q_{p,i,j} B_j \quad (3.42)$$

$$Q_{p,t} C_{p,t} = \sum_{j=1}^S \sum_{i=1}^{N_j} Q_{p,i,j} C_{p,i,j} B_j \quad (3.43)$$

The total and salt mass balance constraints are imposed on mixers. However, only volume balance constraint is required for splitters. Balance over each node in Figure 3.4 representing either mixer or splitter can be expressed as:

For mixer:

$$Q_{mx,out} = \sum_1^Y Q_y \quad y \in Y \quad (3.44)$$

$$Q_{mx,out} C_{mx,out} = \sum_1^Y Q_y C_y \quad y \in Y \quad (3.45)$$

Y is the total number of streams leaving the mixer. $Q_{mx, out}$, $C_{mx,out}$, Q_y , C_y are the outlet flow, outlet concentration, inlet flow and concentration of the inlet stream to the mixer, respectively.

For splitter:

$$Q_{sp,in} = \sum_1^X Q_x \quad x \in X \quad (3.46)$$

X is the total number of streams leaving the splitter, $Q_{sp,in}$, and Q_x are the flow rate of the inlet and outlet streams of the splitter, respectively. Unlike the mixer, concentrations of streams entering and leaving the splitter will remain constant.

The overall water and salt mass balance for the RO network constraints are employed to estimate the properties of the streams leaving or entering RO network as:

$$Q_{f,t} = Q_{r,t} + Q_{p,t} \quad (3.47)$$

$$Q_{f,t} C_{f,t} = Q_{r,t} C_{r,t} + Q_{p,t} C_{p,avg} \quad (3.48)$$

The following constraints are established on binary variables B_{pu} and B_{tu} associated with the existence or non-existence of the booster pump prior to second stage and turbine prior and/or after second stage, respectively:

$$\Delta P_{pu,j} \leq \Delta P_{pu}^U B_{pu,j} \quad \text{For } j=1 \dots S \quad (3.49)$$

$$-\Delta P_{tu,j} \leq \Delta P_{tu}^U B_{tu,j} \quad \text{For } j=1 \dots S \quad (3.50)$$

The binary variable $B_{pu,1}$ always has a value of 1. In case of inter-stage pump exist, equation (3.38) can be written as:

$$P_{fj} = P_{r,j-1} + \Delta P_{pu,j} \quad \text{For } j=2 \dots S \quad (3.51)$$

The exit streams from the pumps and turbines were carefully examined when constricting the superstructure to avoid losing energy and to ensure that there is no co-existence of turbine and pump in series.

Several other constraints such as membrane module design constraints and product characteristics variables constraints are required to have a well-defined MINLP problem:

$$Q_f^L \leq Q_f \leq Q_f^U \quad (3.52)$$

$$P_f^L \leq P_f \leq P_f^U \quad (3.53)$$

$$Q_{p,t} \geq Q_{p,t}^{\min} \quad (3.54)$$

$$C_{p,avg} \leq C_{p,avg}^{\max} \quad (3.55)$$

3.3.4 Cost Functions

The cost components and the objective function employed in the optimization problems involving spiral wound and hollow fibre membrane modules are presented here. The total annualized cost is presented as (Malek et al., 1996):

$$TAC = (C_{SWP} + C_{pu} + C_{ERD} + C_{me})1.411 \times 0.08 + OC_{pu} + OC_{me} + OC_{ch} + OC_{sc} \quad (3.56)$$

In the above equation, the total annualized cost is a combination of the capital and operating costs for one year of operation. The constant 1.411 represent site development cost and indirect costs connected to the capital cost (Malek et al., 1996) while 0.08 is the capital charge rate. The most important cost components affecting the produced water price are included. The capital cost of energy recovery device is the same as the pump cost in the case of turbine is employed to recover energy from the effluent brine.

The cost of proposed RO process structure consists of the following components (Malek et al., 1996):

1. Pump or turbine capital cost

$$C_{pu} \text{ or } C_{ERD} = \begin{cases} 52Q_{HP} \Delta\Delta_{HP} & \text{if } Q_{HP} < 200 \text{ m}^3/\text{h} \\ 81(Q_{HP} \Delta\Delta_{HP})^{0.96} & \text{if } 200 \text{ m}^3/\text{h} < Q_{HP} < 450 \text{ m}^3/\text{h} \end{cases} \quad (3.57)$$

Where Q_{HP} is the flow entering pump or turbine (m^3/h), ΔP_{HP} pressure difference across the pump or turbine in (bar).

2. Membrane modules cost and pressure vessels cost (\$)

For spiral wound module

$$C_{me} = \sum_{j=1}^s \sum_{i=1}^N C_{mele} B_j + \sum_{j=1}^s \sum_{i=1}^N C_{PV} B_j \quad (3.58)$$

For hollow fibre module

$$C_{me} = \sum_{j=1}^s \sum_{i=1}^N C_{mele} B_j \quad (3.59)$$

B_j is binary variable for membrane stage selection.

3. Feed pretreatment cost (\$)

$$C_{SWP} = 996(Q_{f,t} 24)^{0.8} \quad (3.60)$$

$Q_{f,t}$ is the feed flow to RO unit in (m³/h).

4. Net pumping cost (\$/year)

$$OC_{pu} = (E_{pu} - E_{t,recv}) E_c l_f 365 \times 24 \quad (3.61)$$

5. Membrane replacement cost (\$/year)

$$OC_{me} = 0.2C_{me} \quad (3.62)$$

6. Chemical treatment cost (\$/year)

$$OC_{che} = Q_{f,t} l_f 24 \times 365 \times 0.018 \quad (3.63)$$

7. Annual Spares cost (\$/year)

$$OC_{sc} = Q_{p,t} l_f 24 \times 365 \times 0.033 \quad (3.64)$$

$Q_{p,t}$ is the total production from all membrane elements in the existing stages (m³/h).

3.4 gPROMS Simulator

The general Process Modelling System package commonly known as gPROMS is one of the modelling platforms of Process System Enterprise (PSE) for steady-state and dynamic simulation, optimization, experiment design and parameter estimation of plant operation. It can be used for any process that can be described by a mathematical model and can be exported as a package to the most state of the art modelling software such as HYSYS, FLUENT, Aspen Plus, Matlab, and Simulink. In addition, it has a built-in interface to MS EXCEL that allows the user to statistically examine the results. gPROMS has been widely applied for different process industries such as petrochemicals, refining industry, food and pharmaceuticals.

There are many advantages that make gPROMS software an attractive tool for engineers in modelling and optimization of different industrial applications and also competitive

to the simulators packages available on the market. The key benefits of using gPROMS are:

- Reversible-symmetric, reversible-asymmetric, and irreversible discontinuities of the physical and chemical processes behaviour can be handled within gPROMS. This can enhance the solution speed, and also overcome the problems faced solution prediction in the conventional simulators by a high level mathematical research, and automatically detect discontinuities, lock on to them, and then re-initialize.
- Multiple activities from the same model, once the simulation model is built in gPROMS, it can be used for many different activities that available within gPROMS.
- It can handle a large number of algebraic, differential and partial differential equations, over 100,000 equations can be simulated using this software (gPROMS, 2004).
- The model validation techniques available in gPROMS enable a user to fit the models predictions to closely match observed data using experimental data.

3.4.1 Model Development using gPROMS

For the advantages mentioned above, gPROMS was selected for the modelling and optimization of the RO process. gPROMS (version 3.0.3 model builder) which is available in the University of Bradford has been used to simulate the RO system by implementing a set of algebraic equations in the model entity. The variables used in the simulation are defined and the lower and upper bounds for them are specified in variable type entity, the input data and module specification in the process entity, and finally two types of optimization problems (non-linear optimization problems and MINLP optimization problems) are implemented in the optimization entity.

3.4.2 Solvers in gPROMS

Several solvers are provided in gPROMS as standard that may be used for simulation and optimization. The solvers which are used in the simulation and optimization are specified in SOLUTION PARAMETERS section of the PROCESS entity.

Simulation solvers

- Solvers for sets of linear algebraic equations

Both MA28 and MA48 employ direct LU-factorisation algorithms.

- Solvers for sets of non-linear algebraic equations

BNDSOL: Block Decomposition Non-Linear solver with reversible symmetric discontinuities.

NLSOL: is nonlinear solver, with and without block decomposition.

SPARSE: is sophisticated implementation of a Newton-type method without block Decomposition.

- Solvers for mixed sets of non-linear algebraic and differential equations

DASOLV: solver based on a variable time step/Backward Differentiation Formulae (BDF).

A SRQPD: employs a Sequential Quadratic Programming (SQP).

Optimization solvers

(DOSOL V): solver manager which specifies the solvers for the steady state and dynamic.

CVP_SS and CVP_MS: based on a Control Vector Parameterisation (CVP) approach

OAERAP: employs an outer approximation (OA) algorithm for MINLP problems.

3.5 Conclusion

Detailed modelling and optimization approaches of RO processes have been described in this chapter. The RO steady state model consists of a set of algebraic equations that approximate the hydrodynamics in the membrane module channels as well as the

permeation phenomena through the membrane layer. The model also comprises all the required physical property correlations which are depended on temperature and salinity. An optimal design methodology has been presented in this chapter. A superstructure is developed based on two-stage RO system to accommodate all possible connections between streams and unit operations and used in the synthesis of RO process. The problem was formulated using MINLP approach and the mathematical model describes the RO network is presented.

The methodologies developed in this chapter for RO process will be used in the next chapters for different simulation and optimization problems.

A brief discussion of the gPROMS software package is summarized in this chapter. gPROMS has several competitive advantage mentioned above, and others not listed here, that make it an attractive and suitable tool for the modelling and optimization of any plant process (steady state and dynamic). Therefore, gPROMS was selected to perform the computational task in this thesis.

Chapter 4

Effective Design of RO Process under Variable Seawater Temperature

4.1 Introduction

Many experimental and theoretical researches have appeared to investigate the effect of the feed temperature on the operation of RO processes. According to their findings, the effect of temperature on membrane performance is the most important parameter as it influences the key performance parameters of the RO systems as water recovery, concentration polarization and salt rejection (Goosen et al. 2002; Jin et al., 2009). Water production increases with higher feed temperature. Meanwhile salt passage through the membrane layer also increases. Therefore, it is essential to increase the operating pressure to realize the same water quality which means more operational costs.

Based on the above aforesaid, for a fixed RO design, the production of freshwater from an RO process can significantly vary with seasonal temperature variation of seawater. The operation of RO process has to be continuously adjusted with the variation of seawater temperature to maintain the required demand.

As discussed in the previous chapter, gPROMS is a reliable tool for simulation and optimization, of highly complex processes. In this chapter, the design of RO networks is investigated based on the steady state model (no fouling) developed in chapter three for hollow fibre module and using gPROMS software tool.

In order to find the optimal design and operation of RO systems, the design of RO network for water desalination process is formulated as an MINLP problem using hollow fibre module. The influence of the operational and design parameters on the total annualized cost is investigated for a fixed water demand and quality as the feed salinity vary from low salinity of 15,000 ppm up to very high salinity water sources (50,000 ppm). A wide range of seawater temperatures and high temperatures water resources

such as warm feed from cooling systems (Al-Enezi and Fawzi, 2003), varying from 15°C to 40°C representing seasonal variation in seawater temperature are also investigated.

4.2 Modelling of RO Process

4.2.1 Membrane Model

The steady state RO model that takes into account concentration polarization (CP) has been developed for hollow fiber module. A suitable mathematical description of the transport through RO membranes is given by the widely accepted Kimura–Sourirajan model (Kimura and Souriraja, 1967). Details of the mathematical model for the RO module used in this work are given in chapter three (Section 3.2.1.2).

The pressure drop in a hollow fiber membrane module is considered in the model. However, the entire module is taken as a single element and the pressure drop across each hollow fiber element is assumed to be constant (Lu et al., 2006).

4.2.2 Network Model

The objective of the developed optimization model is to find optimal design for RO network involves different seawater salt concentrations and temperatures. A superstructure of the RO network for water desalination process is developed based on two stages RO network shown in Figure 3.4. The formulation of the flexible superstructure allows the optimizer to identify the optimal design of RO process whether two stages or only one RO stage.

4.2.3 Temperature Effect on Membrane Permeability

There are some works carried out for optimization of the design of various RO systems under different feed concentration using MINLP technique (Marcovecchio et al., 2005; Lu et al., 2007). However, their work was limited to the determination of the optimal design and operation of RO networks for only one temperature and the interactions between varying feed concentration and feed temperature is still not well understood.

Membrane characteristics change with varying feed temperature. This effect is included empirically in the relationship between feed water temperature and membrane permeability as (Sarkar et al., 2008):

$$A_w^T = A_w^{T_o} \frac{\mu^{T_o}}{\mu^T} \quad (4.1)$$

$$A_s^T = A_s^{T_o} \frac{\mu^{T_o}}{\mu^T} \frac{T_o}{T} \quad (4.2)$$

Dependence of diffusivity coefficient on temperature is approximated as:

$$D^T = D^{T_o} \frac{\mu^{T_o}}{\mu^T} \frac{T_o}{T} \quad (4.3)$$

T_o is the reference temperature. Note, all physical properties and osmotic pressure are function of temperature.

The steady state model of RO process is coupled with the above equations to represent the temperature effect on the membrane performance.

4.3 RO Network Optimization Validation

The problem of designing a flexible RO system using a combination of RO membranes, pumps, and energy recovery turbines for RO based desalination process is examined here using hollow fibre membrane module.

The proposed MINLP optimization formulation simultaneously integrates the aspects of flexibility with cost effectiveness. The process is represented as brine staging arrangement with two RO stages as the superstructure shown in Figure 3.4.

For the sake of comparison with the MINLP formulation given by El-Halwagi (1992), this network design problem described in this section for hollow fibre module applies the same methodology that has been presented before. This problem is also formulated as a MINLP problem for minimizing the total annualized cost (TAC) subject to process constraints and flexibility constraints. Outer approximation algorithm within gPROMS environment is used to solve the MINLP problem.

The mathematical model that describes the solvent and solute transport via the membrane layer was presented by Evangelista (1985) for the hollow fibre module is used in this case for comparison purpose only.

All the cost parameters and unit operation parameters were taken from El-Halwagi (1992). Table 4.1 presents the geometrical properties of DuPont hollow-fibre RO modules. Table 4.2 lists the parameters that are used in MINLP optimization. The economic data estimated for this case are as follows (El-Halwagi, 1992):

Annual fixed cost of pumps (\$/year) = $0.0157[\text{flow rate through the pump (kg/s)} \times \text{pressure difference across the pump (N/m)}]^{0.79}$

Annual fixed cost of turbines (\$/year) = $0.4182157[\text{flow rate through the turbine (kg/s)} \times \text{pressure difference across the turbine (N/m)}]^{0.47}$

Electrical power = 0.06 \$/kWh

Mechanical efficiency of pump /turbine = 65%

Annualized cost of RO modules (DuPont B-10) = 1,450 \$/module

Table 4.1 Hollow fibre RO modules specifications (El-Halwagi, 1992)

Property	Value
Fibre length (m)	0.75
Outer radius of fibre (m)	50×10^{-6}
Inner radius of fibre (m)	21×10^{-6}
inner radius of the fibre bundle (m)	1.27×10^{-2}
outer radius of the fibre bundle (m)	5.334×10^{-2}
Membrane area (m ²)	152

Table 4.2 Input Data for the hollow fibre optimization case study

Parameter	Value
Feed flow rate (kg/s)	19.29
Feed salt concentration (kg/ m ³)	34.8
Permeate minimum flow rate (kg/s)	5.787
Permeate maximum salt concentration (kg/m ³)	0.57
Minimum flow rate per module (kg/s)	0.21
Maximum flow rate per module (kg/s)	0.27
Pressure drop per module (bar)	0.22
Water permeability (kg/s N)	1.2×10^{-10}
Solute permeability (kg/m ² s)	4×10^{-6}

4.3.1 Results

The globally optimum RO network for hollow fibre element was found to require a treatment cost of \$258,729/year while the total annualized cost reported by El-Hlawgi (1992) for the same case study was \$270,000/year. There are several reasons for this difference among them; the MINLP optimization problem was solved by El-Hawagi (1992) using generalized reduced gradient method while outer approximation algorithm within gPROMS software is used here. Also, El-Hawagi's formulation involves the continuous processing of the entire feed flow (19.29 kg/s) but in this work bypass part of the inlet feed flow is allowed. In addition, the superstructure considered in this work has significantly reduced by eliminating non-essential streams. Figures 4.1 and 4.2 present the optimal layout of the global solutions. The optimum layout (Figure 4.1) includes two RO stages in series, feed pump and turbine, following the second RO stage, to extract energy from the second stage reject stream.

The trade-offs between extra expenditure and more permeate quantity recovered yielded neglecting the bypass and recycle streams. Also the existing of booster pump prior to second stage is found to be unnecessary compared with the flux that resulted due to increase (0.22 bar) in the feed pressure of the second stage. The optimum layout results

in a cascade configuration with 57 modules in parallel in the first RO stage and 55 modules in the second stage. The RO-permeate streams are collected and sent to the final permeate product for the network.

The main differences between the RO layout results from this work and El-Hlawgi optimum RO structure (Figure 4.2) are that, the inlet feed flow to the high pressure pump in the configuration of this work is less by 21 %, thus, the outlet brine from second stage is totally fed to the second stage unlike that in El-Hawagi's network.

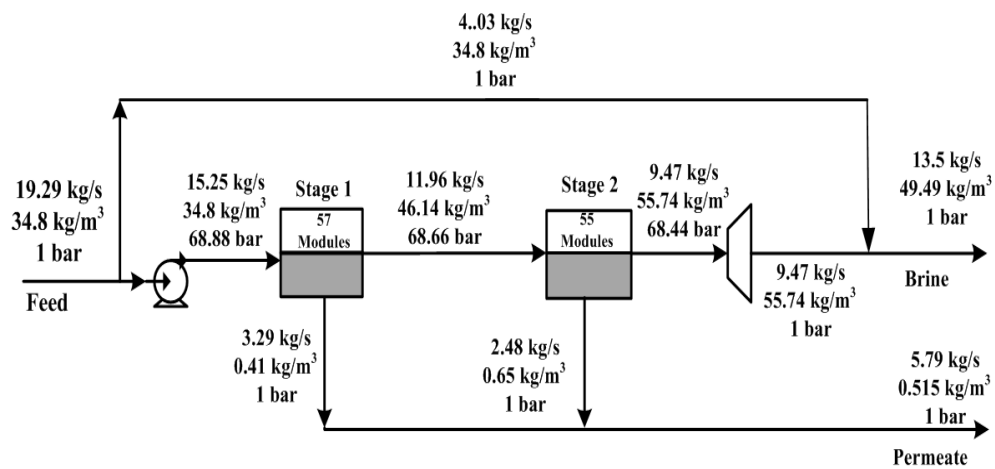


Figure 4.1 Optimal design and operating conditions for the RO network (this work)

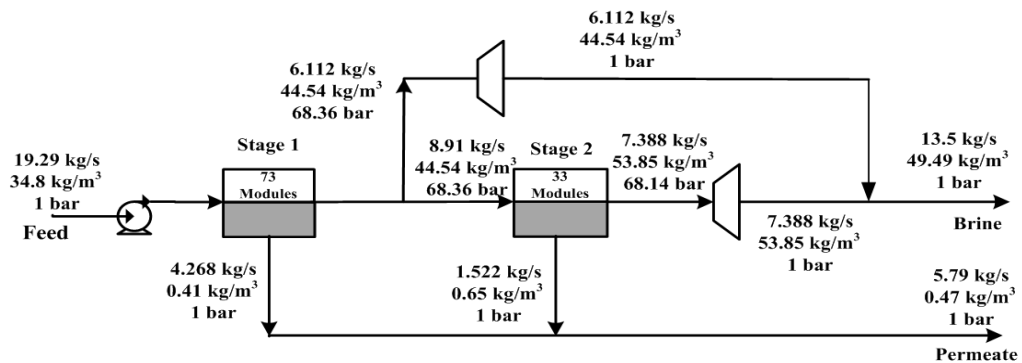


Figure 4.2 Tapered design with brine bypass (El-Halwagi, 1992)

4.4 MINLP Formulation

In this framework, the MINLP optimization formulation presented and validated earlier based on two-stage RO superstructure given in Figure 3.4 is used to find the optimum

design of RO network. The mathematical equations which describe the RO network in chapter three (Section 3.3.3) is used here. Continuous variables are defined for the optimization of operating parameters and discrete variables are used to express discrete decisions such as the existence of process units.

The proposed MINLP optimization approach generates various structures and design alternatives that are all candidates for a feasible and optimal solution. The objective function is the total annualized cost (TAC) which is minimized for every candidate configuration satisfying the operation and design constraints. The cost function is a sum of capital and operating costs as shown in Section 3.3.4. The total annualized cost (TAC) is expressed as:

$$TAC = (C_{WPT} + C_{pu} + C_{ERD} + C_{me})1.411 \times 0.08 + OC_{pu} + OC_{me} + OC_{ch} + OC_{sc} \quad (4.8)$$

The major cost parts that influence the design of the RO process are included as feed pre-treatment, equipment costs (pumps, turbine and membrane modules) which are considered as fixed costs. Also, most operation costs are taken into account as energy consumption cost, membrane replacement cost, chemical cost, and spare costs which are estimated using the equations in Section 3.3.4.

The MINLP optimization problem is stated as follow:

Given: Seawater feed source with different salt contents and temperatures, design specifications of each membrane element, fixed amount of fresh water demand, maximum salt concentration in fresh water.

Optimize: The number of stages, the number of parallel membrane module in each stage, the inter-connections between different streams and equipment, operating conditions (feed flow rate, feed pressure, pressure inlet to second stage, etc.).

So as to minimize: Total annualized cost of fresh water

Subject to: Process constraints: Equality constraints such as process model and inequality constraints such as optimization variables bounds.

Mathematically the optimization problem can be described as:

Minimize	TAC
$P_f, Q_f, S, N_j, N_{pu}, N_{tu}, BY, R$	
Subject to:	Equality constraints Model equations
	Product demand and product quality
Inequality constraints (Control Variables)	(50 bar) $P_f^L \leq P_f \leq P_f^U$ (92 bar)
	(1 m ³ /h) $Q_f^L \leq Q_f \leq Q_f^U$ (2 m ³ /h)
	$1 \leq N_{pu} \leq S ; 1 \leq N_{tu} \leq S ; 0 \leq BY \leq 1 ; 0 \leq R \leq 1$

P_f, Q_f, BY and R are continuous variables and represent feed pressure, feed flow, brine bypass fraction and brine recycle fraction, respectively. S, N_j, N_{pu} and N_{tu} are integer parameters representing number of stages, number of hollow fiber modules in each stage, number of pumps and number of turbines. The subscripts U and L denote the upper and lower bounds of the parameter, respectively.

It is to be noted again that most of the previous researchers optimized the RO process design for fixed feed temperature and did not consider the effects of the seasonal variation in seawater temperature on the RO design and operation. This will be the main focus of this Chapter.

4.5 Case Study

4.5.1 Specifications

The suggested MINLP optimization problem formulation was applied for the desalination process where the optimal structural and operational parameters of RO process were found at given water demand (520 m³/day) and maximum salt concentration in the desalinated water (500 ppm). The membrane modules considered in this case study are DuPont B-10 hollow fiber RO modules. It is assumed that the

membrane module life is 5 years (Lu et al., 2006). The characteristics of hollow fiber module and the parameters used in optimization calculation are listed in Table 4.3 and Table 4.4, respectively.

4.5.2 Results

The optimal operation and configuration of the RO system are displayed in Table 4.5. The range of salt concentration in the feed stream is adopted from Marcovecchio et al. (2005) and Voros et al. (1997) where salt concentration in the feed stream is escalating from a low salinity to an extreme salt content as high as 50,000 ppm. Five different feed concentrations (15,000 to 50,000 ppm) and a set of feed temperatures (ranging from 15°C to 40°C) representing the seasonal variation of seawater temperature are considered in this study.

Table 4.3 DuPont hollow fibre RO modules specifications (Lu et al., 2006)

Property	Value
Fibre length (m)	0.75
Outer radius of fibre (m)	50×10^{-6}
Inner radius of fibre (m)	21×10^{-6}
inner radius of the fibre bundle (m)	1.27×10^{-2}
outer radius of the fibre bundle (m)	5.334×10^{-2}
Water permeability at T_o (m/s)	4×10^{-9}
Salt permeability at T_o (m/bar.s)	3×10^{-8}
Module Feed flow range(m ³ /h)	1-2
Membrane module area (m ²)	152
Pressure drop per module (bar)	0.2
Module operating pressure range (bar)	50-92

Table 4.4 Input data for MINLP optimization

	Value	Reference
Feed pump efficiency (%)	75	Lu et al. (2007)
Turbine efficiency (%)	80	Marcovecchio et al. (2005)
Reference temperature T_o (°C)	25	Lu et al. (2006)
Load factor	0.9	Marcovecchio et al. (2005)
Membrane unit cost (\$)	800	Lu et al. (2006)
Module vessel cost (\$)	200	Lu et al. (2006)
Electricity unit cost (\$/kWh)	0.08	Lu et al. (2006)

Table 4.5 reveals that the brine recycling has not been favoured for any cases. This is due to the fact that the mixing of streams is only allowed for the streams with equal pressure. For any feed salinity (e.g. 35,000 ppm), there is no significant influence of the feed temperature on the unit cost of the optimum RO network. However, for any seawater temperature, the unit cost increases significantly with feed salinity. For example, at 20°C the unit cost at 50,000 ppm salinity is more than double the unit cost at 15,000 ppm salinity. The optimal RO operation is strongly dependent on the feed temperature and feed salinity.

At higher feed salinity and at higher seawater temperature, the optimum RO network structure changes from two stages to one stage with or without bypass and inter-stage pump. Increases in feed temperature results in the increase of permeate flux (Nisan et al., 2005). This effect is dominated in most cases. With increasing feed temperature the required feed pressure decreases significantly with some decrease in the number of the elements. As a result, the production unit cost has decreased despite that the overall system recovery ratio decreased. At higher temperatures, there is both increased water flux and increased salt passage through the membrane.

The impact of these effects on the RO design must be carefully considered in analysing the optimization results at different temperatures. For low and medium seawater

concentrations (15,000–35,000 ppm), the required feed pressure and the unit product cost are inversely proportional of the feed temperature. The water quality constraint is easily realized in this range of feed concentrations. Due to the relatively low salt concentrations in the feed stream, the simple two-stage RO systems without brine bypass or recycle is favoured (Figure 4.3a) for most temperatures. The optimal RO structure for feed concentration 35,000 ppm and 40 °C is two-stage RO network with inter-stage pump and including brine bypass as shown in Figure 4.3b. It is obvious that with increasing feed temperature, pumping and bypass part of brine coming from first stage is necessary to maintain the desired water quality.

For feed salinity of 45,000 ppm, the optimal configuration identified for the RO network design is strongly dependent on the feed temperature. The optimal structure for each individual temperature is quite different. For temperatures ranging from 15°C to 25°C, the simple two-staged networks are favoured (Figure 4.3a).

For higher temperature (30°C), this optimal two-stage design for lower temperature is significantly modified. The brine coming from stage 1 is pressurized and bypasses part of this brine to reduce the amount of salts entering second stage as shown in Figure 4.3b. The unit production cost is increased to maintain water quality requirements. Also, for the same reason, the second stage feed pressure hits the upper bound (92 bar). Only one RO-stage scheme (Figure 4.3d) has been identified as the two-stage structures could not achieve the product quality specifications for higher seawater temperatures (35°C, 40°C).

Table 4.5 MINLP optimization results

T (°C)	Optimum layout	Water recovery (%)	Feed pressure (bar)	Booster pump pressure (bar)	permeate conc. from 1st stage (ppm)	permeate conc. from 2nd stage (ppm)	Average permeate conc. (ppm)	No. of modules in 1st stage	No. of modules in 2nd stage	Total No. of modules	Brine entering 2nd stage (%)	Product unit cost (\$/m ³)
<i>Case 1: Feed conc. 15,000 ppm</i>												
15	Fig. 4.3a	64.14	59.43	-	62	136	92	34	18	52	100	0.530
20	Fig. 4.3a	65.42	58.68	-	92	213	138	33	17	50	100	0.517
25	Fig. 4.3a	66.45	57.72	-	130	315	199	33	16	49	100	0.505
30	Fig. 4.3a	66.14	55.40	-	173	432	266	33	16	49	100	0.497
35	Fig. 4.3a	66.20	54.28	-	225	570	346	33	15	48	100	0.490
40	Fig. 4.3a	66.68	53.11	-	285	784	449	33	15	48	100	0.481
<i>Case 2: Feed conc. 25,000 ppm</i>												
15	Fig. 4.3a	62.65	78.40	-	104	255	158	35	18	53	100	0.634
20	Fig. 4.3a	63.00	78.21	-	153	378	232	34	16	50	100	0.627
25	Fig. 4.3a	62.74	76.99	-	187	522	297	30	18	48	100	0.620
30	Fig. 4.3a	63.13	77.50	-	225	680	369	27	18	45	100	0.616
35	Fig. 4.3a	61.48	73.53	-	285	875	466	27	19	46	100	0.610
40	Fig. 4.3a	62.50	76.72	-	287	1000	495	21	19	40	100	0.610
<i>Case 3: Feed conc. 35,000 ppm</i>												
15	Fig. 4.3a	58.81	91.635	-	145	378	223	37	20	57	100	0.740
20	Fig. 4.3a	59.24	91.32	-	218	593	340	37	19	56	100	0.731
25	Fig. 4.3a	59.27	90.30	-	304	875	478	37	19	56	100	0.727
30	Fig. 4.3a	58.10	90.35	-	305	973	500	28	21	49	100	0.729
35	Fig. 4.3a	56.32	89.86	-	297	997	500	21	21	42	100	0.737
40	Fig. 4.3b	45.29	77.4	92.00	390	629	500	25	11	36	70	0.774
<i>Case 4: Feed conc. 45,000 ppm</i>												
15	Fig. 4.3a	48.88	92.00	-	192	451	281	43	25	68	100	0.873
20	Fig. 4.3a	49.71	91.8	-	294	772	445	44	26	70	100	0.861
25	Fig. 4.3a	48.70	92	-	315	934	500	33	29	62	100	0.866
30	Fig. 4.3b	37.72	64.05	92	528	479	500	31	29	60	95	0.887
35	Fig. 4.3d	35.64	91.2	-	500	-	500	42	-	42	-	1.082
40	Fig. 4.3d	32.31	92.00	-	500	-	500	34	-	34	-	1.170
<i>Case 5: Feed conc. 50,000 ppm</i>												
15	Fig. 4.3c	44.89	92.00	-	231	562	340	49	31	80	98	0.947
20	Fig. 4.3c	44.69	91.87	-	329	861	495	47	31	78	96	0.945
25	Fig. 4.3c	39.84	92.00	-	375	705	500	41	17	58	91	1.006
30	Fig. 4.3d	32.49	92.00	-	500	-	500	51	-	51	-	1.190
35	Fig. 4.3d	28.09	92.00	-	500	-	500	40	-	40	-	1.340

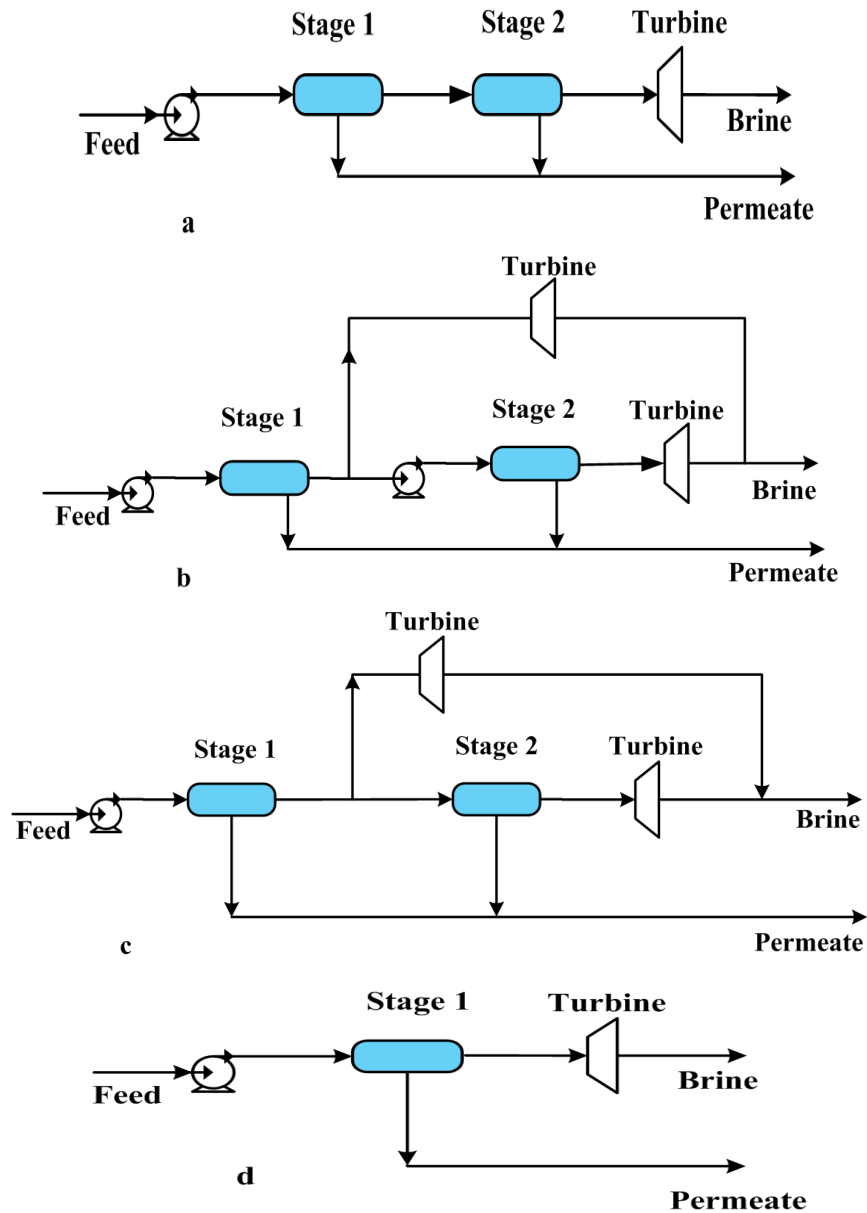


Figure 4.3 Optimum RO networks

For case 5 (feed concentrations is 50,000 ppm), two-stage tapered staging configuration with brine bypass is selected (Figure 4.3c) for feed temperatures 15°C and 25°C. With increasing feed temperature from 15°C to 25°C, it is crucial to increase the operating pressure up to the upper bound to maintain the required salt concentration in the fresh water while the total number of membrane modules and brine flow rate entering second stage were reduced. Despite that, the unit cost is almost unaffected (Table 4.5). This clearly showed that how the optimization becomes a trade-off between the design and the operating variables of the RO network and keeping the production cost as minimum

as possible to ensure an economic design. For higher temperatures (30°C, 35°C), the simple one stage structure is favoured (Figure 4.3d), since two-stage system could not fulfil the required quality of water. In this high range of feed concentration and temperature, the operating pressure hits the upper bound, and feed flow is also increased in order to realize the required water quality. Increased feed temperature to 40°C led to infeasible solution (do not satisfy the constraints).

The product cost results from the optimization of the superstructure and corresponding to various optimal structural configurations are graphically presented in Figure 4.4. Different feed salt concentrations and temperatures are considered to illustrate the effect of these parameters on the optimum design and operation of the RO process. The unit production cost is proportional to the feed concentration. This outcome is consistent with that reported by (Voros et al., 1997; Marcovecchio et al., 2005; Lu et al., 2007). Furthermore, due to the positive effect of the increasing feed temperature on water flux, the total annualized cost decreases with increasing feed temperature until certain point as shown in Figure 4.4 where the product salt concentration reached the maximum allowable limit. After that, the product cost starts to increase as a result of different operating conditions and/or RO structures adopted in order to achieve the required product salinity.

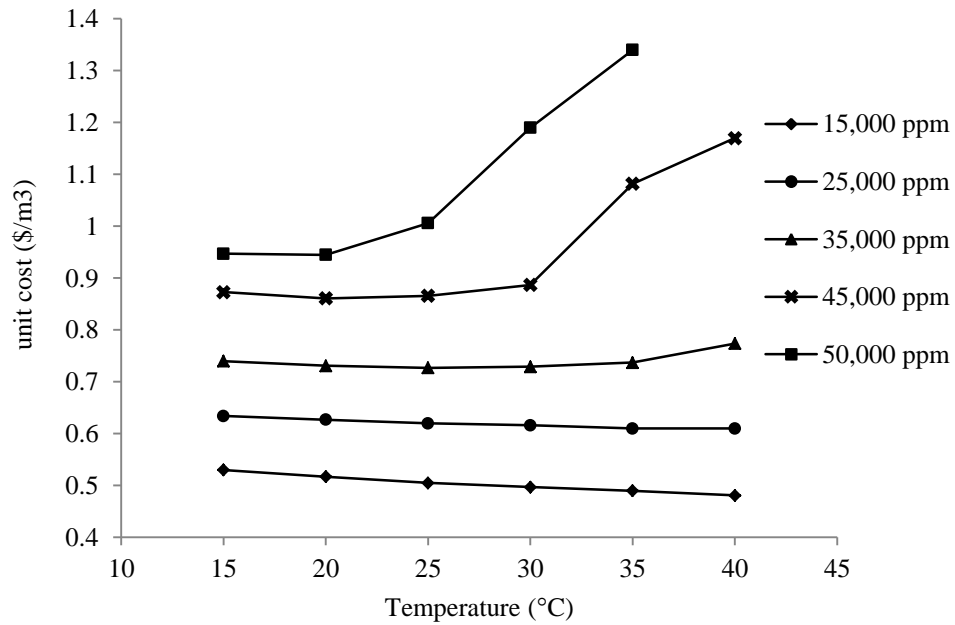


Figure 4.4 Unit costs for the optimal RO networks as a function of temperature at different feed salinity

4.5.3 Maintenance Scheduling

It has been suggested that the RO network could be designed by identifying the number of required membrane maintenance schedules (Zhu et al., 1997). This means the membrane modules can be divided into a number of groups to facilitate the membrane cleaning without complete shutdown of the plant. Based on this approach, the results for the cases 1-3 in Table 4.5 show that, for first stage the RO operation requires more membrane modules in winter than in summer. However, for second stage needs less number of membrane modules for the operation in winter season compared with that in summer season irrespective of the operation condition and system layout adopted for each case. This will allow flexible scheduling for cleaning and maintenance of the membrane modules without interrupting the production of water or fully shutting down the plant. For instance for feed salinity 35,000 ppm, the number of membrane modules utilized in winter (20°C) and summer (35°C) seasons in first stage are 37 and 21 modules, respectively and in second stage 19 and 21 modules, respectively. Based on

these findings, one can conclude that considering the seawater seasonal variation in RO network design can offer flexible scheduling for cleaning and maintenance of the membrane modules without interrupting the production of water or fully shutting down the plant.

For higher salt content range (45,000 ppm and 50,000 ppm), the difficulty of realizing salt content constraint in the final permeate stream forced the optimizer to adopt various layout for each feed temperature (Table 4.5). Therefore, the flexible scheduling of cleaning and maintenance which presented previously for low and medium salt concentrations is not applicable here.

4.6 Conclusion

In this work, the synthesis of RO networks for water desalination, based on an MINLP optimization framework developed in earlier chapter, is investigated. A superstructure, based on two-stage RO systems and incorporates all feasible design alternatives was developed. The RO optimization design problem has been formulated as MINLP problem which was optimizing design and operating parameters while minimizing the total annualized cost of the RO network. The MINLP model showed the ability of handling the trade-offs between optimizing parameters (design and operating variables) and costs for different feasible process alternatives. The feasibility of the optimal design strategy is investigated by considering hollow fibre element as a case study. The total annualized cost for the optimum desalination RO network was less by 4 % compared with that published in the literature. Then, several RO designs and operation conditions were obtained using the MINLP framework for different feed water concentrations and including seasonal variation of seawater temperature. The optimal RO structures vary from one stage to two-stages with and without brine bypass and inter-stage pump. For most cases, the unit production cost of the optimum RO design is fairly decreased as feed temperature increased. For higher feed concentration and also high temperatures,

the unit cost is increased as feed temperature increase due to difficulty of maintaining water quality constraint. The study shows that the salt concentration constraint has a tremendous impact in the RO plant design, especially for high salt concentrations and high temperatures water resources. Also the results demonstrate that the variation in the number of modules required for the operation of RO process in high and low temperature seasons offers the possibility of flexible scheduling of cleaning and maintenance of membrane modules. The latter issue will be also investigated in next chapters (six and seven) for numerous design options and operation conditions with and without membrane fouling.

Chapter 5

Optimal Design of RO Desalination Process with Boron Removal

5.1 Introduction

Boron is essential micronutrient for the living creatures. Boron deficiency leads to negative impact on the growth of both human and plants. It may become toxic depending on the concentration and duration of exposure. Consequently it is important to produce low boron containing water from desalination plants to avoid the negative effects of boron.

In chapter four, the optimization of RO network including seasonal variation of sea temperature and for fixed freshwater demand have been studied using MINLP optimization approach based on two-stage RO superstructure presented in chapter three. In this chapter based also on optimization formulation in chapter three, two passes RO superstructure is considered in the MINLP formulation in order to cope with the WHO boron standards in drinking water, which need to be boron content lower than 0.5 ppm. The seasonal variation of sea temperature is also incorporated. The effect of membrane fouling on the rejection of boron by RO membranes is not included here.

A mathematical analysis tool for the estimation of boron rejection in RO desalination plants is developed based on solution diffusion model and thin film theory. The model was further modified to account for boron rejection by pH and temperature dependence of the model parameters.

A superstructure of the RO network for water desalination process is developed based on double pass RO network. The superstructure includes two passes: seawater (SW) pass contains normal two-stage RO system and housing seawater membrane modules. The second is brackish water pass (BW) accommodates brackish water membrane modules and includes one-stage brackish water desalination added to the RO configuration in order to enhance the boron removal process. An MINLP optimization

formulation is developed based on the superstructure for fixed fresh water demand to determine the optimal design of RO network which sustain boron concentration below the maximum limit.

5.2 Discussion on Boron

5.2.1 Occurrence and Toxicity

Boron is commonly found in the nature in various forms of complex compounds. The average boron concentration in earth crust is from 1 to 500 mg/kg (Aubert and Pinta, 1977) but there is a significant difference in the occurrence of boron mainly due to the nature of the earth.

The majority of boron abundance in the earth normally occurs in the seawater and ocean. The presence of boron in water is usually as a result of natural weathering of rocks and soils where boron may be mobilized into aqueous environments (Magara et al., 1998).

The concentration of boron in seawater varies widely, generally ranging from about 1 to 10 mg/l with an average level of 5 mg/l depending on location, weather conditions, and the level of industrial activity. For example, boron concentration in the Mediterranean Sea and in Arabian Gulf is about 9.6 and 7 mg/l, respectively (Argust, 1998). Boric acid is the dominant form of boron in seawater at normal pH level (7.9 - 8.2) (Sagiv and Semiat, 2004). Groundwater is far more likely to contain low levels of boron than surface water.

Boron plays a vital role as a micronutrient for the plants growth. The concentration of boron observed by the plants in irrigation water or in soils plays a critical role in some metabolic activities (Howe, 1998). There are a number of studies showing that a sufficient supply of boron is essential for the functioning of many biochemical processes for human and animals (Hunt, 2003). However, Boron may become toxic

depending on the concentration and duration of exposure. The margin between boron deficiency and excess is typically narrow.

Many studies illustrate these adverse effects of boron on plants including reduced rate of root, shoot growth and ultimately plant expiration (Hilal et al., 2011). Boron effect on human and animals is still not well understood as was done for plants (Kabay et al., 2010). Exposure to high concentrations of boron may cause toxicity for humans include nausea, vomiting, diarrhea, dermatitis, weight loss, and decreased sexual activity (Tu et al., 2011).

5.2.2 Boron Standards in Drinking Water

Recently boron has been classified as a pollutant of drinking water in national and international drinking water regulations (WHO Guidelines for Drinking-water Quality Fourth Edition: 0.5 mg/l, EU Directive 98/83/EC: 1 mg/l) (Bouguerra et al., 2008).

Table 5.1 summarizes the boron standards and guidelines of drinking water.

Currently WHO guideline value is under revision and boron tolerance is being relaxed to a higher limit of 2.4 mg/ L for the year 2011 (WHO, 2011). In this context Water Desalination Report (2010) reported “Although the new guideline value is based on a human health perspective, some utilities may set seawater desalination plants product water limits as low as 0.5 mg/L to reflect agricultural related issues. These issues include boron's herbicidal effect on some plant species, which is a particular concern in areas of low rainfall” (Kabay et al., 2010). Based on this argument, boron removal from fresh water, to a safe level for plants, remained an essential step especially in the Middle East where desalinated water is frequently used for cultivation. Therefore, in this work boron content limit is kept below 0.5 ppm.

Table 5.1 Regulations for boron in drinking water (Tu et al., 2010)

Region	Maximum boron concentration (mg/L)	Regulation issued year
European Union (EU)	1.0	1998
Canada	0.5	2003
New Zealand	1.4	2000
Australia	4.0	2004
Israel	0.3	2004
Singapore	1.0	2001
Abu Dhabi	1.5	2001
U. S. A. (California)	1.5	2001
Japan	1.5	2000
WHO recommendation	0.3	1990
	0.5	1998
	2.4	2011

5.2.3 Boron in Seawater Chemistry

The elemental form of boron is unstable in nature, but it is often found in combination with oxygen forming a variety of boron compounds as boron salts and acids (Ross and Edwards, 1967).

The chemistry of boron and its compound is unique. At pH ranging from 7 to 8 of most waters used in desalination, boron is predominantly in the form of boric acid as shown in Figure 5.1. At this pH range, the percentage of the non-dissociated species is between 99.3 (pH 7) and 93.2% (pH 8) of total boron (Redondo et al., 2003). Boric acid ($B(OH)_3$) acts as a weak acid and the dissociation of boric acid occurs only via a hydrolysis process:



The value of the dissociation constant of boric acid pK_a has vital role in the distribution of two components, boric acid and borate ion. pK_a value depends on several factors including salinity, pressure, and temperature in addition to pH number. For instance, it

was reported that the pKa of boric acid would decrease from 9.23 to 8.60, when the salinity increased from 0 to 40,000 ppm while the constant decreases by 0.3 unit when the temperature increased from 10°C to 50°C (Tu et al., 2010).

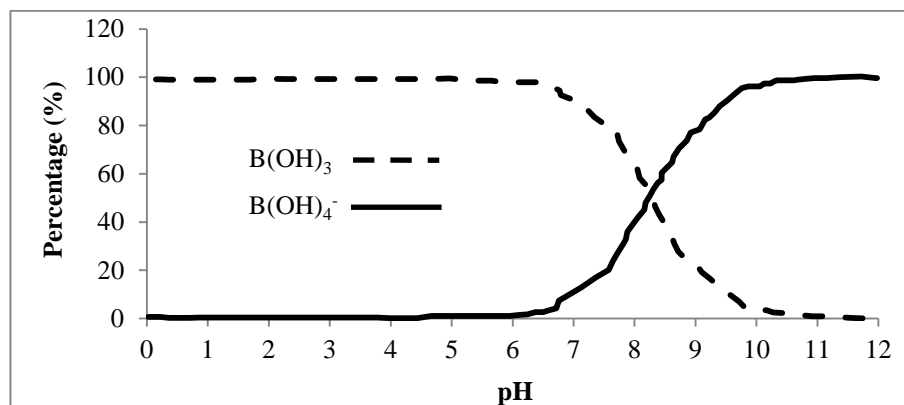


Figure 5.1 Distribution of boric acid and borate in seawater at different pH (at temperature=25 °C, salinity=35,000 ppm, pressure=1 atm) (Hilal et al., 2011)

5.3 Boron Removal by Reverse Osmosis

There are several alternative processes for boron removal from waters has been developed to avoid the boron toxicity including softening, coagulation, electrodialysis, activated carbon and RO membranes (Kabay et al., 2010).

During RO desalination process, some traces of boron present in the final permeate unlike thermal desalination process where boron is removed to nearly zero level (Hilal et al., 2011). Boron rejection by RO is highly depended on the boric acid/borate ion ratio which is mainly function of seawater pH. For example, the rejection of boric acid is between 40 and 60% at pH ranges of 5.5–9.5, and for the same pH range, the rejection of borates reached 90% (Prats et al., 2000).

The configuration of RO process for boron removal depends on several factors, such as feed water characteristics and product water standards (Greenlee et al., 2009). In some cases a complicated RO system may be used to achieve the boron requirements where the boron concentration in permeate set to be lower than 0.4 mg/L such as in Ashkelon, Israel (Gorenflo, et al., 2007).

Different design patterns have been developed to reduce the concentration of boron in RO permeate and fulfil boron standards in drinking water. Several authors have discussed the design concepts for boron removal from RO permeate (Redondo et al., 2003; Tu et al., 2010; Kabay et al., 2010; Hilal et al., 2011). The typical methods used in RO desalination plants for boron removal are summarised in Figure 5.2.

Generally, due to high salinity of seawater, pH is only increased in second and third pass where the feed is the desalinated RO permeate to avoid scale formation (Gluechstren and Priel, 2003). Therefore, the brackish water RO membranes are used in the second pass to save energy and also to maximize the recovery (Tu et al., 2010).

However, some research studies have indicated that the cascade design has several advantages over the two pass system (Hilal et al., 2011), although two pass systems still have comparatively lower cost and can achieve acceptable level of boron rejection (Table 5.2). Therefore, two pass RO system with/without pH changes is chosen in this study for boron removal from RO permeate.

There are many experimental and theoretical studies on boron removal by RO systems (Prats et al., 2000; Taniguchi et al., 2001; Sagiv and Semiat, 2004; Dydo et al., 2005; Hyung and Kim, 2006; Gorenflo et al., 2007; Mane et al., 2009; Tu et al., 2010). However, there are no studies that investigate the detailed design of RO systems that can respond to different operation and design variables.

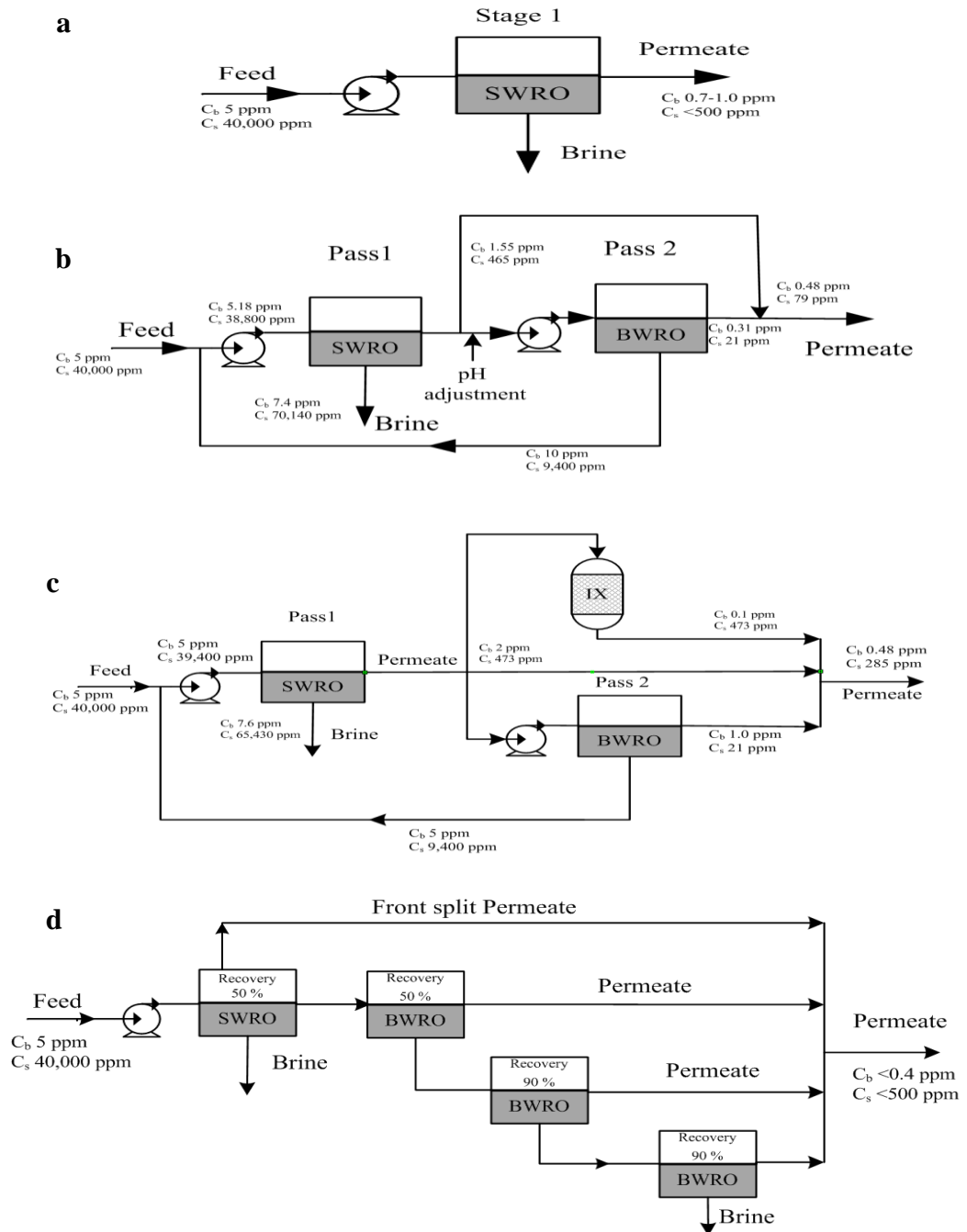


Figure 5.2 Schematic drawings of (a) one pass design (b) the two pass design (c) hybrid design and (d) Cascade design. Modified from (a) (Hilal et al., 2011), (b) and (c) (Jacob, 2007), (d) (Tu et al., 2010)

Table 5.2 RO seawater desalination process for Boron removal (Hilal et al., 2011)
(Feed concentration 4–6.3 mg/L and temperature 18–34 °C)

	pH adjustment	Cost (\$/m³)	Target boron (mg/l)	Configuration
One pass SWRO	No	0.38–0.52	0.8–1.0	Fig. 5.2a
Two pass SWRO	Yes	0.45–0.55	0.4–0.5	Fig. 5.2b
Two pass with BSR (hybrid design)	Yes	0.5–0.55	0.4–0.5	Fig. 5.2c
Cascade design	Yes	0.47–0.52	Less than 0.4	Fig. 5.2d

5.4 Mathematical Model for Boron Rejection by RO

Both solute ions and molecules are transported through the membrane by different mechanisms. These solutes are described using the existing models in the literature. Boron is commonly found in the boric acid and borate salts forms which are essentially typical solutes. Therefore, most of the existing models can be used to illustrate boron rejection phenomena (Tu et al., 2010).

Both irreversible thermodynamic models of Kedem and Katchalsky and the mechanistic models such as the solution-diffusion model are capable for simple and effective representation of the separation process (Tu et al., 2010). These two model types are the most used in boron rejection illustration as shown in Table 2.6. Solution diffusion model is one of the most widely accepted for predicting membrane separation performance (Wijmans and Baker, 1995). And also to have a consensual with the other chapters of this thesis; solution diffusion model will be used to describe boron rejection by RO membranes.

According to the solution–diffusion model, transport of boron across an RO membrane can be expressed as (Taniguchi et al., 2001):

$$j_b^T = A_b^T (C_{m,b} - C_{p,b}) \quad (5.2)$$

Where j_b^T J and A_b^T are flux and permeability of the boron. $C_{p,b}$ and $C_{m,b}$ are the boron concentrations in the permeate and in the feed side of the membrane surface.

The concentration of boron near the membrane surface is different from that in the bulk phase due to concentration polarization. The concentration of boron at the membrane surface $C_{m,b}$ can be derived from the film theory (Section 3.2.1) as follows (Taniguchi et al., 2001; Sagiv and Semiat, 2004):

$$\frac{C_{m,b} - C_{p,b}}{C_{B,b} - C_{p,b}} = \exp\left(\frac{j_w^T}{k_b}\right) \quad (5.3)$$

Where the concentration $C_{B,b}$ is for the boron bulk in the feed side. j_w in equation (5.3) is the pure water flux through the membrane and k_b is for the boron mass transfer coefficient.

The following relationships for permeability and mass transfer coefficient of boron were given by (Taniguchi et al., 2001), and were used in boron rejection modelling for several cases in Sagiv and Semiat, (2004):

Boron permeability

$$A_b^T = 94.3A_s^T \quad (5.4)$$

Mass transfer for boron

$$k = 0.97k_b \quad (5.5)$$

The boron concentration in permeate can be expressed as:

$$C_{p,b} = \frac{J_b^T}{J_w^T} \quad (5.6)$$

Mass balance equation around the spiral wound element is given as:

$$Q_f C_{f,b} = Q_r C_{r,b} + Q_p C_{p,b} \quad (5.7)$$

The total boron rejection for the RO process, which is the measure of the boron removal, is defined as:

$$SR_b = \frac{C_{f,b} - C_{p,b}}{C_{f,b}} 100 \quad (5.8)$$

Temperature has significant effect on the permeation properties of the membrane. This effect is included empirically in the relationship between feed temperature and membrane boron permeability similar to that for salt permeability (Sarkar et al., 2008):

$$A_b^T = A_b^{T_o} \frac{\mu^{T_o}}{\mu^T} \frac{T_o}{T} \quad (5.9)$$

5.4.1 Effect of pH on Boron Permeability

Boron rejection by the RO membrane would improve as pH increased, therefore boron permeability are enhanced by increasing pH of BW pass feed by caustic injection and neutralize by acid injection after BW pass. It is to be noted that elevation of solution pH has only been used in the second pass, after adequate removal of salts in the first pass to eliminate the risk of membrane scaling at high pH.

The observed pH dependence was quantitatively analysed by considering that the overall permeability was function of solution pH. Consequently, data was adopted from (Chillon Arias et al., 2011b) to predict the effect of solution pH on boron permeability constant (pH_f) for brackish water membrane (Filmtec BW30 4040). This data is fitted as:

$$pH_f = 0.99126 pH - 0.18980 pH^2 + 0.0090686 pH^3 \quad (5.10)$$

Figure 5.3 shows the actual data from Chillon Arias et al. (2011b) and the calculated values from the above equation. It can be seen from the Figure that there is a good fit of the predicted boron permeability constant to the Chillon Arias et al. (2011b) data.

When the feed to BW pass is adjusted, the boron permeability in equation (5.2) becomes as:

$$A_{b,pH}(T) = A_b(T) pH_f \quad (5.11)$$

$A_{b,pH}(T)$ will be used instead of $A_b(T)$ in case of pH adjustment.

A superstructure of the RO network for water desalination process is developed based on double pass RO as shown in Figure 5.4. The RO superstructure comprised mainly of two parts: SW represent first pass contains two-stage RO system and BW includes the second pass containing one stage brackish water desalination which is added to the RO configuration in order to enhance the boron removal process. The SW pass is mainly used to reduce salt content in permeate using high pressure seawater RO membranes. Therefore, low pressure RO membranes (brackish water membranes) can be used in the second pass (BW) to save energy and to allow for a high recovery (Tu et al., 2010). In order to increase the boron rejection by BW pass, the operation to increase pH is done. The two passes are connected in series where the permeate output from SW pass becomes feed to BW pass.

The mathematical programming model which describes the RO network (both SW and BW passes) was developed based on this superstructure. The mathematical formulation in chapter three (Section 3.3.3) is used to describe SW pass. The same mathematical equations can be used for BW pass. The binary variables B_j , B_{pu} and B_{tu} are associated with the existence or non-existence of the second stage, booster pump prior to second stage and turbine prior and/or after second stage of SW pass. To eliminate the second stage from the general superstructure, simply set all of these binary variables to zero. The resulting equations will represent one-stage RO network which can used to model BW pass network. The two sets of equations which used to describe SW pass and BW pass are combined and used to describe the general superstructure in Figure 5.4. The boron balance in both SW and BW passes are employed in the same way for salt balance.

Mass balance relationship of boron around the membrane element

$$Q_f C_{f,b} = Q_r C_{r,b} + Q_p C_{p,b} \quad (5.13)$$

Overall mass balance around (SW or BW passes)

$$Q_{p,t} C_{p,b,t} = \sum_{j=1}^S \sum_{i=1}^{N_j} Q_{p,i,j} C_{p,b,i,j} B_j \quad (5.14)$$

The overall water, salt and boron balances constraints for the general RO network are added to the mathematical formulation to estimate the properties of the streams leaving or entering RO network as:

The overall permeate volume balance

$$Q_{p,G} = Q_{p,t,SW} BY^{BW} + Q_{p,t,BW} \quad (5.15)$$

The overall balance of salt in permeate

$$Q_{p,G} C_{p,G} = Q_{p,t,SW} C_{p,t,SW} BY^{BW} + Q_{p,t,BW} C_{p,t,BW} \quad (5.16)$$

Where $Q_{p,G}$, $C_{p,G}$ are flow rate and salinity of the final permeate stream. The subscript SW and BW are denoted to the SW and BW passes respectively. BY^{BW} is the bypass fraction around BW pass. Note that the mixing of different streams is assumed isobaric-mixing since only streams with equal pressures can be mixed. This criterion is watched when constructing the superstructure. A constraint is added to the set of constraints shown in chapter three (Section 3.3.3) to maintain the required boron concentration in the final permeate stream.

$$C_{p,b,avg} \leq C_{p,b,avg}^{\max} \quad (5.17)$$

5.5.2 MINLP Problem Formulation

An MINLP optimization framework is developed to determine the optimal design of RO network based on the superstructure given in Figure 5.4. A set of binary variables with a value of [0, 1] are introduced to account for the existence or non-existence of different structural units.

The proposed MINLP optimization approach generates various structures and design alternatives that are all candidates for optimal solution. The formulation of the optimization problem enables the optimizer to identify the design with two stages or only one RO stage for SW pass while BW contains only one stage.

For RO network with fixed fresh water production and constrained with maximum salt and boron concentrations in the final permeate, the superstructure allows every possible connection between the process units including splitting the feed /brine streams for two-stage RO process in SW pass as well as bypass part of the feed flow to BW pass. Continuous variables are defined for the optimization of operating parameters and discrete variables are used to express discrete decisions such as the existence of process units. The MINLP problem is solved within gPROMS software which implements the outer approximation algorithm.

The MINLP problem is expressed as:

Given: Seawater feed source with variable temperature; design specifications of each membrane element (SW and BW membranes); fixed fresh water demand; maximum salt and boron concentration in fresh water.

Optimize: The number of stages in SW pass; the number of parallel membrane module in each stage in both SW and BW passes; the inter-connections between different streams and equipment; operating conditions (feed flow rate, feed pressure, pressure inlet to second stage, etc.).

So as to minimize: Total annualized cost of fresh water

Subject to: Process constraints: Equality constraints such as process model and inequality constraints such as optimization variables bounds.

Mathematically the optimization problem can be described as:

Minimize TAC

$P_f, Q_f, S, N_{j,SW}, N_{j,BW}, N_{pu}, N_{tu}, BY, R, BY^{BW}$

Subject to: Equality constraints Model equations

Product demand and product quality

$$\begin{aligned}
\text{Inequality constraints} \quad & P_{f,SW}^L \leq P_{f,SW} \leq P_{f,SW}^U ; Q_{f,SW}^L \leq Q_{f,SW} \leq Q_{f,SW}^U ; \\
& P_{f,BW}^L \leq P_{f,BW} \leq P_{f,BW}^U ; Q_{f,BW}^L \leq Q_{f,BW} \leq Q_{f,BW}^U ; \\
& 1 \leq N_{pu} \leq S ; 1 \leq N_{tu} \leq S ; 0 \leq BY \leq 1 ; \\
& 0 \leq BY^{BW} \leq 1 ; 7 \leq pH \leq 10
\end{aligned}$$

P_f , Q_f , BY and R are continuous variables and represent feed pressure, feed flow, brine bypass fraction and brine recycle fraction respectively. The subscript SW denoted to SW pass and BW refer to BW pass. S , $N_{j,SW}$; $N_{j,BW}$; N_{pu} and N_{tu} are integer parameters representing number of stages, number of modules in each stage in SW and BW passes, number of pumps and number of turbines in SW pass, respectively. The subscripts U and L denote the upper and lower bounds of the parameter, respectively. pH of the feed to BW pass is added to control variables when the chemical is injected to the feed stream to adjust feed pH.

5.5.3 Cost Function

The objective function of the model is a sum of capital and operating costs resulting from the process changes configuration and operation conditions. The costs associated with the superstructure in Figure 5.4 include the sum of the annualized costs for SW and BW passes for every candidate configuration. The proposed objective function is presented as:

$$TAC = (C_{WPT} + C_{pu} + C_{ERD} + C_{me})1.411 \times 0.08 + OC_{pu} + OC_{me} + OC_{ch} + OC_{sc} + OC_{reag} \quad (5.18)$$

The total annualized cost is a combination of the capital and operating costs for one year of operation. The electrical power consumed by the feed pump of SW and BW passes and recovered by the turbine from the brine can be expressed in (kw) as:

$$E_{pu} = \sum^{for\ SW} \frac{\Delta P_{HP,pu} Q_{HP,pu}}{36 \eta_{pu}} + \sum^{for\ BW} \frac{\Delta P_{HP,pu} Q_{HP,pu}}{36 \eta_{pu}} \quad (5.19)$$

It is to be noted that for BW pass only one pump is used. The electrical power recovered by the turbine from the brine outlet from SW pass can be expressed in (kw) as:

$$E_{t,recv} = \sum_{for\ SW} \frac{\Delta P_{HP,tu} Q_{HP,tu} \eta_{tu}}{36} \quad (5.20)$$

Energy consumption by feed pumps can be calculated as:

$$E_{tu} = E_{pu} - E_{t,recv} \quad (5.21)$$

The cost of increasing the pH in the BW pass by caustic soda and also acid cost used to neutralize the BW pass discharge are expressed as:

$$OC_{reag} = \frac{CH_{cost}}{100} Q_{f,BW} l_f 24 \times 365 \times 1.28 \quad (5.22)$$

Where $Q_{f,BW}$ is the BW pass feed flow rate in (m³/h) and 1.28 is the exchange rate from Euro to USA \$ (Chillon Arias et al., 2011a). The cost equations in Section 3.3.4 will be used to calculate the costs C_{WIP} , OC_{ch} and OC_{sc} for SW pass only while the cost equations for C_{pu} , C_{ERD} , C_{me} , OC_{pu} and OC_{me} in Section 3.3.4 will also be used to estimate the costs for both SW and BW passes.

5.6 Case Study

The optimization problem presented in Section 5.5 is used here to optimize the configuration and operating parameters of RO process based on a superstructure (Figure 5.4) at a given fresh water demand while minimizing the total annualized cost. The characteristics of seawater module (SW30XLE-400) and brackish water module (BW30-400) used here are listed in Table 5.3. The input optimization parameters used here are presented in Table 5.4.

Five spiral wound modules are connected in series in each pressure vessel in SW pass and three spiral wound modules in BW pass.

The maximum allowable salt concentration in the final desalinated product stream is maintained at 500 ppm and the total water demand is about 80 m³/h. The boron concentration was kept below 0.5 ppm according to WHO boron drinking water standards (2008).

Table 5.3 The characteristics of spiral wound membranes (Lu et al., 2007)

Property	Element type	
	BW30-400	SW30XLE-400
Diameter of the element (m)	0.201	0.201
Feed space (mil)	34	28
Maximum operating pressure (bar)	41	83
Module Feed flow range (m ³ /h)	0.8–19	0.8–16
Membrane module area (m ²)	37	37.2
Water permeability (m/ bar s)	9.39×10^{-7}	3.5×10^{-7}
Salt permeability (m/s)	5.65×10^{-8}	3.2×10^{-8}

mil = 0.0254 mm

1

Table 5.4 Input data for MINLP optimization

	Value	Reference
Feed salinity (ppm)	35,000	
Feed boron concentration (ppm)	5.0	Jacob, (2007)
Turbine efficiency (%)	80	Marcovecchio et al., (2005)
Feed pump efficiency (%)	80	
Load factor	0.9	Marcovecchio et al., (2005)
Pressure vessel unit cost (\$)	1000	Lu et al., (2007)
Seawater module cost (\$)	1200	Lu et al., (2007)
Brackish water module cost (\$)	900	Lu et al., (2007)
Electricity unit cost (\$/kWh)	0.08	Lu et al., (2006)
Maximum operating pressure (bar)		
Sea water(SW)	83	Lu et al., (2007)
Brackish water (BW)	41	
Module Feed flow range (m ³ /h)		
Sea water(SW)	0.8-16	Lu et al., 2007
Brackish water (BW)	0.8-19	

5.7 Results

Two optimization problems were considered. In the first optimization problem, the optimal synthesis of RO networks that takes into account boron content constraint in the RO permeate is formulated as MINLP problem. In the second problem, elevation of pH of BW pass feed is incorporated in the MINLP design problem.

5.7.1 Case Study 1: Optimization of RO Design Without pH Adjustment

The boron rejection across the two passes RO process without pH increase (no chemical injection) was studied here. Table 5.5 shows the optimization results obtained for several cases, in which the feed temperature vary while the fresh water demand, permeate salinity and boron concentration constraints are maintained at a specified levels.

Table 5.5 MINLP results for seawater desalination considering boron limit in fresh water and without pH adjustment

	Seawater temperature (°C)			
	20	25	30	35
Optimum SW scheme	Fig. 5.5a	Fig. 5.5a	Fig. 5.5a	Fig. 5.5a
Boron conc. in final permeate (ppm)	0.6	0.6	0.8	1.0
Number of PV in 1 st stage	22	20	13	13
Number of PV in 2 nd stage	0	0	0	0
Feed pressure (bar)	79.3	82.8	83.0*	82.0
Feed flow (m ³ /h)	188	211	200	201
Inter-stage pump pressure (bar)	0	0	0	0
BW feed pressure (bar)	41.0*	38.2	41.0*	37.9
Number of PV in BW stage	6	6	5	5
BW Bypass (%)	6	3	4	3
Salt conc. outlet from SW (ppm)	216	244	226	290
Boron conc. outlet from SW (ppm)	1.80	1.95	1.88	2.17
Salt conc. outlet from BW (ppm)	1.0	1.0	1.5	2.34
Boron conc. outlet from BW (ppm)	0.50	0.54	0.75	0.96
Permeate flow from SW (m ³ /h)	99.8	111.6	96.0	97.2
Permeate flow from BW (m ³ /h)	78.8	76.7	76.2	77.1
Water recovery in SW (%)	53.0	52.7	47.8	48.3
Water recovery in BW (%)	74.5	71.3	82.6	81.9
Overall water recovery (%)	42.5	37.9	40.0	39.8
Unit cost (\$/m ³)	0.867	0.973	0.899	0.890

*Upper bound

The minimum level of boron removal which may be achieved by RO process was identified by solving the MINLP problem firstly at boron content constraint 0.5 ppm. If the MINLP solver in gPROMS failed to converge, a 0.1 ppm step change is added to boron concentration in the final permeate stream to facilitate the convergence of the optimization algorithm.

Figure 5.5a shows the layout of the global solution for RO network considering boron rejection without pH change. It can be seen that the optimization results in Table 5.5 are oriented to a section of the search region where the one stage process for SW pass in all feed temperatures is favoured. This can be easily related to the high boron concentration resulting from the second stage and the two-stage structures could not achieve the boron quality target.

It can be seen from Table 5.5 that the boron concentration limit increases with the increase of feed temperature. This result is compatible with analysis presented by Hyung and Kim (2006).

Increases in feed pressure results in the increase of boron rejection (Mane et al., 2009). This effect is clearly shown in Table 5.5. The feed pressures for SW and BW passes are in high level in an attempt to reduce boron content in permeate to the desired limit. For instance, the pressures for SW and BW passes at 30°C hit the upper bound (83 bar and 41 bar, respectively).

For the same boron limit (0.6 ppm), despite the positive effect of the increasing feed temperature on water flux (Nissan et al., 2008), the unit production cost for feed temperatures 20°C and 25°C are increased with the increase of feed temperature. Higher temperature enhances boron permeation through the membrane; therefore, higher cost is reported to achieve same boron content.

5.7.2 Case Study 2: Optimization of RO Design with pH Adjustment

The MINLP optimization case study presented here includes boron rejection by the two passes RO process with increased pH in the 2nd pass. Table 5.6 shows the optimal operation and configuration of RO systems for four different feed temperatures in the range from 20°C to 35°C. The maximum allowable boron concentration in the desalinated product is maintained at 0.5 ppm. In addition, pH of BW pass feed is allowed to vary between 7 and 10.

The optimal RO operation and structure shown in Table 5.6 are strongly dependent on the feed temperature as the RO network structures identified vary from one stage to two stages with bypass (Figures 5.5b,c). Due to relatively low boron permeation at low and medium seawater temperatures (20 to 30°C), the simple two-stage RO systems without brine bypass is favoured for SW pass (Figures 5.5b,c). For higher feed temperature (35 °C), the optimal structure changes to the single stage for SW pass (shown as Figure 5.5c).

The optimizer adopted different strategies to reduce the boron level in the final product stream. In Table 5.6, for temperatures 20°C and 30°C the feed pressure to BW pass hits the upper bound, and the bypass percentages are 7% and 4.3% for feed temperatures 20°C and 30°C respectively. Reduction in boron level in the desalinated water is achieved by bypass part of feed stream of BW pass. For seawater temperature 25°C, feed pressure of SW and BW passes remained in the high range (39.4 bar and 81.2 bar, respectively) and this is to maintain low product boron content in the both passes while the BW pass bypass percentage is reduced as low as 1.8%. On the other hand, the boron concentration meets the requirement (0.5 ppm) without bypass stream at feed temperature 35°C and with only one stage in SW pass, showing less operation flexibility in this high range of feed temperatures.

The optimization results in Table 5.6 suggested that boron rejection at higher temperatures demands higher pH values. Boron rejection was highly dependent on pH, especially near pH 9, and this dependency was more pronounced to maintain the lower boron permeability when operating temperatures were higher which represent unfavourable conditions for boron rejection.

Table 5.6 MINLP results for seawater desalination considering boron limit in fresh water and with pH adjustment

	Seawater temperature (°C)			
	20	25	30	35
Optimum SW scheme	Fig. 5.5b	Fig. 5.5b	Fig. 5.5b	Fig. 5.5c
Boron conc. in final permeate (ppm)	0.5	0.5	0.5	0.5
Number of PV in 1 st stage	11	12	12	19
Number of PV in 2 nd stage	6	9	8	0
Feed pressure (bar)	83*	81.2	76.1	79.0
Feed flow (m ³ /h)	165	165	174	177
Inter-stage pump pressure (bar)	0	0	0	0
BW feed pressure (bar)	41*	39.4	41*	39.07
Number of PV in BW stage	6	6	5	7
BW Bypass (%)	7	1.8	4.3	0
Salt conc. outlet from SW (ppm)	210	348	391	477
Boron conc. outlet from SW (ppm)	1.79	2.27	2.46	2.69
Salt conc. outlet from BW (ppm)	1.21	2.23	2.35	4.01
Boron conc. outlet from BW (ppm)	0.40	0.46	0.38	0.50
Permeate flow from SW (m ³ /h)	91.1	94.7	99.2	96.0
Permeate flow from BW (m ³ /h)	73.6	78.2	75.7	80.0
Water recovery in SW (%)	55	57	52	54
Water recovery in BW (%)	86	84	79	83
Overall water recovery (%)	48	48	46	45
pH feed to BW	8.82	8.98	9.17	9.35
Unit cost (\$/m ³)	0.814	0.850	0.953	1.000

*Upper bound

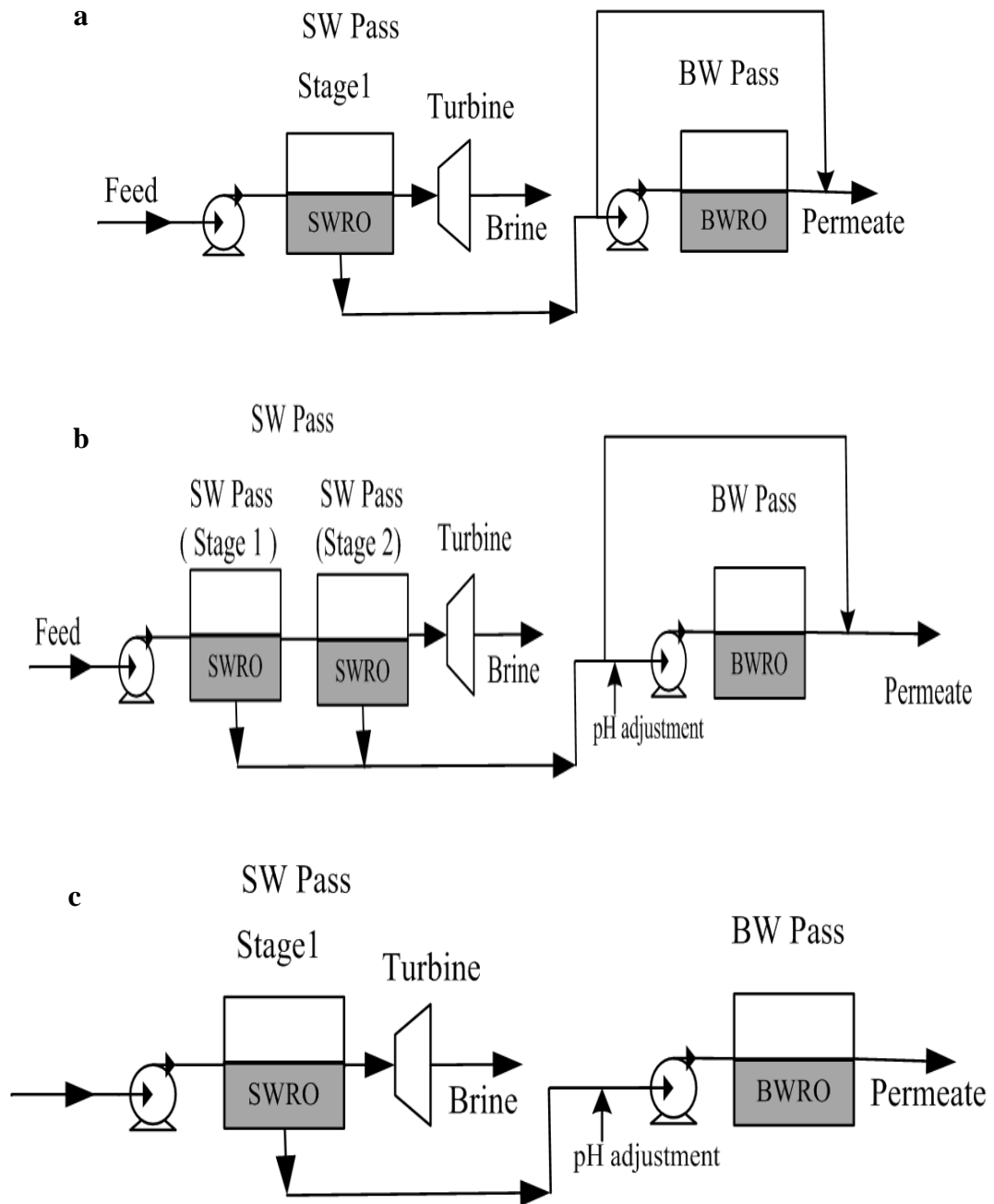


Figure 5.5 Optimum RO configurations for boron removal

A trade-off between the positive effect of increasing feed temperature on water flux and also the contribution of lower boron permeability at high pH and the extra cost needed to achieve the freshwater quality requirements lead to a result that the unit product cost is proportional to the feed temperature. When feed temperature increases, both salt and boron passage are increased (Table 5.6), the operation cost items are significantly

higher, particularly chemical cost (in terms BW pass feed pH) to achieve the required product quality, and as expected, leading to increased total annualized plant costs.

5.8 Conclusion

This chapter has presented a systematic methodology for the optimal design of RO desalination system which considering boron limit in the final permeate. A mathematical model was developed to simulate the boron rejection by RO spiral wound membrane element based on solution diffusion model and film theory. The effects of feed temperature and pH on boron rejection are incorporated in the simulation.

The RO design problem has been formulated as an MINLP problem based on double pass superstructure which minimizes the total annualized cost. For fixed water demand, the design of RO network problem was solved using gPROMS and constrained with maximum salt and boron concentration in the fresh water.

Two optimization problems were carried out to investigate the effect of pH on boron rejection at deferent seawater temperatures. The optimal RO structures vary from one stage to two-stages in SW pass with and without BW pass bypass. The MINLP optimization results suggest that the pH and seawater temperature are very important factors to consider for achieving a target level of boron rejection.

At natural seawater pH, the minimum level of boron removal has not achieved by RO process with SW and BW passes for all feed temperatures. pH elevation is required to satisfy the boron concentration constraint especially at high temperatures (higher temperature increases boron concentration in the fresh water).

Chapter 6

Optimal Operation of RO System with Daily Variation of Fresh Water Demand and Seawater Temperature

6.1 Introduction

Recently, substantial attention was given to RO processes operation optimization in order to enhance the RO process performance and reduce the energy consumption. The optimization of RO systems includes network design and the operating conditions. The RO operating conditions are subject to seawater temperature variation in different seasons and even throughout 24 h a day. This variation affects the RO process key performance parameters such as fresh water production and salinity. Therefore, short term optimization of RO process on the basis of 24 hours gives the operators of the RO plant high chance to respond effectively to the different operation variations.

In the analysis of the previous chapters, it was found that the design optimization problems were solved for fixed water demand and including seasonal variation of seawater temperature. Therefore, it was necessary to study the role of changing fresh water demand on the design and operation of RO process and also, the interaction with varying seawater temperature.

The optimal operation policy of flexible RO systems is studied in this work. The design and operation of RO process is optimized and controlled considering variations in water demands and with changing seawater temperature throughout the day. A storage tank is added to the system layout to provide additional operational flexibility and to ensure the availability of freshwater in all times. A steady state model for the RO process is developed and linked with a dynamic model for the storage tank while membrane dynamic effect of membrane fouling is not included as the operation horizon time is only 24 hours. The membrane modules are divided into a number of groups to add

flexibility in operation to RO network. The total operating cost of the RO process is minimized in order to find the optimal layout and operating variables at discrete time intervals for three design scenarios.

It is important to note that the focus of this chapter was not to provide an in depth investigation of the RO network optimization but rather to find a suitable operation policies that would be appropriate for different design scenarios.

6.2 Variable Operation in RO Systems

During the past decade, scientists have made substantial advances in the RO membranes in terms of cost and separation efficiency. Membranes now cost less, have very high salt rejection rates, and respond effectively to short-term change in operation conditions (Miranda, and Infield, 2003).

Most recently authors who contributed in RO optimization area focused on optimal operation of RO processes based on fixed freshwater demand and for one feed temperature only (Abbas, 2007; Zhu et al., 2009b; Ghobeity and Mitsos, 2010).

There have been many publications in the literature dealing with the operation of RO membrane systems under variable-load. These studies suggested that the RO desalination plant can operate successfully under variable flow rate and pressure without any technical problems (Lising and Alward, 1972; Miranda, and Infield, 2003; Heijman et al., 2009; Emad et al., 2012).

On the daily basis, the operation of one-stage RO desalination plant is optimized while minimizing the operation cost. The problem is formulated as MINLP problem subject to the hourly distribution of the electricity cost (Ghobeity and Mitsos, 2010). Also, the results in the literature (Van Gauwbergenv and Baeyens, 1997; Hasson et al., 2007; Bartman et al., 2009) suggests that the transition from one steady state to another steady state for RO process needs relatively short time and pseudo steady-state model can be assumed for time steps more than 0.25 h.

However, using of finer time steps (0.25 h) lead to cut-down the cost, the execution time for the simulation is prohibitively longer (Ghobeity and Mitsos, 2010). Therefore, one and two hours are selected in this work as a time step.

6.3 Estimation of Dynamic Seawater Temperature and Freshwater Demand Profiles

Figure 6.1 shows the variable fresh water demand profile (Zhou et al., 2002). Figure 6.2a shows seawater temperature throughout the day for summer and for winter season. The actual data (Kawai et al., 2009) and predicted temperatures are plotted in Figure 6.2b. The following relationships are obtained by fitting the data using regression analysis as:

Fresh water demand

$$flow_{out} = \begin{cases} 59.44 - 3.63t - 4.6t^2 + 1.23t^3 & \text{if } t > 0 \text{ and } t \leq 7.5 \\ 1185.6 - 214.9t - 14.1t^2 - 0.297t^3 & \text{if } t > 7.5 \text{ and } t < 24 \end{cases} \quad (6.1)$$

Seawater temperature in summer season

$$T = 3.5 \exp\left(\frac{(t-15.5)^2}{-20.403}\right) + 29.51 \quad (6.2)$$

Seawater temperature in winter season

$$T = 3.5 \exp\left(\frac{(t-15.5)^2}{-20.403}\right) + 20 \quad (6.3)$$

t is operation time in hours (h).

It can be seen from the Figures 6.1 and 6.2; the experimental data of seawater temperature and water consumption are accurately predicted by the above equations.

These relations are considered in the RO model.

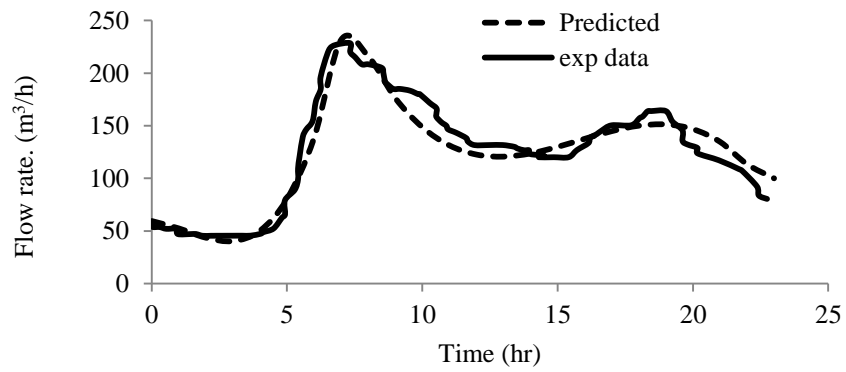


Figure 6.1 Daily time schedule for fresh water consumption by the user

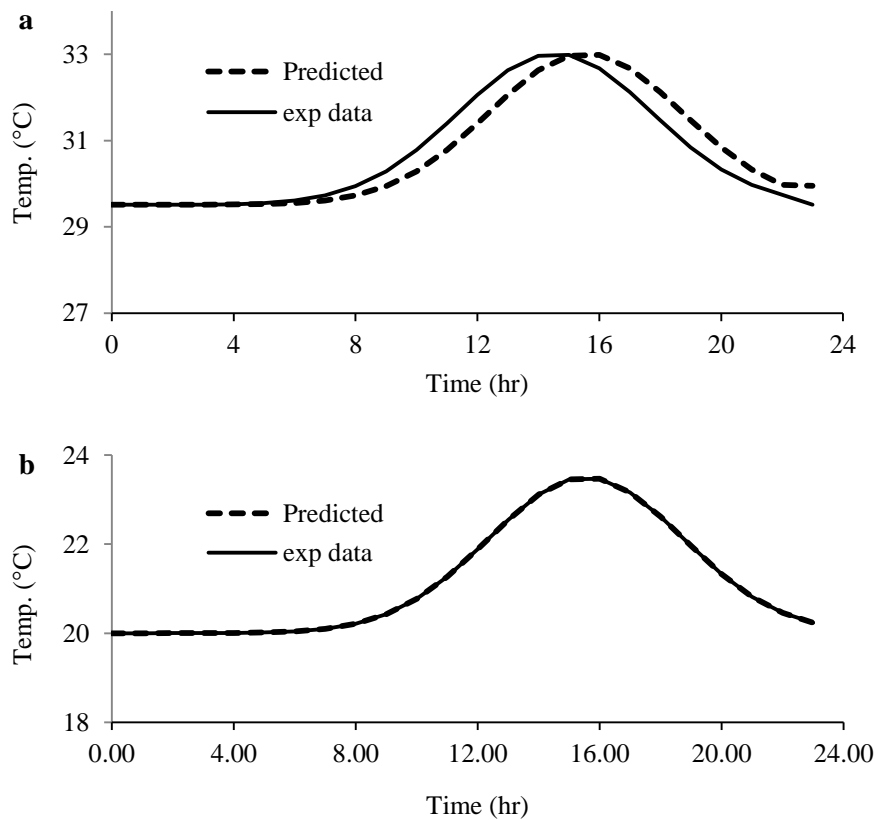


Figure 6.2 Seawater temperature profiles (a) at summer season and (b) at winter season

6.4 Model Development

As mentioned in Section 6.2, the RO system is able to operate successfully under variable conditions of pressure and flow. Also, the transition from one steady state to another steady state requires short time and pseudo steady-state conditions can be assumed even for short time steps. Thus, a steady state model for the RO system can be safely used in the RO simulation. Therefore, a model based on Kimura–Sourirajan

model for spiral wound module that takes into account concentration polarization (CP) is used here. Details of the mathematical model for spiral wound RO module are given in Section 3.2.1.1. Temperature effect on membrane characteristics is also included in model as shown in Section 4.2.3.

Figure 6.3 shows a RO desalination system with an intermediate storage tank between the process and the client. However, the water consumption profile in Figure 6.1 shows a significant variation throughout the day. This entails dynamic model for the storage tank and consequently, changing some operation parameters in order to control the tank operation.

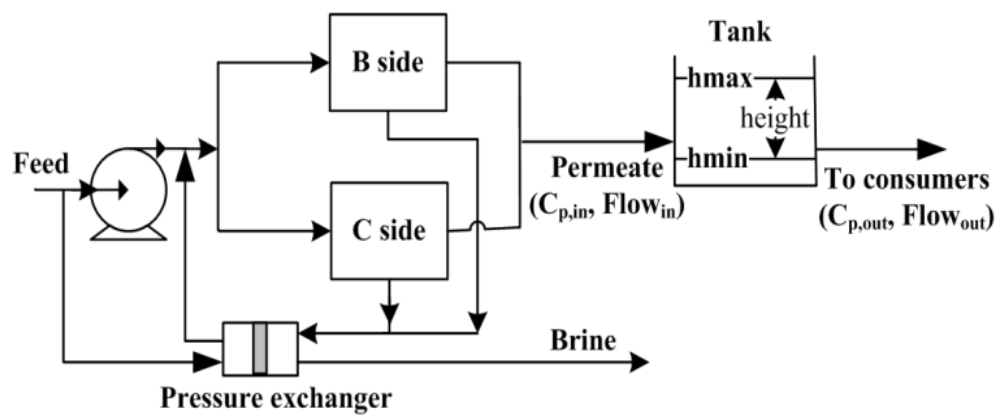


Figure 6.3 RO system with storage tank

6.4.1 Storage tank dynamic model

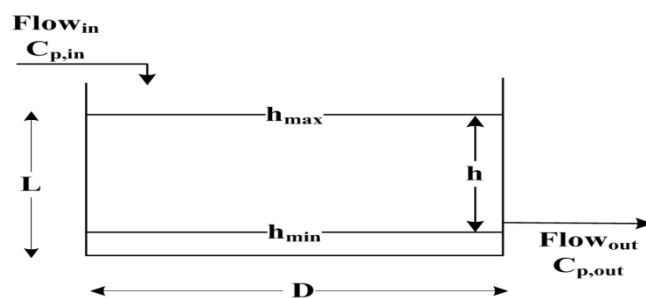


Figure 6.4 Schematic diagram of a storage tank

The dynamic behavior of a storage tank shown in Figure 6.4 can be described as:

Volume balance on the tank

$$\frac{d \text{ holdup}}{dt} = flow_{in} - flow_{out} \quad (6.4)$$

Where $flow_{in}$ is RO permeate production and $flow_{out}$ represents freshwater demand.

Relation between liquid level and holdup

$$Holdup = Tank. Area \times height \quad (6.5)$$

Salt balance on the tank

$$\frac{d C_{p,out}}{dt} = \frac{flow_{in}}{holdup} (C_{p,in} - C_{p,out}) \quad (6.6)$$

$C_{p,in}$ is the salt concentration entering tank from RO process.

The steady state model of RO process is coupled with the above dynamic model for the tank.

6.5 RO process optimization involving storage tank

6.5.1 Process constraints

6.5.1.1 Tank level

In order to make sure that the tank level, (h) does not exceed a given limit (above h_{max} or below h_{min}) at any time; a path constraint on (h) is imposed in the optimization problem. Without this level restriction, h goes above the high and low limits during normal operation of RO process as shown in Figure 6.5a. The level violations (LV_1 , LV_2) can be expressed as:

$$LV_1(t) = \begin{cases} (h(t) - h_{max})^2 & \text{if } h > h_{max} \\ 0 & \text{if } h < h_{max} \end{cases} \quad (6.7)$$

$$LV_2(t) = \begin{cases} (h(t) - h_{min})^2 & \text{if } h > h_{min} \\ 0 & \text{if } h < h_{min} \end{cases} \quad (6.8)$$

These level violations are represented graphically in Figure 6.5b. The total level violation LV_T over the entire processing time (t_p) can be written as:

$$LV_T = \int_{t=0}^{t=t_p} LV_1(t) + LV_2(t) dt \quad (6.9)$$

In other form

$$\frac{dLV_T}{dt} = LV_1(t) + LV_2(t) \quad (6.10)$$

The initial level is assumed in-between h_{\max} and h_{\min} . Therefore, the initial condition of equation 6.10 is zero. The total level violation LV_T is kept in this range of $0 \leq LV_T \leq \alpha$ where α is an infinitesimal positive number (10^{-6}). LV_T will be evaluated at each discrete time interval and will maintain the tank level between the tank level bounds.

The above model was considered by Hawaidi and Mujtaba (2011) for MSF process.

6.5.1.2 Tank Salinity

To ensure that the salinity of fresh water outlet from the tank ($C_{p,out}$) always equal or less than the maximum allowable fresh water salinity, a similar analysis of the tank level control can be done for $C_{p,out}$.

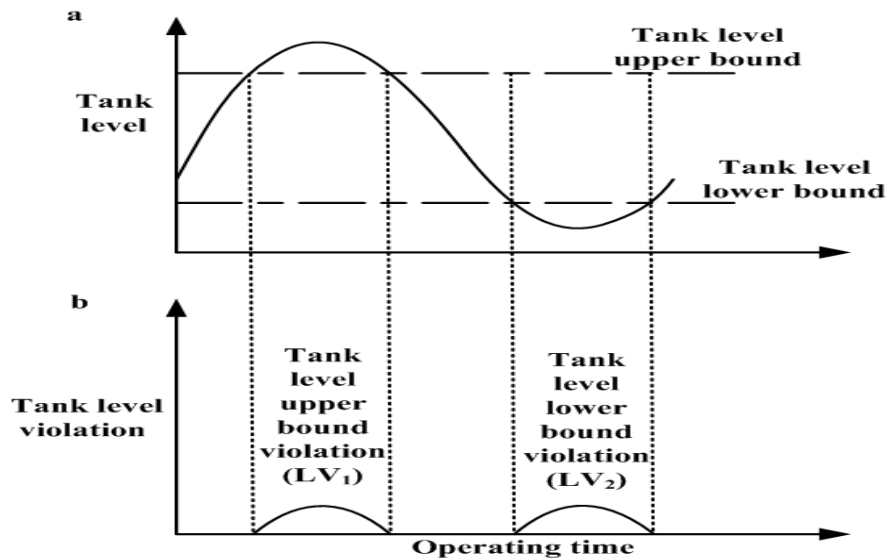


Figure 6.5 (a) Typical tank level profile and (b) Tank level violations

For simplicity, the water in the tank is assumed to be well mixed and the transition times between different operational conditions are neglected in this model (Farmani et al., 2006). Therefore, constraints (equations 6.7 and 6.8) may be rewritten as the following and appended in the optimization model.

$$CV(t) = \begin{cases} (C_{p,out} - C_{p,max})^2 & \text{if } C_{p,out} > C_{p,max} \\ 0 & \text{if } C_{p,out} < C_{p,max} \end{cases} \quad (6.11)$$

Figure 6.6a shows the tank salinity at normal operation without any control and Figure 6.6b represent salt concentration violation in the tank during the operation horizon time. The total accumulated violation CV_T over the entire period (t_p) can be written as:

$$CV_T = \int_{t=0}^{t=t_p} CV(t) dt \quad (6.12)$$

Therefore

$$\frac{d CV_T}{dt} = CV(t) \quad (6.13)$$

The initial tank salinity is assumed below the upper salinity limit; accordingly the initial condition of differential equation 6.13 is set as zero. As in tank level control analysis, the total salinity violation CV_T is kept in this range of $0 \leq CV_T \leq \alpha$.

Optimization of tank operation over a limited time horizon (24h) requires some periodicity in operation. This can be done by returning the final states of the tank to the initial ones. Therefore, two constraints are incorporated in the optimization formulation to keep the water level and salinity in the tank at the end of the operation same as that at the beginning of operation. Other constraints are imposed to the feed pressure and flow inlet to RO spiral wound module to improve the separation efficiency of membrane module.

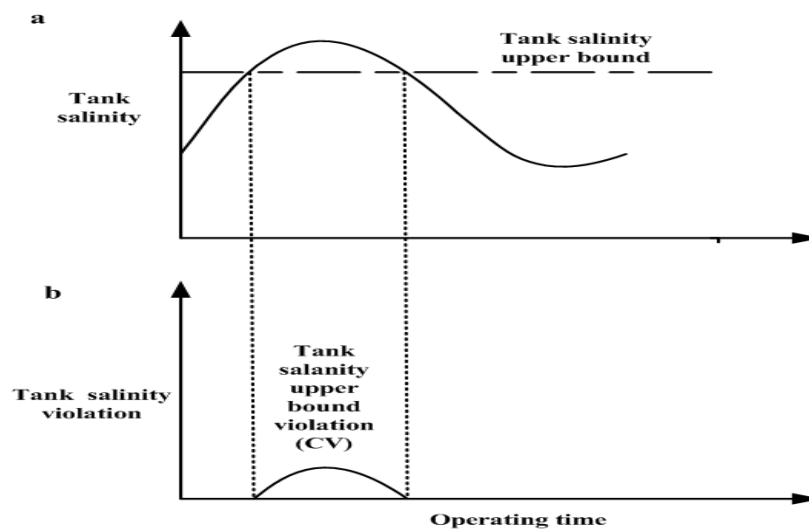


Figure 6.6 (a) Tank salinity profile and (b) Tank salinity violations

6.5.2 Optimization problem formulation

The optimization framework is developed to determine the optimal operation policies of RO process throughout the day. The decision variables are discretized over a 24h time interval and are assumed to be piecewise constant. A set of continuous variables are introduced to account for the existence or non-existence of the membrane sides at each time interval in operation (Figure 6.3). Therefore, they all take the value of [0 or 1] after rounding off. Switching the RO unit to complete shutdown operation mode is not allowed in all time intervals. As long as tank level and salinity constraints are not violated, there is total flexibility in RO operation. Such a strategy enables the optimizer to balance the operation load among the discrete time intervals.

The total operating cost TOC of the RO system was used as objective function. It is composed of many components including net pumping cost OC_{pu} , membrane replacement cost OC_{me} , chemical treatment cost OC_{ch} and annual spares cost OC_{sc} . The total operating cost components were given in Section 3.3.4 on the annual basis. Thus, it was adjusted on the daily basis as follows:

- Net pumping cost (\$/day)

$$OC_{pu} = (E_{pu} - E_{t,recv}) E_c I_f 24 \quad (6.14)$$

- Chemical treatment cost (\$/day)

$$OC_{che} = Q_{f,t} I_f 0.018 \times 24 \quad (6.15)$$

- Annual Spares cost (\$/day)

$$OC_{sc} = Q_{p,t} I_f 0.033 \times 24 \quad (6.16)$$

The objective function TOC (\$/m³) can be written as:

$$TOC = \frac{OC_{pu} + OC_{me} + OC_{ch} + OC_{sc}}{Q_{p,t}} \quad (6.17)$$

$Q_{p,t}$ represent the daily production rate.

The optimization problem OP is described as:

Given: RO plant configurations, design specification of each RO membrane module, storage tank volume, seawater temperature and fresh water demand profiles throughout 24 h.

Optimize: The number of membrane sides in operation; feed pressure and flow.

Minimize: The total operating cost of freshwater per cubic meter of permeate

Subject to: process constraints

The problem OP can be written mathematically as

Minimize TOC

P_f, Q_f, LV_T, CV_T

Subject to: Equality constrains Model equations

$$C_{p,out,initial} = C_{p,out,end}; h_{initial} = h_{end}$$

Inequality constrains Linear bound on P_f and Q_f ;

$$0 \leq LV_T \leq \alpha; 0 \leq CV_T \leq \alpha$$

$C_{p,out,initial}$, $C_{p,out,end}$, $h_{initial}$ and h_{end} are tank salinity and height at initial and last interval, respectively. These constraints are imposed to the optimization formulation to ensure the periodicity in operation where the final level and salinity of the tank are equal to the initial ones.

6.5.3 Optimization Methodology

It has been suggested that the RO network could be designed by identifying the number of required membrane maintenance schedules (Zhu et al., 1997). This means that the membrane modules may be divided into a number of groups for flexible operation to facilitate the membrane cleaning. This approach is adopted in this work, a number of pressure vessels in one stage RO system are distributed into two main sides. Each side is divided into sub-groups containing a number of pressure vessels each as shown in Figure 6.7.

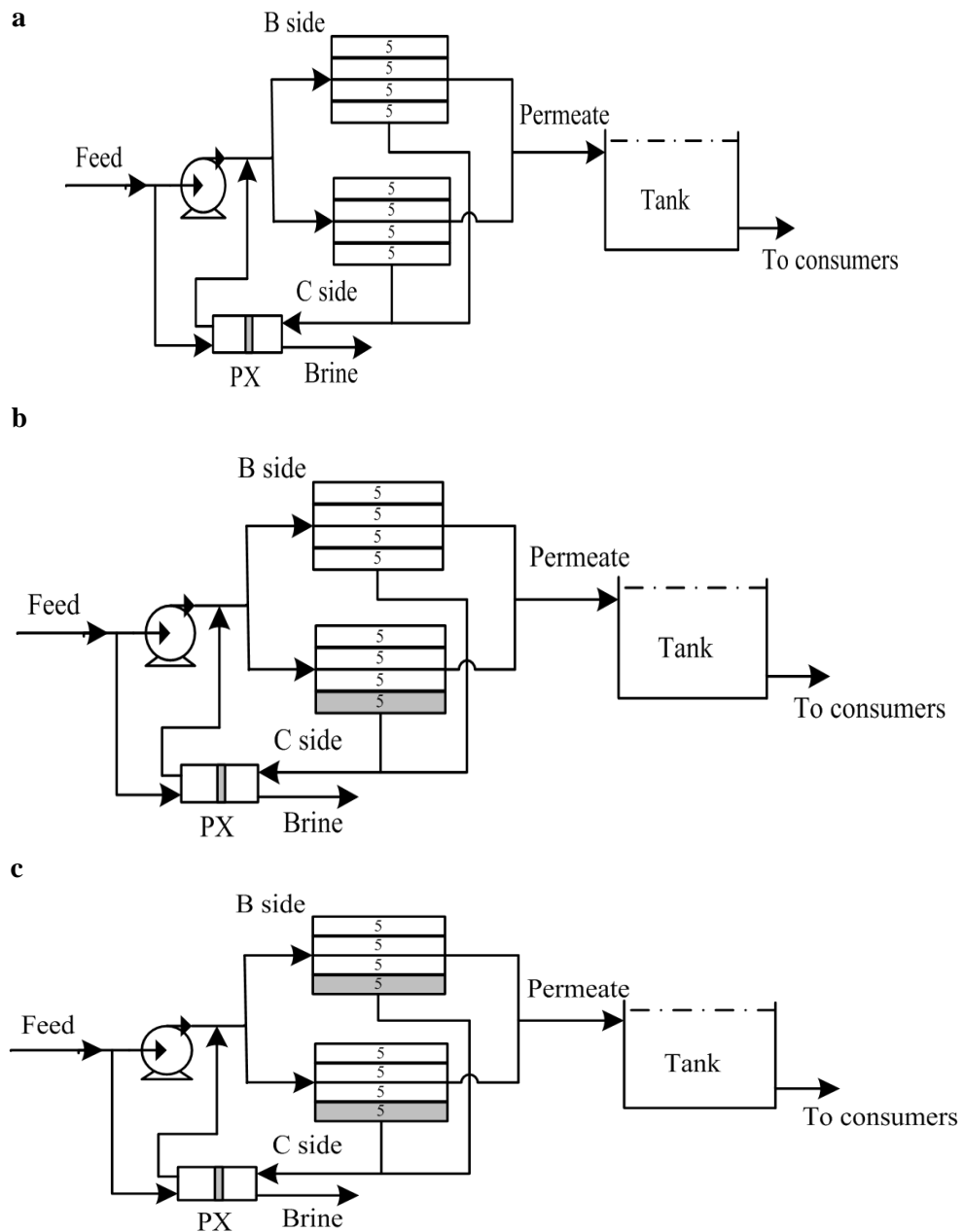


Figure 6.7 The RO process flow diagram with storage tank (a) Scenario 1 all sub-groups in operation, (b) Scenario 2 only one sub-group out of operation (c) Scenario 3 two sub-groups out of operation (■ out of operation)

The objective of optimization formulation was to find an optimal control variables profiles that minimize the total operating cost of the RO plant while satisfying all design and operating constraints and response to the variations in water demand and temperature over a day. Therefore, feed pressure and flow rate are optimized at discrete

time intervals in order to meet the fresh water flow and quality requirements and fulfilling storage tank level and salinity constraints. Storage tank levels (minimum and maximum) and salinity (maximum) are monitored dynamically and path constraints are added to the optimization formulation to keep them within the limits.

Two cases were carried out with two seawater temperature profiles representing summer and winter seasons in which the daily fresh water consumption profile is remained fixed in all cases. For each case, the corresponding optimal operation profile is generated using the optimization model.

Several cases are investigated using the proposed optimization framework in which the RO process configuration and operation are varied as the following:

- 1 All membrane sub-groups in operation at summer temperature profile.
- 2 All membrane sub-groups in operation at winter temperature profile.
- 3 Only one membrane sub-group out of operation at summer temperature profile.
- 4 Only one membrane sub-group out of operation at winter temperature profile.
- 5 Two membrane sub-groups out of operation at summer temperature profile.
- 6 Two membrane sub-groups out of operation at winter temperature profile.

Figure 6.7 shows the three operational flexibility scenarios considered here.

6.6 Presentation of the Illustrative Example

The previous methodology is applied to a RO system from the literature. The forty pressure vessels in one stage RO process which is described in Lu et al. (2007) with feed salinity 48,000 ppm are distributed into two main sides. Each side is divided into four sub-groups containing five spiral wound modules each as shown in Figure 6.7. The characteristics of the membrane module used here are taken from Lu et al. (2007) (Table 5.3). The minimum and maximum levels of the storage tank are 1 m and 5 m respectively. The storage tank has a diameter ($D = 10$ m) and aspect ratio $L/D = 0.5$. The parameters used in optimization calculation are listed in Table 6.1.

6.7 Results and Discussion

Two operational flexibility cases of the RO process are considered. For each case, the corresponding optimal operation profile is generated using the optimization model. Feed flow rate, pressure and the number of membrane sides in operation are optimized at each discrete time period in order to meet the variable freshwater demand. The significance of these cases is in investigating operation flexibility potentials of cleaning and maintenance scheduling of membrane modules without interrupting the RO operation or full plant shut-downs.

Table 6.1 Input data for optimization

	Value	Reference
Feed salinity (ppm)	48,000	Lu et al., (2007)
Feed pump efficiency (%)	80	assumed
Pressure exchanger efficiency (%)	90	Lu et al., (2007)
Load factor	0.9	Marcovecchio et al., (2005)
Module Feed flow range (m ³ /h)	0.8-16	Lu et al., 2007
Maximum operating pressure (bar)	83	Lu et al., (2007)
Initial tank level (m)	2	assumed
Initial tank salinity (ppm)	450	assumed
Electricity unit cost (\$/kWh)	0.08	Lu et al., (2007)

6.7.1 Case Study 1: Optimization of RO Operation in Summer

Using the daily variation of seawater temperature in summer season, the three RO design scenarios described above are investigated.

Figure 6.8 shows the optimal operation schedule for the three scenarios. This solution indicates that all membrane modules in B side in all scenarios are to be in operation in all time intervals while intermittent operation mode was identified for C side. The number of off-operation hours of C side for the three operation scenarios are proportional to the number of membrane modules in operation. The elimination of C

side from operation in certain hours is utilized to maintain the tank level and salinity constraints.

Figure 6.9 illustrates the results of the optimum operating pressure at discrete time intervals. For scenario one, pressure follows the path similar to that for fresh water demand to maintain the required freshwater consumption (Figure 6.1). The same occurs for the scenarios two and three until 4 pm. After that the pressure remained at a high level. This is due to two reasons. First, lower number of membrane elements used in these two cases compared with scenario one and second, to maintain the required fresh water salinity at high temperature period (Figure 6.2a).

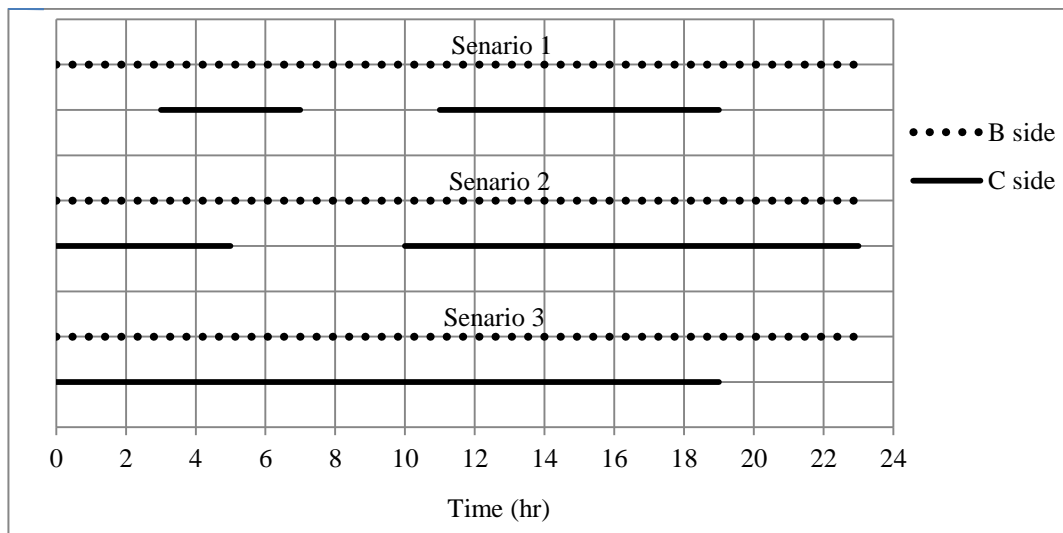


Figure 6.8 Daily RO operation cycle at summer season

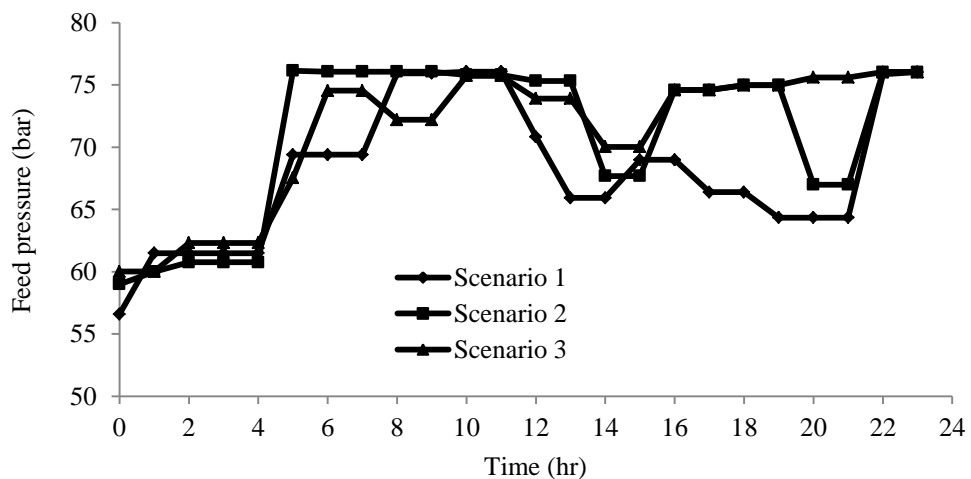


Figure 6.9 Optimal operating pressure profile using summer temperature profile

The trend of tank level in Figure 6.10 is consistent with the water demand and production profile in Figure 6.11. The optimizer determines the best time of storage tank filling. The tank uses all operational volumes during the cycle, as shown in Figure 6.10. It is clear that the tank filling occurs mainly during low demand periods; where the production rate of freshwater is higher than freshwater consumption resulting in increase in tank water level. The storage tank level falls down immediately after the demand peaks period at around 7 am and 7 pm to avoid high level constraint violation.

Figure 6.12 shows the periodic behaviour of the salt concentration in the tank and in RO permeate for scenario one. One can see clearly that the fresh water salinity objective is satisfied over the optimization period, with the salt concentration of the tank remaining close to the maximum limit within the period between 3 pm and 9 pm. This can be attributed to the deterioration of the membrane salt rejection due to increasing seawater temperature (Figure 6.2a). Also, increases in feed temperature results in the increase of permeate flux (Jin et al., 2009), lowering the operating pressure (Figure 6.9) and consequently higher salt concentration in the permeate.

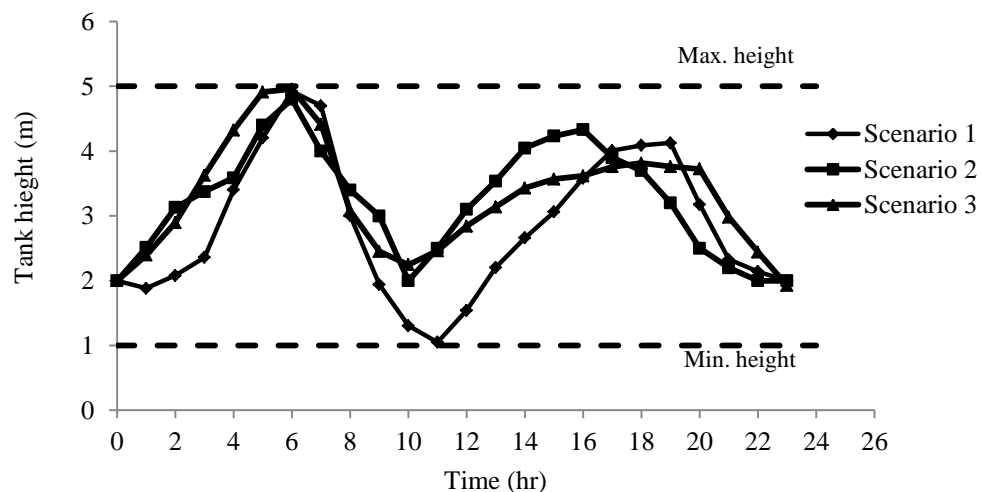


Figure 6.10 Storage tank level profiles at summer operation

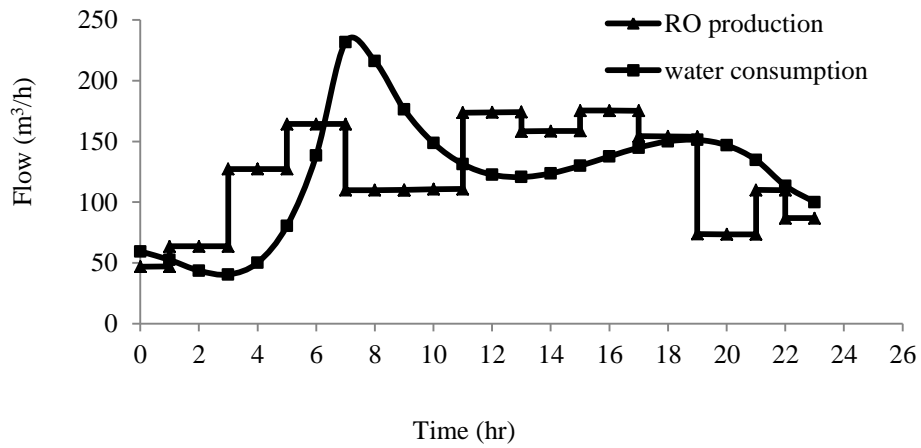


Figure 6.11 Fresh water consumption and RO production profiles (Scenario 1)

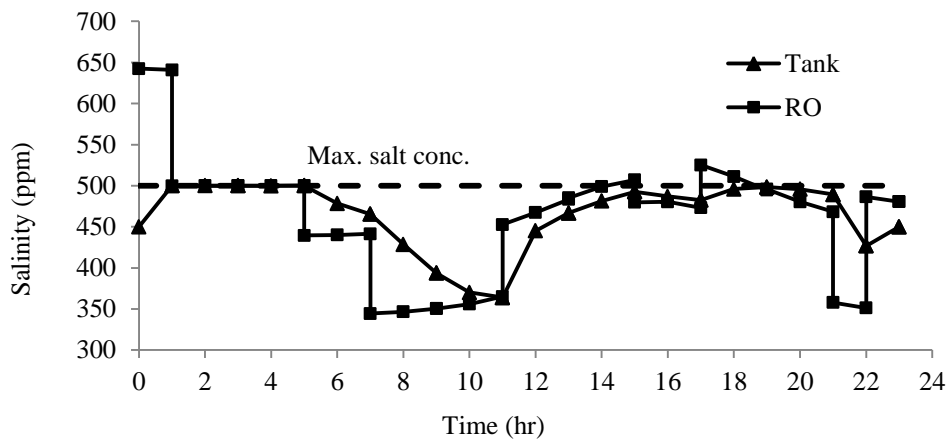


Figure 6.12 Salt concentration of fresh water from RO and tank profiles (Scenario 1)

6.7.2 Case Study 2: Optimization of RO Operation in Winter

Seawater temperature influences the key performance parameters of the RO systems. The permeate production increases in direct relationship to seawater temperature increase. But, increased seawater temperature also results in increased salt passages across the membrane (Jin et al., 2009). Therefore, by using different seawater temperature profiles, it is expected to have significant variations in the RO operation plan to fulfil the freshwater demand.

It is to be noted that water consumption profile used in this case study is the same as that used in case study one. However, water consumption pattern is likely to vary

between seasons. Different water consumption functions could be incorporated into the formulation if desired.

Figure 6.13 illustrates different operating modes for three operation scenarios .by plotting the optimal operation schedule of RO process. As shown in Figure 6.13, the optimal operation schedule involves taking off C side from operation for certain hours for the operation scenarios one and two. The number of off-operation hours decreases with increasing the number of membrane sub-groups in operation for the three operation scenarios. The number of off operation hours for scenario one is 7 hours and 4 hours for scenario two which occurs during relatively low demand period (10 am to 2 pm). Both membrane sides B and C are operated continuously during the optimization period for scenario three. This mode of operation is picked by the optimizer to compensate the shortage of production due to less membrane sub-groups in operation in this operation scenario and also the negative impact of low seawater temperature in winter season on the water production.

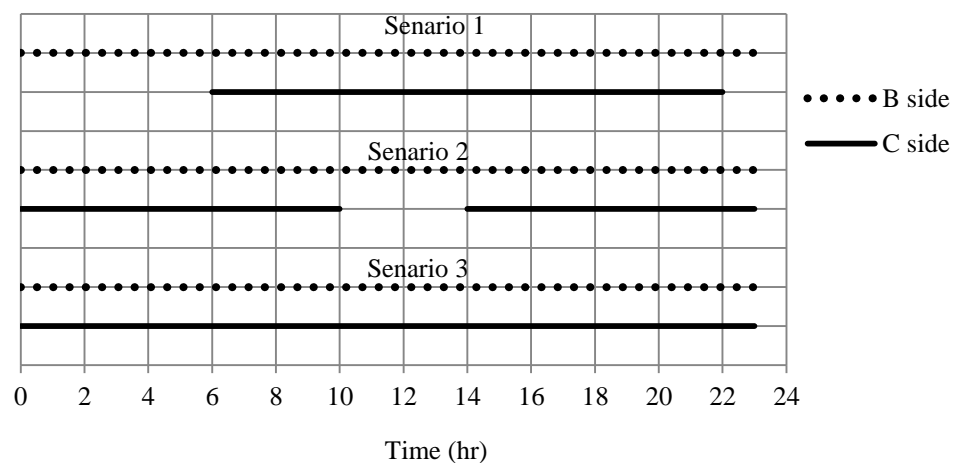


Figure 6.13 Optimal operation schedule of RO at winter season

In comparison to Figure 6.10 in Case study one, it can be seen in Figure 6.14 that the optimizer is still forced to choose to continue the operation of the tank in consistent with fresh water demand rate required (Figure 6.15). Figure 6.14 shows that the storage tank level exhibited periodic behaviour and the tank level is adjusted to avoid any level

violations. The optimizer have chosen to start filling the tank when the production rate of freshwater is higher than freshwater consumption resulting in increase in tank water level. Had the fresh water demand been higher than RO production (Figure 6.15), the storage tank level falls down (Figure 6.14). The storage tank levels tend to peak just before the water demand peaks. The storage tank level reached its upper level bound between the periods 4am to 6am and 4pm to 6pm to supply the peak demand where the peak of fresh water demand occurs mainly in 7 am and 7 pm.

The operating pressure trajectory for the three operation scenarios is shown in Figure 6.16. Unlike pressure profile in Case study one, operating pressure remained at a high level most of the optimization period. This illustrates the level of reliability of the RO operation. The high pressure was used to compensate the negative impact of low seawater temperature in winter on water productivity. However, it has positive impact on the salt concentration in permeate. It can be seen from Figure 6.17 that the average salt concentration produced from RO process does not exceed the salinity upper bound (500 ppm). At first sight, permeate salt concentration was very low as it remained below 400 ppm most of the day (2 am to 8 pm). This illustrates the consequences of high pressure on the permeate salinity.

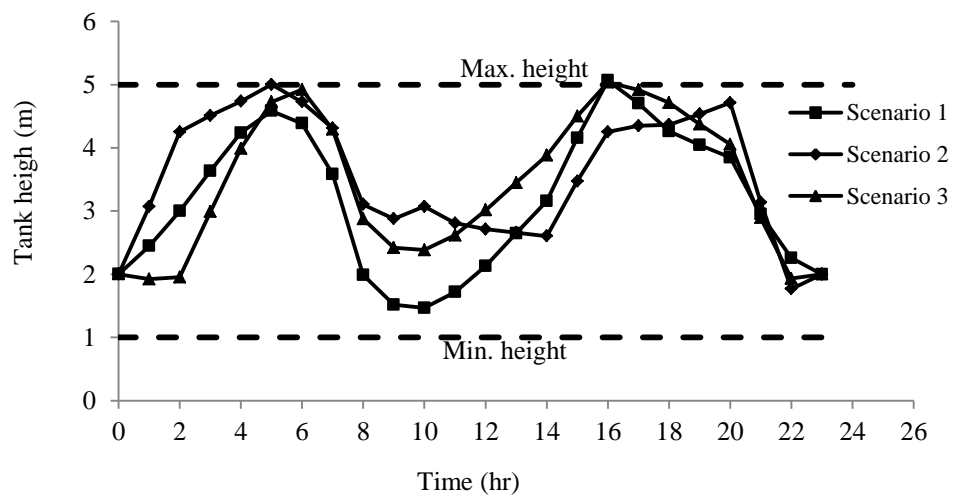


Figure 6.14 Tank operating levels over a cycle of 24 h at winter season

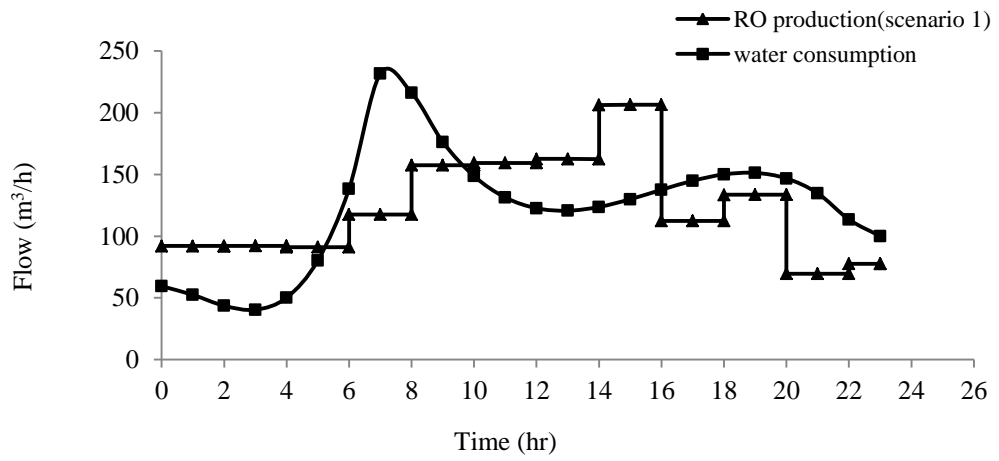


Figure 6.15 Fresh water production and consumption during the day.

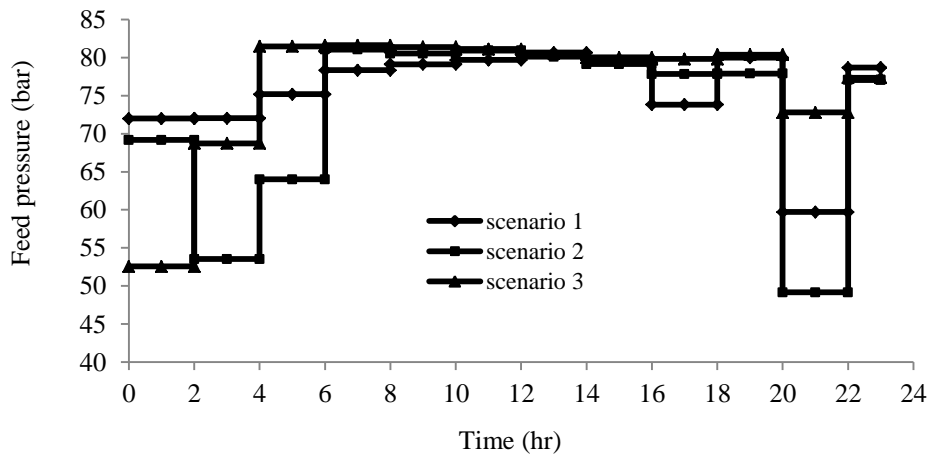


Figure 6.16 Optimal operating pressure profile at winter season

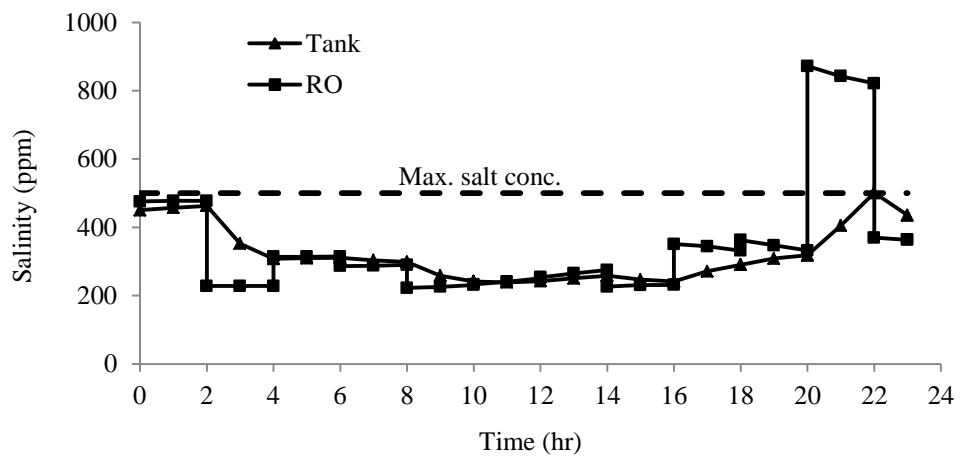


Figure 6.17 RO permeate salinity and tank salinity profiles at winter (Scenario 3)

6.7.3 Comparison between Case Study One and Two

The optimization results show that winter operation requests the RO process to utilize more membrane modules than in summer. According to Figure 6.18 winter seawater temperature profile makes the operation of RO process less flexible. C side in winter season has lower off-operation hours compared to the same membrane side in summer. For instance, the off-operation hours for scenario two in summer and winter are 5 hours and 4 hours respectively. Based on this, one can conclude that RO operation in summer has higher level of operation flexibility in terms of number membrane sub-group in operation. This will offer additional flexibility in maintenance of the RO process throughout the day.

Figure 6.19 shows clearly the difference between the required pressure in summer and winter. Summer operation requires less pressure to meet the variable demand of freshwater. This consequently results higher salt concentration in RO permeate in summer (Figure 6.20).

Table 6.2 presented the average daily specific energy consumption in terms of permeate produced. It can be noted from the Table that the required specific energy in the winter season are the highest due to lower seawater temperature. At the same temperature, the same freshwater demand during the day can be fulfilled by using less number of membrane sub-groups but the operating cost will be higher as shown in Table 6.2. For instance, the specific energy required in summer season for scenario one operation mode is increased by 15 % when the operation switched to the scenario three. Also the difference between seawater temperature in summer and winter seasons demands an increase in specific energy by about 9 % when scenario two is adopted in operation.

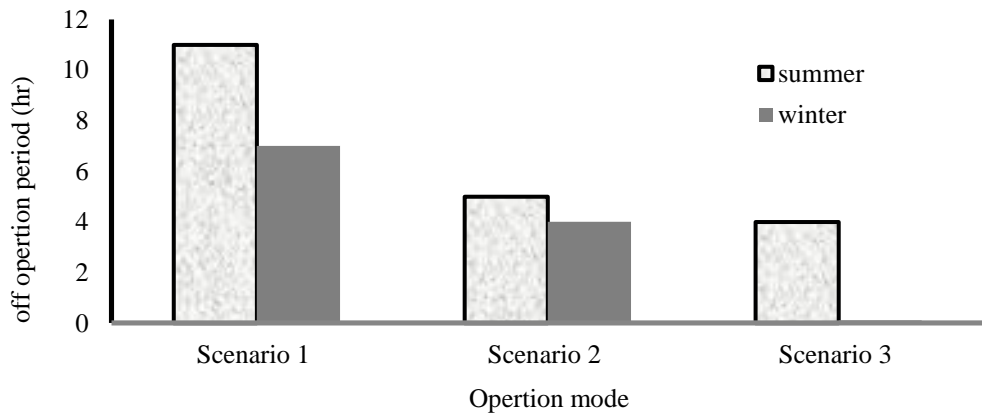


Figure 6.18 Comparison of different operation schedules

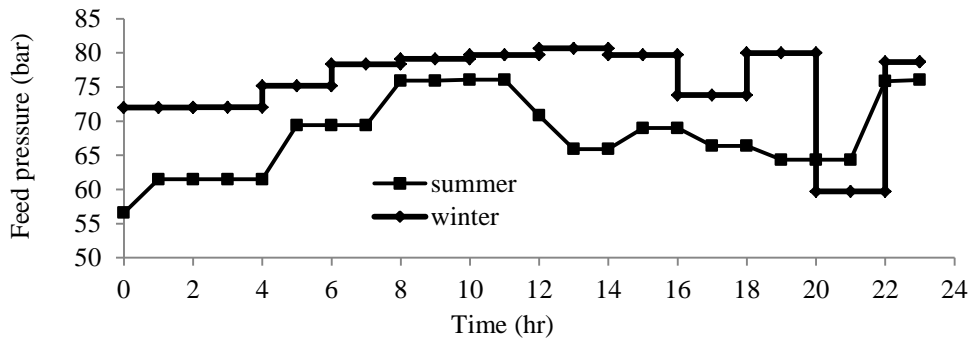


Figure 6.19 Pressure pattern for summer and winter (Scenario 1)

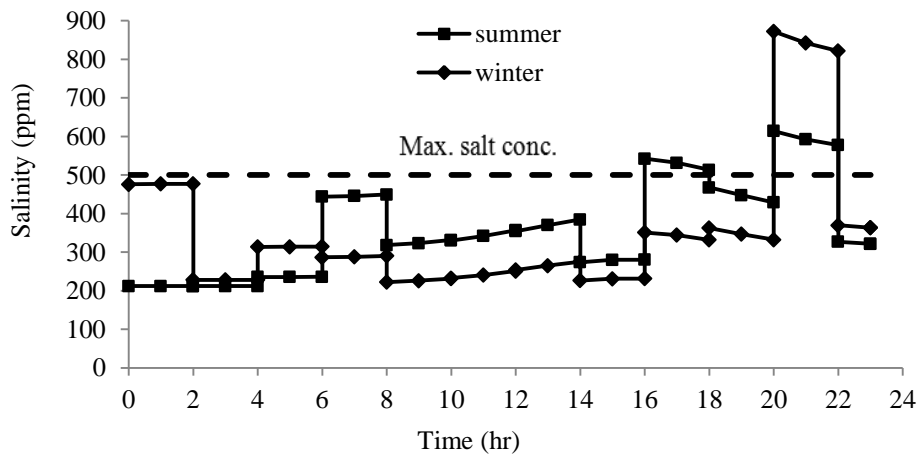


Figure 6.20 RO permeate salinity in summer and winter (Scenario 3)

Table 6.2 Specific power consumption (kwh/m³ of permeate)

	Scenario 1	Scenario 2	Scenario 3
Summer	2.397	2.610	2.774
Winter	2.647	2.844	3.044

6.8 Conclusion

The optimal operation strategies are established for different process designs in terms of number of membrane sub-groups in operation and including variable seawater temperature and water demand for a 24 h operational time horizon. The RO process operation was optimized at discrete time intervals while minimizing the total operation cost.

A steady state model for RO process and dynamics model for storage tank are incorporated in the optimization framework. In this work, hourly time step is used. However, longer time steps could reduce the computational time, but it is not in favor of cost reduction.

Several RO configurations in terms of number of membrane sub-groups are considered incorporating two daily temperature profiles representing the daily temperature variations at summer and winter seasons.

For each case, the corresponding optimal operation profile is generated using the optimization model. Feed flow rate, feed pressure and the number of membrane sides in operation are optimized at each discrete time period in order to meet the variable freshwater demand.

The optimization results show that winter operation requests the RO process to utilize more membrane modules than in summer. On the other hand, summer operation requires less pressure compared to that in winter season to meet the variable demand of freshwater leading to lower power consumption.

The optimization results demonstrated that it is possible to meet the variable fresh water demand throughout the day even-though with less number of membrane modules but with higher operation cost. This will offer the possibility of flexible scheduling of cleaning and maintenance of membrane modules particularly when scaling and fouling become serious problems and more frequent cleaning is required.

Based on the findings in the previous chapters, daily and seasonal seawater temperature variations may offer the possibility of flexible scheduling of cleaning of membrane modules. In next chapter, the role of membrane fouling on the design and cleaning schedule of RO systems with varying seawater temperature will be explored.

Chapter 7

Optimal Design and Cleaning Schedule of RO Process

7.1 Introduction

Membrane fouling is inevitable for any desalination plant. It occurs due to deposition of common impurities of the feed solution and causes decline in permeate flux, decrease in salt rejection, increase in differential pressure, and irreversible membrane damage in severe cases.

In earlier chapters, the design and operation optimization problems have been solved using RO steady state model. In this chapter, an actual fouling model which can appropriately describe the RO performance is embedded in the optimization formulation. Accurate estimation of membrane permeability decline due to fouling is important in developing a reliable process model. Therefore, NNs based correlation is developed in this work based on the actual water and salt permeability data to estimate the performance decline factors. Annual seawater temperature variation is considered in the NNs model. This correlation is embedded in the gPROMS simulation code with rest of the model equations in the process model and the optimal design and operation policies of the RO desalination systems are found. The optimal design of RO networks is formulated as MINLP problem utilizing spiral wound membrane module. Several cases are solved in which the membrane maintenance schedules are varied.

7.2 Previous Formulations of RO Maintenance Scheduling

The previous studies carried out on the design and scheduling of RO networks are limited to the determination of the optimal design and scheduling of RO networks for only one temperature and the impact of varying feed temperature on the optimal design and operation of RO systems is overlooked. Although, spiral-wound module occupies the largest market share (Kaghazchi et al., 2010) all the studies contributed in the optimal design and scheduling of RO networks (Zhu et al., 1997; See et.al., 1999; Lu et

al., 2006) were based on hollow fiber module and none was based on spiral-wound module.

See et.al. (1999) and Lu et al. (2006) formulated the RO maintenance scheduling as discrete time problem. The scheduling problem was solved using MINLP approach for long operation periods. Zhu et al. (1997) solved the optimal design problem of RO processes using MINLP approach for one year operation horizon. The numbers of membrane maintenance schedules are identified for the whole operation time.

7.3 Estimation of Dynamic Seawater Temperature Profile

The actual average seawater temperature data throughout the year in the island of Porto Santo, (Portugal) (Pais et al., 2007) is fitted using nonlinear regression analysis. The following relationships are obtained (also shown in Figure 7.1):

$$T = \begin{cases} 23.8 \exp\left(-\frac{222}{t}\right) + 19.6 & \text{if } t \leq 180 \\ 293240 \exp\left(-\frac{912}{t} - 0.026 t\right) + 0.04997 t & \text{if } t > 180 \end{cases} \quad (7.1)$$

t is continuous operation time (days).

Figure 7.1 shows the actual average seawater temperature (Pais et al., 2007) and predicted temperatures using equation 7.1. There is a good fit of the predicted sea water temperature values to the experimental data. It can be seen that seawater temperature can drop as low as 19.5°C in January and the variation which occurred during the summer months reaches 6.3°C. The variable seawater temperature throughout the year is considered in the RO model.

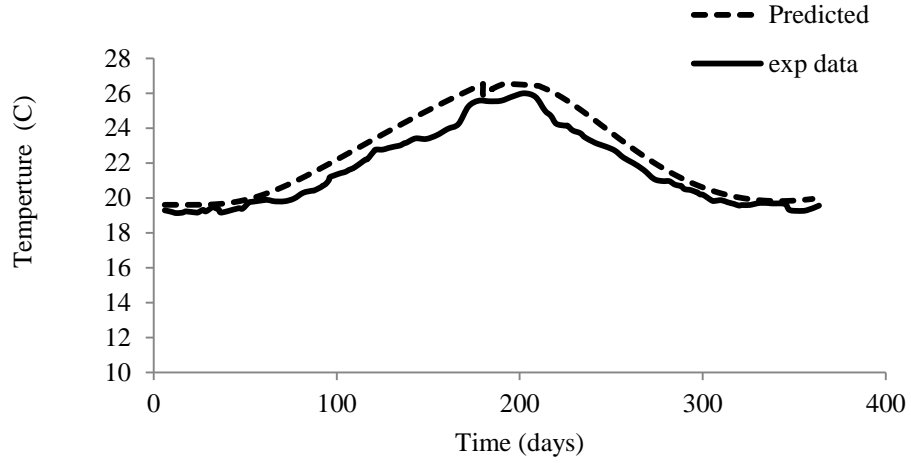


Figure 7.1 Evolution of feed temperature in one year

7.4 RO Network Model

It has been suggested that the RO network could be designed by identifying the number of required membrane maintenance schedules (Zhu et al., 1997). This means that the membrane modules may be divided into a number of groups to facilitate the membrane cleaning. This approach is adopted in this work, a number of pressure vessels in single stage RO system (each pressure vessel contains a number of spiral wound modules connected in series) are distributed into a number of membrane groups (N_g) determined based on the number of inter-maintenance cycles. Each membrane group contains equal number of pressure vessels (n_p) as shown in Figure 7.2.

After the pressurization process, the pump-exit stream is split into (N_g) streams and also again each stream split into (n_p) streams as a feed to the parallel membrane pressure vessels. The number of pressure vessels (n_p) in each group will be determined by the optimizer for each membrane schedule scenario.

$$Q_{fj} = \frac{Q_{f,t}}{N_g} \quad j \in N_g \quad (7.2)$$

$$Q_{fi} = \frac{Q_{fj}}{n_p} \quad i \in n_p \quad (7.3)$$

$Q_{f,j}$ and $Q_{f,i}$ are feed flow rate to membrane group j and to individual pressure vessels i may exist in this group, respectively.

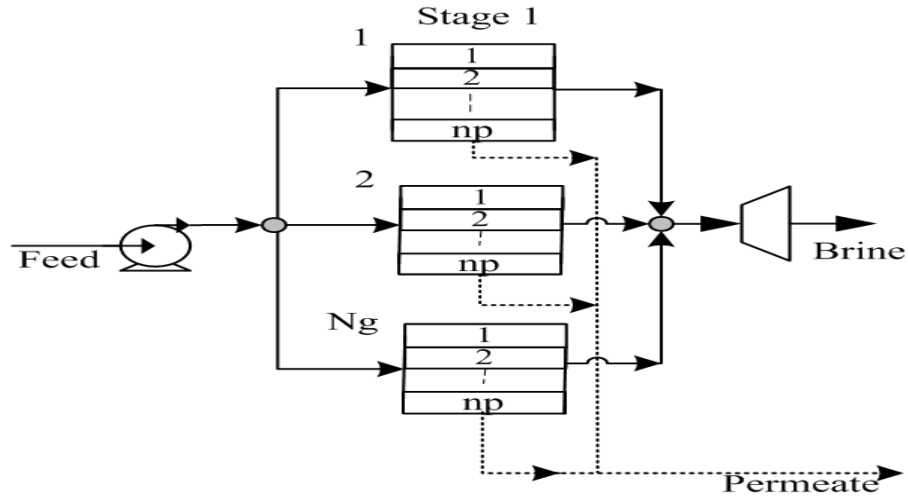


Figure 7.2 One-stage RO process flow diagram.

The total permeate flow and concentration from all spiral wound membrane modules can be determined by imposing volume and material balance constraints on the membrane network.

$$Q_{p,t} = \sum_{j=1}^{Ng} \sum_{i=1}^{np} Q_{p,i,j} \quad j \in Ng, i \in np \quad (7.3)$$

$$Q_{p,t} C_{p,t} = \sum_{j=1}^{Ng} \sum_{i=1}^{np} Q_{p,i,j} C_{p,i,j} \quad j \in Ng, i \in np \quad (7.4)$$

The reject streams from all membrane groups are mixed in one stream which can fed to the turbine for energy recovery.

Several other constraints such as spiral wound module design constraints and product characteristics constraints are included in the MINLP problem to improve the membrane separation efficiency.

$$Q_f^L \leq Q_f \leq Q_f^U \quad (7.4)$$

$$P_f^L \leq P_f \leq P_f^U \quad (7.5)$$

$$Q_{p,t} \geq Q_{p,t}^{\min} \quad (7.6)$$

$$C_{p,avg} \leq C_{p,avg}^{\max} \quad (7.7)$$

The RO network is modelled by combining the above equations with that used in network description for mixers and splitters (Section 3.3.3).

7.5 Maintenance Scheduling Formulation

The formulation of the maintenance scheduling problem of RO network proposed by Zhu et al. (1997) is used in this work. The scheduling problem is formulated by partitioning the time horizon, t , into a number maintenance cycle/cycles (nc) of equal duration. The following is the description of the terms used in the scheduling problem formulation:

Maintenance cycle (nc): Periodical time during which all membrane modules in all membrane groups are cleaned once.

Inter-maintenance cycle (Ng): Time between two membrane cleaning events. In One maintenance cycle, there may be more than one inter-maintenance cycles.

It is necessary that the number of inter-maintenance cycles equal to the number of membrane groups (Ng). Thus, the cleaning operation during one maintenance cycle will be exchanged between the membrane groups during each maintenance cycle.

Figure 7.3 shows the time distribution of the RO membrane maintenance schedules. Figure 7.4 shows the flow diagrams for different maintenance schedules options. The membrane modules are distributed into a number of membrane groups (Ng) determined based on the number of inter-maintenance cycles as shown in Figure 7.4 to facilitate the membrane cleaning. For instance, in three inter-maintenance cycles cleaning schedule option (Figure 7.4c), the membrane modules divided into three groups, each membrane module group (side) will be cleaned at different time.

For example, Figure 7.3f illustrates the formulation of scheduling problem for two maintenance cycles (nc=2) and two inter-maintenance cycles (Ng=2). All pressure vessels in a stage are divided into two main groups as shown in Figure 7.3b. The

optimal number of pressure vessels in each membrane main group is found through the optimization procedure. At the end of the first inter-maintenance cycle at 90 days membrane modules inside one which contains half of the membrane modules are cleaned and membranes in side two are cleaned at the end of the second inter-maintenance cycle (after 180 days of continuous operation), thus the two sides are cleaned once in the first maintenance cycle but in different time. The same cleaning sequence will continue for the second maintenance cycle. It is assumed that no downtime is incurred for membrane cleaning as the time involved (a few hours) is negligible compared to the length of each interval (Lu et al., 2006).

7.6 Development of Neural Network Model

As mentioned before, there is some work carried out for determination the optimal design and scheduling of RO networks using MINLP technique (Zhu et al., 1997; See et al., 1999; Lu et al., 2006). However, in their work an exponential function was used to represent uniform decline in membrane permeability. Also, their work was limited for one temperature only.

In this work therefore, NNs based correlations are developed to estimate the decay in water and salt permeability coefficients ($A_w^f; A_s^f$) based on the actual RO desalination plant data as a function of annual seawater temperature profile and operation time.

7.6.1 Neural Network Architecture

The neural network topology in which the inputs and outputs of the neurons are organized is known as architecture of the neural network. A typical neural network consists of an input layer, one or more hidden layers; output layer and transfer functions. Multi-layer feed-forward neural network is the most common method of implementing NNs models as it is more able to deal effectively with the complex nonlinear problems (Khayet et al., 2011).

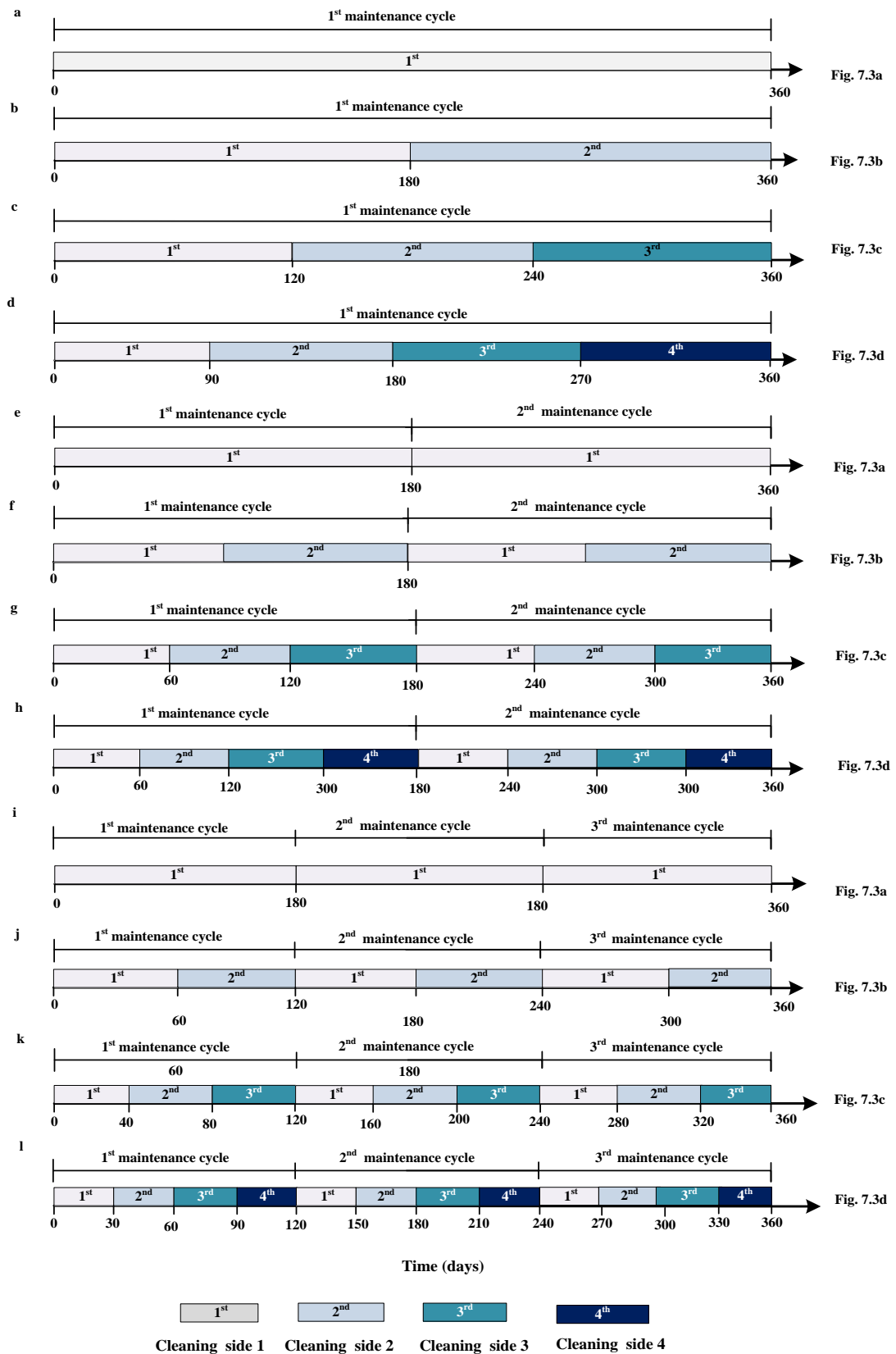


Figure 7.3 Scheduling of cleaning of RO membranes and corresponding flow diagram (maintenance /inter- maintenance):(a) 1/1; (b) 1/2; (c) 1/3; (d) 1/4; (e) 2/1; (f) 2/2; (g) 2/3; (h) 2/4; (i) 3/1; (j) 3/2; (k) 3/3; (l) 3/4

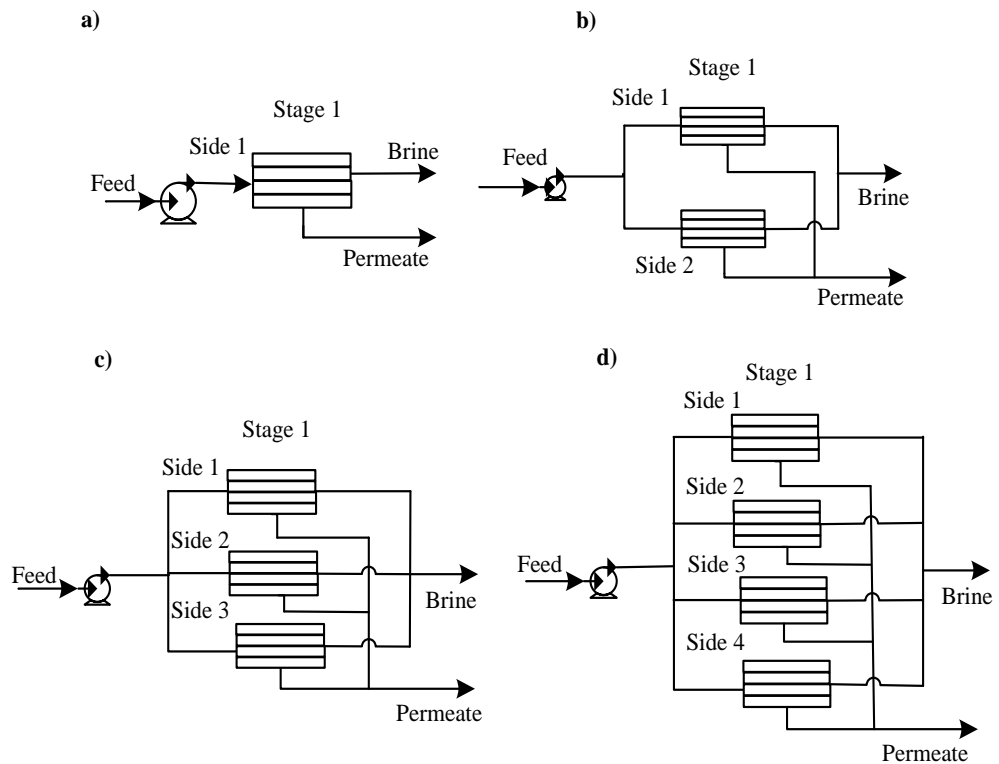


Figure 7.4 RO process configurations for different maintenance schedules

Commonly neural networks are adjusted, or trained so that a particular input leads to a specific target output. The connections are made between the neurons of adjacent layers allowing the neuron to receive a signal from a neuron in the preceding layer and allow it to transmit signals to neurons in the immediately succeeding layers.

The processing neuron receives a number of inputs (a_i). A weighted sum of these signals is calculated, using the neuron's assigned weights (w_i), which is transferred by the transfer function to produce output signal, that is send to the neurons in the succeeding layer. Also a bias neuron (b) supplies an invariant output which is connected to each neuron in the hidden and output layers. The performance of NNs models are strongly influenced by the choice of the input-output function, transfer functions and the weights. Figure 7.5 shows the main categories of transfer functions.

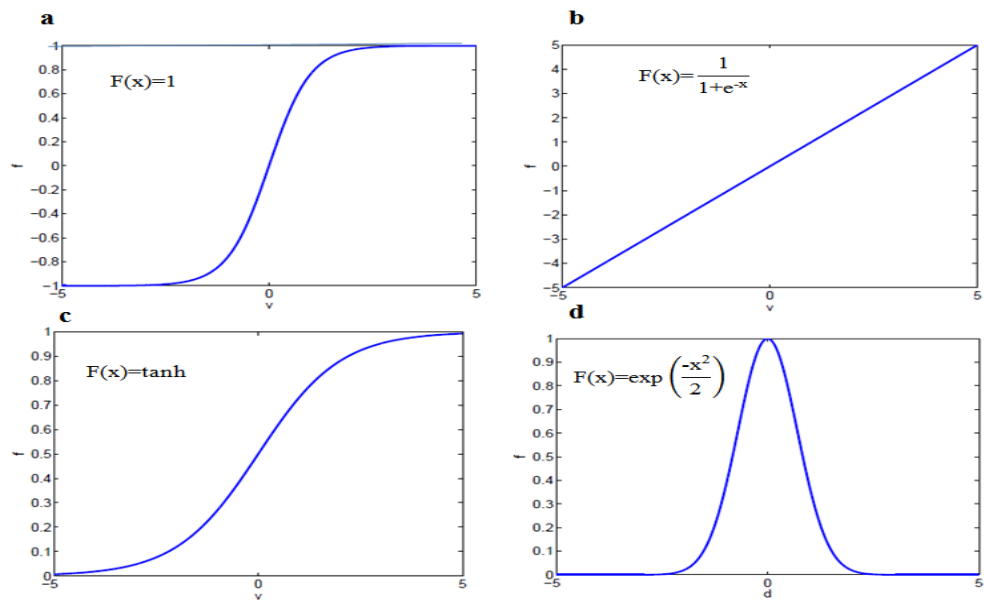


Figure 7.5 Different Neuron transfer Functions: (a) linear (b) Sigmoid (c) hyperbolic (d) Gaussian (Niemi et al., 1995)

7.6.2 Estimation of water and salt permeability coefficients using NNs

Data from Pais et al. (2007) was used for this study that was collected from one stage RO desalination plant utilizing spiral wound modules. These data were selected from the published data presented in graphical form with time range (0-454 days) and were digitized to obtain coordinate values. Data for one year (365 days) only used in neural network model.

The time-dependent variables such as permeate fluxes and membrane permeability are commonly normalized with their initial values (Song et al., 2004). Normalization on the experimental data is required to avoid the effects of different operating conditions. The experimental membrane permeability data obtained for Koch spiral wound membranes (Pais et al., 2007) are normalized using their initial permeability coefficients. The resulting normalized membrane permeability decline factors for water and salt (A_w^f ; A_s^f) (Table 7.1) is used to represent the membrane permeability decline for spiral NNs tool is used to develop two correlations for estimating water and salt permeability decline factors (A_w^f ; A_s^f) for a given seawater temperature profile and operation time.

The seasonal variation of seawater temperature is embedded in the predicted permeability decline factors. A four layered NNs architecture shown in Figure 7.6 is used in this propose. In the proposed NN based correlations, optimal network architecture (in terms of number of hidden layers and neurons in each layer) is chosen for each network by trial and error approach (multiple runs).

Two NN models are developed to estimate water and salt permeability decline factors (A_w^f ; A_s^f), each model consists of two neurons in the input layer, two hidden layers containing four and two neurons respectively, and one neuron in the output layer. The outputs of hidden and output layers are determined as follow:

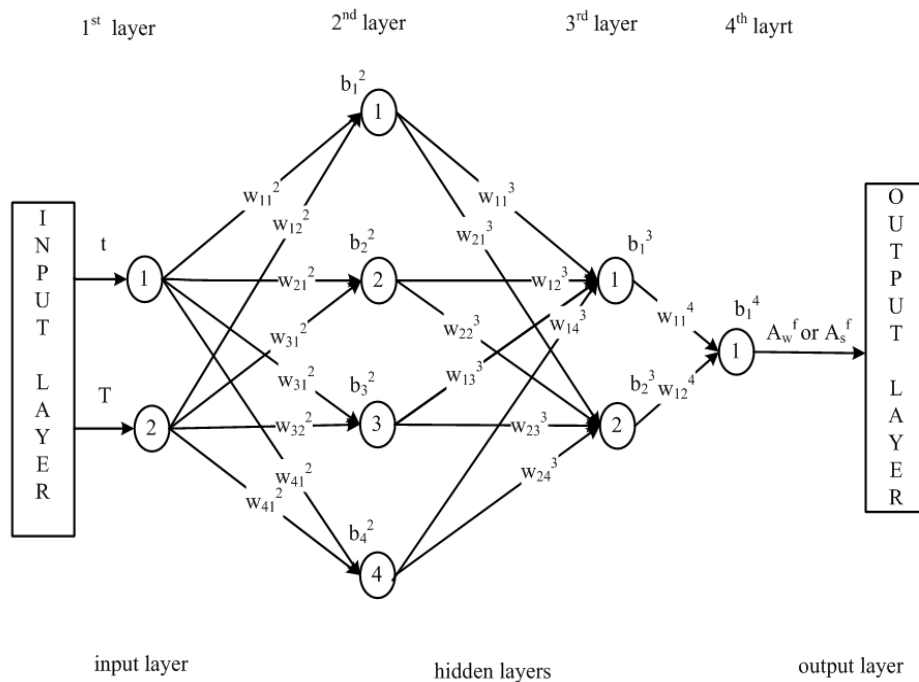


Figure 7.6 Four layer neural network

Table 7.1 Water and salt permeability vs. seawater temperature throughout the year.

Water permeability

Salt permeability

Time (days)	Temp (°C)	(A _w) 10 ⁷ (m/s bar)	A _w ^f (A _w /A _{w0})
6.06	19.28	2.31	1.000
7.51	19.25	2.32	1.004
10.3	19.18	2.34	1.013
11.84	19.13	2.32	1.004
13.76	19.13	2.31	1.000
14.73	19.14	2.31	1.000
15.98	19.16	2.3	0.996
17.33	19.22	2.29	0.991
18	19.22	2.29	0.991
22.91	19.16	2.27	0.983
24.16	19.16	2.29	0.991
25.8	19.25	2.32	1.004
27.14	19.31	2.3	0.996
28.49	19.22	2.27	0.983
32.63	19.5	2.32	1.004
33.78	19.4	2.26	0.978
35.52	19.34	2.29	0.991
36.48	19.16	2.3	0.996
39.94	19.22	2.26	0.978
46.39	19.4	2.3	0.996
48.51	19.37	2.27	0.983
52.07	19.74	2.25	0.974
53.52	19.77	2.24	0.970
59.77	19.86	2.23	0.965
60.16	19.89	2.28	0.987
63.33	19.86	2.23	0.965
65.84	19.8	2.26	0.978
71.42	19.8	2.25	0.974
76.62	19.95	2.25	0.974
81.72	20.29	2.26	0.978
86.82	20.41	2.28	0.987
87.49	20.41	2.3	0.996
91.63	20.63	2.32	1.004
92.21	20.69	2.29	0.991
93.84	20.78	2.31	1.000
95.77	21.02	2.3	0.996

Time (days)	Temp (°C)	(A _s) 10 ⁸ (m/s)	A _s ^f (A _s /A _{s0})
3.37	19.41	2.62	1.000
6.75	19.28	2.55	0.973
9.28	19.16	2.48	0.947
10.5	19.16	2.46	0.939
16.12	19.13	2.42	0.924
20.06	19.19	2.35	0.897
24.46	19.16	2.29	0.874
25.3	19.21	2.48	0.947
26.99	19.25	2.67	1.019
27.74	19.22	2.59	0.989
29.61	19.22	2.75	1.050
31.3	19.56	2.9	1.107
32.05	19.53	2.82	1.076
33.74	19.47	2.69	1.027
38.42	19.16	2.74	1.046
39.83	19.22	2.82	1.076
40.39	19.22	2.9	1.107
41.7	19.22	2.98	1.137
44.33	19.4	3.05	1.164
45.64	19.3	3.01	1.149
46.58	19.4	2.93	1.118
59.04	19.86	2.69	1.027
62.42	19.86	2.62	1.000
63.73	19.84	2.74	1.046
64.1	19.8	2.72	1.038
66.73	19.77	2.79	1.065
69.16	19.77	2.7	1.031
71.69	19.8	2.63	1.004
72.82	19.86	2.62	1.000
79.28	20.2	2.64	1.008
80.97	20.29	2.63	1.004
85.19	20.35	2.6	0.992
87.72	20.41	2.52	0.962
88.94	20.47	2.78	1.061
90.62	20.63	2.7	1.031
92.97	20.69	2.67	1.019

cont'd next page

cont'd next page

Table 7.1 Water and salt permeability vs. seawater temperature throughout the year (cont'd)

Water permeability

Salt permeability

Time (days)	Temp (°C)	(A_w) 10⁷ (m/s bar)	A_w^f (A_w/A_{w0})	Time (days)	Temp (°C)	(A_s) 10⁸ (m/s)	A_s^f (A_s/A_{s0})
96.15	21.18	2.32	1.004	93.9	20.75	2.82	1.076
98.18	21.27	2.29	0.991	103.9	21.27	2.98	1.143
102.31	21.42	2.33	1.009	105.9	21.54	3.06	1.168
104.62	21.48	2.29	0.991	107.68	21.63	2.98	1.137
106.74	21.6	2.29	0.991	111.34	21.85	2.92	1.115
108.96	21.69	2.31	1.000	112.18	21.88	2.84	1.084
111.17	21.85	2.28	0.987	122.3	22.76	3.23	1.233
112.81	21.97	2.33	1.009	126.61	22.76	3.16	1.206
115.6	22.18	2.34	1.013	130.83	22.95	3.24	1.237
116.75	22.21	2.29	0.991	137.76	23.13	3.23	1.233
118.68	22.46	2.32	1.004	138.33	23.16	3.24	1.237
120.12	22.64	2.31	1.000	140.86	23.19	3.09	1.179
121.28	22.76	2.31	1.000	142.64	23.31	3.01	1.149
125.13	22.76	2.31	1.000	143.86	23.4	3.21	1.225
128.21	22.85	2.31	1.000	147.98	23.37	3.15	1.202
132.06	22.95	2.37	1.026	149.39	23.37	3.01	1.149
134.85	23.01	2.34	1.013	151.82	23.47	3.18	1.214
136.87	23.13	2.35	1.017	152.01	23.56	3.26	1.244
138.12	23.16	2.38	1.030	153.51	23.71	3.5	1.336
143.03	23.4	2.38	1.030	159.51	23.71	3.46	1.321
148.8	23.37	2.38	1.030	166.16	24.23	3.45	1.317
154.67	23.59	2.36	1.022	171.22	24.29	3.28	1.252
160.74	23.95	2.36	1.022	174.5	24.5	3.43	1.309
166.51	24.23	2.37	1.026	177.13	24.78	3.51	1.340
171.9	24.23	2.38	1.030	183.4	24.53	3.48	1.328
177.49	24.56	2.39	1.035	185.84	24.5	3.45	1.317
183.45	24.53	2.4	1.039	188.09	24.47	3.37	1.286
189.81	24.56	2.41	1.043	189.31	24.56	3.44	1.313
196.16	24.81	2.4	1.039	191.28	24.9	3.21	1.225
202.51	24.99	2.4	1.039	194.74	24.81	3.28	1.252
208.67	24.78	2.39	1.035	195.21	24.81	3.44	1.313
213.77	24.56	2.38	1.030	205.71	24.96	3.47	1.324
217.04	24.29	2.36	1.022	226.14	24.14	3.29	1.256
219.93	24.26	2.34	1.013	227.64	24.05	3.17	1.210
224.74	24.14	2.33	1.009	228.11	23.86	3.22	1.229
226.09	24.14	2.37	1.026	229.33	23.71	3.11	1.187

cont'd next page

cont'd next page

Table 7.1 Water and salt permeability vs. seawater temperature throughout the year (cont'd)

Water permeability

Time (days)	Temp (°C)	(A _w) 10 ⁷ (m/s bar)	A _w ^f (A _w /A _{w0})
228.98	23.86	2.34	1.013
233.02	23.71	2.37	1.026
235.62	23.47	2.33	<i>1.009</i>
239.95	23.22	2.37	1.026
242.45	23.1	2.33	1.009
247.56	22.92	2.32	1.004
252.08	22.7	2.31	<i>0.996</i>
256.7	22.31	2.28	0.987
261.9	22	2.27	0.983
267.67	21.6	2.25	0.974
273.35	21.08	2.24	<i>0.970</i>
281.53	20.96	2.21	0.957
283.55	20.84	2.21	0.957
285	20.75	2.19	0.948
287.88	20.69	2.19	<i>0.948</i>
288.27	20.69	2.17	0.939
290	20.5	2.21	0.957
293.56	20.44	2.17	0.939
296.55	20.32	2.2	<i>0.952</i>
297.03	20.32	2.17	0.939
298.47	20.2	2.19	0.948
300.3	20.17	2.18	0.944
307.13	19.83	2.17	<i>0.939</i>
310.21	19.86	2.17	0.939
313.78	19.74	2.17	0.939
317.14	19.65	2.17	0.939
321.57	19.59	2.19	<i>0.948</i>
325.52	19.59	2.2	0.952
331.49	19.71	2.21	0.957
337.93	19.68	2.21	0.957
344.86	19.65	2.21	<i>0.957</i>
347.27	19.31	2.2	0.952
351.6	19.25	2.21	0.957
356.7	19.28	2.2	0.952
362.96	19.53	2.19	<i>0.948</i>
363.54	19.56	2.19	0.948

Salt permeability

Time (days)	Temp (°C)	(A _s) 10 ⁸ (m/s)	A _s ^f (A _s /A _{s0})
235.23	23.47	3.08	1.176
237.01	23.47	3.09	1.179
239.26	23.22	3.01	<i>1.149</i>
240.85	23.19	2.99	1.141
245.63	22.98	2.93	1.118
245.63	22.98	2.93	1.118
249.48	22.82	3.05	<i>1.164</i>
278.43	20.96	2.62	1.000
287.71	20.69	2.71	1.034
243.2	23.04	2.95	1.126
291.27	20.5	2.78	1.061
294.08	20.35	2.72	1.038
297.18	20.23	2.74	1.046
299.24	20.2	2.7	<i>1.031</i>
300.36	20.17	2.7	1.031
301.3	20.02	2.68	1.023
304.86	19.9	2.68	1.023
305.33	19.83	2.64	<i>1.008</i>
307.58	19.83	2.57	0.981
310.95	19.86	2.54	0.969
314.14	19.71	2.63	1.004
315.55	19.68	2.71	<i>1.034</i>
317.7	19.65	2.54	0.969
325.39	19.59	2.45	0.935
332.13	19.71	2.45	0.935
335.7	19.71	2.45	<i>0.935</i>
338.88	19.71	2.44	0.931
342.44	19.65	2.45	0.935
345.35	19.47	2.42	0.924
355.47	19.25	2.46	<i>0.939</i>
360.16	19.44	2.51	0.958
365.31	19.56	2.5	0.954

Note: Training data in plain, Validation data in *italic*, Test data in **bold**

$$a_1^4 = f_1^4 \left(\sum_{k=1}^2 (w_{1k}^4 a_{1k}^3) + b_1^4 \right) \quad (7.8)$$

Where a_k^3 is given as:

$$a_k^3 = f_i^3 \left(\sum_{k=1}^4 (w_{1k}^3 a_k^2) + b_j^3 \right) \quad (7.9)$$

In general for the 3rd layer, the value of jth neuron can be given as:

$$a_j^3 = f_i^3 \left(\sum_{k=1}^4 (w_{1k}^3 a_k^2) + b_j^3 \right) \quad (7.10)$$

Where a_k^2 is determined as:

$$a_k^2 = f_i^2 \left(\sum_{k=1}^2 (w_{1k}^2 a_k^1) + b_j^2 \right) \quad (7.11)$$

In general for the 2nd layer, the value of jth neuron can be given as:

$$a_j^2 = f_j^2 \left(\sum_{k=1}^2 (w_{jk}^2 a_k^1) + b_j^2 \right) \quad (7.12)$$

The transfer functions describes the relationship between output layer and input layer of each neuron are hyperbolic tangent function ($f_j^2, f_j^3 = \tanh$) between the input and the first hidden and between the two hidden layers. While the linear function ($f_j^4 = 1$) is used between the last hidden layer and the output layer.

The data collected from the field are rarely fed to the NNs. The raw data are normally scaled into an appropriate range (usually between zero and one or one and negative one) (Tanvir and Mujtaba, 2006). The data in Table 7.1 are scaled before used as input data.

The relations used in data scale up are as follow:

Time

$$time_{scal} = \frac{time - time_{mean}}{time_{std}} \quad (7.13)$$

Temperature

$$T_{scal} = \frac{T - T_{mean}}{T_{std}} \quad (7.14)$$

Water permeability

$$A_{w scal}^f = \frac{A_w^f - A_{w mean}^f}{A_{w std}^f} \quad (7.15)$$

Salt permeability

$$A_{s scal}^f = \frac{A_s^f - A_{s mean}^f}{A_{s std}^f} \quad (7.16)$$

Where the subscripts mean, std and scal refer to average, standard deviation and scale up variables respectively.

Two NNs models are solved in order to determine correlations which can be used to calculate water and salt permeability decline factors (A_w^f ; A_s^f). The output values from the NNs are rescaled to find the value in original units. The experimental data was divided into three sets a set of 50% of the data are selected for training , 25 % of the data for validation and last set (25 %) is selected for testing.

The back propagation algorithm (Tanvir and Mujtaba, 2006) is used for training a multilayer feed forward neural network. The Neural Network Toolbox available in MATLAB software is implemented in this study to design and train the data.

The value of neurons (a_j) at the first, second or third layer can be expressed by the following equations:

$$a_1^2 = \tanh (w_{11}^2 time_{scal} + w_{12}^2 T_{scal} + b_1^2) \quad (7.17)$$

$$a_2^2 = \tanh (w_{21}^2 time_{scal} + w_{22}^2 T_{scal} + b_2^2) \quad (7.18)$$

$$a_3^2 = \tanh (w_{31}^2 time_{scal} + w_{32}^2 T_{scal} + b_3^2) \quad (7.19)$$

$$a_4^2 = \tanh (w_{41}^2 time_{scal} + w_{42}^2 T_{scal} + b_4^2) \quad (7.20)$$

$$a_1^3 = \tanh (w_{11}^3 a_1^2 + w_{12}^3 a_2^2 + w_{13}^3 a_3^2 + w_{14}^3 a_4^2 + b_1^3) \quad (7.21)$$

$$a_2^3 = \tanh (w_{21}^3 a_1^2 + w_{22}^3 a_2^2 + w_{23}^3 a_3^2 + w_{24}^3 a_4^2 + b_2^3) \quad (7.22)$$

Water and salt permeability decline factors $A_{w_{scal}}^f$ and $A_{s_{scal}}^f$ can be obtained from the output layer (a_1^4) which produces the final results of processing by the NNs model as:

$$a_1^4 = \tanh(w_{11}^4 a_1^3 + w_{12}^4 a_2^3 + b_1^4) \quad (7.23)$$

The results of two NNs models of $A_{w_{scal}}^f$ and $A_{s_{scal}}^f$ are shown in Table 7.2 and Table 7.3.

The weights and bias between the input layer, hidden and the output layer are included in the results.

The permeability decay factors predicted by the NNs are plotted versus their corresponding experimental values in Figures 7.7 and 7.8. The results illustrate good agreement between the predicted and experimental data. Also, it can be seen from the Figures 7.9, 7.10 that the experimental data of water and salt permeability decay factors are accurately predicted by the NNs model.

7.7 Fouling Model Formulation

Both fresh water production and salt rejection are declined as consequences of formation of fouling layer on the membrane surface. Determination of the optimum maintenance schedule is essential for the optimal RO design and operation where the membrane can be chemically or mechanically cleaned and consequently, membrane performance restored.

See et al. (1999) and Zhu et al. (1997) assumed an exponential decay in water permeability over time and the impact of fouling on salt permeability was ignored. In this work, the fouling model that described by Lu et al. (2006) and taking into account the impact of fouling on both water and salt permeability coefficients are combined with NNs based correlations for water and salt permeability decay factors. The permeability coefficients are given as follows:

$$A_w = A_{w0}(1 - \theta_1 t_2) A_w^f(t_1) \quad (7.24)$$

$$A_s = A_{s0}(1 + \theta_2 t_2) A_s^f(t_1) \quad (7.25)$$

Where A_{w0} and A_{s0} denoted to initial water and salt permeability coefficients, respectively. A_w^f and A_s^f are water and salt membrane permeability decline factors, respectively. t_1 denotes to the length of period since the last cleaning was performed in which the operation time for the cleaned membrane modules will restart at the begging of each cleaning event. The t_2 represents the continuous operation time. The variation in water and salt membrane permeability resulting from the difference between actual seawater temperature (Figure 6.2) and seawater temperature at t_1 time domain is considered in the model.

Table 7.2 NNs parameters for estimation water permeability factor

Weights		bias		Transfer function	
2nd layer					
$w_{11}^2 = 1.15622$	$w_{12}^2 = -1.72079$	$b_1^2 = 3.09386$		tanh	
$w_{21}^2 = -0.05138$	$w_{22}^2 = 0.20847$	$b_2^2 = 0.150153$		tanh	
$w_{31}^2 = 2.04809$	$w_{32}^2 = -3.43108$	$b_3^2 = -3.30951$		tanh	
$w_{41}^2 = 1.42777$	$w_{42}^2 = -0.96244$	$b_4^2 = -1.61448$		tanh	
3rd layer					
		bias			
$w_{11}^3 = 1.76307$	$w_{12}^3 = -0.95896$	$w_{13}^3 = 2.15917$	$w_{14}^3 = 2.20172$	$b_1^3 = -3.03812$	tanh
$w_{21}^3 = 0.28681$	$w_{22}^3 = 1.96992$	$w_{23}^3 = -0.37512$	$w_{24}^3 = 0.67162$	$b_2^3 = 0.29936$	tanh
4th layer					
		bias			
$w_{11}^4 = 0.58228$	$w_{12}^4 = 3.76995$	$b_1^4 = -0.13469$		1	
time mean	time std	T mean	T std	A_w^f <small>w_{mean}</small>	A_w^f <small>w_{std}</small>
167.74	109.41	21.19	1.82	0.99	0.03

Table 7.3 NNs parameters for estimation salt permeability factor

Weights		bias		Transfer function	
2nd layer					
$w_{11}^2 = 1.777414$	$w_{12}^2 = -2.29036$	$b_1^2 = -4.52089$		tanh	
$w_{21}^2 = 0.35902$	$w_{22}^2 = -2.04543$	$b_2^2 = -1.60477$		tanh	
$w_{31}^2 = 1.059634$	$w_{32}^2 = -2.37573$	$b_3^2 = 3.447281$		tanh	
$w_{41}^2 = -4.97533$	$w_{42}^2 = -5.77942$	$b_4^2 = -14.6048$		tanh	
3rd layer					
				bias	
$w_{11}^3 = -1.39766$	$w_{12}^3 = 3.38951$	$w_{13}^3 = 3.07388$	$w_{14}^3 = 1.95439$	$b_1^3 = 0.80823$	tanh
$w_{21}^3 = -1.84938$	$w_{22}^3 = 1.33817$	$w_{23}^3 = -0.16574$	$w_{24}^3 = -4.00229$	$b_2^3 = -6.24591$	tanh
4th layer					
				bias	
$w_{11}^4 = -1.34286$	$w_{12}^4 = 2.575753$	$b_1^4 = 2.617429$		1	
time mean	time std	T mean	T std	A_s^f mean	A_s^f std
177.46	104.73	21.53	2.03	1.108	0.125

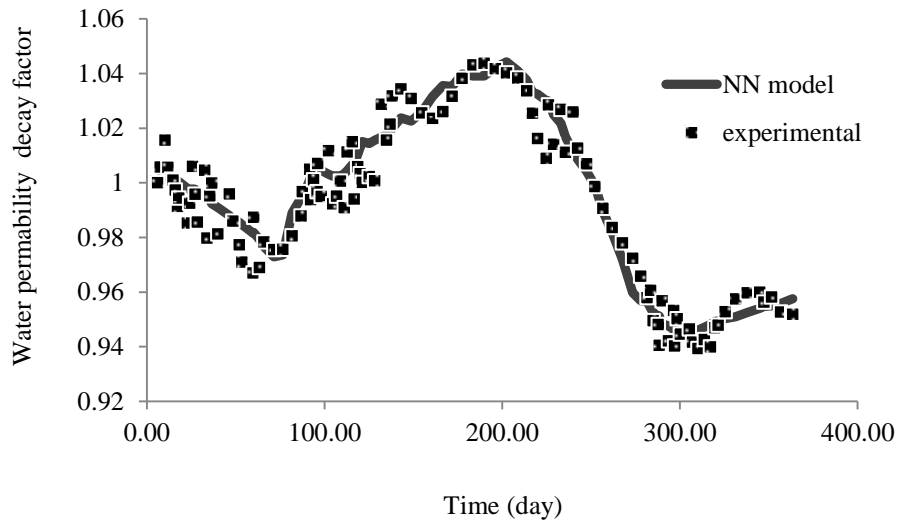


Figure 7.7 Actual water permeability decline factor and the predicted by NNs

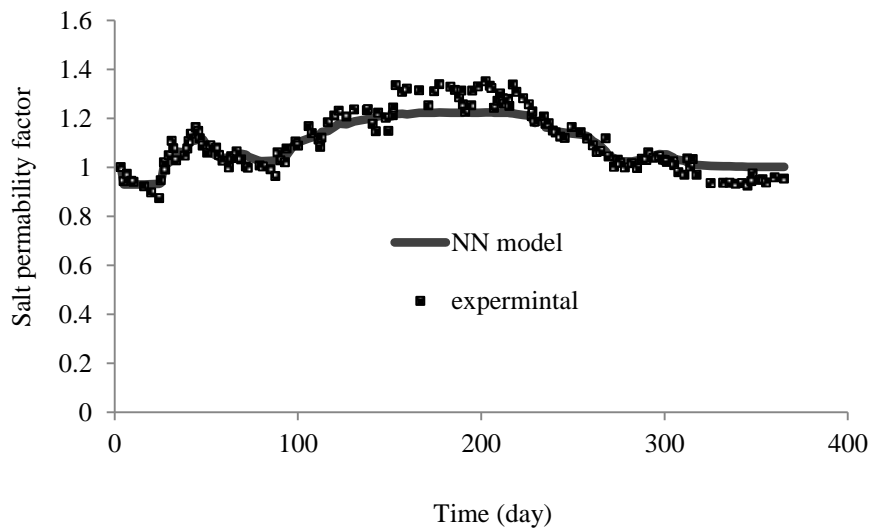


Figure 7.8 Actual salt permeability decline factor and the predicted by NNs

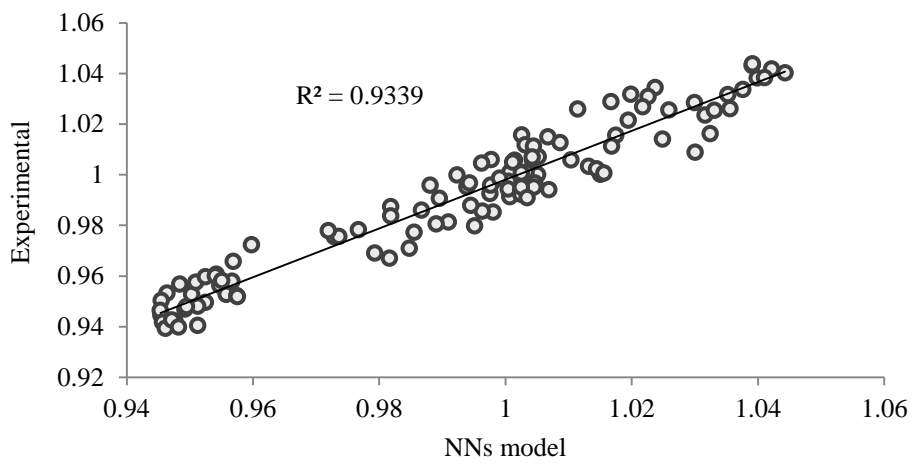


Figure 7.9 Actual and predicted water permeability decay factor

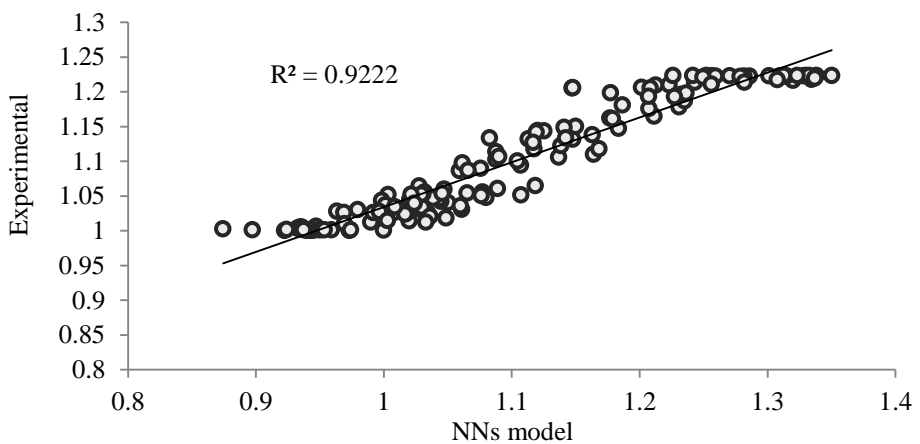


Figure 7.10 Actual and predicted salt permeability decay factor

Generally, RO membranes show better recovery of permeability after chemical cleaning (Hoek et al., 2008). However, the membrane permeability after cleaning was still lower

than initial value and the initial permeability level could not be recovered completely. Therefore, two constants θ_1 and θ_2 are added to the fouling model to represent the membrane degradation extent for water and salt, respectively.

Temperature variation has a significant impact on the RO membrane fouling. However, it is rarely included in the studies related to the design and operation of RO systems (Mo et al., 2008). Jin et al. (2009) pointed out that higher temperature enhances the performance of filtration process by increasing salt diffusivities and diffusion coefficients and, as a result, more salt in permeate and higher permeate flux. Also, when feed temperature increases salt and water membrane permeability also increased. However, higher temperature can also increase the rate of membrane fouling as a consequence of the increase of the tendency of aggregation or adsorption to the membrane surface. Therefore, the temperature dependence of water and salt permeability are empirically included in the NNs model. Note, all physical properties and osmotic pressure are function of temperature.

7.8 MINLP optimization formulation

An MINLP optimization framework is developed to determine the optimal design of RO network scheduling based on the superstructure shown in Figure 7.2.

For a given maintenance and inter-maintenance cycles, the RO design and operation variables are to be optimized in order to maintain the required fresh water demand and including the sea water temperature variation throughout the year.

A mathematical description of RO network and membrane fouling (equations 7.24 and 7.25) are included in the MINLP formulation. The membrane pressure vessels in one-stage RO network (Figure 7.2) are distributed into a number membrane groups (N_g) which are determined prior to optimization based on the number of inter-maintenance cycles. It is to be noted that all membrane groups (N_g) contains equal number of pressure vessels.

For predetermined cleaning schedules, the design of RO networks problem is optimized and the number of pressure vessel (n_p) in each membrane group is found. For each selected schedule (n_c, N_g), the corresponding decision variables are fixed. For each cleaning schedule, the optimal design and operation are obtained by solving the MINLP problem.

The number of membrane groups shown in the superstructure illustration (Figure 7.2) is identified for each maintenance schedule scenario. Discrete variables are used to express discrete decisions such as the number of pressure vessels in each membrane group (n_p) and continuous variables are defined for the optimization of operation variables.

The MINLP problem has the form:

Given: Seawater feed source with variable temperature; design specifications of each membrane element; fixed fresh water demand; maximum salt concentration in fresh water; number of maintenance and inter-maintenance cycles; number of membrane groups

Optimize: The number of parallel pressure vessels in each membrane group; operating conditions (feed flow rate, feed pressure).

So as to minimize: Total annualized cost of fresh water

Subject to: Process constraints: Equality constraints such as process model and inequality constraints such as optimization variables bounds.

Mathematically the optimization problem can be described as:

Minimize TAC

P_f, Q_f, n_p

Subject to: Equality constraints Model equations

Product demand and product quality

$$\text{Inequality constraints} \quad P_f^L \leq P_f \leq P_f^U ; Q_f^L \leq Q_f \leq Q_f^U$$

P_f , Q_f are continuous variables representing feed pressure, feed flow. (np) is an integer parameters representing number of pressure vessels in each membrane group (Ng). The subscripts U and L refer to the upper and lower bounds of the variables, respectively.

7.8.1 The Objective Function

The objective function employed in the MINLP optimization model is defined to minimizing the total annualized cost which is the summation of the annualized capital cost and the annual operating cost. The annualized investment cost is composed into many components including the costs of pre-treatment unit C_{wip} , membrane module C_{me} , booster pumps C_{pu} and ERD C_{ERD} . The annual operating cost consists of net pumping cost OC_{pu} , membrane replacement cost OC_{me} , chemical treatment cost OC_{ch} and annual spares cost OC_{sc} . The cost of membrane module cleaning OC_c is incorporated in the objective function. The cost model equations in section 3.3.4 are used to represent the different cost components.

$$TAC = (C_{WPT} + C_{pu} + C_{ERD} + C_{me})1.411 \times 0.08 + OC_{pu} + OC_{me} + OC_{ch} + OC_{sc} + OC_c \quad (7.26)$$

The membrane cleaning cost is expresses as:

$$OC_c = \sum_{j=1}^{nc} \sum_{i=1}^{Ng} 200 + 200np \quad j \in nc, i \in Ng \quad (7.27)$$

Where (nc) and (Ng) are the number of maintenance and inter-maintenance cycles respectively. The membrane cleaning cost consists of variable cost of \$200 for cleaning of each pressure vessel, and \$200 as a fixed cleaning cost of for downtime during cleaning operation (Lu et al., 2006).

The fixed costs of the pump and the turbine are calculated from the maximum power requirements while the pre-treatment unit cost was calculated based on the maximum feed flow rate.

This objective function allows economic comparison of the candidate configuration of the optimum RO process meanwhile satisfying the operation and design restrictions by adjusting the design and operation variables.

7.9 Case study

The goal is to determine the optimal arrangement and operating conditions for the RO system minimizing the cost of the fresh water at different predetermined cleaning schedules. The annual temperature variation and its subsequent effect on the membrane permeability are considered in this study.

The MINLP design strategy is used to derive optimal design and operation of RO network. A number of membrane modules are divided into groups as shown in Figure 7.2. Each group features an undefined number of pressure vessels, which are arranged in parallel. The optimization was conducted for a single stage configuration with turbine as energy recovery device using spiral wound RO modules. The optimal structural and operational parameters of RO process for each membrane cleaning schedule are found at given water demand ($100 \text{ m}^3/\text{h}$) and maximum salt concentration in the desalinated water (500 ppm).

The characteristics of RO spiral wound membrane (SW30XLE-400) are listed in Table 5.3. Each pressure vessel is assumed to house five spiral wound elements. The parameters used in optimization calculation are listed in Table 7.4.

7.10 Optimal Design and Scheduling Results

Table 7.5 summarizes the process selection for the optimum RO arrangement along with the corresponding membrane maintenance schedules. Cost components displayed in the Table include fixed and variables costs. For more clarification of the cost trend the total cost of fresh water production are also shown in Figure 7.11. A full comparison with the detailed MINLP optimization results for different membrane cleaning schedules are given in Table 7.6.

Table 7.4 Input data for MINLP optimization

	Value	Ref.
Feed pump efficiency (%)	80	
Feed salinity (ppm)	35,000	
Turbine efficiency (%)	80	Marcovecchio et al., (2005)
Load factor	0.9	Marcovecchio et al., (2005)
Pressure vessel unit cost (\$)	1000	Lu et al., 2007
Seawater module cost (\$)	1200	Lu et al., 2007
Electricity unit cost (\$/kWh)	0.08	Lu et al., 2006
Maximum operating pressure (bar)	83	Lu et al., 2007
Module Feed flow range (m ³ /h)	0.8-16	Lu et al., 2007
Coefficient in Equation (7.24) θ_1	1.67×10^{-4}	Lu et al., 2006
Coefficient in Equation (7.25) θ_2 ,	1.67×10^{-4}	Lu et al., 2006

From Table 7.5 and Figure 7.11, the optimum maintenance schedule of the RO network which has the lowest cost is found to have one maintenance cycle and two inter-maintenance cycles. The results specify that half of the membrane modules (14 modules) are to be cleaned in the first six months and the remaining half at the end of the year. The optimum maintenance schedules cost (444.8 k\$/year) is only less by 1.8 % compared to the next optimal schedule one maintenance cycle and three inter-maintenance cycles option (452.9 k\$/y). This shows the high precision trade-off between the design and operation variables where the optimizer efficiently utilizes the advantages of cleaning process in the reduction of the fixed costs of the membrane modules for one maintenance cycle and three inter- maintenance cycles option but with notable increase in the pumping cost.

Cost associated with pump energy consumption for the optimum membrane schedule (one maintenance cycle and two inter- maintenance cycles) shown in Table 7.5 is the heights share where it accounts for 38.6% of the total product cost. This percentage is very close to that found in the literature (Geraldes, et al., 2005).

Three maintenance cycle and one inter-maintenance cycle scheduling option is proven to be the most expensive option (476.8 k\$/year) with the highest variable cost (TOC) about 250.7 k\$/year (Table 7.5). The pumping cost is dominated by the duty required to pressurise the feed to 75 bar (Table 7.6). And consequently, a relatively low salt concentration in the final permeate stream is reported for all inter- maintenance cycles in this scheduling option.

Table 7.5 Cost breakdown for optimal RO systems at different maintenance schedules in (k\$/year)

Maint. cycles	Inter-Maint. Cycles	C_{WIP}	C_{me}	C_{pu}	C_{ERD}	OC_{pu}	TOC	TCC	TAC
1	1	89.3	12.6	78.4	32.9	188.7	248.8	213.2	462.0
	2	88.0	22.1	72.9	31.4	169.0	228.2	216.6	444.8
	3	88.3	16.6	76.1	31.7	178.6	239.0	213.8	452.9
	4	88.3	15.8	77.1	31.6	182.0	240.9	212.8	453.7
2	1	90.1	19.7	73.9	31.9	171.5	232.9	235.3	468.3
	2	89.4	17.4	75.5	31.7	176.2	241.5	214.0	455.8
	3	89.4	17.4	75.5	31.7	176.2	241.5	214.0	455.8
	4	88.6	15.8	76.9	31.7	180.7	244.5	213.0	457.5
3	1	88.4	15.0	76.3	31.5	183.2	250.7	226.0	476.8
	2	89.4	17.4	75.6	31.8	175.9	246.1	214.2	460.2
	3	95.0	19.0	74.8	34.1	164.5	236.6	222.9	459.5
	4	88.9	15.8	76.6	31.7	180.0	248.7	213.0	461.8

For all schedules options shown in Table 7.5, the pumping cost represents the major part of fresh water cost as it is comprise between 36% and 40 % of the total production cost. Also, there is little effect on the fixed cost components (pretreatment, turbine and pump costs) and most of the differences observed were in membrane modules cost which is clearly linked to the pumping cost. The pumping cost increases when the membrane modules cost reduces. This trade-off exists due to increase of the operating pressure to maintain the permeate rate steady when lower number of membrane modules is identified by the optimizer.

It can be seen from Figure 7.11 that three maintenance cycles scheduling option has higher fresh water cost for all inter- maintenance cycles compared with that for one and two maintenance cycles. This may attributed to the high frequency of cleaning operations required.

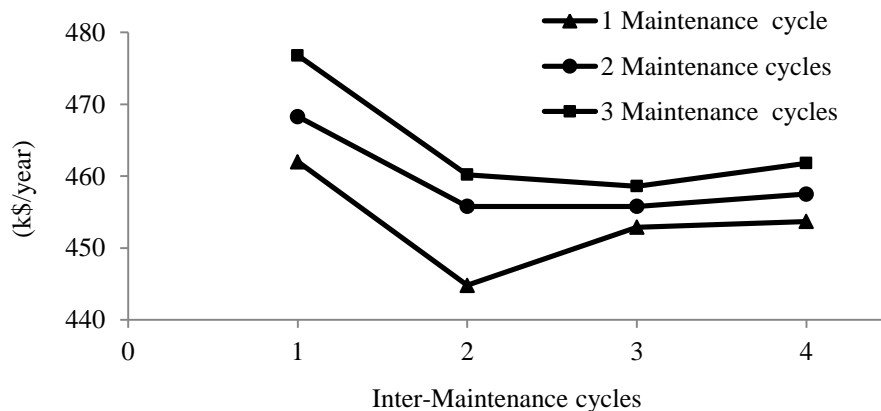


Figure 7.11 Total production cost of the optimal maintenance schedules

Figure 7.12 shows the optimum feed pressure trajectory (one maintenance cycle and two inter-maintenance cycles.) where the feed pressure is varied between 53 and 68 bar depending on the membrane fouling conditions. At the start of the operation all membranes are assumed to be new, the feed pressure is maintained at lower value (52 bar). Due to fouling effect, the feed pressure is gradually increased where it reached 68 bar at the end of the first inter-maintenance period. It was assumed that the membrane

permeability cannot be restored completely after cleaning, therefore, after membrane cleaning at the end of first inter-maintenance cycle, the feed pressure is sharply decreased but to a level higher the initial (54 bar).

In order to display the effect of the annual variation of seawater temperature on RO process operation, Figure 7.13 shows the optimal operation policy for the feed pressure and the resulting permeate salt concentration profile for three maintenance cycle and three inter-maintenance cycles scheduling option. Increases in feed temperature results in increase of water flux but also increase in permeate salinity (Nisan et al., 2005). The impact of these effects on the RO operation is obviously revealed in Figure 7.13. The permeate salinity follows path similar to that for seawater temperature profile (Figure 7.1). Due to the frequent cleaning processes in this scheduling option, the water quality constraint is easily realized for all temperatures. Consequently, the feed pressure trend in Figure 7.13 is consistent with the seawater temperature profile in Figure 7.1. Taking the advantages of the high temperature (higher water flux), feed pressure tends to decline in the high temperature periods. The higher temperature operation compensates the reduction in fresh water production resulting from lower feed pressure as the fresh water salinity constraint not violated.

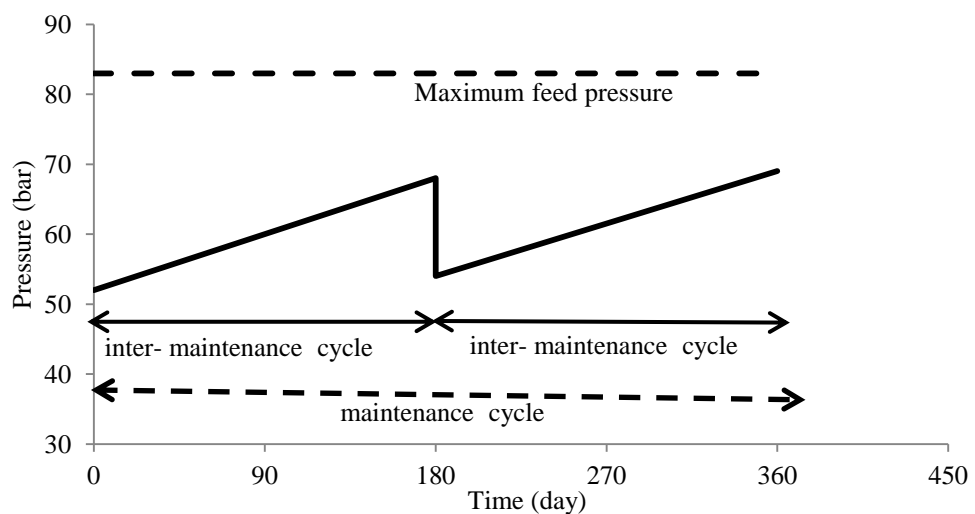


Figure 7.12 Optimal feed pressure profile for one maintenance cycle and two inter-maintenance cycles

Table 7.6 MINLP results for spiral wound membrane scheduling problem

Maintenance Cycle -inter- Maintenance cycle	N o. of P V	Inter-maintenance cycles															
		1				2				3				4			
		Feed pressure (bar).		Permeate conc. (ppm).		Feed pressure (bar).		Permeate conc. (ppm).		Feed pressure (bar).		Permeate conc. (ppm).		Feed pressure (bar).		Permeate conc. (ppm).	
		start	end	start	end	start	end	start	end	start	end	start	end	start	end	start	end
1-1	16	70	76	135	500												
1-2	28	52	68	176	500	54	69	448	344								
1-3	21	59	74	137	237	57	71	245	476	57	74	272	260				
1-4	20	63	74	152	229	63	74	214	418	62	74	339	406	64	76	235	246
2-1	25	55	70	157	445	52	70	352	304								
2-2	22	57	72	141	248	56	72	195	428	55	71	314	477	58	74	209	261
2-3	24	55	67	149	237	55	66	167	288	54	66	267	433	53	66	332	500
2-4	20	64	74	151	218	64	74	165	234	63	74	212	338	62	73	289	423
3-1	17	62	75	127	251	62	75	127	252	72	75	128	251				
3-2	22	57	72	140	246	57	72	157	312	56	71	247	454	55	71	314	500
3-3	24	55	67	151	240	55	67	163	251	54	66	198	341	54	66	272	437
3-4	20	64	74	153	209	64	74	165	223	64	74	172	244	63	73	217	312

cont'd next page

Table 7.6 MINLP results for spiral wound membrane scheduling problem (cont'd)

Cycle - inter-cycle	Inter-maintenance cycles															
	5				6				7				8			
	Feed pressure (bar).		Permeate conc. (ppm).		Feed pressure (bar).		Permeate conc. (ppm).		Feed pressure (bar).		Permeate conc. (ppm).		Feed pressure (bar).		Permeate conc. (ppm).	
	start	end	start	end	start	end	start	end	start	end	start	end	start	end	start	end
2-3	54	67	297	390	56	70	185	269								
2-4	62	73	337	463	62	74	321	397	63	75	238	273	66	76	175	243
3-2	56	73	274	332	59	74	169	244								
3-3	53	66	315	500	53	66	338	486	54	67	300	397	55	68	219	280
3-4	63	73	276	384	62	73	311	429	62	73	342	456	62	73	339	443

cont'd

Table 7.6 MINLP results for spiral wound membrane scheduling problem (cont'd)

Cycle - inter-cycle	Inter-maintenance cycles															
	9				10				11				12			
	Feed pressure (bar).		Permeate conc. (ppm).		Feed pressure (bar).		Permeate conc. (ppm).		Feed pressure (bar).		Permeate conc. (ppm).		Feed pressure (bar).		Permeate conc. (ppm).	
	start	end	start	end	start	end	start	end	start	end	start	end	start	end	start	end
3-3	56	70	173	271												
3-4	62	73	304	385	64	74	245	296	65	76	178	236	65	75	174	238

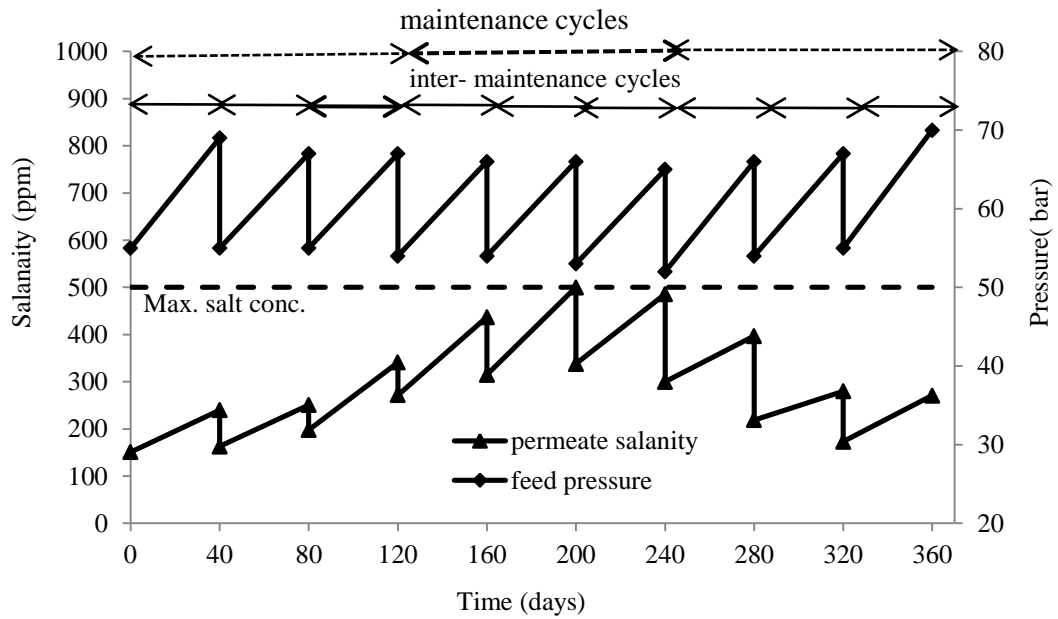


Figure 7.13 Optimal trajectory of feed pressure and permeate salinity for three maintenance cycle and three inter-maintenance cycles

7.11 Conclusion

The present work addresses the optimal design and scheduling of one-stage RO network using gPROMS optimization tool.

NNs based correlation was developed for estimating the permeability decline factors over one year of operation. The NNs model predictions are in good agreement with the experimental data. Then, the predicted permeability decline factors are embedded within the optimization problem formulation.

The design and scheduling of RO network has been formulated as an MINLP problem using spiral wound modules. The scheduling problem is formulated based on systematic technique involves selecting the number of membrane maintenance and inter-maintenance cycles and consequently the corresponding decision variables are fixed for each selected schedule.

The outcomes obtained by solving the MINLP problem showed that a one maintenance cycle with two inter-maintenance cycles scheduling option provides lower total production cost than other scheduling alternatives. The optimum maintenance schedules

cost is only less by 1.8 % compared to the next optimal scheduling option (one maintenance cycle and three inter- maintenance cycles). This infinitesimal difference in the fresh water cost is debatable whether the sensitivity study of cost parameters such as cleaning cost is needed.

However, the results obtained here are for one-stage RO process, this work can be extended for multi-stage RO process provided that long-term performance data for multi stage process is available.

Chapter 8

Brackish Water RO Process: Simulation and Optimization

8.1 Introduction

The RO process performance can be improved by enhancing the efficiency of the equipment used in the RO process (pre-treatment, pumps, energy recovery devices, high permeability membranes, etc.). The improvement of the RO process network design and adapting the optimal operating conditions to this network is the decisive task of RO process manufactures.

This chapter focuses on steady state performance predictions of the brackish water RO desalination plant based on combining Kimura–Sourirajan model with film theory approach, the simulation results were compared with operational data. The sensitivity of different operating and design parameters on RO process performance were investigated via the simulation program.

The RO process performance was enhanced by implementing an NLP optimization framework to minimize specific energy consumption. The optimal operating variable and design parameters are determined by solving the optimization problem.

In chapter six, actual membrane permeability data representing the effect of membrane fouling in one-stage RO process is considered. While in this chapter, Due to the absence of detailed actual data of multi-stage RO process, an exponential decay in membrane permeability over time from literature is assumed to represent the fouling in entire RO system and the influence of fouling on the individual RO stages is rearranged.

The synthesis of RO networks for water desalination is also investigated by state space approach via a superstructure problem (chapter 3). The fouling is assumed to have different values depending on the stage position in the processing array. The optimal

designs of brackish water RO network based desalination using MINLP technique are obtained utilizing spiral wound membrane element.

8.2 Fouling Description

Fouling and scaling have significant impact on the design of RO process, and lead to dynamic adjustment of operation parameters if certain fresh water demand is to be met. In spite of this, most previous models of RO systems do not take in account the effect of fouling (Oh et al., 2009). In this work, an exponential function was used to represent the decline in water permeability coefficient. The water permeability is approximated as follows (Al-Bastaki and Abbas, 2004).

$$A_w = A_{w0} F \quad (8.1)$$

Where A_{w0} is the initial water permeability, F is the fouling factor representing the decay in permeability coefficient caused by the effect of fouling and scaling. Fouling factor (F) for brackish water RO plant described in (Abbas, 2005) is given (Al-Bastaki and Abbas, 2004) as:

$$F = 0.68 \exp\left(\frac{79}{t + 201.1}\right) \quad (8.2)$$

Note, under fouling condition, water flux given by equation (3.1) will become:

$$j_w = A_w^{fo} (\Delta P - \Delta \pi) \quad (8.3)$$

This equation clearly shows the effect of fouling on the water flux. Note, water flux may also affect the rate of fouling build up on the membrane surface which requires a detailed hydrodynamic model of the membrane channels which is beyond the scope of this work. Note the purpose of this study is to analyse the effect of fouling on a given membrane and how it affects the network design and operation of the RO system. This work does not include study on how the fouling would affect the design of the membrane itself.

In the past, for simulation and optimization purposes the effect of fouling on RO unit (which has more than one stage) is assumed to be equal, i.e. the decrease in water permeability with time has the same rate for all stages. And the prediction of water flux through membrane surface (which is function of fouling) has been carried out using fixed permeability decline rate for all stages. Many researchers showed that the fouling level in different stages of RO process varies and depends on the stage location in the process layout (Alqahtany and Albastaki., 1995; See et al., 1999; Huiting, et al., 2001; Karime et al., 2008; Vrouwenvelder et al., 2009b) as discussed in Section 2.3.3.2.

The fouling effect for the two-stage RO is incorporated within the simulation model. The fouling factor F is assumed to have different values depending on the stage position in the processing array. For two stages RO process, the fouling factor for the first stage at any time F^1 is approximate as:

$$F^1 = F S X_{f1} \quad (8.4)$$

And the fouling factor for second stage F^2 as:

$$F^2 = F S (1 - X_{f1}) \quad (8.5)$$

Where X_{f1} is the fraction of fouling level in the first stage. For RO process with two stages, if fouling factor is assumed equal in all stages (average) then. $X_{f1}=0.5$.

8.3 Model Validation

In this work, RO based desalination process is considered using three stages unit described by (Abbas, 2005) as shown in Figure 8.1. The plant nominal operating and design parameters are given in Table 8.1. Commercial Film Tec spiral wound RO membrane elements have been used in the simulation. Three membrane elements in each pressure vessel are connected in series; each element is modelled by a set of non-linear algebraic equations using solution-diffusion model, thin film theory, total and salt balances, etc. (Section 3.2.1.1). The membrane element model is solved sequentially.

The output of first element in the pressure vessel becomes the input for the second element and the same for the pressure vessels in different stages.

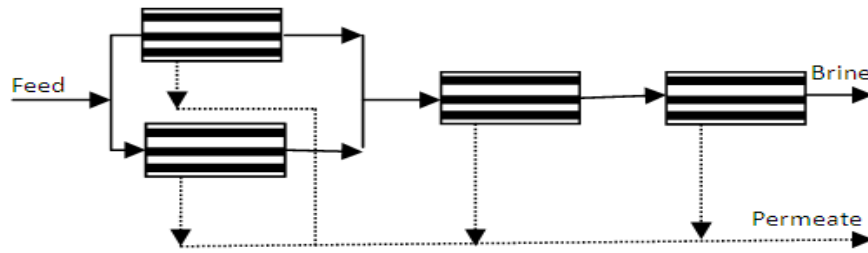


Figure 8.1 Schematic diagram of RO process (Abbas, 2005)

Table 8.1 Membrane parameters and operating conditions

Parameter	Value
Feed conditions	
Q_f (m ³ /h)	20.4
C_f (kg/m ³)	2.54
P_f (bar)	12.2
T_o (°C)	28.8
Membrane and spacer characteristics	
A_w (m/bar s)	9.39×10^{-7}
A_s (m/ s)	5.65×10^{-8}
L_f (m)	2.77×10^{-3}
L (m)	1.0
w (m)	37.2
A (m ²)	37.2
h_{sp} (m)	5.93×10^{-4}
d_h (m)	8.126×10^{-4}

The results using the developed model are validated by comparing the results of Abbas (2005) under identical conditions. As shown in Table 8.2, the model yielded an overall water recovery of 58.0 % and salt rejection of 98.6%. The relative deviations of the simulated results compared to the results of Abbas (2005) are 0.71% and 1.02% for water recovery and salt rejection, respectively.

Further validation of the model is performed by comparing the water recovery and salt rejection at different operating conditions with those predicted by Abbas (2005) (Table 8.3 and Table 8.4). The predictions of this model have good agreement with those

reported by Abbas (2005). The model gives data that have overall absolute average deviation for water recovery 1.45% and 0.41% for salt rejection.

Table 8.2 Comparison operational data with Abbas data and this work results

	Plant Data	Abbas (2005)	% Dev.	This work	% Dev.
Water recovery %	58.82	58.6	0.37	58.0	0.71
Salt rejection %	97.6	98.9	1.33	98.6	1.02

Table 8.3 Comparison of data predicted by Abbas and this work
(Feed concentration 2540 ppm, Feed flow 20.4 m³/h)

Pressure (bar)	Water Recovery %			Salt Rejection %		
	Abbas (2005)	This work	% Dev.	Abbas (2005)	This work	% Dev.
10	44.10	45.32	2.72	98.75	98.4	0.35
11	50.7	51.64	1.77	98.83	98.48	0.35
12	57.00	57.70	1.22	98.87	98.5	0.37
13	63.22	63.51	0.47	98.867	98.515	0.35
14	68.34	68.96	0.96	98.83	98.47	0.36
15	74.20	73.9	0.40	98.82	98.39	0.43

Table 8.4 Compression of data predicted by Abbas and this work
(Feed concentration 2540 ppm, Feed pressure 12.2 bar)

Feed flow (m ³ /h)	Water Recovery %			Salt Rejection %		
	Abbas (2005)	This work	% Dev.	Abbas (2005)	This work	% Dev.
15	74.2	73.3	1.21	98.45	97.76	0.70
16	72	70.6	1.94	98.57	97.99	0.58
18	66	65.12	1.33	98.75	98.3	0.45
20	59	59.8	1.35	98.88	98.5	0.38
22	54.5	55	0.91	98.93	98.62	0.31
24	49.2	50.74	3.13	98.95	98.7	0.25

The model discussed in chapter three (Section 3.2.1.1) is used to predict the system profiles. The parameters used in the calculations are shown in Table 8.1. Stage one contains two identical parallel membrane pressure vessels and the feed was split into two equally streams prior to entering stage one. Thus, in Table 8.5 the same results are presented for the two parallel vessels. Table 8.5 shows that the water feed to the membrane elements are declined as more permeate is recovered in each subsequent element. The pressure drop decreases along the elements in the first stage followed by sudden increase in lead element in the second stage due to the combination of the exit brine from the two pressure vessels in the first stage prior to entering the second stage. Pressure drop in the feed channel should be taken into account in the design stage. Higher pressure drop means higher feed pressure is required at the feed pump.

Another important parameter in membrane design is the individual membrane element recovery, which should not exceed the maximum value recommended by the membrane manufacturer. The individual membrane element recovery is gradually declined while the feed pressure and feed salt concentration decreased and increased respectively (Table 8.5).

The osmotic pressure was only 2.18 bar in the first element of the first stage creating a massive driving force and high water flux for the membrane elements in the first stage (Figure 8.2). As expected, the salt flux gradually increased with the flow direction as the brine becomes more concentrated. At the tail element in the third stage, the osmotic pressure was 4.72 bar while the feed pressure for this element is 10.16, considerable driving force is still there.

From Figure 8.3 it can be noticed that the concentration polarization is much higher in stage one due to the high flux. The decrease in mass transfer coefficient as the feed water moves downstream from element one to element three and the same from elements in stage two and three is as a result of decreasing the brine flow rate in the feed

side. The recombining the feed streams prior to entering stage two and increasing the axial velocity lead to a significant enhancement in the mass transfer from element three in stage one to the first element in the second stage, whereas the concentration polarization is suddenly plunged in the lead element of the stage two. The concentration polarization factor and mass transfer profiles in Figure 8.3 explained the huge enhancement of the mass transfer in the membrane stages and clearly demonstrated the advantages of the tapered configuration for RO systems.

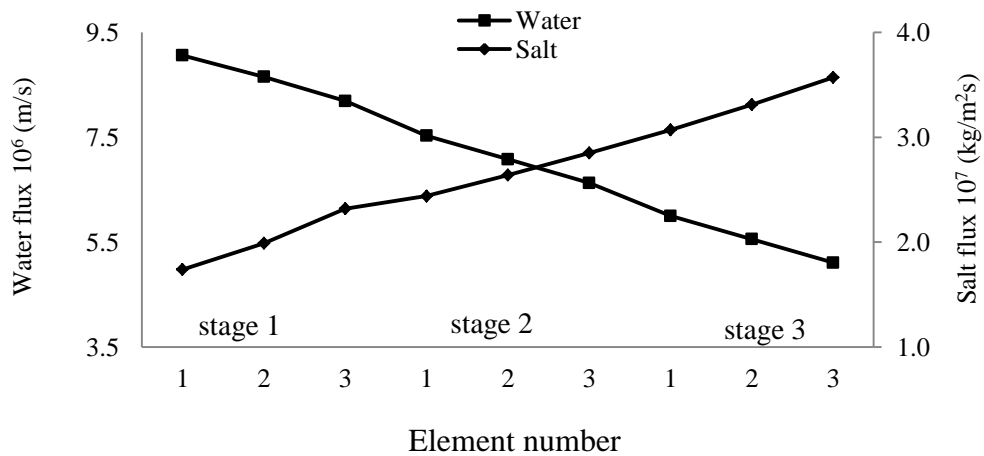


Figure 8.2 Water and salt flux for different RO elements

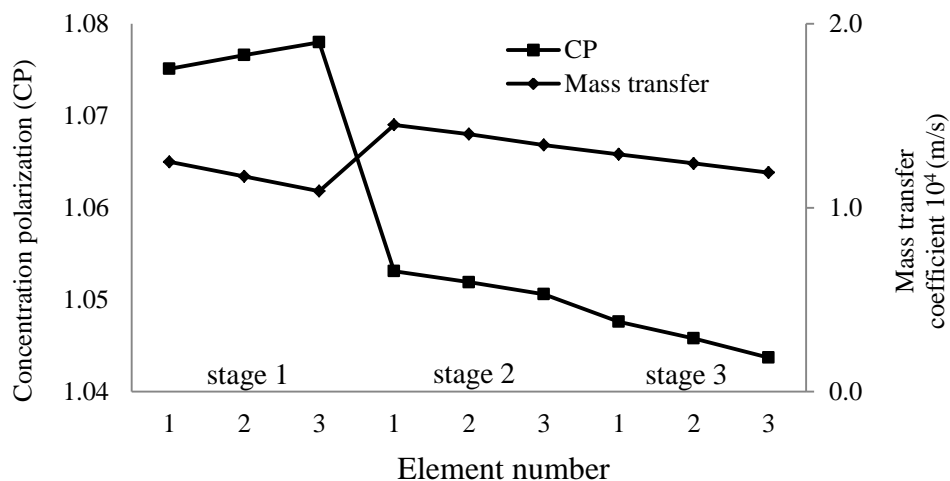


Figure 8.3 Average concentration polarization factor and Mass transfer coefficient for the different RO elements.

Table 8.5 Predicted profiles for the three stages RO process

Membrane elements in PV	Stage 1			Stage 2			Stage 3		
	1	2	3	1	2	3	1	2	3
Feed flow rate (m ³ /h)	10.20	8.99	7.83	13.46	12.46	11.51	10.62	9.82	9.07
Brine flow rate (m ³ /h)	8.99	7.83	6.73	12.46	11.51	10.62	9.82	9.07	8.39
Permeate flow rate (m ³ /h)	1.21	1.16	1.10	1.01	0.95	0.89	0.80	0.74	0.68
Feed salt concentration (kg/m ³)	2.54	2.88	3.30	3.84	4.14	4.48	4.85	5.25	5.67
Brine salt concentration (kg/m ³)	2.88	3.30	3.84	4.14	4.48	4.85	5.25	5.67	6.13
Permeate salt concentration (kg/m ³)	0.02	0.02	0.03	0.03	0.04	0.04	0.05	0.06	0.07
Feed pressure (bar)	11.83	11.70	11.59	11.22	11.00	10.81	10.44	10.29	10.16
Pressure drop (bar)	0.13	0.11	0.08	0.22	0.19	0.17	0.15	0.13	0.11
Water recovery %	11.90	12.89	14.01	7.49	7.61	7.72	7.57	7.58	7.54
Salt rejection %	99.25	99.20	99.14	99.15	99.10	99.04	98.95	98.86	98.77
Water flux 10 ⁶ (m/s)	9.06	8.65	8.19	7.53	7.08	6.63	6.00	5.56	5.11
Salt flux 10 ⁷ (kg/m ² .s)	1.74	1.99	2.32	2.44	2.64	2.85	3.07	3.31	3.57
Concentration polarization factor	1.0751	1.0766	1.0780	1.0531	1.0519	1.0506	1.0476	1.0458	1.0437
Osmotic across membrane (bar)	2.18	2.48	2.86	3.20	3.46	3.74	4.04	4.37	4.72
Axial velocity (m/s)	0.13	0.12	0.10	0.18	0.16	0.15	0.14	0.13	0.12
Mass transfer coefficient 10 ⁴ (m/s)	1.25	1.17	1.09	1.45	1.40	1.34	1.29	1.24	1.19

8.4 Case Study 1: Sensitivity Analysis

The fixed configuration three-stage RO based desalination process of Abbas (2005) (Figure 8.1) is used to study the effect of different operating and design parameters on membrane performance by varying one parameter at a time and keeping the other parameters as listed in Table 8.1.

8.4.1 Sensitivity of Operating Variables

8.4.1.1 Pressure

Figure 8.4a shows the effect of operating pressure on RO plant performance. Salt rejection increases linearly at low to moderate pressure. At higher pressure, salt rejection decreases dramatically due to the increase in osmotic pressure along the feed channel. Average permeates flux curve is divided into two regions. In the lower pressure region, water flux increases linearly which illustrates a linear relationship between the permeate flux and the driving pressure (Equation 3.1). In the higher pressure region water flux starts to level-off at 16 bar (corresponding to flux 1.2×10^{-4} m/s). This may be due to the accumulation of the salt along the membrane channel that exerts an increasing osmotic pressure. The limiting flux is (1.4×10^{-4} m/s) where the flux cannot be increased even when the applied pressure increases.

Variations of specific energy consumption (kWh/m^3) and concentration polarization factor (CP) are shown in Figure 8.4b for operating pressure ranging from 6 to 25 bar. Higher pressure required less specific pumping energy. The minimum specific energy consumption is observed at 12 bar corresponding to water recovery rate 57 %, followed by increase in specific energy due to the stabilization in the permeate production despite increasing applied pressure. As expected CP increase with increase in operating pressure due to the increase in convective transport of salts towards membrane surface.

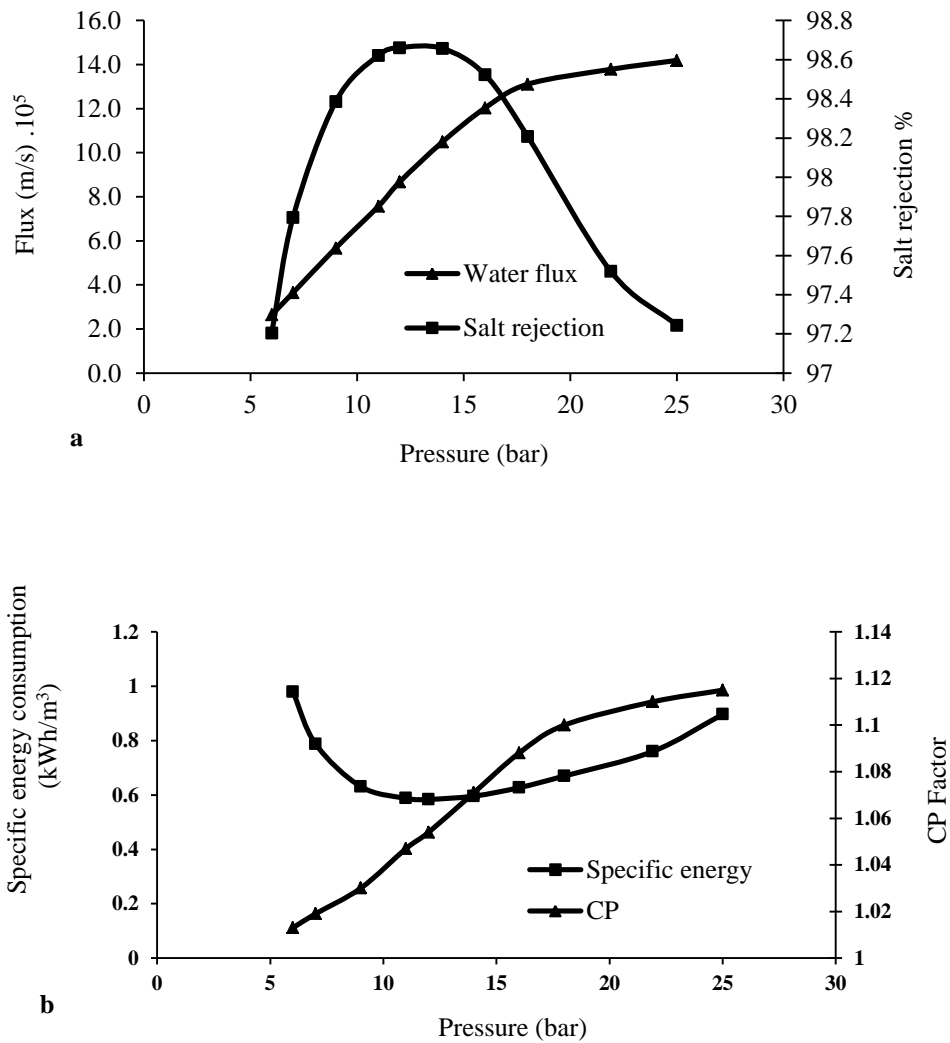


Figure 8.4 Dependence of RO process performance on operating pressure

8.4.1.2 Number of Elements in Pressure Vessel

As shown in Figure 8.5, water recovery ratio increased as number of element in pressure vessel increased due to the greater membrane area. There was a sharp increase at low number of elements and a slow increase at higher number of elements. This was due to the salt build up on the brine channel as flux increases. Therefore adding more elements after a certain limit was not worthy.

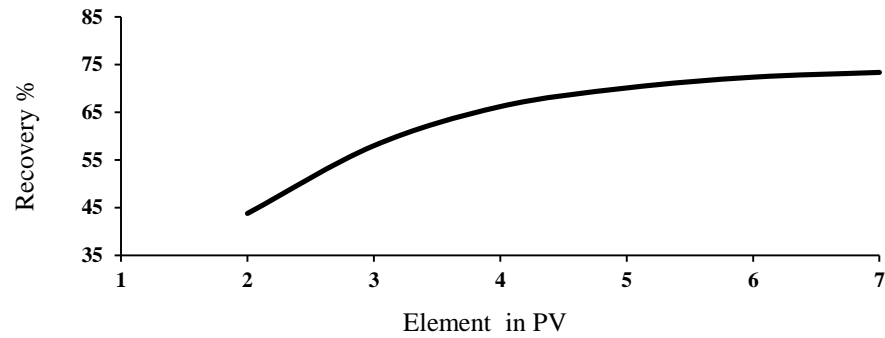


Figure 8.5 Effect of the number of membrane element on the recovery ratio

8.4.1.3 Feed Salinity

The effect of feed salinity on the total recovery ratio can be observed in Figure 8.6a. Two alternative feeds with 2500 ppm and 5000 ppm salt have been studied. Feed with low salt concentration produced 40 % higher recovery ratios more compared to that produced by high feed (5000 ppm). This is a consequence of the much higher driving force for the same exerted pressure to the feed. This is due to the fact that the osmotic pressure is proportional to the feed salt concentration.

8.4.2 Sensitivity of Design Variables

Feed spacer channel can affect RO performance significantly, compared to that with slit feed channel. The effect of neglecting the presence of the spacer in the feed channel is investigated by recalculated the mass transfer coefficients and pressure drop in the feed side for open channels while the other variables will remain as in Table 8.1.

Sherwood number (Al-Bastaki and Abbas, 2003)

$$sh = 1.86(Re Sc d_h/L)^{0.33} \quad (8.6)$$

Pressure drop (Lu et al., 2007)

$$\Delta P_f = \frac{0.0033 Q_f L \mu}{W H_{sp}} \quad (8.7)$$

Even though the pressure drop is increased from 0.122 bar for empty channel to 1.23 bar, the mass transfer is enhanced by 80%. Concentration polarization on membrane

surface is reduced by about 27 %, and the specific energy consumption is reduced by 10%.

8.4.2.1 Length of Filament Mesh in Feed Spacer

Figure 8.6a,b show the recovery of fresh water and pressure drop when mesh length is varied for the two transverse filament thicknesses. It can be seen the recovery rate increases with the increase of mesh length until a turning point at mesh length 3 mm, after which the recovery rate remained relatively stable regardless of further increase of mesh length. Small mesh length has the advantage of more turbulent flow and consequently the polarization phenomenon is decreased. On the other hand smaller mesh length has the drawback of higher pressure drops along feed channel and therefore less water flux as in Figure 8.6a.

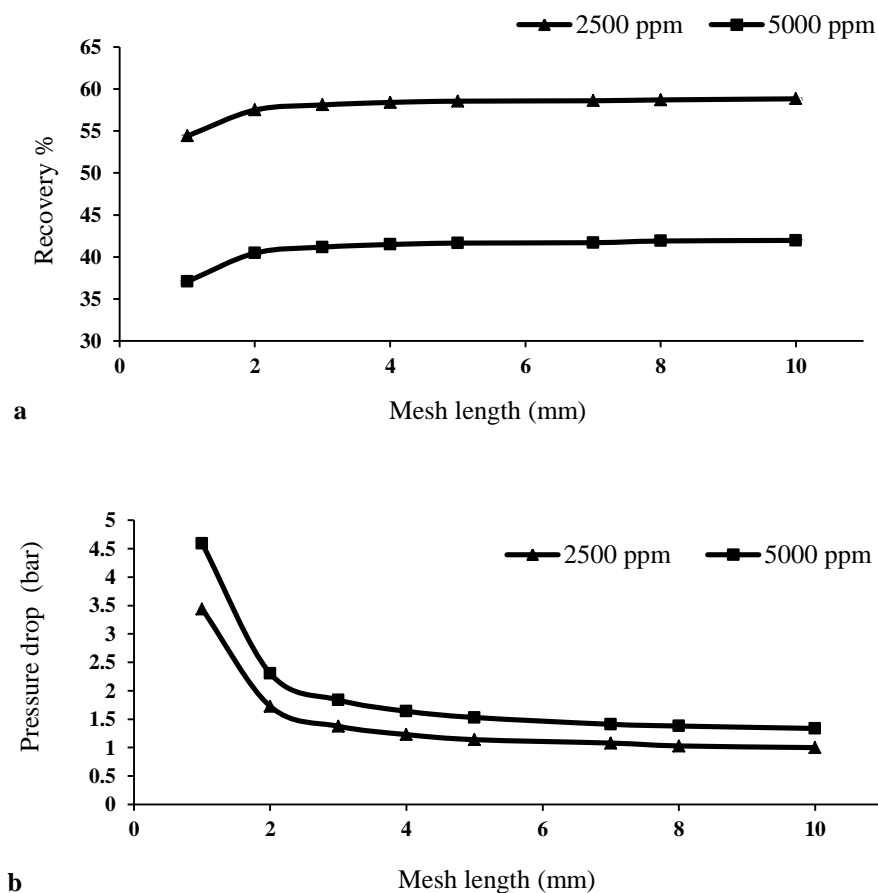


Figure 8.6 Effect of mesh length on water recovery and axial pressure drop at different feed salinity

8.4.2.2 Filament Diameter to Spacing Ratio

Figure 8.7 presents the water recovery, average concentration polarization factors and axial pressure drops for filaments of different diameter to feed spacer ratio. Pressure drop is significantly affected (increase by 342 %) while the concentration polarization is reduced by 8 % at filament ratio 0.6. In general, larger filaments to spacing ratio slightly enhance mass transfer by reducing concentration polarization, but significantly increase hydraulic pressure losses and consequently more expenditure. Therefore, spacers design should be optimized specifically for the particular operating conditions of the real application.

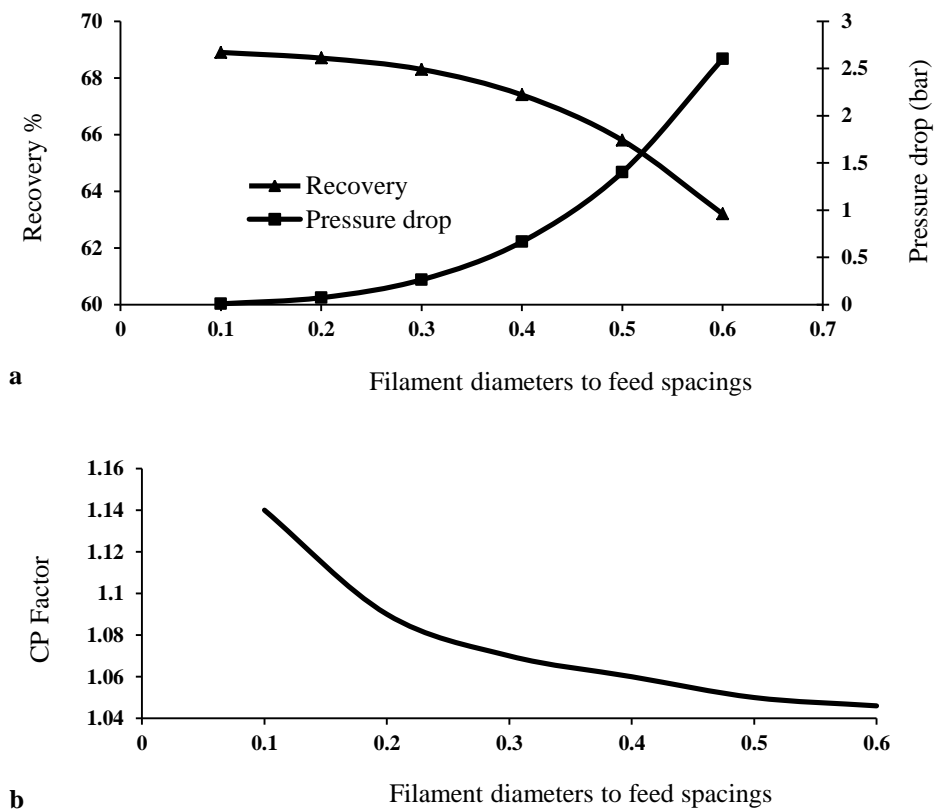


Figure 8.7 RO performance for different spacer diameters and filament spacing

8.4.3 Energy Recovery

Three different options have been considered in this work (i) no energy recovery, (ii) energy recovery by turbine and (iii) energy recovery using pressure exchanger. The efficiencies for the feed pump, turbine and pressure exchanger are assumed as 0.8, 0.8

and 0.97 (Stover, 2007), respectively. Villafafila and Mujtaba (2003) studied different pressure exchanger efficiency in comparison with other energy recovery devices. Figure 8.8 shows the energy recovered by the three alternatives against water recovery ratio. Obviously, using pressure exchanger is seen to be the most profitable option as the pumping cost reduces up to 50 % compared with 20 % when turbine used as energy recovery choice.

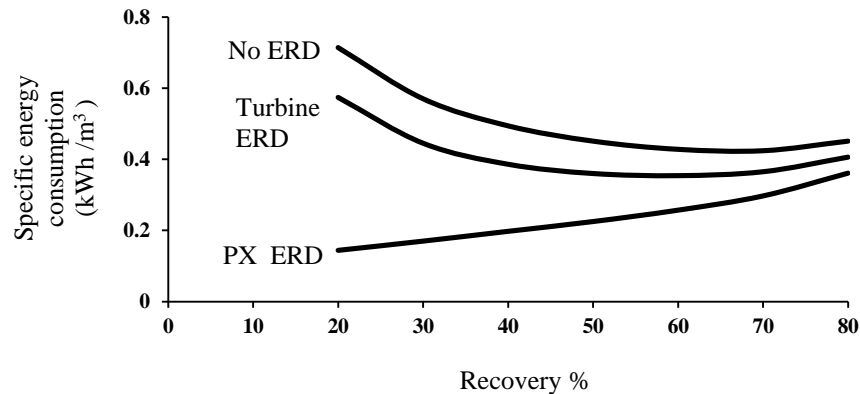


Figure 8.8 RO energy recovery for different recovery devices

8.5 Optimization Study

For the same type of spiral wound membrane two optimization problems are formulated and solved (Case study 2 and 3). In the first problem the operating and module design parameters of the existing RO process in Figure 8.1 is optimized while minimizing specific energy consumption (OP1). The second optimization problem develops an optimized layout for RO process using MINLP approach (OP2). The total annualized cost is considered as objective function.

8.5.1 Case study 2: Optimization of Operating and module Design Parameters (OP1)

In this work, for a fixed water demand and salt concentration the external energy supplied to the system (specific energy consumption) is minimized while the operating and module design variables of the existing three stages RO process (Figure 8.1) are

optimized. Note that electrical energy supply to the pumps is a measure of operating cost and therefore, will reflect the production cost of the fresh water.

A non-linear optimization problem was solved using SQP method within gPROMS software. An optimization strategy which considers both operating variables and module design parameters are formulated as follows:

Given: Feed water conditions; membrane properties and specifications;
freshwater flow and salinity

Optimize: Feed pressure; feed flow; module specifications (feed spacer
filament length and thickness)

So as to minimize: Specific energy consumption E (kWh/ m³).

Subject to: Equality and inequality constrains

Mathematically optimization problem can be represented as:

Minimize E

P_f, Q_f, L_f, H_{sp}

Subject to: Equality constraints: Process model; Product demand;
Product specification

Inequality constrains $P_f^L \leq P_f \leq P_f^U ; Q_f^L \leq Q_f \leq Q_f^U$

$L_f^L \leq L_f \leq L_f^U ; H_{sp}^L \leq H_{sp} \leq H_{sp}^U$

All the variables are defined in the nomenclature.

The optimized values for different parameters (at fixed product demand 11.8 m³/h and permeate salt concentration less than 100 ppm) are shown in Table 8.6. A substantial saving about 20 % and equivalent to 1.7 kWh can be acquired by only optimizing operating parameters (Investigation 1). Reduction in feed flow and slightly increase in operating pressure yields higher driving force in the brine channel. This result is concordant with sensitivity analysis presented before. Further reduction in specific energy can be achieved in Investigation 2 by enlarging feed spacer thickness and

shortening in the filament length. This gives less pressure drop and consequently, less pumping energy and more water flux.

Table 8.6 Optimization Results of Problem 1 (OP1) results

	Optimized parameter	Base case (Abbas, 2005)	Optimized conditions (This work)
Investigation 1	Feed pressure (bar)	12.2	13.6
	Feed flow (m ³ /h)	20.4	14.6
	Specific energy consumption (kWh/m ³)	0.7304*	0.5865
	Feed pressure (bar)	12.2	13.1
Investigation 2	Feed flow (m ³ /h)	20.4	14.9
	Spacer thickness (mm)	0.593	2.2
	Mesh length (mm)	2.77	2.37
	Specific energy consumption (kWh/m ³)	0.7304*	0.5781

*Calculated in this work

8.5.2 Case study 3: RO Network Optimization

The synthesis of RO desalination network is formulated as MINLP problem which seeks to minimize the total annualized cost and subject to process constraints. The representation of membrane network via a superstructure takes into account parallel/series arrangements, bypass and recycle streams among the membrane modules and equipment that may exist in the RO configuration (El-Halwagi, 1992).

The MINLP optimization problem is described as:

- Given: Fixed water demand; permeate salt concentration; membrane module specifications; feed water specifications; membrane properties
- Optimize: Number of series stages; number of parallel pressure vessels in each stage; number of pumps; number of energy recovery devices (turbine); optimal feed pressure; feed flow; other RO network options (Recycle; Bypass)

So as to minimize: Total annualized cost of fresh water

Subject to: Equality constraints such as process model and inequality constraints
such as variables bounds

Mathematically the optimization problem can be represented as:

Minimize TAC

$P_f, Q_f, S, N_j, N_{pu}, N_{tu}, BY, R$

Subject to: Equality constraints: Model equations; Product demand;
Product specification

Inequality constraints $P_f^L \leq P_f \leq P_f^U ; Q_f^L \leq Q_f \leq Q_f^U ;$

$1 \leq N_{pu} \leq S ; 1 \leq N_{tu} \leq S ;$

$0 \leq BY \leq 1 ; 0 \leq R \leq 1$

Two cases of membrane network design based desalination are studied.

The characteristics of spiral wound membrane used are listed in Table 8.1. The parameters used in optimization calculation are given in Table 8.7.

Table 8.7 Input parameters for optimization calculations

Parameter	Value	Reference
Maximum operating pressure (bar)	41	Abbas, 2005
Maximum flow rate per module (m ³ /h)	19.3	Abbas, 2005
Minimum flow rate per module (m ³ /h)	3.6	Abbas, 2005
Pump efficiency (%)	80	Assumed
Turbine efficiency (%)	80	Marcovecchio et al., 2005
Electricity cost (\$/kWh)	0.08	Marcovecchio et al., 2005
Membrane element unit cost (\$)	1000	Marcovecchio et al., 2005
PV unit cost (\$)	1000	Marcovecchio et al., 2005

Before presenting the RO network optimization results, effect of membrane fouling on RO performance is presented.

8.5.2.1 Effect of Membrane Fouling on RO Performance

For a two-stage RO configuration (two PVs in each stage), the new fouling distribution (Equations 8.4 and 8.5) is implemented in the gPROMS simulation code to examine the effect of fouling change between stages on the water permeability, water recovery and water flux. The operating and design conditions remained as shown in Table 8.1.

It can be seen in Figure 8.9 that there is a continuous reduction in the water permeability (A_w) magnitude for all fouling levels in the two stages. The permeability coefficient values have higher values for all fouling levels in the second stage compared with the permeability coefficient in first stage. These differences are observed mainly due to the higher fouling percentage assumed in the first stage. For $X_{f1}=0.5$, the average A_w is reduced about 11% for a period of 90 days, and 16 % during the period between 90 days and 180 days operation.

The effect of fouling level in each stage is shown in Figure 8.10. The recovery rate follows different paths depending on the fouling rate between stages. It is obvious that the higher fouling in the first stage the lower water recovery achieved despite the overall decline rate was the same for all cases investigated.

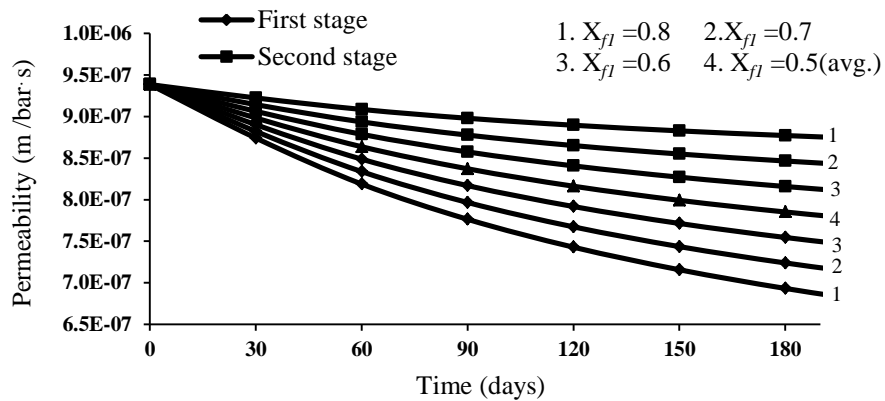


Figure 8.9 Variation of water permeability with different fouling levels for RO stages

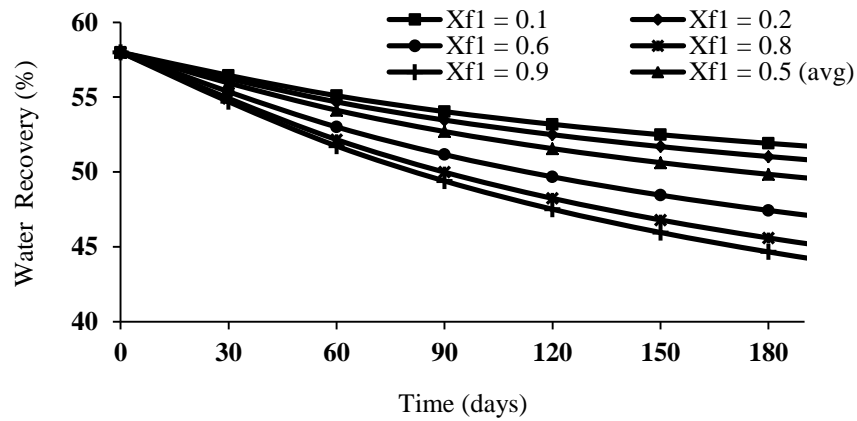


Figure 8.10 Water recovery decline for various fouling percentage at different stages

Figure 8.11 illustrates the influence of fouling level in the first stage on the water flux decline for two stage RO process. For the same fouling extent in each stage (i.e. $X_{f1}=0.5$), the water flux in the first stage is higher than in the second stage and the overall water flux decline over a period of 180 days (shown in Figure 8.11c) are 41 % and 38 % for the first stage and second stage respectively. For $X_{f1}=0.8$ (Figure 8.11a), the water flux in the first stage is also found to be higher than that of the second stage but only up to the period of 60 days and the reduction in water flux for the same period are 66 % and 9% for the first stage and second stage respectively. Note, while the decline rate for the first stage with $X_{f1}=0.8$ is much higher than that observed with $X_{f1}=0.5$, it is opposite for the second stage. These observations have not been reported in the literature.

Figure 8.11a shows that there is no considerable decline in water flux for the second stage at $X_{f1}=0.8$. There are two reasons which can explain this phenomenon. First, it can be due to much lower decline rate in the water permeability for $X_{f1}=0.8$ in the second stage compared to that in the first stage for other fouling distributions (as shown in Figure 8.12). Second, it can be due to the lower feed concentration in the second stage at $X_{f1}=0.8$ compared to that with other fouling distribution (Figure 8.12) leading to decrease in osmotic pressure and thus enhancing water flux.

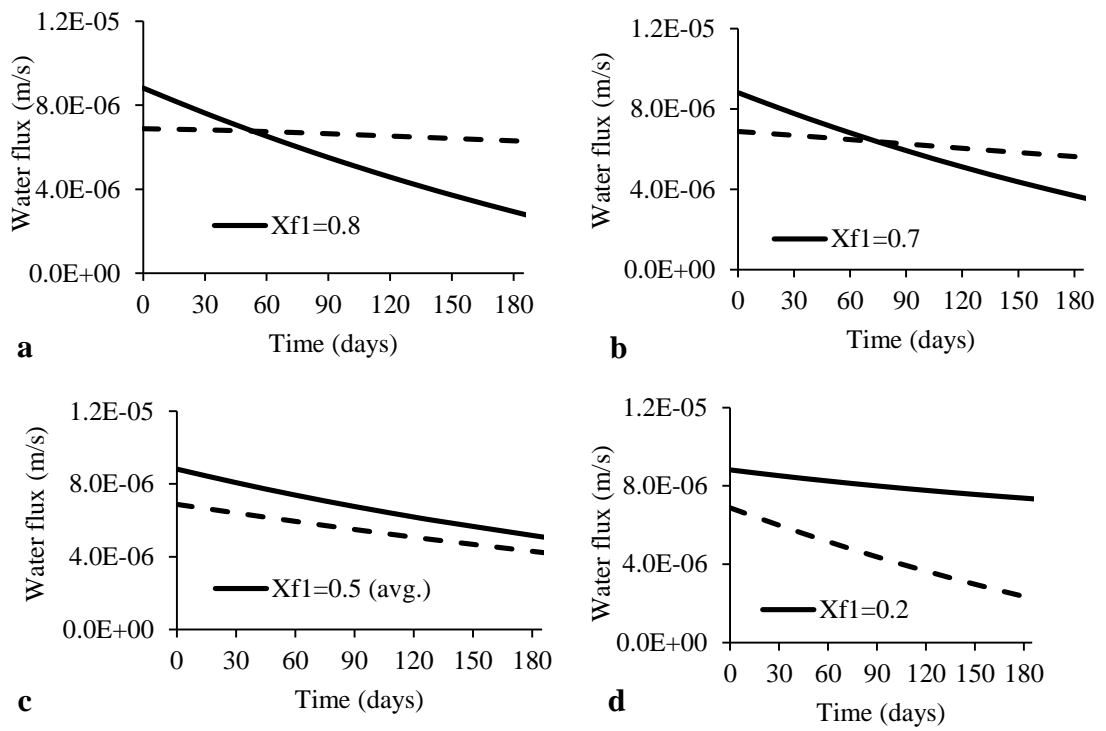


Figure 8.11 Water flux profile for different fouling levels

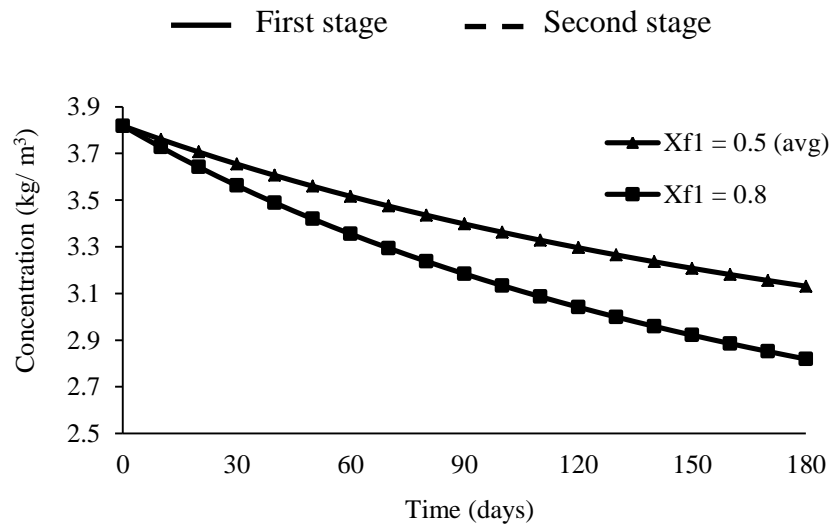


Figure 8.12 Second stage feed concentration at two levels of fouling

8.5.2.2 RO Network Optimization Results

While the search space of the proposed MINLP problem is defined by the superstructure, the starting point of the iterative solution is provided by an initial guess. The initial guess usually has a profound influence on the convergence of the search process (as the MINLP solver used in gPROMS provides local minimum rather than

global minimum). Several starting points with different initial guesses for each case in MINLP problem were performed. Several cases were solved, in which the fouling level into stages vary while the total production is maintained about 40 m³/h and the maximum salt concentration is less than 100 ppm.

Table 5.8 shows the results obtained for different fouling distribution sequences. It can be seen that the optimization results are oriented to a section of the search region where the installing new pump in all fouling distribution scenarios is not favoured because the added cost of installing new booster pump prevail over the gain from the extra quantity of permeate produced. The dilution of feed stream by bypass part of the brine also is not desirable because brine bypass increases the operating cost without considerable enhancement in product quantity.

Table 8.8 Summary of MINLP optimization results

	% Fouling in 1 st stage (X_{f1})			
	Average (0.5)	0.6	0.7	0.8
Optimum process layout	Fig. 8.13b	Fig. 8.13b	Fig. 8.13a	Fig. 8.13b
Feed flow (m ³ /h)	46.3	46.8	45.3	45.45
Feed pressure (bar)	18.44	17.8	19.6	21.16
Overall water recover %	87.4	86.3	87.9	89.2
Permeate concentration (ppm)	99.6	77.8	70.2	46.2
Number of PV in stage 1	8	7	6	4
Number of PV in stage 2	2	3	4	4
Outlet brine Recycle (%)	0	0	0.119	0
Annual operating cost (\$/year)	43513	43514	45001	45802
Total annualised cost (\$/year)	84827	84535	85558	86032
Product cost (\$/m ³)	0.239	0.238	0.241	0.242

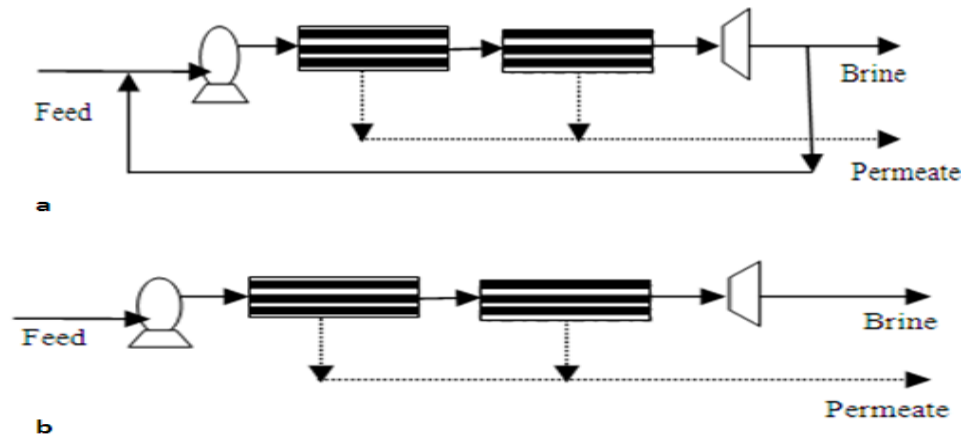


Figure 8.13 The optimum RO process arrangements

There are no mixing between streams with different pressure was set as a condition in constructing the superstructure. Consequently, the recycle of brine should be done after passing through energy recovery device (turbine). This makes the brine recycle option is not attractive. In an attempt to minimize pretreatment and chemical costs about 12% of the brine is recycled at $X_{f1}=0.7$ (Figure 8.13a).

The process layout identified is changed as the fouling level in the first stage varies. As feed pressure is relatively low, two stages configuration was selected in all cases whereas one stages layout is appropriate for process with higher feed salinity (Abbas, 2005).

In Table 8.8, it has been observed that the number of pressure vessels (PV) decreased as the fouling level in first stage increase while the number of PV in second stage are increased in reasonable way to compensate the flux reduction in first stage due to rise in the fouling percentage.

Figure 8.14 presents optimal process pressure trajectory for different fouling distributions between stages. It can be seen that for higher fouling percentage in the first stage more feed pressure needed to met the water demand. The maximum value of feed pressure is reached at $X_{f1}=0.8$. The variations in initial values of feed pressures are caused by the diversity of processes configurations that adapted for each fouling level. It

is illustrated very clearly that the feed pressure increases with the increase the fouling share in first stage regardless lowering the fouling in second stage.

Figure 8.15 shows the change in annual operating cost of the optimum arrangement for different scenario of fouling percentages in RO stages at a fixed demand. It can be seen that the operating cost is proportional to the fouling levels in first stage and this may be caused by the effect of increasing feed pressure (Figure 8.14).

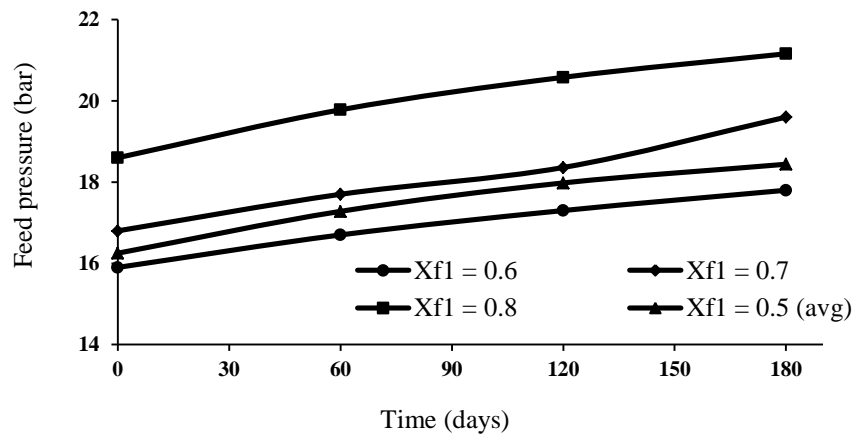


Figure 8.14 Predicted feed pressure-+ at various fouling levels

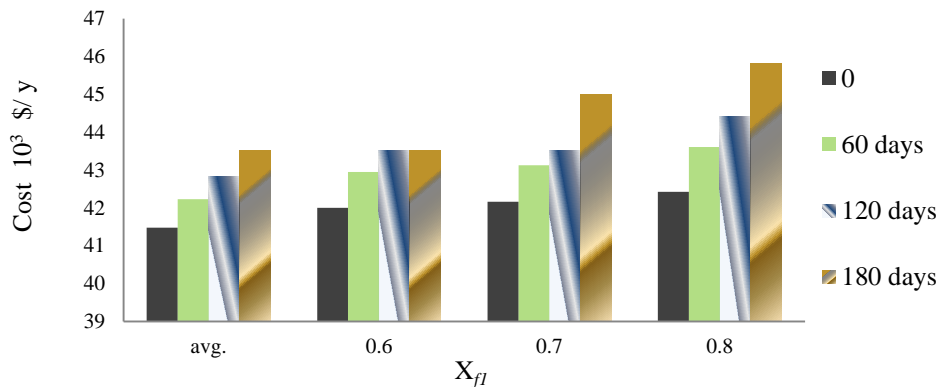


Figure 8.15 Annual operating cost profiles at various fouling levels

8.6 Conclusion

This chapter discusses the process simulation and optimization of brackish water RO desalination process. The steady state RO process model have been developed to investigate the effect of different operating and design parameters on the performance of the system. The model is verified against the operational data and a good agreement was

found. The model is then used to study the sensitivity of the important operating parameters (feed concentration and feed pressure) and design parameters (number of elements, spacer thickness, length of filament) on the plant performance. The simulation results provide reasonable insight of the process performance. Based on the obtained results, the following remarks can be drawn:

- 1) The RO system is found to be sensitive to the variation in the feed pressure and salinity. Increasing the feed pressure increases the plant productivity till certain level and decreases the permeate salinity. Also higher feed water salinity results lower water recovery and higher freshwater salinity.
- 2) Based on RO desalination process utilizing spiral wound element, the effect of membrane element design parameters on the RO process performance were studied:
 - The most remarkable result is that adding more elements in the pressure vessel after certain limit was not worthy. Therefore the number of elements should be optimized to avoid unnecessary cost. In this work, for small brackish water RO desalination it found that the optimum number of elements per pressure vessel is four.
 - Larger filaments length in spiral wound module enhances mass transfer by reducing concentration polarization, but significantly increases hydraulic pressure losses. Therefore, spacers design should be optimized.

Comparison of the two energy recovery alternatives including turbine and pressure exchanger showed that energy recovery by pressure exchanger yields the best results by 50 % reduction in the pumping energy.

For a given RO design, optimization problem formulation is presented to minimize a specific energy consumption while optimizing membrane module design and operating parameters of the process. It is found that considerable reduction in specific pumping energy around 20 % is achievable.

The optimum RO design with spiral wound membrane is studied here for different fouling levels in RO stages. For each fouling level, the optimal operating parameters are also determined. The optimal designs of RO layout are obtained using MINLP approach while optimizing the operating parameters. The study shows that the optimal design and operation of RO process are sensitive to the fouling distribution between stages although the overall fouling remains constant.

Chapter 9

Conclusions and Future Work

9.1 Conclusions

Desalination is one of the most widely used techniques to produce pure water from seawater, groundwater, wastewater or brackish water as highlighted in Chapter one. Several desalination technologies exist nowadays and among them RO process. It is one of the most widely used desalination techniques, and it produces 60% of the total desalinated water (IDA 2010). This work has presented different approaches for effective design and operation of the RO process. Particular attention is given to two aspects in the synthesis of RO networks: 1- The flexible design, scheduling and operation of RO process incorporating variation in sea water temperature and/or fresh water demand (Chapters four, five and six). 2- The effect of membrane fouling on the separation process of the membrane as in Chapter seven and eight.

To carry out meaningful simulation and optimization to generate alternative design and operation scenarios cheaply, development of a reliable process model is the first step.

In this work, gPROMS modelling tool has been used to model an RO process incorporating two theories. The passage of solvent and solute through the membrane layer is simulated by solution-diffusion model while thin film theory is used to account concentration polarization phenomena.

To design an optimal RO system, a superstructure is developed based on two-stage RO system to accommodate all possible connections between streams and equipments. The optimization of RO systems was formulated as a MINLP problem. The objective function was the total annualized cost for the RO process; this objective function allowed economic comparison of different potential arrangements of RO process and operating conditions. The following conclusions can be drawn from this work.

Chapter 4

The capability of the developed MINLP approach was proven by considering hollow fibre module as a case study. The results show that, The MINLP model was able to handle the trade-offs between optimizing variables and costs for different feasible process alternatives. The total annualized cost for the optimal RO network is less by 4 % compared to the optimum layout in literature.

Using the MINLP optimization procedure, the optimum design of various RO systems using hollow fibre modules under different feed concentration and temperatures are obtained. The MINLP framework is based on two-stage RO superstructure and minimizing the total annualized cost. The formulation of the optimization problem enables the optimizer to identify the design with two stages or only one RO stage.

For low and medium feed concentration, the results indicate that the unit production cost of the optimum RO design is decreased as feed temperature increased. For higher feed concentration, the production cost is increased as feed temperature increase due to difficulty of maintaining product quality in the required limit.

The results also show that variation in sea water temperature and salinity will alter the optimum configurations identified from one stage to two-stages with different layout options. A substantial difference in the number of modules required for the operation in high and low temperature seasons suggests the possibility of flexible maintenance scheduling of RO membranes.

Chapter 5

This study aimed to determine the feasibility of using double pass RO desalination process for boron removal from RO permeate. RO membranes boron rejection efficiency was found to be governed by the temperature and solution pH. Mathematical model has been presented to describe boron rejection by RO spiral wound membrane

based on solution-diffusion model and film theory. The developed model was further improved to take into account effect of solution pH and temperature on boron rejection. The major contribution of this aspect of the research is through development of general superstructure for boron removal by double pass RO based desalination process. The RO design problem has been formulated as an MINLP which minimize the total annualized cost based on the superstructure. Two case studies are considered: in first case, double pass RO network with natural seawater feed pH while in second case solution pH is elevated before the second pass. Operating parameters like seawater temperature and pH were studied to see how they affect the performance of boron rejection. The solution pH appears to be the most important factor governing the rejection of boron by a RO process.

the results suggest that a possibility of using RO membranes with natural pH (6–7) at the first pass and elevated pH up to 10 at the second pass to effectively remove boron to the level of the WHO guideline for drinking water (<0.5 mg/L).

Chapter 6

A steady state model for the RO process is developed and linked with a dynamic model for the storage tank. An optimization problem was formulated based on RO model considering variations in water demands and seawater temperature throughout the day to find optimal design decision variables and control operational variables at discreet time intervals that minimize the total operating cost of the RO plant.

Using daily variation of seawater temperature in summer and winter seasons, three RO design scenarios were investigated in which the number of RO modules in operation is varied. The optimization results showed that the winter operation demands more pressure to meet the variable demand due to lower seawater temperature, and consequently, winter operation requires higher specific energy compared to summer operation.

During winter and summer operation, the results clearly show the freshwater demand throughout the day can be fulfilled by using less number of membrane modules despite the changing in seawater temperature but the operating cost will be higher. This allows for a higher degree of flexibility in scheduling where maintenance could be carried out without interrupting the production of water or fully shut down the plant

Chapter 7

Development of a reliable fouling model is required to carry out meaningful optimization of design and maintenance scheduling of RO networks. NNs based correlations are developed based on the actual data for accurate prediction of the RO performance decline. The NNs based correlations predicted water and salt permeability decline factors accurately compared to the actual plant data.

Systematic modeling approach is presented for RO process scheduling problems based on preselected membrane cleaning schedules. The membrane modules were divided into a number of groups depends on a number of the maintenance cycles. This approach provides more flexibility to the RO process operation.

The design and scheduling of RO networks has been formulated as an MINLP problem incorporating NNs based correlation for RO performance decline and including the annual seawater temperature variation. The MINLP problem is solved for each maintenance schedule generating the corresponding optimal design and operation policy. Operating pressure and seawater flow rate are optimized while minimizing the total annualized cost.

The optimum maintenance schedule of the network is found to have one maintenance cycle and two inter-maintenance cycles per year. Also, it has been found that the optimal feed pressure trajectories are depended on the seawater temperature profile as the water quality constraint is easily realized for all temperatures due to the membrane cleaning.

Chapter 8

The developed model successfully predicts the key RO performance parameters i.e. salt rejection and permeate recovery for the simulated feed water. The results generated from the gPROMS simulation code were in good agreement with the published results.

The influences of the operating and design parameters on the RO desalination system performance were investigated.

The simulation results in this chapter provided reasonable insight of the process performance. The next logical step was to formulate an appropriate optimization problem where design and operating parameters are simultaneously optimized.

In this study, a methodology was developed for optimization of the RO process performance. The optimization of RO process operation was achieved by solving the NLP optimization problem. The optimization problem was to find the optimum feed pressure and flow rate while minimizing specific energy consumption, also to fulfil the permeate flow and salinity constraints. The results showed a 20% savings in specific energy consumption compared to the base case. Furthermore, commercial module designs might be further refined in order to reach more economic improvements for RO processes by optimization of spiral wound membrane element design parameters such as mesh length, channel spacing subject to technical limitations. Therefore existing RO commercial module designs should be modified to reduce concentration polarization in the membrane channel and pressure drop as well as to enhance mass transfer.

An MINLP approach for the optimal design and operation of RO process which takes into account fouling effect has been proposed. Different fouling percentages in the RO process stages are assumed and spiral wound module is used in constructing RO network constrained to fixed fresh water production and salt concentration. It is found that the optimal process layout is varied as the fouling percentages in RO first stage

increased; also the annual operating cost of the optimum RO design is increased as the fouling level in the first stage increase.

9.2 Future Work

Some suggestions for future research are addressed here based on the extensive survey and case studies presented in this work:

- A stand-alone RO desalination process system was only investigated in this research. The interaction of RO process with other unit operations or plants was not discussed. The superstructure approach developed in this work can be used as a basis for RO hybrid design. For instance based on the outcomes from this work, seawater temperature variation was found to have a significant impact on the optimal RO design and operation. By hybrid design, it is possible to recover some of the wasting energy, and utilize it either for heating or cooling the RO feed water to the desired temperature.
- Rejection of boron using double pass or single pass RO process could be linked to boron-selective ion exchange resins within the general superstructure developed in this work, with several operational options.
- The results in Chapter 5 show low salinity of freshwater produced from RO process involves boron removal. Therefore, the boron removal MINLP optimization problem can be updated by using NF membranes in the second pass to avoid over-demineralisation of the final product water.
- In this research, the single day operation and design of RO process subject to varying seawater temperature and including storage tank is optimized. Nevertheless, the incorporation of annual temperature variations was not considered in this optimization problem. Thus, using annual temperature profile provides direction and focus for further research.

- The instantaneous energy fluctuations in the case of RO installations powered by renewable energy could be incorporated in the optimization framework developed in Chapter 6.
- The assumption of constant decay of the RO process performance over time may lead to inaccurate prediction of the optimal RO design and operation. Therefore, an accurate model that describes the local fouling in a multi-stage RO process can be considered. NNs tool may be used to develop such a model as in Chapter 7.
- Preliminary results in Chapter 8 show that the RO operation is sensitive to the number of modules in a pressure vessel. Thus, the synthesis of RO networks could be optimized for the optimum number of modules in a pressure vessel.
- A dynamic simulation model could be used in the optimization formulations developed in this work for control and design of RO processes.

References

- Abbas, A. (2005) Simulation and analysis of an industrial water desalination plant, *Chemical Engineering and Processing* 44, 999-1004.
- Abbas, A. (2006) Model predictive control of a reverse osmosis desalination unit, *Desalination* 194, 268-280.
- Abbas, A. (2007) Enhancement of productivity in reverse osmosis desalination processes, *Asian Journal of Water, Environment and Pollution* 4, 23-29.
- Abbas, A. and Al-Bastaki, N. (2001) Performance decline in brackish water FilmTec spiral wound RO membranes, *Desalination* 136, 281-286.
- Abuzinada, A. H., Barth, H. J., Krupp, F. and Böer, B., Al Abdessalaam, T. Z. (2008) Protecting the Gulf's Marine Ecosystems from Pollution, Basel.
- Alahmad, M. (2010) Prediction of performance of sea water reverse osmosis units, *Desalination* 261, 131-137.
- Alatiqi, I. M., Ghabris, A. H. and Ebrahim, S. (1989) System-identification and control of reverse-osmosis desalination, *Desalination* 75, 119-140.
- Alatiqi, I., Ettouney, H. and El-Dessouky, H. (1999) Process control in water desalination industry: an overview, *Desalination* 126, 15-32.
- Al-Bastaki, N. and Abbas, A. (2003) Permeate recycle to improve the performance of a spiral-wound RO plant, *Desalination* 158, 119-126.
- Al-Bastaki, N. and Abbas, A. (2004) Long-term performance of an industrial water desalination plant, *Chemical Engineering and Processing* 43, 555-558.
- Al-Bastaki, N. M. and Abbas, A. (1999) Modeling an industrial reverse osmosis unit, *Desalination* 126, 33-39.
- Al-Bastaki, N. M. and Abbas, A. (2000) Predicting the performance of RO membranes, *Desalination* 132, 181-187.
- Al-Enezi, G., and Fawzi, N. (2003) Design consideration of RO units: case studies, *Desalination* 153, 281-286.
- Alqahtany, H. I. and Albastaki, N. M. S. (1995) Effect of aging on the performance of RO hollow-fiber membranes in a section of an RO plant, *Desalination* 101, 177-183.

- Amiri, M. C. and Samiei, M. (2007) Enhancing permeate flux in a RO plant by controlling membrane fouling, *Desalination* 207, 361-369.
- Argust, P. (1998) Distribution of boron in the environment, *Biological Trace Element Research* 66, 131-143.
- Assef, J. Z., Watters, J. C., Deshpande, P. B. and Alatiqi, I. M. (1997) Advanced control of a reverse osmosis desalination unit, *Journal of Process Control* 7, 283-289.
- Aubert, H. and Pinta, M. (1977) Trace elements in soils, Elsevier Scientific, Amsterdam.
- Australian Drinking Water Guidelines, (2004).
- Avlonitis, S., Hanbury, W. T. and Benboudinar, M. (1991) Spiral wound modules performance - an analytical solution .1, *Desalination* 81, 191-208
- Bagajewicz, M. J. and Manousiouthakis, V. (1992) Mass heat-exchange network representation of distillation networks, *AIChE Journal* 38, 1769-1800.
- Bartman, A. R., Christofides, P. D. and Cohen, Y. (2009) Nonlinear model-based control of an experimental reverse-osmosis water desalination system, *Industrial & Engineering Chemistry Research* 48, 6126-6136.
- Bartman, A. R., Zhu, A., Christofides, P. D. and Cohen, Y. (2010) Minimizing energy consumption in reverse osmosis membrane desalination using optimization-based control, *Journal of Process Control* 20, 1261-1269.
- Bergamini, M. L., Aguirre, P. and Grossmann, I. E. (2005). 'Logic based outer approximation for global optimization of synthesis of process networks', *Computers and Chemical Engineering*, 29, 1914–1933.
- Bhattacharyya, D., Back, S. L., Kermode, R. I. and Roco, M. C. (1990) Prediction of concentration polarization and flux behavior in reverse-osmosis by numerical-analysis, *Journal of Membrane Science* 48, 231-262.
- Bielik, P., Smutka, L. and Horská, E. (2010) Water-Strategic commodity for the 21st century: the role of global business activities and social responsibility, *DSM Business Review*, 2, 2-21.

- Borchers, B. and Mitchell, J. E. (1997) A computational comparison of branch and bound and outer approximation algorithms for 0-1 mixed integer nonlinear programs, *Computers & Operations Research* 24, 699-701.
- Boudinar, M. B., Hanbury, W. T. and Avlonitis, S. (1992) Numerical simulation and optimisation of spiral-wound modules, *Desalination* 86, 273-290.
- Bouguerra, W., Mnif, A., Hamrouni, B. and Dhahbi, M. (2008) Boron removal by adsorption onto activated alumina and by reverse osmosis, *Desalination* 223, 31-37.
- Busch, J., Cruse, A. and Marquardt, W. (2007) Run-to-run control of membrane filtration processes, *AIChE Journal* 53, 2316-2328 (b)
- Cabassud, M., Delgrange-Vincent, N., Cabassud, C., Durand-Bourlier, L. and Laine, J. M. (2002) Neural networks: a tool to improve UF plant productivity, *Desalination* 145, 223-231
- Chaaben, A.B., Andoulsi, R., Sellami A. and Mhiri, R. (2011) MIMO Modeling approach for a small photovoltaic reverse osmosis desalination system, *Journal of Applied Fluid Mechanics* 4, 35-41
- Chatterjee, A., Ahluwalia, A., Senthilmurugan, S. and Gupta, S. K. (2004) Modeling of a radial flow hollow fiber module and estimation of model parameters using numerical techniques, *Journal of Membrane Science* 236, 1-16.
- Chen, J. S., Wang, F. Y., Meybeck, M., He, D. W., Xia, X. H. and Zhang, L. T. (2005) Spatial and temporal analysis of water chemistry records (1958-2000) in the Huanghe (Yellow River) basin, *Global Biogeochemical Cycles* 19.
- Chen, K. L., Song, L. F., Ong, S. L. and Ng, W. J. (2004) The development of membrane fouling in full-scale RO processes, *Journal of Membrane Science* 232, 63-72.
- Cheryan, M. (1998) Ultrafiltration and Microfiltration Handbook. *Technomic Publishing Co., Inc., Lancaster, PA.*
- Chillon Arias, M. F., Valero i Bru, L., Prats Rico, D. and Varo Galvan, P. (2011a) Approximate cost of the elimination of boron in desalinated water by reverse osmosis and ion exchange resins, *Desalination* 273, 421-427.

- Chillón Arias, M., Bru, L. and Rico D., Galvañ, P. (2011b) Kinetic behaviour of sodium and boron in brackish water membranes, *Journal of Membrane Science*, 368, 86–94.
- Chiolle, A., Gianotti, G., Gramondo, M. and Parrini, G. (1978) Mathematical model of reverse osmosis in parallel-wall channels with turbulence promoting nets, *Desalination* 26, 3-16.
- Choi, H., Zhang, K., Dionysiou, D. D., Oerther, D. B. and Sorial, G. A. (2005) Influence of cross-flow velocity on membrane performance during filtration of biological suspension, *Journal of Membrane Science* 248, 189-199.
- Council of the European Union, (1998) Council Directive 98/83/EC, November 3, on the quality of water intended for human consumption.
- Curcio, S., Calabro, V. and Iorio, G. (2006) Reduction and control of flux decline in cross-flow membrane processes modeled by artificial neural networks, *Journal of Membrane Science* 286, 125-132.
- Dacosta, A. R., Fane, A. G. and Wiley, D. E. (1994) Spacer characterization and pressure-drop modeling in spacer-filled channels for ultrafiltration, *Journal of Membrane Science* 87, 79-98.
- Dendukuri, D., Karode, S. K. and Kumar, A. (2005) Flow visualization through spacer filled channels by computational fluid dynamics-II: improved feed spacer designs, *Journal of Membrane Science* 249, 41-49.
- Desalination Market, (2010) Global Forecast and Analysis, *Global Water Intelligence*.
- Djebedjian, B., Gad, H., Khaled, I. and Abou Rayan M. (2008) Optimization of reverse osmosis desalination system using genetic algorithms technique, *twelfth international water technology conference, iwtc12*, Alexandria, Egypt.
- Duran, M. A. and Grossmann, I. E. (1986) An outer-approximation algorithm for a class of mixed-integer nonlinear programs, *Mathematical Programming* 36, 307-339.
- Dydo, P., Turek, M., Ciba, J., Trojanowska, J. and Kluczka, J. (2005) Boron removal from landfill leachate by means of nanofiltration and reverse osmosis, *Desalination* 185, 131-137.

- Edgar, T. F., Himmelblau, D. M. and Ladson, L. S. (2001) Optimization of chemical processes, Boston, Mc-Graw Hill.
- ElHalwagi, A. M. and Manousiouthakis, V. (1996) Analysis and simulation of hollow-fiber reverse-osmosis modules, *Separation Science and Technology* 31, 2505-2529.
- Elhalwagi, M. M. (1992) Synthesis of reverse-osmosis networks for waste reduction, *AICHE Journal* 38, 1185-1198.
- Eltawil, M. A., Zhengming, Z. and Yuan, L. Q. (2009) A review of renewable energy technologies integrated with desalination systems, *Renewable & Sustainable Energy Reviews* 13, 2245-2262.
- Emad, A., Ajbar, A. and Almutaz, I. (2012) Periodic control of a reverse osmosis desalination process, *Journal of Process Control* 22, 218-227.
- Evangelista, F. (1985) A short cut method for the design of reverse-osmosis desalination plants, *Industrial & Engineering Chemistry Process Design and Development* 24, 211-223.
- Farmani, R., Walters, G. and Savic, D. (2006) Evolutionary multi-objective optimization of the design and operation of water distribution network: total cost vs. reliability vs. water quality, *Journal of Hydroinformatics* 8, 165-179.
- Fiacco, A.V. and McCormick, G.P. (1968) Nonlinear programming: sequential unconstrained minimization techniques, John Wiley & Sons, New York.
- Flemming, H. C., Schaule, G., Griebe, T., Schmitt, J. and Tamachkiarowa, A. (1997) Biofouling - the Achilles heel of membrane processes, *Desalination* 113, 215-225.
- Fletcher, R. and Leyffer, S. (1994) Solving mixed-integer nonlinear programs by outer approximation, *Mathematical Programming* 66, 327-349.
- Fritzmann, C., Lowenberg, J., Wintgens, T. and Melin, T. (2007) State-of-the-art of reverse osmosis desalination, *Desalination* 216, 1-76.
- Geoffrion, A.M. (1972) A generalized benders decomposition, *Journal of optimization theory and applications* 10, 237-260.
- Geraldes, V., Pereira, N. E. and de Pinho, M. N. (2005) Simulation and optimization of medium-sized seawater reverse osmosis processes with spiral-wound modules, *Industrial & Engineering Chemistry Research* 44, 1897-1905.

- Geraldes, V., Semiao, V. and de Pinho, M. N. (2002) Flow management in nanofiltration spiral wound modules with ladder-type spacers, *Journal of Membrane Science* 203, 87-102.
- Ghobeity, A. and Mitsos, A. (2010) Optimal time-dependent operation of seawater reverse osmosis, *Desalination* 263, 76-88.
- Gilau, A. M. and Small, M. J. (2008) Designing cost-effective seawater reverse osmosis system under optimal energy options, *Renewable Energy* 33, 617-630.
- Gill, P. E., Murray, W. and Saunders, M. A. (2005) SNOPT: An SQP algorithm for large-scale constrained optimization (Reprinted from SIAM Journal Optimization, vol 12, pg 979-1006, 2002), *Siam Review* 47, 99-131.
- Goosen, M. F. A., Sablani, S. S., Al-Maskari, S. S., Al-Belushi, R. H. and Wilf, M. (2002) Effect of feed temperature on permeate flux and mass transfer coefficient in spiral-wound reverse osmosis systems, *Desalination* 144, 367-372.
- Gorenflo, A., Brusilovsky, M., Faigon, M. and Liberman, B. (2007) High pH operation in seawater reverse osmosis permeate: First results from the world's largest SWRO plant in Ashkelon, *Desalination* 203, 82-90.
- Goyal, V. and Ierapetritou, M. G. (2004) Computational studies using a novel simplicial-approximation based algorithm for MINLP optimization, *Computers & Chemical Engineering* 28, 1771-1780.
- gPROMS Advanced User Guide, (2005) Process Systems Enterprise Ltd., London.
- Greenlee, L. F., Lawler, D. F., Freeman, B. D., Marrot, B. and Moulin, P. (2009) Reverse osmosis desalination: Water sources, technology, and today's challenges, *Water Research* 43, 2317-2348.
- Grote, F., Froehlich, H. and Strube, J. (2012) Integration of Reverse-Osmosis Unit Operations in Biotechnology Process Design, *Chemical Engineering & Technology* 35, 191-197.
- Guidelines for Drinking Water Quality, Boron, (2011) WHO. Water desalination report (46 (7), 15 Feb 2010)

- Guillen, G. and Hoek, E. M. V. (2009) Modeling the impacts of feed spacer geometry on reverse osmosis and nanofiltration processes, *Chemical Engineering Journal* 149, 221-231.
- Guria, C., Bhattacharya, P. K. and Gupta, S. K. (2005) Multi objective optimization of reverse osmosis desalination units using different adaptations of the non-dominated sorting genetic algorithm (NSGA), *Computers & Chemical Engineering* 29, 1977-1995.
- Hameed, M. S. (1989) Design method of reverse-osmosis units used in desalination, *Desalination* 75, 85-96.
- Hasson, D., Drak, A., Komlos, C., Yang, Q. and Semiat, R. (2007) Detection of fouling on RO modules by residence time distribution analyses, *Desalination* 204, 132-144.
- Hatfield, G. B. and Graves, G. W. (1970) Optimization of a reverse osmosis system using nonlinear programming, *Desalination* 7, 147-&.
- Hawaidi, E.A.M. and Mujtaba, I. M. (2011) Meeting Variable Freshwater Demand by Flexible Design and Operation of the Multistage Flash Desalination Process, *Ind. Eng. Chem. Res.*, 50, 10604–10614.
- Health Canada, (2003) Summary of Guidelines for Canadian Drinking Water Quality, Health Canada, Ottawa.
- Heijman, S. G. J., Rabinovitch, E., Bos, F., Olthof, N. and van Dijk, J. C. (2009) Sustainable seawater desalination: Stand-alone small scale windmill and reverse osmosis system, *Desalination* 248, 114-117.
- Hilal, N., Kim, G. J. and Somerfield, C. (2011) Boron removal from saline water: A comprehensive review, *Desalination* 273, 23-35.
- Hoek, E. M. V., Allred, J., Knoell, T. and Jeong, B. H. (2008) Modeling the effects of fouling on full-scale reverse osmosis processes, *Journal of Membrane Science* 314, 33-49.
- Howe, P. D. (1998) A review of boron effects in the environment, *Biological Trace Element Research* 66, 153-166.
- Huiting, H., Kappelhof, J. and Bosklopper, T. G. J. (2001) Operation of NF/RO plants: from reactive to proactive, *Desalination* 139, 183-189.

- Hung, P. V. X., Cho, S. H. and Moon, S.-H. (2009) Prediction of boron transport through seawater reverse osmosis membranes using solution-diffusion model, *Desalination* 247, 33-44.
- Hunt, C. D. (2003) Dietary boron: An overview of the evidence for its role in immune function, *Journal of Trace Elements in Experimental Medicine* 16, 291-306.
- Hyung, H. and Kim, J.-H. (2006) A mechanistic study on boron rejection by sea water reverse osmosis membranes, *Journal of Membrane Science* 286, 269-278.
- Ian, C. Watson, PE.; O.J. Morin, Jr., PE. and Lisa Henthorne PE. (2003), *Desalting Handbook for Planners*, 3rd Edition, ,Desalination and Water Purification Research and Development Program Report No. 72.
- IDA Desalination Yearbook 2008–2009, Global Water Intelligence, 2009.
- IDA Desalination Yearbook 2010–2011, Global Water Intelligence, 2011.
- Jacob, C. (2007) Seawater desalination: Boron removal by ion exchange technology, *Desalination* 205, 47-52.
- Jin, X., Jawor, A., Kim, S. and Hoek, E. M. (2009) Effects of feed water temperature on separation performance and organic fouling of brackish water RO membranes, *Desalination* 239, 346-359.
- Kabay, N., Guler, E. and Bryjak, M. (2010) Boron in seawater and methods for its separation - A review, *Desalination* 261, 212-217.
- Kaghazchi, T., Mehri, M., Ravanchi, M. T. and Kargari, A. (2010) A mathematical modeling of two industrial seawater desalination plants in the Persian Gulf region, *Desalination* 252, 135-142.
- Kallrath, J. (2000) Mixed integer optimization in the chemical process industry - Experience, potential and future perspectives, *Chemical Engineering Research & Design* 78, 809-822.
- Karime, M., Bouguecha, S. and Hamrouni, B. (2008) RO membrane autopsy of Zarzis brackish water desalination plant, *Desalination* 220, 258-266.
- Kawai, Y., Ando, K. and Kawamura, H. (2009) Distortion of near-surface seawater temperature structure by a moored-buoy hull and its effect on skin temperature and heat flux estimates, *Sensors* 9, 6119-6130.

- Kedem, O. and Katchalsky, A. (1989) Thermodynamic analysis of the permeability of biological membranes to non-electrolytes. 1958, *Biochim Biophys Acta* 1000, 413-430.
- Khan, A.H., (1986) 'Desalination Processes and Multistage Flash Distillation Practice', Elsevier Publishers, New York.
- Khawaji, A. D., Kutubkhanah, I. K. and Wie, J. M. (2008) Advances in seawater desalination technologies, *Desalination* 221, 47-69.
- Khayet, M., Cojocar, C. and Essalhi, M. (2011) Artificial neural network modeling and response surface methodology of desalination by reverse osmosis, *Journal of Membrane Science* 368, 202-214.
- Khayet, M., Essalhi, M., Armenta-Deu, C., Cojocar, C., and Hilal, N. (2010) Optimization of solar-powered reverse osmosis desalination pilot plant using response surface methodology, *Desalination* 261, 284-292.
- Khedr, M. (2000) Membrane fouling problems in reverse osmosis desalination applications. *Desalination & Water Reuse* 10, 8-17.
- Kim, J.S., Kim, J.H., Park, J.M., Park, S.M., Choe, W. and Heo, H. (2008) Auto tuning PID controller based on improved genetic algorithm for reverse osmosis Plant, *International Journal of Intelligent Systems and Technologies* 30, 232-237.
- Kim, S., and Hoek, E. M. V. (2005) Modeling concentration polarization in reverse osmosis processes, *Desalination* 186, 111-128.
- Kim, Y. M., Kim, S. J., Kim, Y. S., Lee, S., Kim, I. S. and Kim, J. H. (2009) Overview of systems engineering approaches for a large-scale seawater desalination plant with a reverse osmosis network, *Desalination* 238, 312-332.
- Kimura, S. and Sourirajan, S. (1967) Analysis of data in reverse osmosis with porous cellulose acetate Membranes, *AIChE Journal* 13, 497-503.
- Kumano, A., Sekino, M., Matsui, Y., Fujiwara, N. and Matsuyama, H. (2008) Study of mass transfer characteristics for a hollow fiber reverse osmosis module, *Journal of Membrane Science* 324, 136-141.

- Kumar, M., Adham, S. S. and Pearce, W. R. (2006) Investigation of seawater reverse osmosis fouling and its relationship to pretreatment type, *Environmental Science & Technology* 40, 2037-2044.
- Lee, Y. G., Lee, Y. S., Jeon, J. J., Lee, S., Yang, D. R., Kim, I. S. and Kim, J. H. (2009) Artificial neural network model for optimizing operation of a seawater reverse osmosis desalination plant, *Desalination* 247, 180-189.
- Li, M. H. (2010) Minimization of Energy in Reverse Osmosis Water Desalination Using Constrained Nonlinear Optimization, *Industrial & Engineering Chemistry Research*, 49, 1822-1831.
- Libotean, D., Giralt, J., Giralt, F., Rallo, R., Wolfe, T. and Cohen, Y. (2009) Neural network approach for modeling the performance of reverse osmosis membrane desalting, *Journal of Membrane Science* 326, 408-419.
- Lising, E. R., and Alward, R. (1972) Unsteady state operation of a reverse-osmosis desalination unit, *Desalination* 11, 261-268.
- Lonsdale, H.K., Merten, U. and Riley, R.L. (1965) Transport properties of cellulose acetate osmotic membranes. *J. Appl. Poly. Sci.*, 9, 1341-362.
- Lu, J. and Lu, W. Q. (2010) A numerical simulation for mass transfer through the porous membrane of parallel straight channels, *International Journal of Heat and Mass Transfer* 53, 2404-2413.
- Lu, Y. Y., Hu, Y. D., Xu, D. M. and Wu, L. Y. (2006) Optimum design of reverse osmosis seawater desalination system considering membrane cleaning and replacing, *Journal of Membrane Science* 282, 7-13.
- Lu, Y. Y., Hu, Y. D., Zhang, X. L., Wu, L. Y. and Liu, Q. Z. (2007) Optimum design of reverse osmosis system under different feed concentration and product specification, *Journal of Membrane Science* 287, 219-229.
- Magara, Y., Tabata, A., Kohki, M., Kawasaki, M. and Hirose, M. (1998) Development of boron reduction system for sea water desalination, *Desalination* 118, 25-33.
- Majali, F., Ettouney, H., Abdel-Jabbar, N. and Qiblawey, H. (2008) Design and operating characteristics of pilot scale reverse osmosis plants, *Desalination* 222, 441-450.

- Malek, A., Hawlader, M. N. A. and Ho, J. C. (1994) A lumped transport parameter approach in predicting B10 RO permeator performance, *Desalination* 99, 19-38.
- Malek, A., Hawlader, M. N. A. and Ho, J. C. (1996) Design and economics of RO seawater desalination, *Desalination* 105, 245-261.
- Mane, P. P., Park, P. K., Hyung, H., Brown, J. C. and Kim, J.-H. (2009) Modeling boron rejection in pilot- and full-scale reverse osmosis desalination processes, *Journal of Membrane Science* 338, 119-127.
- Marcovecchio, M. G., Aguirre, P. A. and Scenna, N. J. (2005) Global optimal design of reverse osmosis networks for seawater desalination: modeling and algorithm, *Desalination* 184, 259-271.
- Marcovecchio, M. G., Scenna, N. J. and Aguirre, P. A. (2010) Improvements of a hollow fiber reverse osmosis desalination model: Analysis of numerical results, *Chemical Engineering Research & Design* 88, 789-802.
- Mareth, B. (2006) A reverse osmosis treatment process for produced water: optimization, process control, and renewable energy application, M.S. Thesis in chemical engineering, Texas A&M University.
- Marriott, J. and Sorensen, E. (2003) A general approach to modelling membrane modules, *Chemical Engineering Science* 58, 4975-4990.
- Martin-Rosales, W., Pulido-Bosch, A., Vallejos, A., Gisbert, J., Andreu, J. M. and Sanchez-Martos, F. (2007) Hydrological implications of desertification in southeastern Spain, *Hydrological Sciences Journal-Journal Des Sciences Hydrologiques* 52, 1146-1161.
- Maskan, F., Wiley, D. E., Johnston, L. P. M. and Clements, D. J. (2000) Optimal design of reverse osmosis module networks, *AIChE Journal* 46, 946-954.
- McFall, C. W., Bartman, A., Christofides, P. D., Cohen, Y. and Ieee. (2008) Control of a reverse osmosis desalination process at high recovery, In (2008) *American Control Conference 1-12*, 2241-2247.
- Michaels, A. S. (1968) New separation technique for the chemical process industries, *Chem. Eng. Prog.* 64, 31-43
- Miranda, M. S. and Infield, D. (2003) A wind-powered seawater reverse-osmosis system without batteries, *Desalination* 153, 9-16.

- Mo, H., Tay, K. G. and Ng, H. Y. (2008) Fouling of reverse osmosis membrane by protein (BSA): Effects of pH, calcium, magnesium, ionic strength and temperature, *Journal of Membrane Science* 315, 28-35.
- Murkes, J. and Bohman, H. (1972) Mathematical modeling of reverse-osmosis and ultrafiltration processes, *Desalination* 11, 269-301.
- Niemi, H., Bulsari, A. and Palosaari, S. (1995) Simulation of membrane separation by neural networks, *Journal of Membrane Science* 102, 185-191.
- Nisan, S., Commercon, B. and Dardour, S. (2005) A new method for the treatment of the reverse osmosis process, with preheating of the feedwater, *Desalination* 182, 483-495.
- Oh, H. J., Hwang, T. M. and Lee, S. (2009a) A simplified simulation model of RO systems for seawater desalination, *Desalination* 238, 128-139.
- Oh, H.-J., Choung, Y.-K., Lee, S., Choi, J.-S., Hwang, T.-M. and Kim, J. H. (2009b) Scale formation in reverse osmosis desalination: model development, *Desalination* 238, 333-346.
- Onwubiko, C. (2000) Introduction to engineering optimization. Prentice Hall Inc., Upper Saddle River, NJ.
- Pais, J. A. G. C. R. and Ferreira, L. M. G. A. (2007) Performance study of an industrial RO plant for seawater desalination, *Desalination* 208, 269-276.
- Park, C., Lee, Y. H., Lee, S. and Hong, S. (2008) Effect of cake layer structure on colloidal fouling in reverse osmosis membranes, *Desalination* 220, 335-344.
- Pastor, M. R., Ruiz, A. F., Chillón, M. F. and Rico, D. P. (2001) Influence of pH in the elimination of boron by means of reverse osmosis, *Desalination* 140, 145-152.
- Paul, D. R. (2004) Reformulation of the solution-diffusion theory of reverse osmosis, *Journal of Membrane Science* 241, 371-386.
- Penate, B., and Garcia-Rodriguez, L. (2011) Energy optimisation of existing SWRO (seawater reverse osmosis) plants with ERT (energy recovery turbines): Technical and thermoeconomic assessment, *Energy* 36, 613-626.

- Perrot, N., Me, L., Trystram, G., Trichard, J. M. and Decloux, M. (1996) Optimal control of the microfiltration of sugar product using a controller combining fuzzy and genetic approaches, *Fuzzy Sets and Systems* 94, 309-322.
- Prats, D., Chillon-Arias, M. F. and Rodriguez-Pastor, M. (2000) Analysis of the influence of pH and pressure on the elimination of boron in reverse osmosis, *Desalination* 128, 269-273.
- Quesada, I., and Grossmann, I. E. (1992) An lp/nlp based branch and bound algorithm for convex minlp optimization problems, *Computers & Chemical Engineering* 16, 937-947.
- Redondo, J., Busch, M. and De Witte, J. P. (2003) Boron removal from seawater using FILMTEC (TM) high rejection SWRO membranes, *Desalination* 159, 99-99.
- Robertson, M. W., Watters, J. C., Desphande, P. B., Assef, J. Z. and Alatiqi, I. M. (1996) Model based control for reverse osmosis desalination processes, *Desalination* 104, 59-68.
- Ross, V F, and Edwards. J. O. (1967) The Chemistry of Boron and Its Compounds." In The Chemistry of Boron and its Compounds, by Earl L. Muetterties, Wilmington: John Wiley and Sons, Inc. 155-207.
- Sagiv, A. and Semiat, R. (2004) Analysis of parameters affecting boron permeation through reverse osmosis membranes, *Journal of Membrane Science* 243, 79-87.
- Saif, Y., Elkamel, A. and Pritzker, M. (2009) Superstructure optimization for the synthesis of chemical process flowsheets: Application to optimal hybrid membrane systems, *Engineering Optimization* 41, 327-350.
- Sarkar, P., Goswami, D., Prabhakar, S. and Tewari, P. K. (2008) Optimized design of a reverse osmosis system with a recycle, *Desalination* 230, 128-139.
- Schneider, R. P., Ferreira, L. M., Binder, P., Bejarano, E. M., Goes, K. P., Slongo, E., Machado, C. R., and Rosa, G. M. Z. (2005) Dynamics of organic carbon and of bacterial populations in a conventional pretreatment train of a reverse osmosis unit experiencing severe biofouling, *Journal of Membrane Science* 266, 18-29.
- Schwinge, J., Wiley, D. E. and Fletcher, D. F. (2002) A CFD study of unsteady flow in narrow spacer-filled channels for spiral-wound membrane modules, *Desalination* 146, 195-201.

- See, H. J., Vassiliadis, V. S. and Wilson, D. I. (1999) Optimisation of membrane regeneration scheduling in reverse osmosis networks for seawater desalination, *Desalination* 125, 37-54.
- Sekino, M. (1993) Precise analytical model of hollow-fiber reverse-osmosis modules, *Journal of Membrane Science* 85, 241-252.
- Senthilmurugan, S., Ahluwalia, A. and Gupta, S. K. (2005) Modeling of a spiral-wound module and estimation of model parameters using numerical techniques, *Desalination* 173, 269-286.
- Singh, R. (2008) Sustainable fuel cell integrated membrane desalination systems, *Desalination* 227, 14-33.
- Singh, R. and Tembrock, J. (1999) Effectively control reverse osmosis systems, *Chemical Engineering Progress* 95, 57-64.
- Song, L. F. and Yu, S. C. (1999) Concentration polarization in cross-flow reverse osmosis, *AIChE Journal* 45, 921-928.
- Song, L. F., Chen, K. L., Ong, S. L. and Ng, W. J. (2004) A new normalization method for determination of colloidal fouling potential in membrane processes, *Journal of Colloid and Interface Science* 271, 426-433.
- Sourirajan, S. and J. P. Agrawal (1969) 'Reverse Osmosis', *Industrial and Engineering Chemistry* 61, 62-89.
- Spiegler, K. S. and Kedem, O. (1983) Thermodynamics of hyperfiltration (reverse-osmosis) - criteria for efficient membranes, *Current Contents/Engineering Technology & Applied Sciences*, 16-16.
- Starov, V. M., Smart, J. and Lloyd, D. R. (1995) Performance optimization of Hollow-Fiber reverse-osmosis membranes .1. Development of theory, *Journal of Membrane Science* 103, 257-270.
- Stover, R. L. (2007) Seawater reverse osmosis with isobaric energy recovery devices, *Desalination* 203, 168-175.
- Subramani, A., Kim, S. and Hoek, E. M. V. (2006) Pressure, flow, and concentration profiles in open and spacer-filled membrane channels, *Journal of Membrane Science* 277, 7-17.

- Sundaramoorthy, S., Srinivasan, G. and Murthy, D. V. R. (2011) An analytical model for spiral wound reverse osmosis membrane modules: Part I - Model development and parameter estimation, *Desalination* 280, 403-411.
- Taniguchi, M., Fusaoka, Y., Nishikawa, T. and Kurihara, M. (2004) Boron removal in RO seawater desalination, *Desalination* 167, 419-426.
- Taniguchi, M., Kurihara, M. and Kimura, S. (2001) Boron reduction performance of reverse osmosis seawater desalination process, *Journal of Membrane Science* 183, 259-267.
- Taniguchi, Y. (1978) Analysis of reverse-osmosis characteristics of roga spiral-wound modules, *Desalination* 25, 71-88.
- Tanvir, M. S. and Mujtaba, I. M. (2006) Neural network based correlations for estimating temperature elevation for seawater in MSF desalination process, *Desalination* 195, 251-272.
- Tanvir, M. S. and Mujtaba, I. M. (2008) Optimisation of design and operation of MSF desalination process using MINLP technique in gPROMS, *Desalination* 222, 419-430.
- Technical Manual, Dow Water & Process Solutions, FILMTEC Reverse Osmosis Membranes, Visited on 19 February, 2009
http://www.dowwaterandprocess.com/support_training/literature_manuals/filmtec_manual.htm.
- Thomson, M. and Infield, D. (2002) A photovoltaic-powered seawater reverse-osmosis system without batteries, *Desalination* 153, 1-8.
- Tu, K. L., Nghiem, L. D. and Chivas, A. R. (2011) Coupling effects of feed solution pH and ionic strength on the rejection of boron by NF/RO membranes, *Chemical Engineering Journal* 168, 700-706.
- Van der Meer, W. G. J. and van Dijk, J. C. (1997) Theoretical optimization of spiral-wound and capillary nanofiltration modules, *Desalination* 113, 129-146.
- Van Gauwbergen, D. and Baeyens, J. (1997) Macroscopic fluid flow conditions in spiral-wound membrane elements, *Desalination* 110, 287-299.

- Van boxtel, A. J. B. and Otten, Z. E. H. (1993) New strategies for economic optimal membrane fouling control based on dynamic optimization, *Desalination* 90, 363-377
- Villafafila, A. and Mujtaba, I. M. (2003) Fresh water by reverse osmosis based desalination: simulation and optimisation, *Desalination* 155, 1-13.
- Voros, N. G., Maroulis, Z. B. and MarinouKouris, D. (1997) Short-cut structural design of reverse osmosis desalination plants, *Journal of Membrane Science* 127, 47-68.
- Vrouwenveder, J. S., van Paassen, J. A. M., van Agtmaal, J. M. C., van Loosdrecht, M. C. M. and Kruithof, J. C. (2009)a A critical flux to avoid biofouling of spiral wound nanofiltration and reverse osmosis membranes: Fact or fiction?, *Journal of Membrane Science* 326, 36-44.
- Vrouwenvelde, J. S., van Paassen, J. A. M., Kruithof, J. C. and van Loosdrecht, M. C. M. (2009)b Sensitive pressure drop measurements of individual lead membrane elements for accurate early biofouling detection, *Journal of Membrane Science* 338, 92-99.
- Westerlund, T. and Pettersson, F. (1995) An extended cutting plane method for solving convex MINLP problems, *Computers & Chemical Engineering* 19, Supplement 1, 131-136.
- WHO 2008, Final Regulatory Determinations for the Second Drinking Water Contaminant Candidate List 2008.
- Wijmans, J. G. and Baker, R. W. (1995) The solution-diffusion model - a review, *Journal of Membrane Science* 107, 1-21.
- Wilf, M. (1997) Design consequences of recent improvements in membrane performance, *Desalination* 113, 157-163.
- Wilf, M. and Bartels, C. (2005) Optimization of seawater RO systems design, *Desalination* 173, 1-12.
- Wilf, M. and Schierach, M. K. (2001) Improved performance and cost reduction of RO seawater systems using UF pretreatment, *Desalination* 135, 61-68.
- Wilson, R. B. (1963) A simplicial method for convex programming, *Ph.D. thesis*, Harvard University.

- World Health Organization (1998) Boron, Environmental Health Criteria 204, Geneva, World Health Organization.
- Yang, H. L., Huang, C. and Lin, J. C.-T. (2010) Seasonal fouling on seawater desalination RO membrane, *Desalination* 250, 548-552.
- Zhao, Y., Taylor, J. S. and Chellam, S. (2005) Predicting RO/NF water quality by modified solution diffusion model and artificial neural networks, *Journal of Membrane Science* 263, 38-46.
- Zhou, S. L., McMahon, T. A., Walton, A. and Lewis, J. (2002) Forecasting operational demand for an urban water supply zone, *Journal of Hydrology* 259, 189-202.
- Zhu, A. Z., Christofides, P. D. and Cohen, Y. (2009) Effect of Thermodynamic Restriction on Energy Cost Optimization of RO Membrane Water Desalination, *Industrial & Engineering Chemistry Research* 48, 6010-6021.
- Zhu, M. J., ElHalwagi, M. M. and AlAhmad, M. (1997) Optimal design and scheduling of flexible reverse osmosis networks, *Journal of Membrane Science* 129, 161-174.
- Zilouchian, A. and Jafar, M. (2001) Automation and process control of reverse osmosis plants using soft computing methodologies, *Desalination* 135, 51-59.

Appendix A

PID Control of RO Process

A.1 Introduction

Despite the significant advances in RO membranes such as new membranes with higher permeability and fouling resistance and incorporation of the energy recovery devices in RO systems (Martin-Rosales et al., 2007), maintaining the process conditions in order to realize the production targets while operating the RO systems economically is still a vital task.

Variation in feed water quality and/or water temperatures including changes due to seasonal or even daily climate changes can significantly alter the operation conditions in RO plant and may led to sub-optimal system performance (Chen et al., 2005). Due to its sensitivity to quality of the feed and plant operating conditions, RO desalination process needs an efficient and accurate control system to maintain operation at optimum conditions that ensures the least energy utilization and prevent scaling and fouling.

Having presented a steady state model incorporating changes in several operation variables such as seawater temperature and membrane fouling for repetitive simulation and several optimization problems of RO process in earlier chapters, it was attempted to present an optimal control algorithm and demonstrate its capability with only preliminary results in this chapter.

In this work, a rigorous mathematical model of RO process is developed for Hollow Fibre B-10 Permasep module based on solution diffusion model to describe the RO performance and takes into account concentration polarization through film theory approach. A first order transfer function is built to represent the model and a PID controller is designed and used to control the rigorous model which is assumed to represent a real process. Optimal PID design based on the minimization of the integral of the squared error (ISE) performance index was used to tune the controller.

A.2 Process control variables

RO process often involves many operating parameters and requires the knowledge of several parameters such as pressure, salinity, pH, temperature, etc. (Chaaben et al., 2011). Several researchers have been developed control strategies for the RO desalination plants and addressing the selection of manipulated and controlled variables that can deliver the best control performance.

Robertson et al. (1996), Ballannec et al. (1999), Alatiqi et al. (1999) and Thomson and Infield (2002) have modelled seawater RO based desalination using pH and feed pressure as control variables. Calangelo et al. (1999) developed a control strategy using average hourly solar insolation and ambient temperature. They assumed that temperature is the main control variables.

Permeate flow rate and quality were chosen by Alatiqi et al. (1989) and also adopted in this work as control variables while the manipulated variable is feed pressure.

A.3 Modeling of RO Process

Models that adequately describe the performance of RO membranes are very important since these are needed in the design of RO processes. In this work, a steady state model of RO process that takes into account concentration polarization (CP) has been developed for the hollow fibre module presented in Alatiqi et al. (1989). The mathematical model equations for the RO module used in this work are given in chapter three (Section 3.2.1.2).

The performance of RO processes are affected by membrane fouling. Fouling causes reduction in membrane permeability and consequently decline in permeate flux. The dynamic of RO process is initiated by incorporating the operation disturbances caused by membrane fouling. Using the steady state model incorporating the dynamic behaviour of membrane fouling, optimal control of RO desalination is investigated and also, the optimal PID design is found.

An exponential function proposed by (Zhu et al., 1997) that describes the effect of membrane fouling on water permeability is incorporated in the simulation.

$$F = \exp\left(-\frac{t}{328}\right) \quad (\text{A.1})$$

The water permeability incorporating performance decline due to fouling (F) is approximated as follows:

$$A_w^{fo} = A_w F \quad (\text{A.2})$$

Where A_w is the water permeability without fouling, F is the fouling factor, t is the operation time.

Note, under fouling condition, water flux given by equation (3.1) will become:

$$j_w = A_w^{fo}(\Delta P - \Delta\pi) \quad (\text{A.3})$$

A.3.1 Estimation of Water and Salt Permeability Coefficients

Using the routine for parameter estimation built in gPROMS, the parameter estimation was carried out to predict the values of water and salt permeability coefficients. Experiment and parameter estimation entities in gPROMS are used in estimation of the permeability coefficients. The measured experiment data from Alatiql et al. (1989) is introduced in the experiment entity. In estimation entity the user specifies which experiment to use for parameter estimation. When the simulation model is implemented within gPROMS environment and the experiment are performed by introducing the required experiment data within experiment entity, the next stage in the model development process is the estimation of unknown model parameters using parameter estimation entity to fit the experiment data.

The water and salt permeability coefficients are estimated using gPROMS parameter estimation utility corresponding for each experimental data point (feed pressure, freshwater flux and salinity) shown in Table A.1. Then, the predicted water and salt

permeability coefficients in Table A.1 are fitted to yield general formula for the entire pressure range.

Water permeability

$$A_w = \frac{3.49468 \times 10^{-6}}{P^2} + 1.235 \times 10^{-8} \quad (\text{A.4})$$

Salt permeability

$$A_s = \frac{1}{1.116 \times 10^9 - 1.69 \times 10^8 \ln(P)} \quad (\text{A.4})$$

These relations are implemented in the simulation model within gPROMS.

Table A.2 shows a comparison between the experimental data (Alatiq et al., 1989) and the values calculated from equations A.4 and A.5. The results obtained illustrate good agreement with the experimental data where the average absolute deviations are 0.198 % and 2.477 % for water flux and freshwater TDS, respectively.

Table A.1 Permeability coefficients and experimental data

Pressure (bar)	Experimental data (Alatiq et al., 1989)		Predicted parameters (This work)	
	Flux (m ³ /h)	Permeate salinity TDS (ppm)	Water Permeability 10 ⁸ (m/s bar).	Salt permeability 10 ⁹ (m/s).
	68.02	0.341	201	1.17
61.20	0.286	218	1.21	2.31
54.42	0.232	243	1.23	2.34
47.60	0.177	279	1.25	2.5

Table A.2 Comparison of predicted with experimental data

	(Alatiq et al., 1989)		This work		Absolute Deviation		
	Pressure (bar)	Flux (m ³ /h)	Permeate salinity (ppm)	Flux (m ³ /h)	Permeate salinity (ppm)	Flux (m ³ /h) (%)	TDS (ppm) (%)
	68.02	0.3419	201	0.341	195	0.264	3.000
	61.20	0.2870	218	0.286	210	0.349	3.669
	54.42	0.2323	243	0.232	236	0.129	2.881
	47.60	0.1771	279	0.177	280	0.051	0.358
					Avg. Dev. (%)	0.198	2.477

A.4 Case Study

In this work, first, a rigorous mathematical model of Hollow Fibre module presented in Section 3.2.1.2 has been used. Then, a first order transfer function has been built to provide linear approximation of the rigorous mathematical model. A PID controller has been designed for the linear transfer function and used to control the rigorous model. Optimal PID design based on the minimization of the integral of the squared error (ISE) performance index was used to tune the controller. Only one membrane module is incorporated in the RO process. The characteristics of seawater Hollow Fibre module membrane used here are listed in Table A.3 (Marriott and Sorensen, 2003).

A.5 System Identification

Identification was carried out using MATLAB's system identification tool box where a sum of sinusoids input signal shown in Figure A.1 were generated and fed to the rigorous model. Feed pressure is manipulated (input) to control the permeate flow rate. Then, a linear transfer function was fitted to approximate the response of the rigorous model shown in Figure A.2 to the sinusoidal input.

Table A.3 B10 hollow fibre module (6440-T) specifications

Property	Value
Fibre length (mm)	780
Outer radius of fibre (mm)	0.0425
Inner radius of fibre (m)	0.021
radius of feed distributor (mm)	15
Fibre bundle radius (mm)	5.334×10^{-2}
Membrane area, m ²	187
Temperature range (°C)	0-40
pH range	4-9
Minimum flow rate per module (m ³ /day)	7.57
Maximum flow rate per module (m ³ /day)	56.78

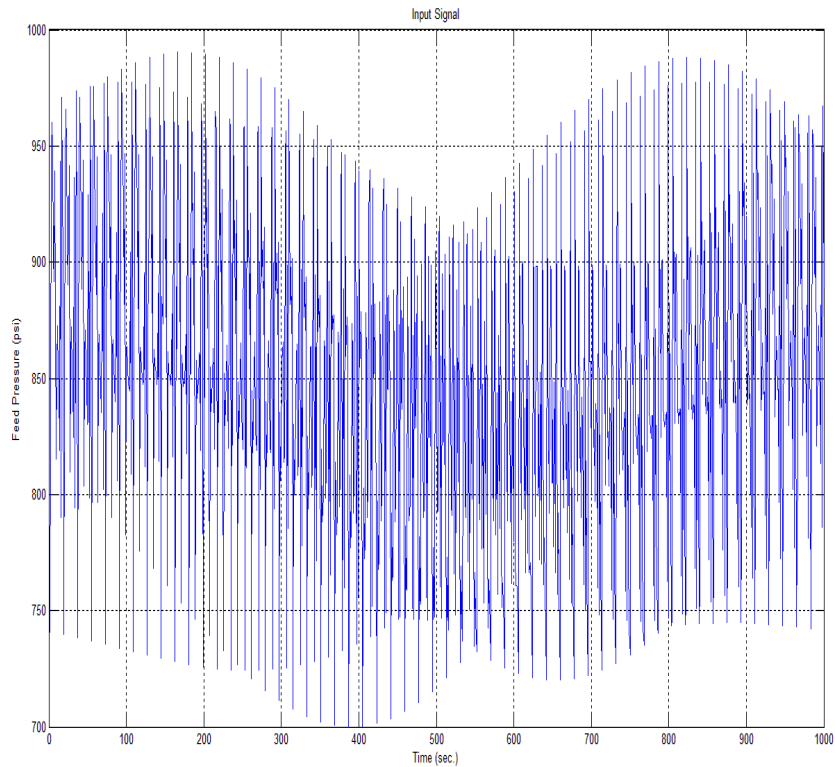


Figure A.1 Identification input signal

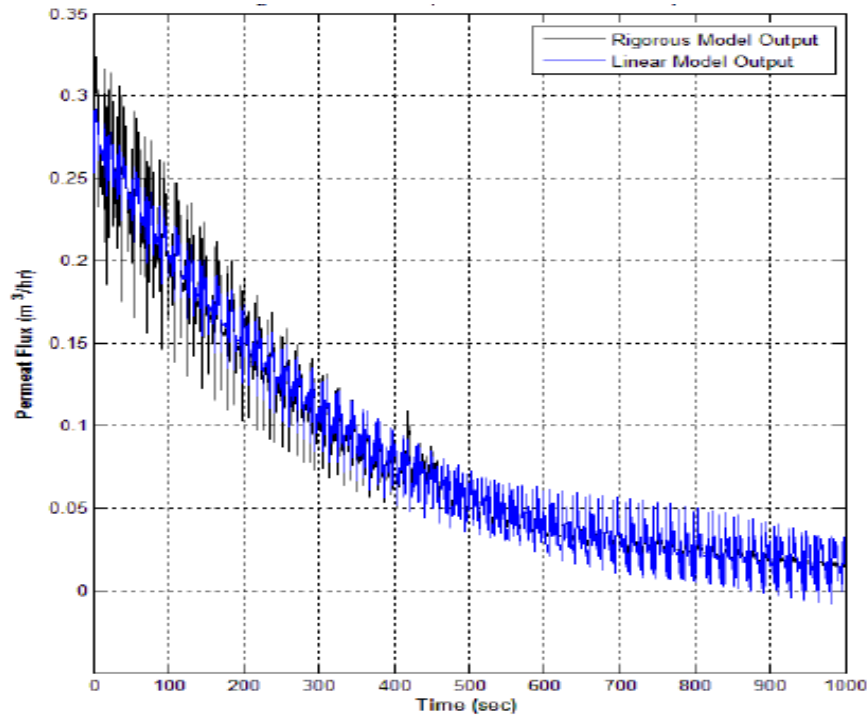


Figure A.2 Identification output signal

The best transfer function to fit the process in the least square sense was found to be:

$$G_p(s) = \frac{-5.207 \times 10^{-6}(1 - 212077 s)}{1 + 341.35 s} \quad (\text{A.6})$$

Figure A.3 shows the response of the process transfer function to the sinusoidal input with fit percentage 85.92%. Recall that the fit percentage is the percentage of the output variation explained by the model and is defined as:

$$fit = 100 \left(1 - \frac{|y - \hat{y}|}{|y - \bar{y}|} \right) \quad (\text{A.7})$$

Where y is the measured output, \hat{y} is the simulated output, and \bar{y} is the mean of y .

A.6 Controller Design and Response

The PID controller is usually used to improve the dynamic response as well as to reduce or eliminate the steady state error. The derivative controller adds a finite zero to the open loop plant transfer function and improves the transient response. The integral controller adds a pole at the origin, thus increasing system type by one and reducing the steady state error due to a step function to zero. Minimizing integral of squared error

(ISE) is commonly referred to as a good performance index in designing PID controllers. A PID controller has been designed for the linear transfer function and used to control the rigorous model. Optimal PID design based on the minimization of the integral of the squared error (ISE) performance index was used to tune the controller. PID controller parameters obtained by implementing the ISE performance index are: $K_p = 5324$, $T_i = 0.0021$, $T_d = 18.8204$.

Closed loop response to the change of permeate flux was done by changing the set point from 0 to 0.3 and then from 0.3 to 0.1 as shown in Figure A.3. It is clear that the closed loop system can follow the set point change in reasonable time and maintain fixed flow rate at steady state regardless of the presence of fouling.

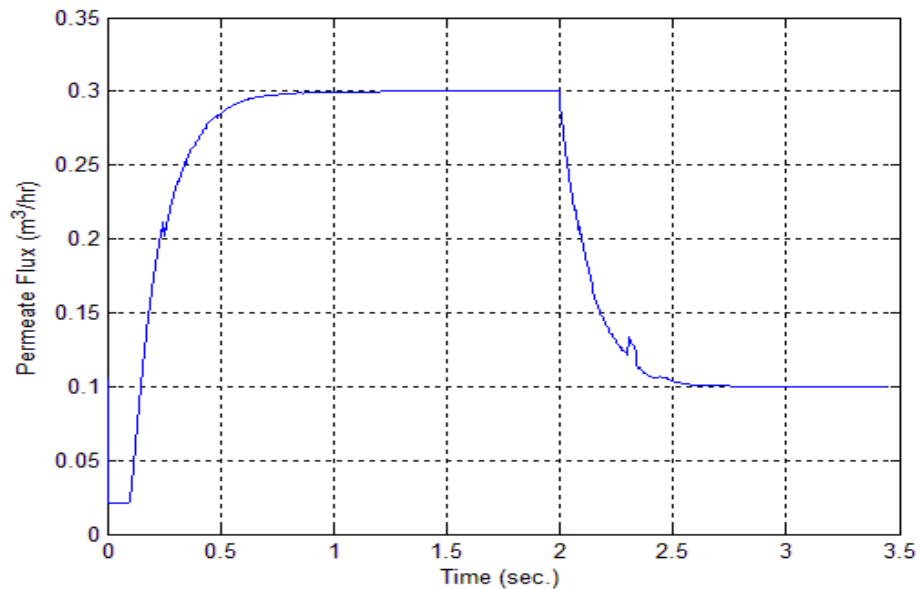


Figure A.3 Closed-Loop Response

A.7 Conclusion

Developing an optimization-based PID controller for a rigorous model (representing the real plant) of a hollow fiber RO process has been addressed in this work. Model parameters are estimated using parameter estimation tool built in gPROMS. Such controller was built based on linear approximation of the dynamics of the rigorous nonlinear mathematical model. Linear regression was used to estimate the linear approximate model. The PID design was based on minimizing integral of square error

performance index. Simulation showed that the process was able to track step change of the set point (in permeate flux) in reasonable time and maintain fixed flow rate at steady state regardless of the presence of fouling.